# Electrical control of magnetism by electric field and current-induced torques

Albert Fert

*Laboratoire Albert Fert, CNRS, Thales, Université Paris–Saclay, 91767 Palaiseau, France, Department of Advanced Polymers and Materials: Physics, Chemistry and Technology, Faculty of Chemistry, University of Basque Country (UPV/EHU), 20018 Donostia–San Sebastian, Basque Country, Spain, and Donostia International Physics Center (DIPC), 20018 Donostia–San Sebastian, Basque Country, Spain*

Ramamoorthy Ramesh

*Department of Materials Science and Engineering, University of California, Berkeley, California 94720, USA, Department of Physics, University of California, Berkeley, California 94720, USA, Department of Physics and Astronomy, Rice University, Houston, TX 77005, USA, and Materials Sciences Division, Lawrence Berkeley National Laboratory, Berkeley, California 94720, USA*

Vincent Garcia

*Laboratoire Albert Fert, CNRS, Thales, Université Paris–Saclay, 91767 Palaiseau, France*

Fèlix Casanova

*CIC nanoGUNE BRTA, 20018 Donostia–San Sebastian, Basque Country, Spain and IKERBASQUE, Basque Foundation for Science, 48009 Bilbao, Basque Country, Spain*

Manuel Bibes*

*Laboratoire Albert Fert, CNRS, Thales, Université Paris–Saclay, 91767 Palaiseau, France*

(published 13 March 2024)

The remanent magnetization of ferromagnets has long been studied and used to store binary information. While early magnetic memory designs relied on magnetization switching by locally generated magnetic fields, key insights in condensed matter physics later suggested the possibility of doing it by electrical means instead. In the 1990s, Slonczewski and Berger formulated the concept of current-induced spin torques in magnetic multilayers through which a spin-polarized current generated by a first ferromagnet may be used to switch the magnetization of a second one. This discovery drove the development of spin-transfer-torque magnetic random-access memories (MRAMs). More recent fundamental research revealed other types of current-induced torques named spin-orbit torques (SOTs) and will lead to a new generation of devices including SOT MRAMs and skyrmion-based devices. Parallel to these advances, multiferroics and their magnetoelectric coupling, first investigated experimentally in the 1960s, experienced a renaissance. Dozens of multiferroic compounds with new magnetoelectric coupling mechanisms were discovered and high-quality multiferroic films were synthesized (notably of $BiFeO_3$), also leading to novel device concepts for information and communication technology such as the magnetoelectric spin-orbit (MESO) transistor. The story of the electrical switching of magnetization, which is discussed in this review, is that of a dance between fundamental research (in spintronics, condensed matter physics, and materials science) and technology (MRAMs, MESO transistors, microwave emitters, spin diodes, skyrmion-based devices, components for neuromorphics, etc.). This *pas de deux* has led to major scientific and technological breakthroughs in recent decades (such as the conceptualization of pure spin currents, the observation of magnetic skyrmions, and the discovery of spin-charge interconversion effects). As a result, this field has not only propelled MRAMs into consumer electronics products but also fueled discoveries in adjacent research areas such as ferroelectrics or magnonics. In this review, recent advances in the control of magnetism by

*manuel.bibes@cnrs-thales.fr

 

electric fields and by current-induced torques are covered. Fundamental concepts in these two directions are reviewed first, their combination is then discussed, and finally current various families of devices harnessing the electrical control of magnetic properties for various application fields are addressed. The review concludes by giving perspectives in terms of both emerging fundamental physics concepts and new directions in materials science.

DOI: 10.1103/RevModPhys.96.015005

**CONTENTS**



## I. INTRODUCTION

### A. Macroscale perspective

The macrosystems perspective in this review is based on the field of information technologies. Microelectronics components and systems form an ever-increasing backbone of our society, pervading many parts of our daily life, for example, through a host of consumer electronics systems, providing sensing, actuation, communication, and processing and storage of information. All of these are built upon an approximately \$470 billion/yr global market that is exponentially growing at a pace of 10%–15% annually (Khan, Hounshell, and Fuchs, 2018; Manipatruni, Nikonov, and Young, 2018). Many such components likely started as materials physics research ideas, which have often first been discussed within the confines of physics and materials conferences worldwide. A few emerging global phenomena will likely completely change this microelectronics landscape. First among them is the "Internet of things," which is the network of physical devices, transportation systems, appliances, and other items embedded with electronics for sensing or actuating, computing, storage, and communications functions; see Fig. 1. As an example, a modern automobile has a large number of embedded sensing,

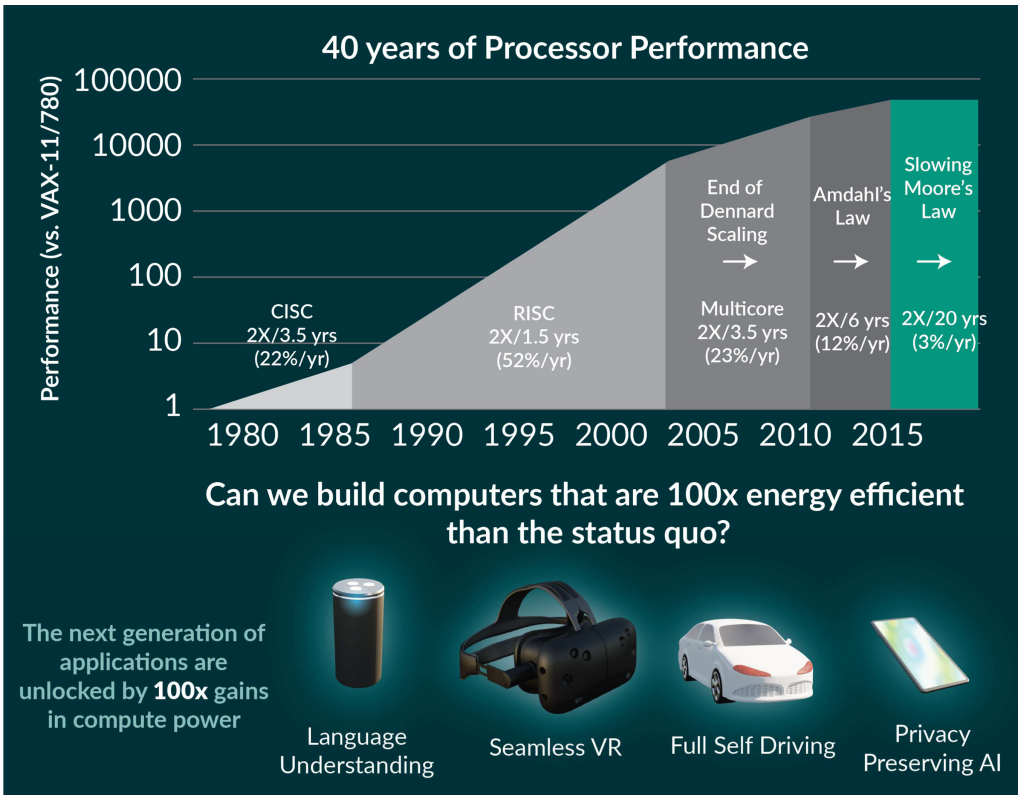


FIG. 1. Schematic illustrating the emergence of the Internet of things and machine learning and artificial intelligence as macroscale drivers for the beyond Moore's law research and development. The leveling off of the various scaling laws (Dennard's law states that as the dimensions of a device go down so does power consumption; Amdahl's law is a principle that states that the maximum potential improvement to the performance of a system is limited by the portion of the system that cannot be improved) is described as a function of time, leading to the end of Moore's law. Courtesy of Sasikanth Manipatruni and Debo Olaosebikan, Kepler Computing.

communicating, and computing components, and this is only going to increase. For example, the emergence of autonomous vehicles will require orders of magnitude higher levels of computing with sustainable power consumption.

The second major phenomenon is the emergence of machine learning and artificial intelligence, which are taking the technology world by storm. They use a large amount of computing and data analytics, which in turn provides the system the ability to "learn" and do things better without human intervention. Of relevance to us is the fact that microelectronic components are critical building blocks for this field.

We can now ask the following question: How do these macroscale phenomena relate to microelectronics and, more importantly, to new materials and physics underpinning them? Stated differently, what can materials physics do to enable this coming paradigm shift? To put this into perspective, we now need to look at the fundamental technoeconomic framework that has been driving the microelectronic field for more than five decades. The well-known Moore's law (Moore, 1968), the technoeconomic principle that has thus far underpinned the field of microelectronics through the scaling of complementary metal oxide semiconductor (CMOS-) based transistors is displayed in Fig. 2.[1] Broadly it states that the critical dimensions of the CMOS transistor shrink by 50% every 18–24 months. At their inception, CMOS transistors were "macroscopic," with the critical dimension well over 1 μm. Dennard scaling provided a path to shrinking such transistors while keeping the power density constant (Dennard *et al.*, 1974). Today this power scaling is no longer possible, while the critical dimensions of modern transistors have entered sub-10-nm scales, the point at which the fundamental science (i.e., classical electron dynamics) is no longer sufficient to adequately describe the physics of the transistor, and ever more complex manufacturing issues must be addressed. Therefore, in the past decade or so, there has been an ever-increasing sense that something has to be done about this issue (Theis and Solomon, 2010; Ferain, Colinge, and Colinge, 2011; Kuhn, 2012; Salahuddin, Ni, and Datta, 2018; Manipatruni *et al.*, 2019).

What is now needed to mitigate this major issue is a paradigm shift similar to the introduction of CMOS technology to replace bipolar transistors in the 1990s (Ellsworth *et al.*, 2008; Ball, 2012; Paredes *et al.*, 2014); see Fig. 3. One can explore many pathways to address this impending crisis. In some sense, this is a matter of perspective: circuit design engineers may prefer to go to specialized architectures (Patterson and Hennessy, 2017) or pivot from the conventional Boolean or von Neumann architecture into a neuromorphic architecture (Borders *et al.*, 2019). Another pathway could be to move away from highly deterministic computing (which tolerates errors at a scale of $10^{-10} - 10^{-12}$) to more of a stochastic computing. The third way overtly involves "quantum materials," materials in which quantum mechanical effects such as exchange interaction or spin-orbit coupling

[1]See https://ourworldindata.org/moores-law.

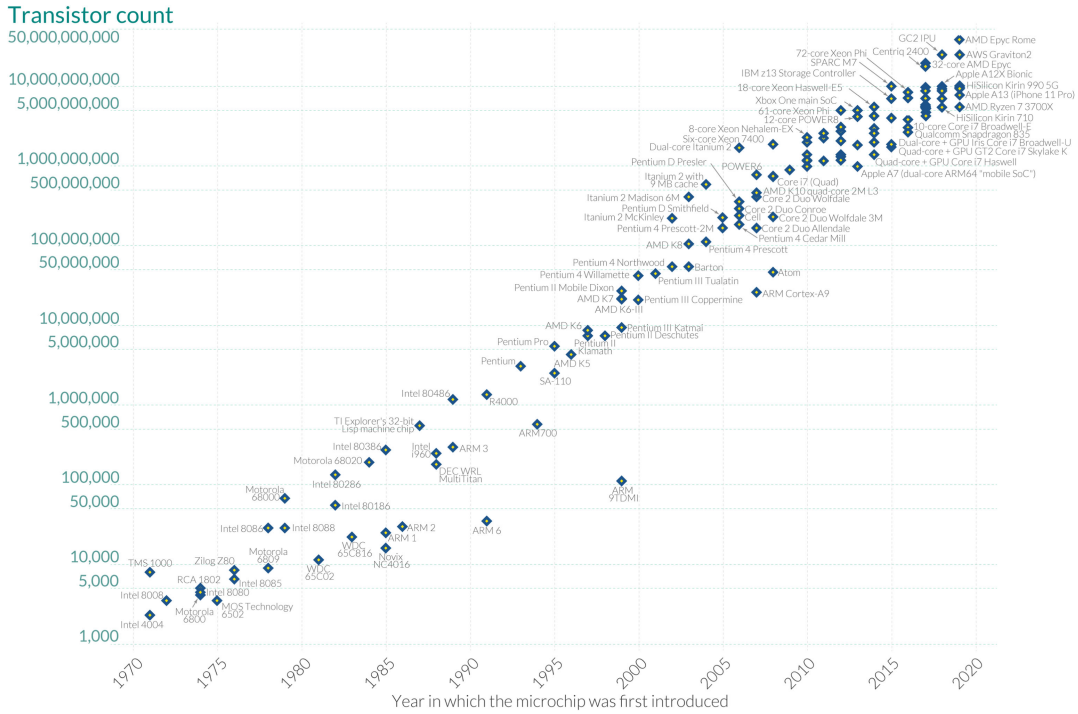


FIG. 2. Moore's law: the evolution of the number of transistors per chip over time.

directly lead to exotic physical phenomena (to start with magnetism, ferroelectricity, multiferroic behavior, and more recently topological behavior arising from band topology). We get to this after a short description of another looming challenge, namely, energy or, more specifically, energy efficiency in computing and how it impacts the global energy consumption in microelectronic systems.

In today's CMOS transistor, the energy consumed per logic operation is of the order of 10–100 pJ for a typical 32-transistor logic circuit. It is noteworthy that, at the single transistor level, the energy consumption in state-of-the-art transistors is ∼50 aJ; however, the design of logic circuits involving a large number of such transistors leads to the eventual energy per logic operation. In this sense, a reduction in the number of transistors required to perform logic operations and/or moving to capacitive elements [as in magnetoelectric spin-orbit (MESO) devices (Manipatruni *et al.*, 2019), which are discussed in Sec. V.A.4] could also reduce the number of building blocks required to perform the logic operations. If we assume that there will be no change to this number in the near future, and at the same time that the demand for and consumption of microelectronic components in the Internet of things, artificial intelligence, and machine learning is predicted to increase, the total energy consumption in all of microelectronics could grow to ∼20% of primary energy by 2030; see Fig. 4. At this scale, microelectronics would become a significant part of worldwide energy consumption and thus should be addressed from an energy efficiency perspective as well.

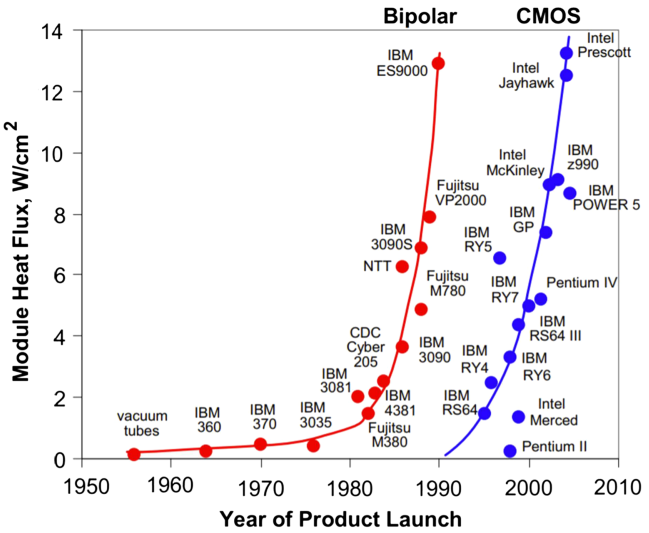


FIG. 3. Heat output over time for bipolar and CMOS transistor chips. From Ellsworth *et al.*, 2008.

The end of the conventional Si-CMOS-based Moore's law thus emerges as a fantastic opportunity to explore pathways for beyond Moore's law architectures. Indeed, the past decade has witnessed innovations at multiple levels. In particular, there have been many fundamental-physics-based innovations in spintronics and spin-based devices. Thus, if pathways are found to reduce their energy consumption, notably to control magnetization, then this presents an interesting opportunity to create the next generation of computing paradigms. This includes logic-in-memory architectures departing from von Neuman's architectures by embedding memory and logic, thereby removing the energy-costly transfer of data beween separated memory and computing units.

### B. The need for a paradigm shift and for new materials

We begin our exploration of new materials physics by going back to the fundamentals of CMOS devices. CMOS

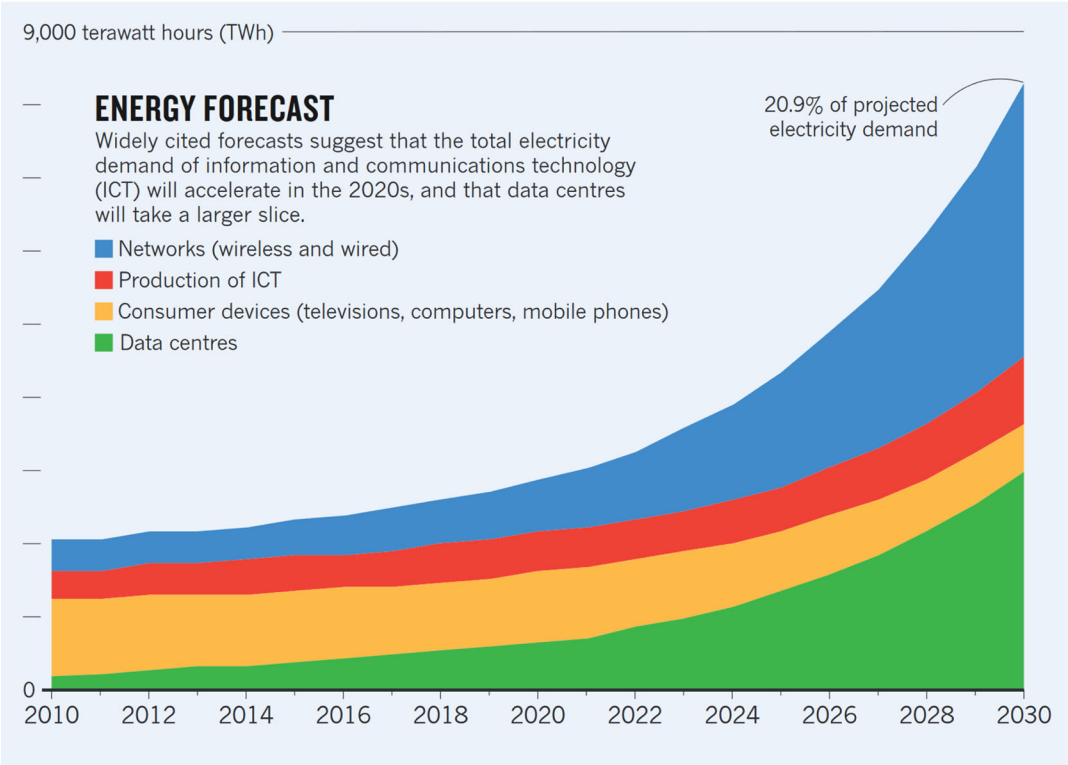


FIG. 4. Energy consumption of information and communication technology systems over time. From Jones, 2018.

transistors utilize a gate voltage to control the flow of current between the source and the drain. By adjusting the energy bands in the semiconducting channel, the gate voltage either permits the movement of electrons (the *on* state) or obstructs it (the *off* state). However, the electron energies from the source are spread out at finite temperatures. Consequently there is a finite density of electrons with sufficiently high energy to surpass the barrier that would otherwise impede their journey between the source and drain in the off state. This leakage current leads to energy wastage. According to fundamental thermodynamic principles, reducing this current by a factor of 10 necessitates increasing the barrier by approximately 60 meV at room temperature (Salahuddin, Ni, and Datta, 2018). However, to prevent energy wastage caused by leakage current, the current must be reduced by a factor of at least 100 000, thereby requiring a minimum barrier of 300 meV. Consequently a minimum gate voltage of at least 300 mV becomes necessary. This minimum gate voltage establishes a lower limit on switching energy. This limitation is referred to as Boltzmann's tyranny. It was named after Ludwig Boltzmann, who elucidated the spreading of particle energies due to temperature. Boltzmann's tyranny is believed to restrict the extent to which the operating gate voltage can be reduced for a transistor, irrespective of the material used.

In recent years, the community realized that Boltzmann's tyranny needs to be addressed, setting the stage for new materials and new phenomena, with a view toward designing entirely new computing building blocks to replace CMOS transistors operating at low voltage and dissipating much less power. One proposed pathway identifies a broad class of quantum materials, for instance, materials exhibiting a metal-to-insulator transition (Imada, Fujimori, and Tokura, 1998) and those possessing a ferroic order such as ferromagnets or ferroelectrics. In these compounds the exchange energy (in ferromagnets) or the dipolar energy (in ferroelectrics) makes the spins or the dipoles align collectively without the need for an external source of energy such as an applied field. Thus, if one could use a spontaneous magnetic-dipole moment as the primary order parameter rather than electronic charge in a CMOS device, one could take advantage of such internal collective order to reduce the energy consumption. Indeed, this was the premise behind two notable research articles (Manipatruni, Nikonov, and Young, 2018; Manipatruni *et al.*, 2019) in which the rudiments of a possible MESO coupled memory-logic device were discussed. As we see in this review, harnessing the electric-field control of magnetism offers promising opportunities to realize ultralow-power, beyond-CMOS computing devices.

### C. Magnetism and spintronics

While magnetic phenomena have been known since ancient times, spintronics is a relatively new field of electronics that acts not only on the charge of electrons but also on their spin. The field of spintronics was initially sparked by the discovery of the giant magnetoresistance (GMR) in magnetic multilayers in 1988 (Baibich *et al.*, 1988; Binasch *et al.*, 1989), which introduced new concepts for utilizing spin-polarized currents and demonstrated potential applications for spin-based technology. In the early days of spintronics, spin-polarized currents were generated by utilizing the influence of the orientation of spin on the transport properties of electrons in ferromagnetic conductors. This influence, which was first suggested by Mott (1936), had been experimentally

demonstrated and theoretically described a decade before the GMR discovery (Fert and Campbell, 1968, 1971, 1976). This method of generating spin-polarized currents was used in "classical spintronics" during the first decade after the GMR discovery. Major advancements during this time included the discovery of tunneling magnetoresistance (TMR) (Miyazaki and Tezuka, 1995; Moodera *et al.*, 1995) and spin-transfer torque (STT) (Berger, 1996; Slonczewski, 1996). Additionally, important concepts such as spin accumulation and pure spin current (a current of spin without a current of charge) were introduced. In more recent times, it has become possible to produce spin-polarized currents and pure spin currents without using magnetic materials by utilizing spin-orbit interactions in nonmagnetic materials, which is known as spin-orbitronics. Today, spintronics is expanding in various directions, with promising new areas of research including spintronics with topological systems, such as the interface states of topological insulators, and spintronics with magnetic skyrmions.

The idea that magnetism could be used to store digital information dates back to the 1950s and the development of soft-core ferrite-based memories (Eckert, 1953). In these destructive readout devices, magnetic tori made of ferrites were organized into an array and magnetized in one or the other direction by the magnetic field produced by currents running in two perpendicular electrical wires passing through each torus. This technology remained the dominant random-access computer memory until the introduction of semiconductor memory in the late 1960s, which allowed for both an increase in density and a decrease in cost. Magnetic disk technology appeared in the 1960s as well and led to the development of hard-disk drives and floppy disks. The write process involved passing a current into an electromagnetic write head, thus generating a local magnetic field. Initially, the readout process was based on magnetic induction, but in 1990 IBM introduced read heads relying on anisotropic magnetoresistance (AMR), thereby pioneering a new method to sense magnetization through its influence on electrical transport. The discovery of GMR in 1988 (Baibich *et al.*, 1988; Binasch *et al.*, 1989) prompted the development of GMR-based read heads that replaced AMR-based ones in 1997, thus marking the beginning of spintronics-based technologies. However, magnetic information writing continued to rely on the generation of a local magnetic field by electrical current. The Oersted field produced by current running through perpendicular current lines (as in soft-core memories) was also the method used to write information in the first prototype of magnetic random-access memories (MRAMs), which was announced in 1995 (Tang *et al.*, 1995) and released in 2006. In today's generation of STT MRAMs, which have been on the market since 2019, writing has become purely electrical thanks to the use of the STT mechanism for the conversion of spin-polarized current into torques acting on the magnetization. Current MRAM dice density is 1 Gbyte at the 28 nm technology node and MRAM will continue to gain market share as stand-alone nonvolatile memories for specific applications, for example, when radiation hardness is needed or where the endurance and speed of Flash are not enough. Embedded MRAM will also start replacing SRAM in applications where the nonvolatility versus speed compromise is advantageous. Commercial products are already on the market. The next generation will be spin-orbit torque (SOT) MRAMs, which exploit pure spin current induced by spin-orbit coupling in heavy metals or topological materials and the resulting SOTs; see Sec. V.A.1.

With this as the technological background, in this review we discuss efforts in the endeavor focusing on controlling magnetism not from the magnetic field but instead from electrical means, namely, voltage and electric current. Research in this field has been fueled by advances in condensed matter physics and materials science, along directions that have remained parallel for several decades. As we later see, research on multiferroics and magnetoelectrics started in the 1960s but remained confidential for 40 years, while spintronics entered the stage upon the discovery of GMR in 1988. Both fields developed nearly without interacting until the 2000s and the rediscovery of multiferroic materials and magnetoelectric coupling. Magnetoelectric coupling precisely aims to achieve an electrical control of magnetization, mostly using multiferroics, and its revival prompted the development on voltage-controlled magnetic anisotropy in classical spintronic devices such as magnetic tunnel junctions (MTJs), not those involving magnetoelectric or multiferroic materials *per se*.

### D. Magnetoelectric coupling and multiferroics

Multiferroics exhibit more than one primary ferroic ordering (i.e., ferromagnetism, ferroelectricity, ferroelasticity, or ferrotoroidicity) in the same phase (Schmid, 1994); see Fig. 5. This terminology is usually extended to include other types of order such as antiferromagnetism and composites of individual ferroics and is used most often to refer specifically to magnetoelectric materials combining ferroelectric and magnetic behavior into a single phase (Fiebig, 2005). The coexistence of ferroic orders can lead to coupling between them, so one ferroic property can be manipulated with the conjugate field of the other (Ramesh and Spaldin, 2007). A good example of a multiferroic is the case of ferromagnetic shape memory alloys, which exhibit ferromagnetism along with a spontaneous strain (Ullakko, 1996). In contrast, the coexistence of spin and charge orders (particularly ferromagnetism and ferroelectricity) is challenging since ferroelectricity requires an insulator, while typical ferromagnets require electronic exchange interactions (Hill, 2000). Many insulating magnets are either antiferromagnets or ferrimagnets (driven by superexchange interactions); ferrimagnets are antiferromagnets with uncompensated magnetic sublattices and thus possess a finite magnetization. Therefore, progress in multiferroic research requires (i) understanding the electronic structure at the most fundamental level, (ii) new material chemistries to implement them, (iii) the development of new tools to compute and characterize the novel properties associated with the coupled behaviors, and (iv) new approaches to synthesize such materials with atomic-scale precision. When this is successful, it presents possible routes to entirely new device architectures (Wood and Austin, 1974; Bibes and Barthélémy, 2008; Fusil *et al.*, 2014), as exemplified by Intel's MESO device (Manipatruni *et al.*, 2019). The field of multiferroics is now vast, and we direct the interested reader to other articles with different emphases (Eerenstein,

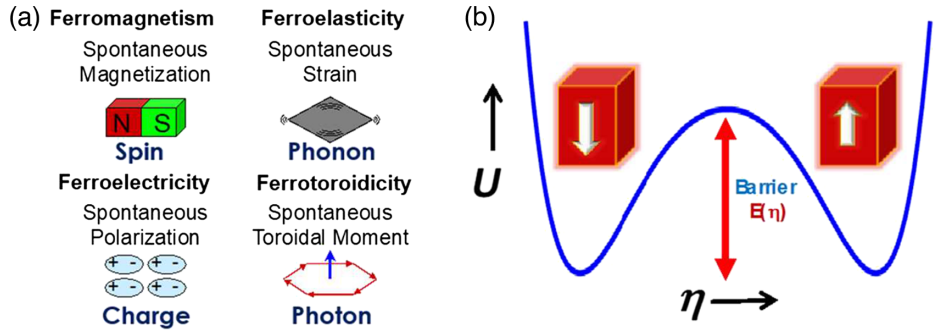


FIG. 5. Fundamental taxonomy of solid-state order parameters. (a) Emergence of ferromagnetism due to spontaneous time-reversal symmetry breaking, ferroelectricity due to spontaneous spatial inversion symmetry breaking, and ferroelasticity, which is characterized by a spontaneous strain, and ferrotoroidicity, which breaks both time and spatial inversion symmetry (Van Aken *et al.*, 2007). The coexistence of at least two order parameters defines multiferroics and the coupling between them leads to magnetoelectricity, piezoelectricity, and piezomagnetism. (b) Scheme of a classical double-well energy $U$ landscape that characterizes the emergence of the order parameters (here $\eta$) described in (a). Switching between equivalent states requires an energy barrier $E(\eta)$, often described as the Landau barrier, to be overcome.

Mathur, and Scott, 2006; Wang *et al.*, 2010; Pyatakov and Zvezdin, 2012; Tokura, Seki, and Nagaosa, 2014; Dong *et al.*, 2015; Fiebig *et al.*, 2016; Lu *et al.*, 2019; Batoo *et al.*, 2021; Cano, Meier, and Trassin, 2021) as a complement to what we present in this review.

There are now many established routes to circumvent the "contraindication" between ferroelectricity (associated with ionic species with empty *d* orbitals) and magnetism (associated with partially filled *d* orbitals) (Hill, 2000). Although there are several known multiferroics, there is still a dearth of technologically viable multiferroics, i.e., those that can be manipulated at room temperature and exhibit strong coupling between spin and charge degrees of freedom. Thus, there should be no doubt that a more diverse palette of new materials with robust room-temperature coupling of magnetism and ferroelectricity is still urgently needed and indeed should be the focus of interdisciplinary research. Table I summarizes five main physical principles that have led to the discovery of multiferroics. Of these, the two most studied are multiferroics in which the polar order comes from one of the crystal sites and the magnetic order is built into the other chemical site, as exemplified by $BiFeO_3$. The second type, which has received considerable interest from the physics community, is based on a polar order emerging as a consequence of a magnetic transition, as for manganites (Kimura, Goto *et al.*, 2003). An emerging third pathway is via the power of heteroepitaxy and superlattice design (Mundy *et al.*, 2016). In this regard, although there were numerous attempts in the past to synthesize complex crystal symmetries to induce multiferroic behavior, this has not been extensively revisited in recent years. There appears to be a significant opportunity to "design" multiferroic behavior by selecting magnetic materials with low symmetry and then induce inversion symmetry breaking through heterophase epitaxy. We use these as examples to explore both the fundamental materials physics of coupling and the potential for future applications; see Sec. V.

### E. Outline

We start this review by covering advances on the control of magnetism by an electric field (Sec. II) using magnetoelectric effects within multiferroics (Sec. II.A), strain-driven magnetoelectric coupling in composites and multilayers (Sec. II.B), and electric-field effects using dielectrics, ferroelectrics, or ionic liquids (Sec. II.C). More recent progress in electric-field control of magnetism has been dedicated to two-dimensional (2D) magnets (Sec. II.D), magnetic skyrmions (Sec. II.E), and magnons (Sec. II.F). Section III is devoted to the control of magnetism by current-induced torques. We start by recalling the definition and generation of spin currents (Sec. III.A), then introduce STTs (Sec. III.B) and SOTs (Sec. III.C) for magnetization switching. We also discuss specific systems and application of particular interest such as the current-induced motion of domain walls (Sec. III.D), skyrmions (Sec. III.E), and the control of magnetism by current-induced torques in the recently discovered 2D magnets (Sec. III.F). In Sec. IV we cover the combined use of electric-field- and current-induced torques. Finally, Sec. V reviews advances in devices harnessing the electrical control of magnetism, including devices for logic and memory such as MRAMs and the MESO transistor (Sec. V.A), spin-torque nano-oscillators and spin diodes (Sec. V.B), and devices based on domain walls and skyrmions (Sec. V.C). We conclude by giving perspectives for this vast and vibrant field (Sec. VI).

## II. CONTROL OF MAGNETISM BY AN ELECTRIC FIELD

### A. Electric-field control of magnetism in multiferroics

#### 1. Single phase multiferroics

*a.* $BiFeO_3$

Of the known multiferroics, bismuth ferrite ($BiFeO_3$) remains arguably the most important, and certainly the most widely studied, with more than 6000 papers published in the last decade. The establishment of its large (90–100 $\mu C/cm^2$) ferroelectric polarization, combined with magnetic ordering well above room temperature (Wang *et al.*, 2003), has spawned an intense research effort that continues to unveil interesting new physics and potential new applications (Catalan and Scott, 2009).

TABLE I. Summary of the various identified mechanisms for creating multiferroics and magnetoelectrics. For generalities on oxides and their structural and electronic properties, we refer the interested reader to Cox and Cox (1995).

| Pathway | Fundamental mechanism | System examples | Type of magnetic order |
|---|---|---|---|
| *A*-site driven | Stereochemical activity of lone pairs on the *A* site leads to ferroelectricity; magnetism comes from the *B* site | $BiFeO_3$<br>$BiMnO_3$ | Antiferromagnet<br>Ferromagnet |
| Geometrically driven | Long-range dipole-dipole interactions and oxygen rotations break inversion symmetry | $YMnO_3$<br>$BaNiF_4$<br>$LuFeO_3$ | Antiferromagnet<br>Antiferromagnet<br>Antiferromagnet |
| Charge ordering | Noncentrosymmetric charge ordering leads to ferroelectricity in magnetic materials (such as a Vervey transition) | $LuFe_2O_4$ | Ferrimagnet |
| Magnetic ordering | Magnetic-field-driven ferroelectricity induced by a lower symmetry ground state | $TbMnO_3$<br>$DyMnO_3$ | Antiferromagnet<br>Antiferromagnet |
| Atomically designed superlattices | Still under investigation; likely lattice mediated | $LuFeO_3 - LuFe_2O_4$ | |
| Vertical epitaxial nanocomposites | Coupling mediated by 3D interfacial epitaxy, for instance, a spinel-perovskite interface | $CoFe_2O_4 - BiFeO_3$<br>$NiFe_2O_4 - BiFeO_3$<br>$CoFe_2O_4 - BaTiO_3$ | Ferrimagnet-antiferromagnet |

$BiFeO_3$ formally belongs to the perovskite family of oxides, albeit it is rhombohedrally distorted from the cubic prototypical structure with $R3c$ crystal symmetry in which the spontaneous polarization points along the eight equivalent $\langle 111 \rangle$ directions (Fig. 6). While there was considerable debate in the early days regarding the magnitude of the spontaneous polarization (Teague, Gerson, and James, 1970) (due to the difficulty of making high-quality single crystals), it is now well established to be 90–100 $\mu C/cm^2$ in both films and single crystals (Wang *et al.*, 2003; Lebeugle *et al.*, 2007) and has been confirmed theoretically (Neaton *et al.*, 2005; Daumont *et al.*, 2012). In parallel with the scientific debate on the ferroelectric properties, there was an equal degree of debate as to the state of magnetism, particularly since it is complicated. Although the dominant superexchange interaction stabilizes a *G*-type (ferromagnetic coupling in a $\{111\}$ plane and antiferromagnetic coupling perpendicular to this plane) antiferromagnetic structure (Kiselev, Ozerov, and Zhdanov, 1963), the magnetic structure is much more sophisticated. As a consequence of the antisymmetric magnetoelectric interaction (Sosnowska and Zvezdin, 1995), the spins are forced to rotate in an incommensurate spin cycloid (62–64 nm; green arrows in Fig. 6) in a plane containing the polarization and the propagation vector [along the three high-symmetry $\langle -110 \rangle$ of the (111) plane] (Sosnowska, Neumaier, and Steichele, 1982; Lebeugle *et al.*, 2008). A second Dzyaloshinskii-Moriya interaction, arising from the antiphase rotations of the oxygen octahedra along the $\langle 111 \rangle$ polarization direction [Fig. 6(c)], favors an additional canting perpendicular to the cycloidal plane. This small canting is varying in space in the form of a spin-density wave (red areas in Fig. 6) locked to the spin cycloid, which gives rise to zero net magnetization (Ramazanoglu *et al.*, 2011).

In $BiFeO_3$ single crystals, this canted moment does not exhibit a macroscopically measurable magnetic moment until the spin cycloid is broken, such as through the application of a magnetic field of ~16–18 T (Zvezdin *et al.*, 2006). While it was initially considered not to exist in thin films (Bai *et al.*, 2005;

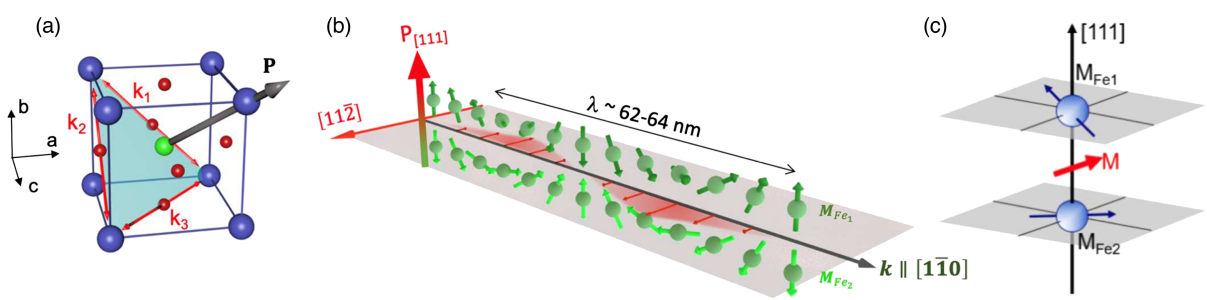


FIG. 6. (a) Sketch of the $ABO_3$ perovskite unit cell of $BiFeO_3$. The Bi atoms are at the corners of the cell (*A* site), the Fe atom is at the center of the cell (*B* site) and the oxygen atoms form an octahedron around the Fe. The polarization points along the $\langle 111 \rangle$ plane. The three corresponding propagation directions ($k_1$, $k_2$, and $k_3$) are contained along the $(111)$ plane. (b) Sketch of the spin cycloid in which antiparallel spins are rotating in a plane defined by the polarization $P$ and the propagation vector $k$. A small canting perpendicular to the cycloidal plane and varying in space forms a coupled spin-density wave (propagating in the gray plane). (c) Small canted moment resulting from the Dzyaloshinskii-Moriya interaction; see Sec. II.E for the definition. From Ederer and Spaldin, 2005.

Ederer and Spaldin, 2005; Béa *et al.*, 2007), there was experimental evidence over the last decade indicating that the spin cycloid is preserved for moderate epitaxial strain in $BiFeO_3$ thin films using macroscopic averaging techniques (Ke *et al.*, 2010; Sando *et al.*, 2013) or scanning nitrogen-vacancy color center in diamond (N-*V*) magnetometry (Gross *et al.*, 2017; Haykal *et al.*, 2020). In addition, varying the epitaxial strain is an effective tool for controlling the antiferromagnetic textures in $BiFeO_3$ thin films from bulklike to exotic cycloids, or pseudocollinear *G*-type orderings (Agbelele *et al.*, 2017; Haykal *et al.*, 2020). In addition, domain walls can play a key role in the emergence of a magnetic moment, which typically manifests in the form of a spin glass (Martin *et al.*, 2008).

Understanding electric-field control of antiferromagnetism in $BiFeO_3$ thin films requires probing antiferromagnetism using x rays, neutrons, second harmonic generation (SHG), or scanning N-*V* magnetometry. These studies of $BiFeO_3$ showed that, when the polarization state switches with the application of an electric field, there is a corresponding rotation of the magnetic order (Zhao *et al.*, 2006; Lebeugle *et al.*, 2008; Chauleau *et al.*, 2017; Gross *et al.*, 2017). As illustrated in Figs. 7(a) and 7(b), this change can be spatially probed using a combination of piezoresponse force microscopy [(PFM); to image the ferroelectric order] and x-ray magnetic linear dichroism (XMLD) photoemission electron microscopy [(PEEM); to image the antiferromagnetic order] (Zhao *et al.*, 2006). SHG shows that, in the canted antiferromagnetic state (large compressive strain), a single ferroelectric domain can correspond either to multiple submicron antiferromagnetic domains or to single domains, depending on the switching path [Figs. 7(c) and (d)] (Chauleau *et al.*, 2017). Scanning N-*V* magnetometry revealed that the electric field enables a deterministic control of antiferromagnetic domains in the cycloidal state [Figs. 7(e)–7(h)]. Note that there has been little detailed work leading to a full understanding of the dynamics of the manipulation of the antiferromagnetic state by an electric field, with most studies assuming that the magnetic order merely follows that of the polar order, but not clarifying that pathway. This is an opportunity for future ultrafast dynamics research since the antiferromagnetic resonance frequencies are in the several hundred gigahertz range and $BiFeO_3$ has electromagnons in the 600 GHz–1 THz range (Cazayous *et al.*, 2008; Rovillain *et al.*, 2010; Nagel *et al.*, 2013); see Sec. II.F.2. Given the current surge of interest in antiferromagnetic spintronics (Baltz *et al.*, 2018), such insulating multiferroics would also garner more attention, especially through the use of nonlocal spin transport.

While first-principles density functional theory calculations remain central for understanding and predicting the properties of multiferroics, second-principles calculations with embedded model Hamiltonians are proving to be increasingly valuable in the study of larger systems, for example, heterostructures, domain walls, and defects, as well as, on longer timescales, in molecular dynamics. They have been applied to describe structural phase transitions of prototypical ferroelectrics (Zhong, Vanderbilt, and Rabe, 1994; Rabe and Waghmare, 1995), and recent extensions to include additional

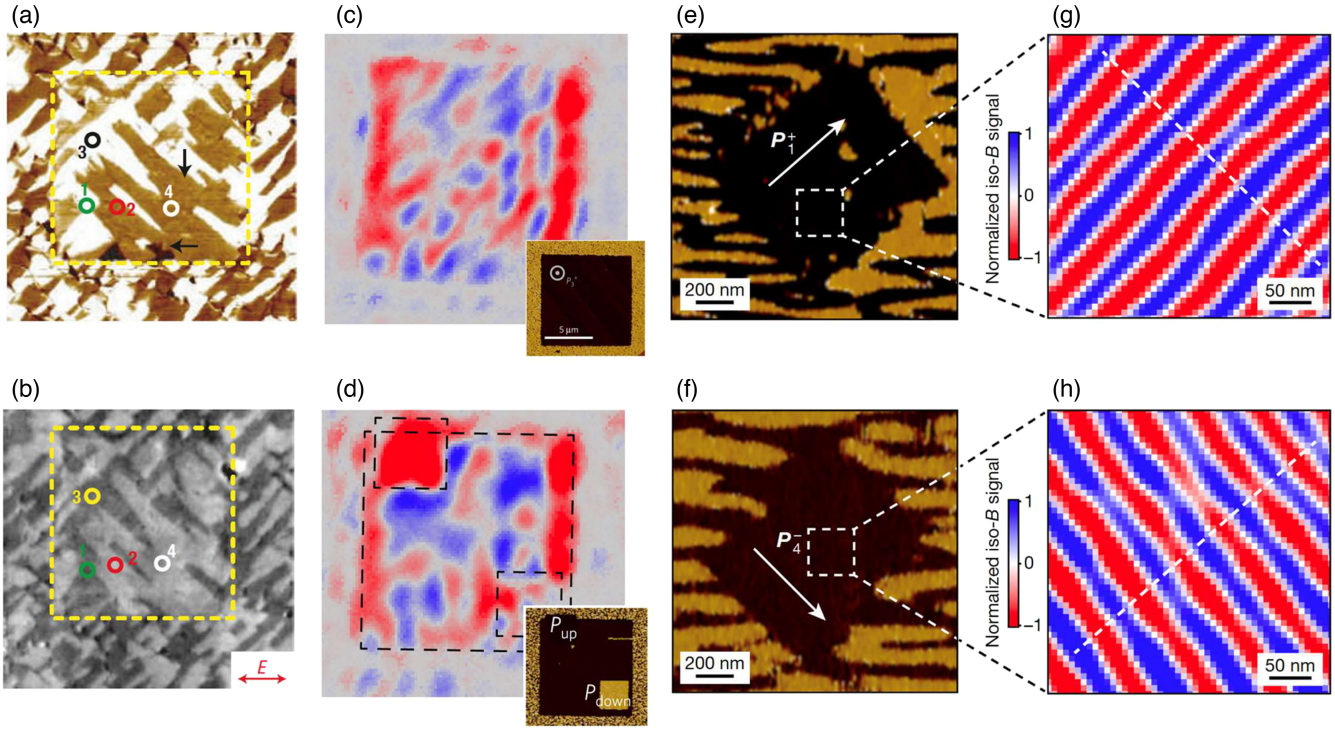


FIG. 7. Electric-field control of antiferromagnetism in $BiFeO_3$. (a) In-plane PFM and (b) XMLD PEEM on a central area that has been electrically switched. From Zhao *et al.*, 2006. (c) Reconstructed antiferromagnetic configurations from SHG images in a single ferroelectric domain and (d) after switching in plane (top left inset) and out of plane (bottom right inset). (c),(d) From Chauleau *et al.*, 2017. (e),(f) In-plane PFM and (g),(h) corresponding scanning N-*V* magnetometry images of two different single ferroelectric domains defined by applying an electric field to the PFM tip. (e)–(h) From Gross *et al.*, 2017.

lattice degrees of freedom (Liu, Grinberg, and Rappe, 2013), as well as magnetic interactions (Rahmedov *et al.*, 2012), have extended their applicability to multiferroics. For example, an effective Hamiltonian consisting of a lattice part incorporating ferroelectric distortions, octahedral rotations and strain, a contribution from the interaction of the magnetic moments with each other, and coupling between the magnetic moments and the lattice were shown to accurately reproduce the crystal and magnetic structures of bulk $BiFeO_3$ (Rahmedov *et al.*, 2012). On a larger length scale, a Landau-Ginzburg thermodynamic potential that includes both polar and antipolar distortions and their coupling to magnetism was successful in reproducing the bulk behavior of $BiFeO_3$ and offers promise for predicting properties in thin-film heterostructures and nanostructures (Karpinsky *et al.*, 2017). Multiscale approaches that allow the electronic and lattice degrees of freedom to be treated on the same footing (García-Fernández *et al.*, 2016) could lead to vastly enhanced system sizes and accuracy when combined with improved tools for generating effective potentials using input from first principles (Wojdeł *et al.*, 2013). Modeling of the dynamics of ferroelectric switching (Liu, Grinberg, and Rappe, 2016) and its effect on magnetic order (Bhattacharjee *et al.*, 2014), both of which are on timescales and length scales that are far outside the ranges accessible using density functional methods, has now become feasible. These models in combination with molecular dynamics start to allow calculation of dynamical magnetoelectric responses in the terahertz region (D. Wang *et al.*, 2013), which is particularly timely as it coincides with advances in experimental methods for generating terahertz radiation (Rana *et al.*, 2009). Finally, the possibility of magnetoelectric multipole as an order parameter for phase transitions that break both space inversion and time reversal (Spaldin, Fiebig, and Mostovoy, 2008; Tolédano *et al.*, 2015) seems intriguing, although it has not been fully explored experimentally.

### *b. Manganites*

Multiferroic perovskite manganites can be classified into three families: (i) $BiMnO_3$ and related phases, (ii) orthorhombic rare-earth manganites $RMnO_3$, and (iii) hexagonal manganites. Some materials from the second family can be metastable members of the third one, and vice versa.

$BiMnO_3$ is a monoclinic perovskite first synthesized in Japan and the Soviet Union in the 1960s (Sugawara *et al.*, 1965; Bokov *et al.*, 1966). $BiMnO_3$ was soon recognized as a ferromagnetic insulator with a $T_{CM}$ of about 105 K (Sugawara *et al.*, 1965, 1968; Bokov *et al.*, 1966). This ferromagnetic behavior was unexpected because the similar compound $LaMnO_3$ [the ionic radii of $Bi^{3+}$ and $La^{3+}$ ions are 1.24 and 1.22 Å, respectively (Shannon and Prewitt, 1969)] is an *A*-type (ferromagnetic coupling in a $\{001\}$ plane and antiferromagnetic coupling perpendicular to this plane) antiferromagnet (Wollan and Koehler, 1955). In fact, while the Jahn-Teller effect lifts the degeneracy of the $e_g$ states in both compounds, the presence of stereochemically active $6s^2$ lone pairs on the Bi ions (Seshadri and Hill, 2001) triggers a peculiar three-dimensional (3D) orbital ordering of the Mn $d_{x2-z2}$ orbitals (Moreira dos Santos *et al.*, 2002) that induces globally ferromagnetic superexchange interactions between the Mn ions.

Based on reports of a noncentrosymmetric space group [$C2$; see Atou *et al.* (1999)], $BiMnO_3$ has been conjectured to be ferroelectric, and thus multiferroic. Later neutron diffraction experiments, however, indicated a centrosymmetric structure (Belik *et al.*, 2007), ruling out ferroelectricity in bulk $BiMnO_3$. We note that first-principles calculations (Diéguez and Íñiguez, 2015) have predicted a ferroelectric ground state for compressively strained films and that indications of ferroelectricity have been provided in thin films (Jeen *et al.*, 2011; N. Yang *et al.*, 2019). $BiMnO_3$ (De Luca *et al.*, 2013) and $La_{0.1}Bi_{0.9}MnO_3$ (Gajek *et al.*, 2007) ultrathin films were also shown to be ferroelectric at room temperature. To date there have been no clear indications that $BiMnO_3$ and related phases are magnetoelectric, aside from magnetocapacitance measurements showing a peak at the ferromagnetic $T_C$ (Kimura, Kawamoto *et al.*, 2003).

Orthorhombic rare-earth manganites such as $TbMnO_3$ are so-called type II multiferroics, in which ferroelectricity arises as a consequence of noncollinear spin ordering that breaks inversion symmetry. Multiferroicity in this compound was first discovered by Kimura, Goto *et al.* (2003), and the existence of an incommensurate spiral spin order was clarified by Kenzelmann *et al.* (2005). Arima *et al.* (2006) later confirmed the same spin order in $(Tb, Dy)MnO_3$ compounds. The mechanism leading to the onset of ferroelectricity in the presence of spiral spin order was elucidated through the spin-current model (Katsura, Nagaosa, and Balatsky, 2005); see Fig. 8. Experimentally these compounds become ferroelectric below about 30 K, and their polarization is small (in the 0.1 $\mu C/cm^2$ range). However, because the ferroelectric character arises from spin ordering, the compounds display substantial magnetoelectric coupling. Early on, it was shown that the application of a magnetic field has a strong influence on ferroelectric properties, notably on the amplitude and direction of the polarization, also leading to large magnetocapacitance effects (Goto *et al.*, 2004); see Fig. 8.

In perovskite manganites, when the size of the *A*-site rare-earth cation is further reduced beyond that of Dy, or *A* is Y or Sc, the hexagonal structure becomes more stable than the orthorhombic structure. Hexagonal manganites are also multiferroic with a high ferroelectric $T_C$ of around 1000 K, and they are antiferromagnetic with a Néel temperature typically lower than 100 K (Lorenz, 2021). Coupling between the two orders was first detected as an anomaly in the dielectric constant at the Néel point for $YMnO_3$ (Huang *et al.*, 1997). Dielectric anomalies at magnetic phase transitions were later found in other compounds of the series (Lorenz, Litvinchuk *et al.*, 2004; Lorenz, Wang *et al.*, 2004). In general, hexagonal manganites with a magnetic ion at the *A* site have complex phase diagrams (Fiebig, Lottermoser, and Pisarev, 2003) [as, for instance, $HoMnO_3$ (Fiebig, Degenhardt, and Pisarev, 2002], with spin reorientation temperatures where the dielectric constant shows a pronounced peak (Lorenz, Litvinchuk *et al.*, 2004) and the polarization displays a kink (Hur *et al.*, 2009). Application of a magnetic field allows the system to be tuned into various

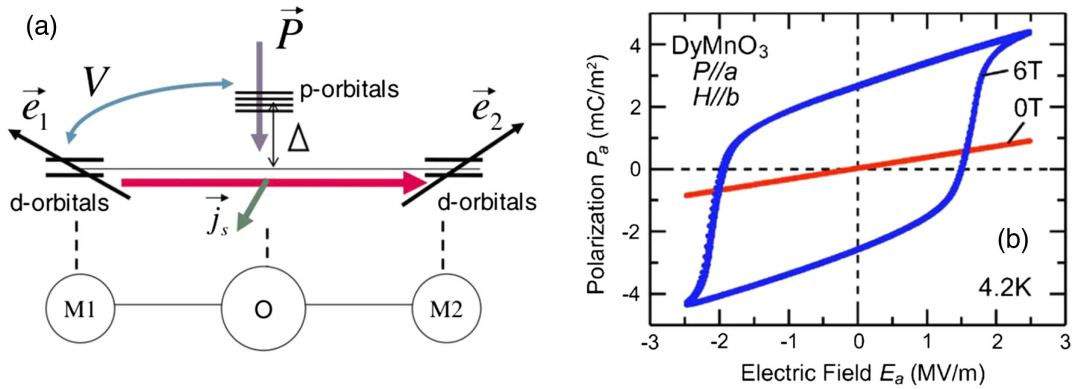


FIG. 8. (a) Spin-current model. Two transition metal ions $M1$ and $M2$ are separated by an O ion. $M1$ and $M2$ carry noncollinear spin moments $\vec{e_1}$ and $\vec{e_2}$. In this situation, a spin current arises and is expressed as $\vec{J_s} \propto \vec{e_1} \times \vec{e_2}$, with the direction of the $\vec{J_s}$ vector corresponding to the spin polarization. The electric polarization is then given by $\vec{P} \propto \vec{e_{12}} \times \vec{j_s}$, where $\vec{e_{12}}$ is the unit vector connecting $M1$ and $M2$. This mechanism is analogous to the inverse Dzyaloshinskii-Moriya interaction; see Sergienko and Dagotto (2006). (b) $P$ and $E$ curves obtained at magnetic fields of 0 (red line) and 6 T (blue curve) for a $DyMnO_3$ crystal, illustrating the magnetic-field control of ferroelectric in this compound. From Kimura *et al.*, 2005.

magnetic states that have different dielectric properties. Thus far this magnetoelectric coupling has not been harnessed to control magnetism by electric fields.

*c. Ferrites*

Besides $BiFeO_3$, several other Fe-containing oxides have been explored as possible multiferroics with a sizable magnetoelectric coupling. Fe-based compounds often have larger magnetic moments and high magnetic transition temperatures, which is appealing for applications.

Fe-based perovskites, i.e., orthoferrites, are directly related to $BiFeO_3$ but lack the lone pair provided by Bi ions that are responsible for the robust ferroelectricity in that compound. Nevertheless, $GdFeO_3$ and $DyFeO_3$ were shown to be ferroelectric at low temperatures. The mechanism is different from that at play in $BiFeO_3$; here ferroelectricity is improper and is believed to be driven by magnetic order through exchange striction below the ordering temperature of the rare-earth ion, which is around 3 K (Tokunaga *et al.*, 2008, 2009). While polarization was shown to strongly depend on magnetic field, only a moderate change of magnetization was induced by the electric field (Tokunaga *et al.*, 2009). Recently nonstoichiometric $YFeO_3$ was reported to display ferroelectricity at room temperature, qualifying it as multiferroic (Ning *et al.*, 2021). It will be interesting to see if this behavior can be reproduced in other systems and if magnetoelectric coupling is present in this new phase.

When the $A$ cation size is small, $AFeO_3$ compounds can be stabilized in a hexagonal structure resembling that of hexagonal manganites that are ferroelectric. Hexagonal $AFeO_3$ compounds have thus been predicted to be ferroelectric and to display magnetoelectric coupling (Das *et al.*, 2014). Their Néel temperature is around 100 K, which is much lower than in their orthorhombic cousins (Li, Tan, and Duan, 2020). Various reports indeed indicate a ferroelectric response at room temperature (Jeong *et al.*, 2012; W. Wang *et al.*, 2013). Electric control of magnetism has been elusive thus far with this family of compounds.

A promising yet complex family of ferrites for the electrical control of magnetism is hexaferrites. These compounds have large unit cells with many magnetic sites and can be grouped into six subfamilies coined $M$-, $W$-, $Y$-, $Z$-, $X$-, and $U$-type hexaferrites. Their structure is built from blocks labeled $R$, $S$, and $T$ (the $R$ block is $[(Ba, Sr)Fe_6O_{11}]^{2-}$, the $S$ block or spinel block is $Me^{2+}[Fe_4O_8]$, the $T$ block is $[(Ba, Sr)_2Fe_8O_{14})]$), and Me is a divalent metal ion, for instance, $Zn^{2+}$ or $Co^{2+}$) (Kimura, 2012). The most well known is the $M$-type structure magnetoplumbite, which is built from alternating the $S$ and $R$ blocks. While most hexaferrites are ferrimagnetic, some (and, in particular, $Y$-type compounds) display noncollinear magnetic order. What is unique compared to other noncollinear systems is that in some hexaferrites this order exists at and above room temperature.

The magnetic moments within hexaferrites can be viewed as being organized into two types of stacks with large or low moments. The stacks are then coupled together by superexchange in a fashion that is sensitive to the concentration of Ba or Sr ions and that tunes the Fe–O–Fe bond angles at the interface between blocks. This results in noncollinear order, such as a proper screw for $Y$-type ferrites. When a magnetic field is then applied perpendicular to the hexagonal axis, the materials undergo magnetic phase transitions to conical structures that cause the appearance of a spontaneous polarization (Kimura, Lawes, and Ramirez, 2005). In most compounds, the finite conductivity impedes the observation of such a magnetoelectric coupling at room temperature, but it has been realized in some $Z$- and $U$-type ferrites (Okumura *et al.*, 2011; Soda *et al.*, 2011).

Electric-field control of magnetization has been demonstrated in some of these ferrites. In a Co-based $Z$-type compound, Chun *et al.* (2012) reported a change of the magnetization of about 0.6 μB/f.u. over 2 MV/m at room temperature. In these experiments, the field dependence comprised linear and quadratic terms, but later, working with a Zn-based $Y$-type compound, Chai *et al.* (2014) reported magnetization switching between about −2 and +2 μB/f.u. in a field of ±2 MV/m, albeit at 15 K; see Fig. 9. A similar

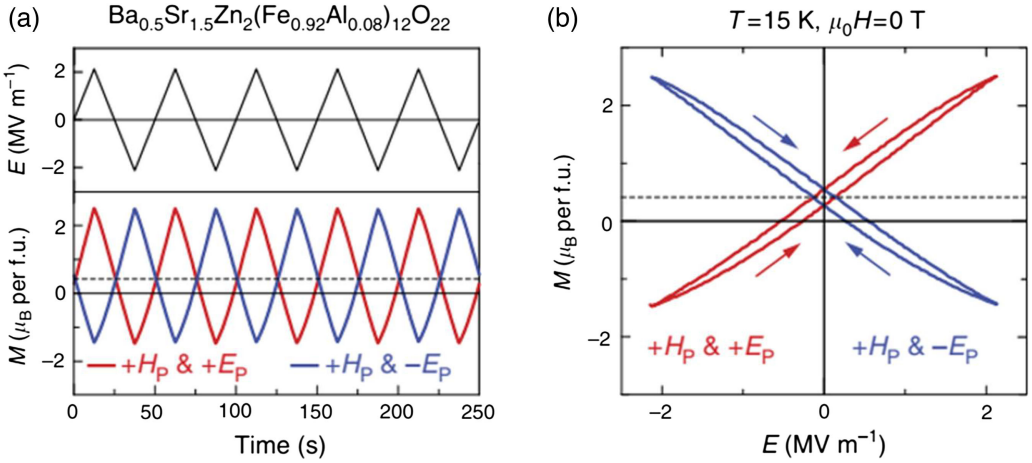


FIG. 9. Electric-field modulation of magnetization in a *Y*-type hexaferrite. (a) Periodic modulations of $M$ along the [100] crystallographic direction at zero magnetic field under repeating triangular waves of $E$ applied parallel to the [120] direction after preparing the system by cooling it to the measurement temperature in the electric and magnetic fields (magnetoelectric annealing). (b) Corresponding magnetization vs electric-field loops illustrating the reversal. The red and blue traces in (a) and (b) correspond to the opposite directions of the applied electric field during the magnetoelectric annealing procedure. From Chai *et al.*, 2014.

effect of up to 250 K was subsequently reported in a related system (Kocsis *et al.*, 2019), even at room temperature, with, however, a reduced amplitude (Zhai *et al.*, 2020).

### *d. Other systems including organics*

In contrast to the heavily studied inorganic multiferroics, organic multiferroics have not been extensively explored (Qin, Xu, and Ren, 2015). Organic materials provide an equally broad palette of materials design building blocks but face similar challenges, as do their inorganic counterparts. Inducing a magnetic state, especially at room temperature, requires strong exchange interactions, thus invariably necessitating the introduction of transition metal ions into an organic framework. One could envision a multiferroic tree, for example (Spaldin and Ramesh, 2019). Before converging into possible multiferroic systems, it is perhaps appropriate to discuss the possible origins of ferroelectricity and magnetism separately in these compounds.

Ferroelectricity in organic materials has been extensively studied (Lines and Glass, 2001), with the polyvinylidene difluoride (PVDF) and *P*-(*n*-decyloxybenzylidene)-*p*-amino-(2-methylbutyl) systems having received considerable scientific attention. Ferroelectric liquid crystals have also been investigated (Meyer, 1977; Lagerwall and Dahl, 1984). Recent developments in molecular ferroelectrics such as diisopropyl ammonium bromide (and related compounds) are showing a lot of promise, with spontaneous polarization almost equal to the model system barium titanate (Zhang *et al.*, 2017). The robustness of the ferroelectric order parameter through charge, permittivity, and piezoelectric measurements is a strong positive sign. Further work on the switching dynamics in such order-disorder ferroelectrics would be welcome. Pathways to introduce magnetism into such materials would be equally rewarding. Organic charge-transfer-based ferroelectrics such as tetrathiafulvalene-*p*-chloranil (Giovannetti *et al.*, 2009) are another possible class of ferroelectrics, but with a much lower spontaneous polarization. Large polarization values have been reported, but the experimental measurements likely require further validation. Another class of organic ferroelectrics, metal-organic frameworks (MOFs) such as $[NH4]\text{-}M(HCOO)_3$ and $[(CH3)2NH2]M(HCOO)_3$ ($M$ = Zn, Mn, Fe, Co, and Ni), showed promising spontaneous polarization due to their order-disorder transition, which, however, occurs well below room temperature (Zhang and Xiong, 2012). Given the large body of research into metal-organic-framework compounds for a wide range of possible applications, such organics hold promise for future study.

Regarding organic multiferroics, the challenges of obtaining magnetic and ferroelectric order are almost exactly the same as in their inorganic counterparts, namely, the contradictions in the requirements for these two order parameters to coexist. One example is tetrathiafulvalene-*p*-bromanil, which derives its ferroelectric order from a spin-Peierls-like instability (spin-lattice interaction), albeit at a low temperature of 53 K (Kagawa *et al.*, 2010; Ding, Yao, and Fu, 2011). This is accompanied by the emergence of a relatively small polarization, much like the emergence of ferroelectricity in the magnetic manganites. Another organic multiferroic of spin-driven polarization is the crystalline thiophene-$C_{60}$ charge-transfer complex (Ren and Wuttig, 2012). By utilizing the supramolecular assembly strategy to build electron donor thiophene and acceptor $C_{60}$ cocrystals, Qin *et al.* (2014) observed room-temperature magnetism and spontaneous polarization. There have been a few demonstrations of multiferroic behavior (once again with a low ferroelectric $T_C$) in MOFs that contain 3*d* transition metal species. Organic charge-transfer salts such as $\kappa$-[bis(ethylenedithio)tetrathiafulvalene]2Cu[N(CN)2]-Cl exhibit the converse behavior, i.e., a charge ordering induced magnetism, typically at temperatures ~25 K (Lunkenheimer *et al.*, 2012). Thus, organic multiferroics provide a unique set of chemical frameworks to explore spin-charge coupling, but the challenges for potential translation to devices remain in terms of the ordering temperatures or the strength of the individual order parameters. In this sense, the large room-temperature

polarization of the diisopropyl ammonium bromide seems promising for further research to make them magnetic. More broadly, organic ferroelectrics or ferromagnets and multiferroics seems to be a topic that is rich for an even deeper and more comprehensive investigation using fundamental materials design principles. It is particularly noteworthy that organics typically do not require the high process temperatures that are characteristic of inorganics such as oxides, and thus should be more amenable to integration efforts once the correct materials system is discovered.

### 2. Multiferroic heterostructures

#### *a. $BiFeO_3$-based heterostructures*

Thin-film syntheses of $BiFeO_3$ (and other multiferroics) have been a fruitful pathway to study the materials physics of magnetoelectric coupling and have pointed the way to possible applications. The perovskite symmetry and lattice parameters (pseudocubic lattice parameter of 3.96 Å) close to a large number of oxide-based substrates means that epitaxial synthesis is possible and has indeed been widely demonstrated (Sando, Barthélémy, and Bibes, 2014). Films with thicknesses down to just a few unit cells and as large as a few microns have been synthesized by physical-vapor deposition [for example, pulsed laser deposition (Wang *et al.*, 2003; Béa *et al.*, 2005; Sando, Barthélémy, and Bibes, 2014), sputtering (Ichinose, Miura, and Naganuma, 2021), and molecular beam epitaxy (Ihlefeld *et al.*, 2007)], chemical-vapor deposition (Singh, Yang, and Takoudis, 2009), and chemical-solution deposition. Many studies have used conducting perovskite electrodes (such as $SrRuO_3$, $La_{1x}Sr_xMnO_3$, and $La_{1-x}Sr_xCoO_3$) as bottom electrodes to both template the perovskite phase and provide a bottom contact for electrical measurements. These synthesis studies have led to enabling a wide range of materials physics studies.

A particularly important aspect is the stability of the polar state as the thickness is scaled down. Such size effects have been extensively studied in classical ferroelectrics (Rabe, Ahn, and Triscone, 2007) and are characterized by a suppression of the order parameter as the thickness is scaled down. Similar studies have been undertaken in the case of the $BiFeO_3$ system (Béa *et al.*, 2006; Béa, Fusil *et al.*, 2006; Chu *et al.*, 2007; Maksymovych *et al.*, 2012), albeit in an incomplete sense. Several studies showed that the polar order parameter is reduced but still maintained. The ferroelectric switching process in $BiFeO_3$ is believed to be limited by the nucleation and growth of the reverse domains (Yamada *et al.*, 2013; Boyn *et al.*, 2017; Steffes *et al.*, 2019) broadly captured by the Kay-Dunn model (Chandra *et al.*, 2004), in which the coercive field scales as the film thickness $d^{-2/3}$. Consequently progressively larger reductions in film thickness are needed to reduce the coercive voltage as it is pushed to smaller values. In $BiFeO_3$, lanthanum substitution (Chu *et al.*, 2008) has been shown to reduce the switching energy by reducing the polarization (Maksymovych *et al.*, 2012), although to an insufficient extent to date. Pushing $BiFeO_3$ close to a phase boundary between

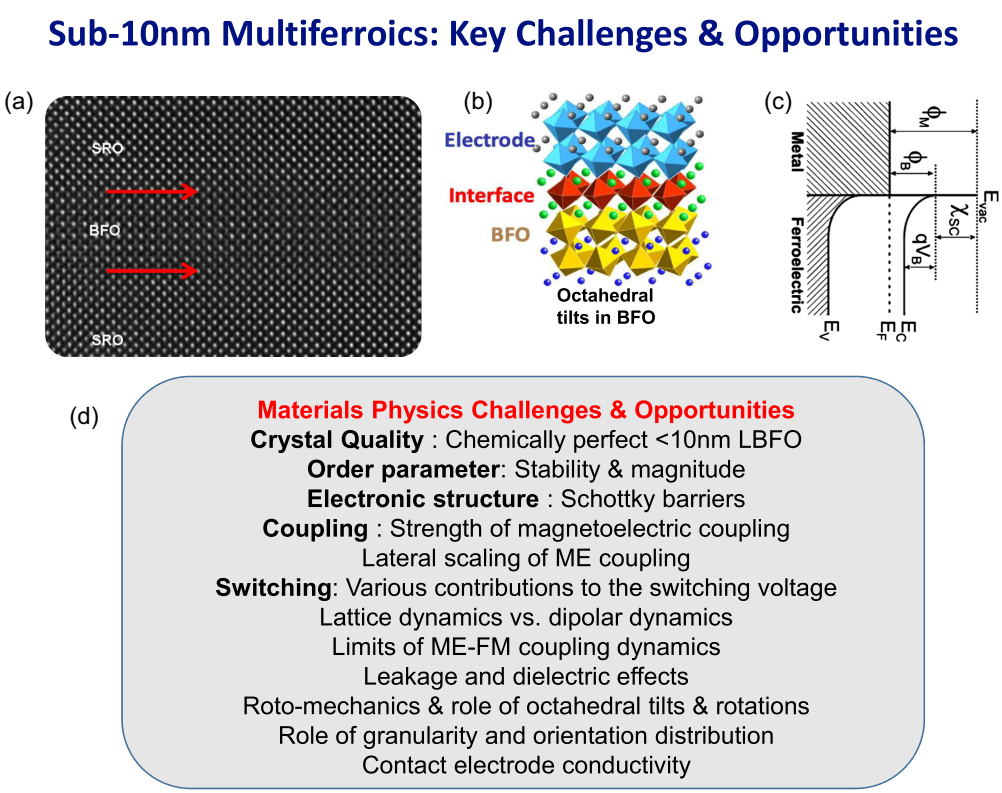


FIG. 10. (a) Atomic resolution image of a six-unit-cell-thick $BiFeO_3$ (BFO) layer sandwiched between epitaxial $SrRuO_3$ (SRO) top and bottom electrodes as a representative of sub-10-nm-thick multiferroics as a model system. (b) The corresponding crystal model showing the octahedral tilts (in both the SRO and $BiFeO_3$ layers). (c) Schematic depiction showing how the formation of a Schottky barrier at the contact metal—$BiFeO_3$ interface can lead to potential drops. (d) List of materials physics challenges and opportunities for multiferroic heterostructures.

ferroelectric and antiferroelectric states or identifying materials without the octahedral rotations of $BiFeO_3$ could be an alternative pathway to smaller coercive fields.

The antiferromagnetic order has also been shown to exist at room temperature in films that are as thin as 4 nm (ten unit cells). What has not been shown is the coupling between the two order parameters at such length scales or electric-field manipulation of this coupling. Thus, a deeper quantitative understanding of the stability of the individual order parameters, the coupling between them, and the *E*-field manipulation of this coupling at a thickness of less than ∼10 nm would be of significant interest. This is captured in Fig. 10.

*i.* $BiFeO_3/La_{0.7}Sr_{0.3}MnO_3$

Perhaps the most significant breakthrough in the past few years is the demonstration that the magnetization direction in conventional ferromagnets (such as $Co_{1-x}Fe_x$) can be rotated by 180° with an electric field (Heron *et al.*, 2014) when it is exchange coupled to $BiFeO_3$ (Béa *et al.*, 2008; Martin *et al.*, 2008). The extension to all-oxide $La_{0.7}Sr_{0.3}MnO_3/BiFeO_3$ interfaces (Béa *et al.*, 2006) (Fig. 11) with chemically abrupt *A*-site termination (P. Yu *et al.*, 2012) allowed for electric-field control of exchange-bias coupling at temperatures below 100 K (Wu *et al.*, 2010). Exchange bias refers to the horizontal shift of the magnetization versus the field loop of a ferromagnetic layer due to the exchange coupling to an adjacent antiferromagnetic layer.

Earlier work on the same system has demonstrated the ability to reversibly switch between two exchange-biased states with the same polarity (unipolar modulation) without the need of additional magnetic or electric fields in a multiferroic field-effect device (Wu *et al.*, 2010), but eventually the ability to reversibly switch between these two states with opposite polarity (bipolar modulation) was demonstrated as well (Fig. 12). The key was modifying the direction of the magnetization in the $La_{0.7}Sr_{0.3}MnO_3$ with respect to the current in the device channel. A reversible shift of the polarity of exchange bias through the zero applied magnetic-field axis was thus achieved with no magnetic- or electric-field cooling and no additional electric or magnetic bias fields: in essence, full direct electric-field control of exchange bias. This also helped clarify the mechanism underlying the change in exchange-bias coupling.

An important open problem is the development of oxide ferromagnets or ferrimagnets with high $T_C$, a significant remanent moment, and strong exchange coupling and Ohmic contacts with $BiFeO_3$ or other multiferroics. Spinels and double perovskites are promising candidates in this regard (Suzuki, 2001; Serrate, Teresa, and Ibarra, 2007). In a complementary direction, the antiferromagnetic domain orientation in magnetoelectric $Cr_2O_3$, which can be controlled by an electric field, has been shown to affect the exchange-bias coupling to a ferromagnetic overlayer (He *et al.*, 2010), thereby opening a pathway to electric-field switchable exchange-bias devices.

*ii.* $BiFeO_3$*/ferromagnetic metals*

Metallic ferromagnets such as the well-studied CoFe system provide a good starting point to explore electric-field

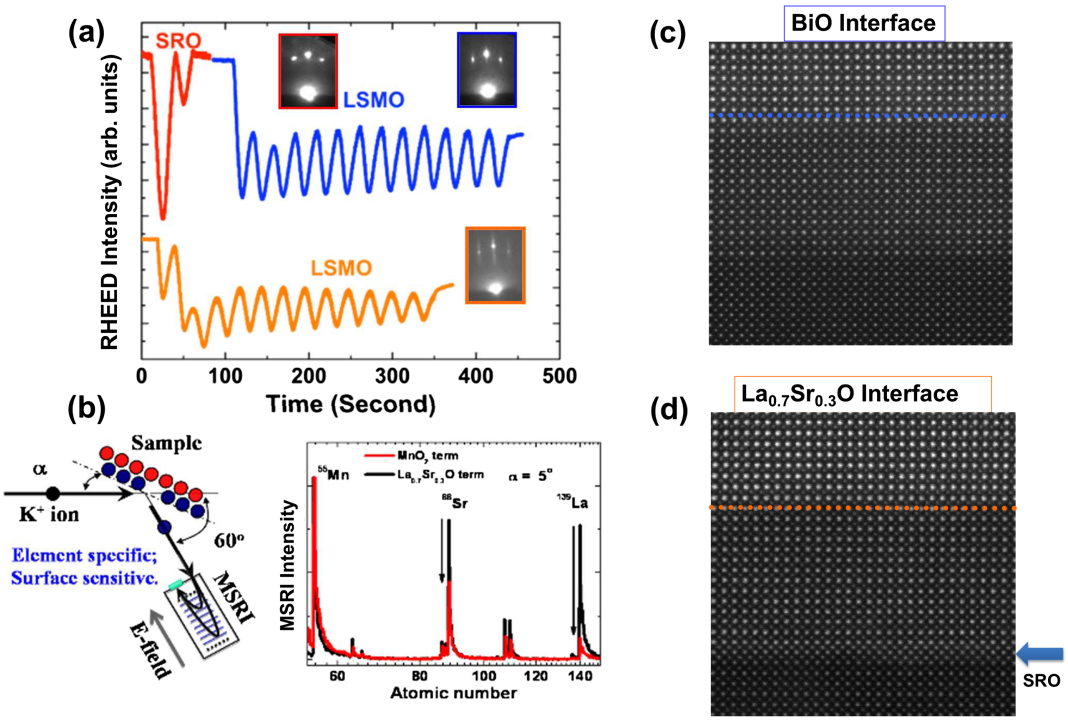


FIG. 11. Synthesis of model systems illustrating epitaxial synthesis as a pathway to create model systems at the scale of a single unit cell. (a) Reflection high-energy electron diffraction (RHEED) pattern of the growth of the $La_{0.7}Sr_{0.3}MnO_3$ bottom electrode on a $TiO_2$-terminated $SrTiO_3$ substrate. The insertion of two unit cells of $SrRuO_3$ leads to a conversion of the termination from the *B* site to the *A* site. (b) Time of flight ion scattering and recoil spectroscopy of the two types of substrate surfaces. The spectra are normalized to the Mn peak, and it is clear that the La content is much higher for one of them than for the other. (c),(d) Atomic resolution STEM images of the two types of interfaces showing that atomically sharp interfaces can be obtained. From P. Yu *et al.*, 2012.

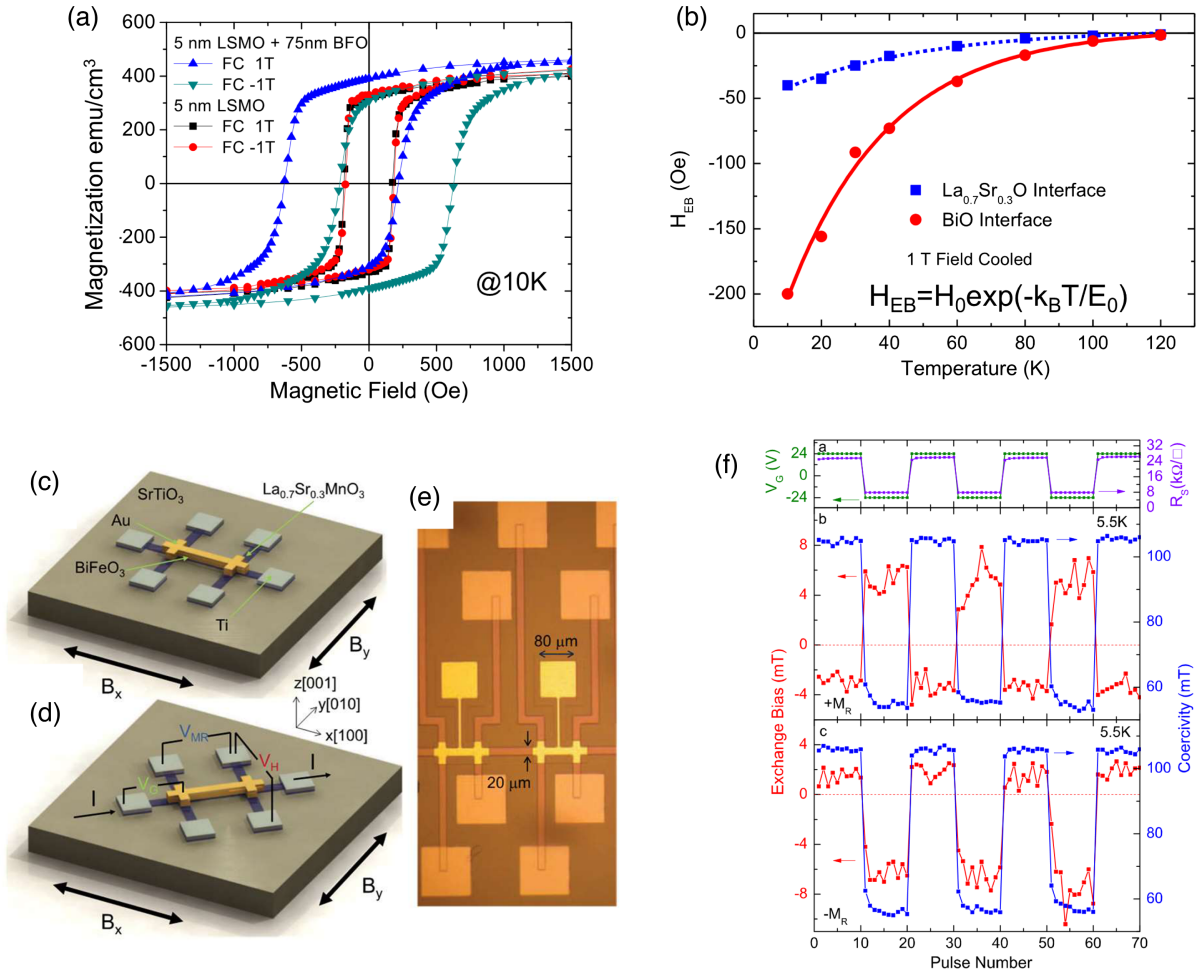


FIG. 12. Electric-field manipulation of interfacial magnetic coupling in epitaxial heterostructures. (a) 1 T, field cooled magnetic hysteresis loops at 10 K showing a strong exchange bias of 200 Oe for a $La_{0.7}Sr_{0.3}MnO_3$(5 nm)/$BiFeO_3$(75 nm) heterostructure. (b) Magnitude of the exchange-bias field as a function of temperature and interface termination (La/Sr-Ovs Bi-O interfaces). (a), (b) From P. Yu *et al.*, 2010. (c),(d) Device layouts for magnetoelectric measurements, with the corresponding SEM image shown in (e). (f) Bipolar voltage profile and the corresponding exchange bias and coercivity showing full electric-field switching of the exchange bias. (c)–(f) From Wu *et al.*, 2013.

control of ferromagnetism. Although chemically much different than oxides, metallic ferromagnets generally have higher $T_C$ values, and thus a greater likelihood of strong exchange coupling. The push for ultralow-power logic-memory devices builds from observations of the potential of magnetoelectric control using multiferroics, with the key being the ability to control magnetism with an electric field at room temperature (Heron, Schlom, and Ramesh, 2014) using a spin-valve device [Fig. 13(a)] to demonstrate such a coupling (Bibes and Barthélémy, 2008). For example, magnetoelectric switching of a magnetoresistive element was recently shown to operate at or below 200 mV, with a pathway to get down to 100 mV (Prasad *et al.*, 2020). Reducing the thickness is an obvious pathway to get to such low voltages. A combination of structural manipulation via lanthanum substitution and thickness scaling in multiferroic $BiFeO_3$ has helped to scale the switching energy density to $\approx 10\ \mu J\,cm^{-2}$ and provides a template to achieve attojoule-class nonvolatile memories. Using La-$BiFeO_3$, it was possible to show that the switching voltage of the GMR response can be progressively reduced from $\approx 1$ V to 500 mV by decreasing the film thickness to 20 nm [Fig. 13(a)]. Electric-field control of the magnetization direction in the bottom $Co_{0.9}Fe_{0.1}$ layer was shown in measurements both in a magnetic field of 100 Oe and in the remanent state (i.e., zero magnetic field) [Figs. 13(b) and 13(c)]. The low-voltage magnetoelectric switching in multiferroic $Bi_{0.85}La_{0.15}FeO_3$ was further probed using x-ray magnetic circular dichroism (XMCD-) PEEM imaging at the Co $L_3$ edge via studies [Fig. 13(d) insets and Fig. 13(e)] where application of $\pm 500$ mV revealed contrast changes consistent with reversal of the in-plane magnetization.

### B. Strain-driven control of magnetism using ferroelectrics and piezoelectrics in multilayers

#### 1. Piezoelectric and ferromagnet heterostructures

Another way to control magnetism with an electric field is to combine piezoelectric materials and magnetic materials in thin-film heterostructures. The simplest geometry is to grow a magnetic thin film on top of a ferroelectric (or relaxor) substrate with large piezoelectric coefficients [a relaxor is a ferroelectric with large electrostriction and piezoelectric

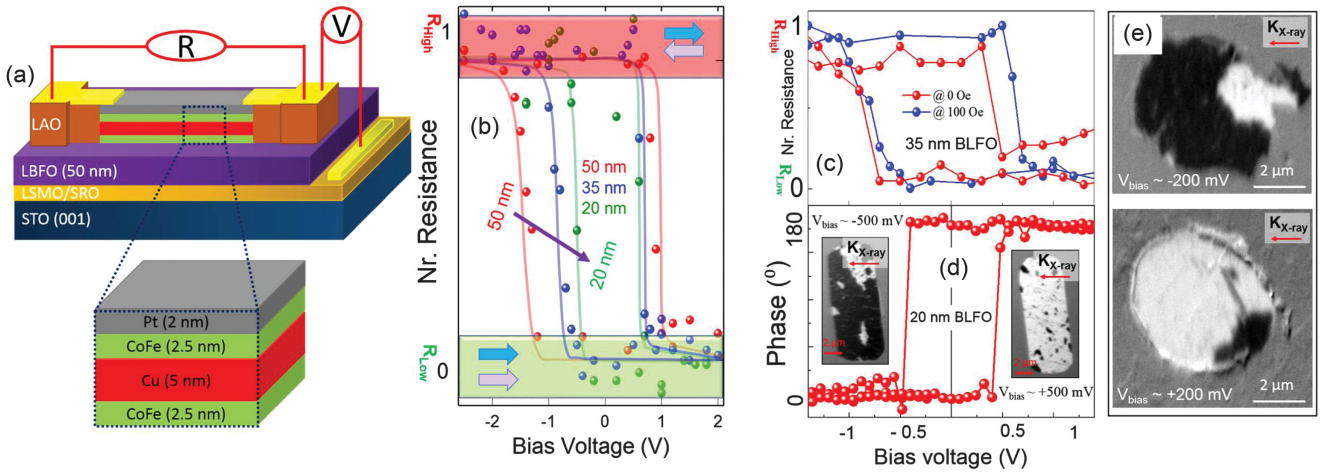


FIG. 13. *E*-field control of magnetism at room temperature. (a) Schematic of the magnetoelectric test structure comprising the multiferroic La-$BiFeO_3$ layer that is in contact with a CoFe-Cu-CoFe spin valve used as a readout element. (b) The normalized resistance of the spin valve as a function of applied voltage to the La-$BiFeO_3$ layer. (c) The normalized resistance vs electric field at zero magnetic field and at 100 Oe showing no significant difference, and thus illustrating that the switching of the spin valve is due to the electric field. (d) Piezoelectric hysteresis loop for the 20 nm La-$BiFeO_3$ layer showing the full switching at ~500 mV. Insets: XMCD-PEEM images of a Co layer that is in contact with the La-$BiFeO_3$ layer. The contrast reversal illustrates a change in the magnetization direction due to the applied voltage of 500 mV. (e) XMCD-PEEM image of a CoFe 10 nm La-$BiFeO_3$ test structure that has been switched by −200 mV (dark) and +200 mV (bright) contrast showing that the magnetization direction has mostly been switched. From Huang *et al.*, 2020, and Prasad *et al.*, 2020.

coefficient (Cowley *et al.*, 2011)]. Pertsev (2008) predicted that giant magnetoelectric susceptibility might be achieved in such a geometry as a result of the strain-driven spin reorientation in the ferromagnetic thin film. Nickel is often chosen as the magnetic thin film due to its sizable magnetostriction at room temperature ($T_C \gg 300$ K). Modifications of the remnant magnetization, magnetic anisotropy, or even magnetization direction of a Ni thin film induced by the electric field applied onto its ferroelectric or piezoelectric substrate have been reported (Weiler *et al.*, 2009; Geprägs *et al.*, 2010; Wu *et al.*, 2011; Ghidini *et al.*, 2013). This is illustrated in Figs. 14(a)–14(c), where the magnetic easy axis of the Ni layer reversibly rotates by 90° (along the in-plane $x$ or $y$ axis), depending on the sign of the voltage applied to the $x$ axis of the $Pb(Zr_xTi_{1-x})O_3$ substrate (Weiler *et al.*, 2009). The electric-field strain-induced modifications of magnetization or magnetic anisotropy were extended to other artificial multiferroics, including Fe or $La_{0.7}Sr_{0.3}MnO_3$ on $BaTiO_3$, $Co_{40}Fe_{40}B_{20}$ or $La_{0.7}(Ca,Sr)_{0.3}MnO_3$ on $Pb(Mg_{1/3}Nb_{2/3})_{0.7}Ti_{0.3}O_3$, $Ga_{1-x}Mn_xAs$ on $Pb(Zr_xTi_{1-x})O_3$,

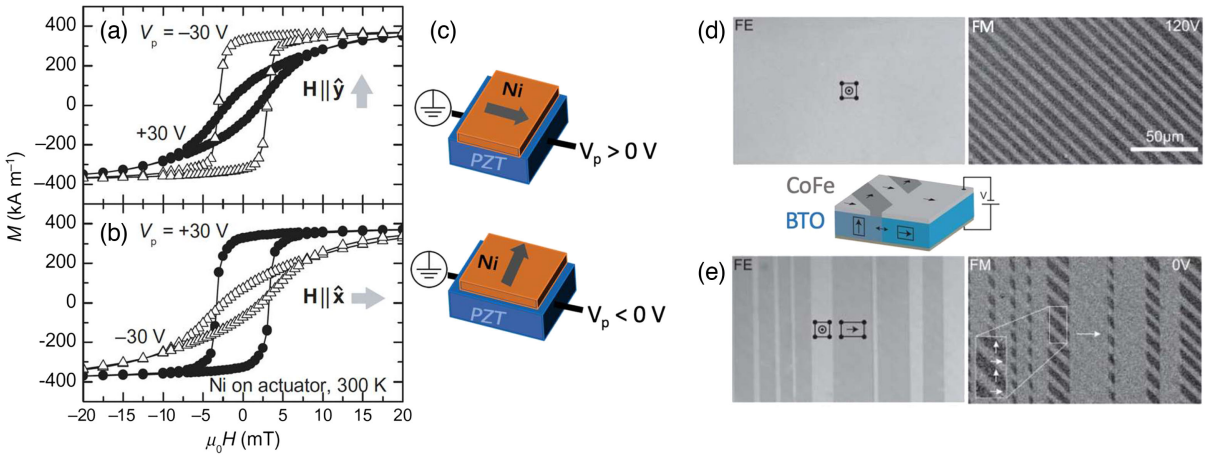


FIG. 14. Piezoelectric control of the magnetic anisotropy. Magnetization vs magnetic field aligned along the (a) $y$ and (b) $x$ axes in Ni thin films on $Pb(Zr_xTi_{1-x})O_3$-based actuators under +30 V and −30 V (along the $x$ axis). (c) Sketch showing that the magnetic anisotropy of the Ni thin film rotates by 90° and depends on the sign of the voltage applied to the piezoelectric actuator. (a)–(c) From Weiler *et al.*, 2009. (d),(e) Ferroelectric domain (left panels, birefringent contrast) and magnetic domains (right panels, magneto-optic Kerr contrast) for a CoFe thin film on a $BaTiO_3$ substrate (d) under a vertical voltage of 120 V and (e) when the voltage is turned off. As depicted in the sketch between (d) and (e), the voltage changes the population of ferroelastic domains in $BaTiO_3$ and, consequently, in the local strain and magnetic anisotropy. (d),(e) From Lahtinen, Franke, and van Dijken, 2012.

and FeGaB on $Pb(Zn_{1/3}Nb_{2/3})O_3$-$PbTiO_3$ (Eerenstein *et al.*, 2007; Sahoo *et al.*, 2007; Thiele *et al.*, 2007; Bihler *et al.*, 2008; Lou *et al.*, 2009; Zhang *et al.*, 2012).

In ferroelectrics in which polarization is associated with a strong deformation of the lattice (such as $BaTiO_3$), application of an electric field can result in a modification of ferroelastic domains and modify the average strain on the adjacent magnetic layer. Combining optical imaging techniques, Lahtinen, Tuomi, and van Dijken (2011) demonstrated a full imprint of the ferroelastic domains of a $BaTiO_3$ substrate on the magnetic domains of a CoFe thin film grown on top. Furthermore, they were able to electrically control the magnetic domain patterns of CoFe by the voltage applied through the $BaTiO_3$ substrate [Figs. 14(d) and 14(e)] (Lahtinen, Franke, and van Dijken, 2012).

### 2. FeRh-based structures

In parallel to these efforts to control the orientation of magnetization with an electric field, attempts have been made to achieve an electrical control of the magnetic order. For this approach, the archetypical magnetic material is FeRh with the CsCl-type structure, which displays a first-order metamagnetic phase transition from a low temperature antiferromagnetic phase to a high temperature ferromagnetic phase that is slightly above room temperature (350–370 K) (Kouvel and Hartelius, 1962). This first-order magnetic phase transition is accompanied by sharp changes in the volume and resistivity. FeRh thus displays strong coupling between lattice, magnetization, and electronic properties. Because of the volume change at the ferromagnetic-to-antiferromagnetic transition in $Fe_{1-x}Rh_x$ (Moruzzi and Marcus, 1992; Gruner, Hoffmann, and Entel, 2003), an electric field was used to drive the reciprocal effect, a ferromagnetic-to-antiferromagnetic transition induced by a structural deformation. This makes this system promising for the electric-field control of magnetism and resistivity via piezoelectric effects.

Cherifi *et al.* (2014) grew 20-nm-thick epitaxial thin films of FeRh using rf sputtering on $BaTiO_3$ single crystals. Applying a voltage to the $BaTiO_3$ crystal and changing the proportion of *c*- and *a*-ferroelastic domains, they were able to modulate the average epitaxial strain and trigger a giant change of magnetization at 385 K [Fig. 15(a)]. These results were supported by *ab initio* calculations as well as XMCD-PEEM images, which demonstrated that turning off the electric field leads to a transition from an antiferromagnetic state (pure *c* domains) to a ferromagnetic one (*a* domains) [Figs. 15(a) and 15(b)] (Phillips *et al.*, 2015). The strain-driven magnetic transition results in a 260% change of the magnetic coercive field ($H_C$) for FeRh thin films grown on $(1-x)Pb(Mg_{1/3}Nb_{2/3})O_3$-$xPbTiO_3$ (PMN-PT) (Xie *et al.*, 2018). Note that the electric-field-induced phase transition in FeRh and PMN-PT further enables the spin dynamics of FeRh to be modulated with a 120% adjustment of the magnetic damping [Figs. 15(c) and 15(d)]

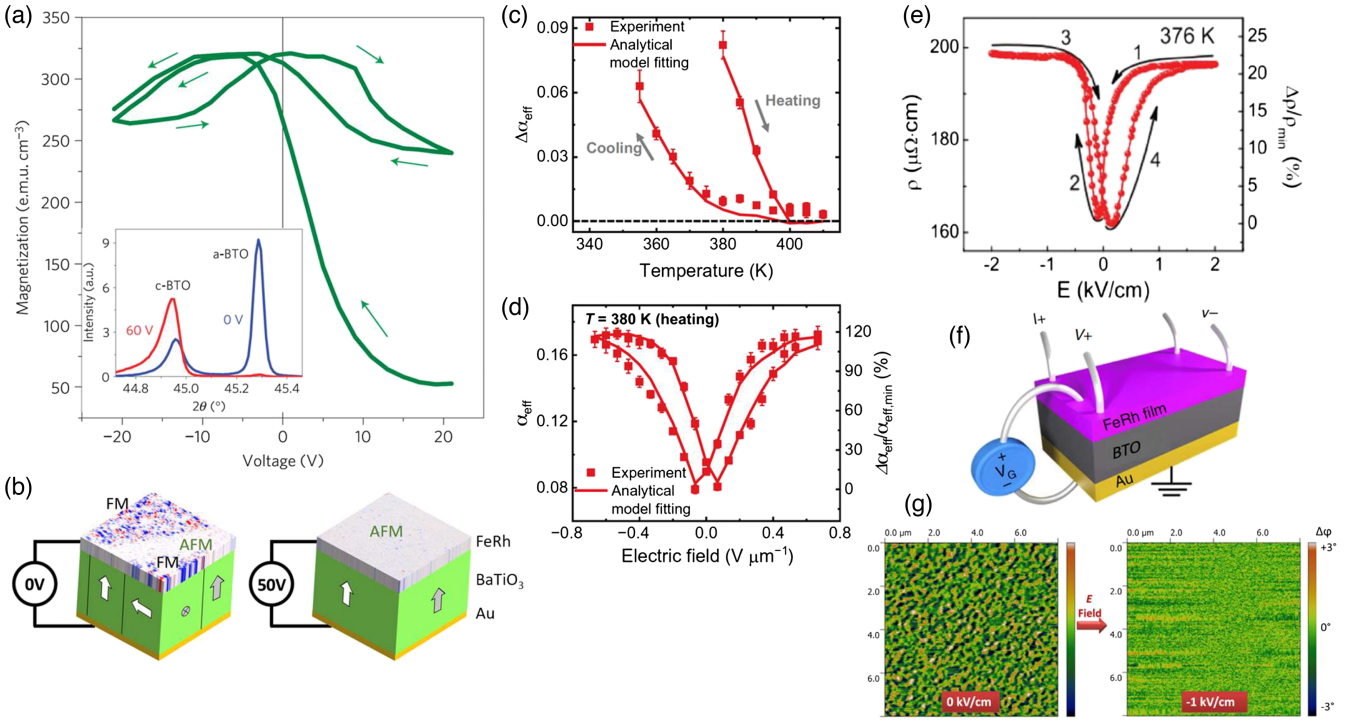


FIG. 15. (a) Variation of the magnetization with voltage in FeRh grown on $BaTiO_3$ single crystals at 385 K. Inset: x-ray diffraction pattern of the (002) and (200)/(020) reflections of $BaTiO_3$ as a function of voltage at 390 K. Under 60 V, the $BaTiO_3$ is a purely *c* domain, while it consists of mixed *a* and *c* domains at 0 V. (b) Sketch of the electric-field-induced magnetic phase transition at 385 K with the XMCD-PEEM image overlayed. (a),(b) From Cherifi *et al.*, 2014. (c) Temperature dependence of the magnetic damping in FeRh thin films grown on PMN-PT. (d) Electric-field modulation of the damping at 380 K. (c),(d) From Nan *et al.*, 2020. (e) Large electroresistance of FeRh thin films on $BaTiO_3$ substrates at 376 K. (f) Principle of the experiment. (g) MCD phase images collected at 376 K at 0 and −1 kV/cm electric field. (e)–(g) From Lee *et al.*, 2015, and Liu *et al.*, 2016.

resulting from the modification of the relative fraction of the antiferromagnetic-ferromagnetic phases (Nan *et al.*, 2020).

Since the resistivities of the two magnetic phases of FeRh differ, the magnetic transition is accompanied by a ~25% change in film resistivity. Using FeRh thin films on PMN-PT, Lee *et al.* (2015) demonstrated an electroresistance of 8% using the piezoelectric strain modulations at 368 K. This electroresistance is attributed to a variation of the antiferromagnetic-to-ferromagnetic phase proportions. Similar observations were later made about $FeRh/BaTiO_3$ with an electroresistance of 22% at 376 K [Figs. 15(e) and 15(f)] (Liu *et al.*, 2016). Magnetic force microscopy (MFM) investigations under an electric field revealed a full magnetic transition in the film [Fig. 15(g)]. This electric readout of the first-order phase transition opens possibilities for nonvolatile magnetic memories in a simple architecture. For more details on the electric-field control of magnetic and resistive properties in FeRh, see the reviews by Feng, Yan, and Liu (2019) and Fina and Fontcuberta (2020).

Open challenges with this approach include reducing the optimal working temperature from around 100 °C to room temperature, tuning the chemical composition to optimize the strengths of the exchange interactions, achieving complete conversion between the ferromagnetic and antiferromagnetic phases, and reducing the required applied voltages. Other promising systems are the Mn-Pt intermetallics and half-doped perovskite manganites such as $La_{0.5}Sr_{0.5}MnO_3$, in which an electric-field-driven charge-ordered antiferromagnetic insulator to ferromagnetic metal transition could be possible (Yi *et al.*, 2013), although then the Curie temperature ($T_C$) is below 300 K.

#### 3. $LuFeO_3/LuFe_2O_4$

There is considerable potential in designing magnetoelectrics at the atomic scale using epitaxial superlattices. The original work of Mundy *et al.* (2016) on $LuFeO_3$-$LuFe_2O_4$ superlattices showed that the epitaxial pathway to magnetoelectric coupling is indeed possible (Fig. 16). $LuFeO_3$ belongs to the class of ferroelectrics, termed as improper ferroelectrics (Bousquet *et al.*, 2008), in which the fundamental order parameter is a structural distortion: this distortion coupled to a polar mode leading to a spontaneous polarization of 3–5 $\mu C/cm^2$ along the $c$ axis of the hexagonal structure; see Sec. II.A.1.b). Using the power of epitaxy, atomically perfect superlattices were prepared by combining $LuFeO_3$ with its sister compound $LuFe_2O_4$ (which is ferrimagnetic with a $T_N$ of ~240 K). The magnetic state in the $LuFe_2O_4$ layer has been switched with an electric field (Mundy *et al.*, 2016), with the coupling most likely mediated through the lattice [Figs. 36(c) and 36(d)].

S. Fan *et al.* (2020) revealed the microscopic details of the coupling across the ferroelectric ($LuFeO_3$) and ferrimagnet ($LuFe_2O_4$) interface. A key issue with $LuFe_2O_4$ is that the $T_C$ is lower than room temperature [~240 K in the bulk, ~280 K in epitaxial superlattices (Mundy *et al.*, 2016)]. Thus, it is desirable to replace this with other structurally and chemically compatible ferrites. Research in this regard is under way, with $CoFe_2O_4$ used as the replacement for $LuFe_2O_4$.

### C. Electric-field effects in magnetic semiconductors, oxides, and metal ultrathin films

Since magnetism is usually intimately linked to the electronic structure and carrier density of materials, accumulating or depleting charges in a magnet may influence its transition temperature, magnetization, anisotropy, and even magnetic order. Charge accumulation (depletion) can be achieved using a ferroelectric instead of a dielectric, in which case the amount of added (removed) charge is typically higher (in the $10^{13}$–$10^{14}$ $cm^{-2}$ range, depending on the ferroelectric polarization value, versus $10^{11}$–$10^{13}$ $cm^{-2}$ with a dielectric, depending on its dielectric constant and the electric field applied) and remanent. This provides a means to electrically control magnetism in a nonvolatile fashion. Another possibility to accumulate or deplete charge is to use an ionic liquid. When a voltage is applied, a large electric field of the order of 10 MV/cm is generated at the interface between the liquid and the magnetic film due to the formation of an electric double layer. Ionic liquid gating can lead to charge density accumulation up to $\sim 10^{15}$ $cm^{-2}$.

While the elastic interaction harnessed in strain-driven magnetoelectrics can extend over several hundreds of nanometers, the field effect operates over distances of the order of the Thomas-Fermi screening length ($\lambda_{TF}$), which is a few angstroms in metals and a few nanometers in semiconductors. In magnetic materials, it has been argued that changes in the magnetic properties may be perceived over distances set by the exchange interaction length, which is usually larger than $\lambda_{TF}$ and can approach 10 nm (Ovchinnikov and Wang, 2009).

Several mechanisms occur to electronically drive changes in the magnetic properties. The first one corresponds to electrostatic doping [that is, charge accumulation and depletion in a conductor at the interface with a dielectric or a ferroelectric (Ahn, Triscone, and Mannhart, 2003)] of the interfacial region in the ferromagnet: if the magnetic properties are strongly doping dependent, as in carrier-mediated ferromagnets such as (Ga, Mn)As and mixed-valence manganites, charge accumulation or depletion will lead to changes in the magnetic response. The second mechanism is related to the spin-dependent screening in the ferromagnetic of the interface-bound charges of the ferroelectric. In ferromagnetic metals, owing to the different density of states for spin-up and spin-down electrons at the Fermi level, the screening is spin dependent. This spin-dependent screening leads to changes in the surface magnetization and surface magnetocrystalline anisotropy (Niranjan *et al.*, 2009). The third contribution is due to changes in the electronic bonding at the interface between the ferroelectric and the ferromagnet (electronic reconstruction). The displacements of atoms in the ferroelectric due to the polarization reversal influence the overlap between the orbital of the ferroelectric and ferromagnet materials at the interface (Yin *et al.*, 2013). This leads to charge redistribution, which affects the magnetization, anisotropy, and spin polarization at the interface. Related to this, magnetic reconstruction may occur upon accumulating or depleting charges. This mechanism is particularly appealing in materials such as manganites that possess rich phase diagrams, with competing magnetic phases as a function of carrier doping.

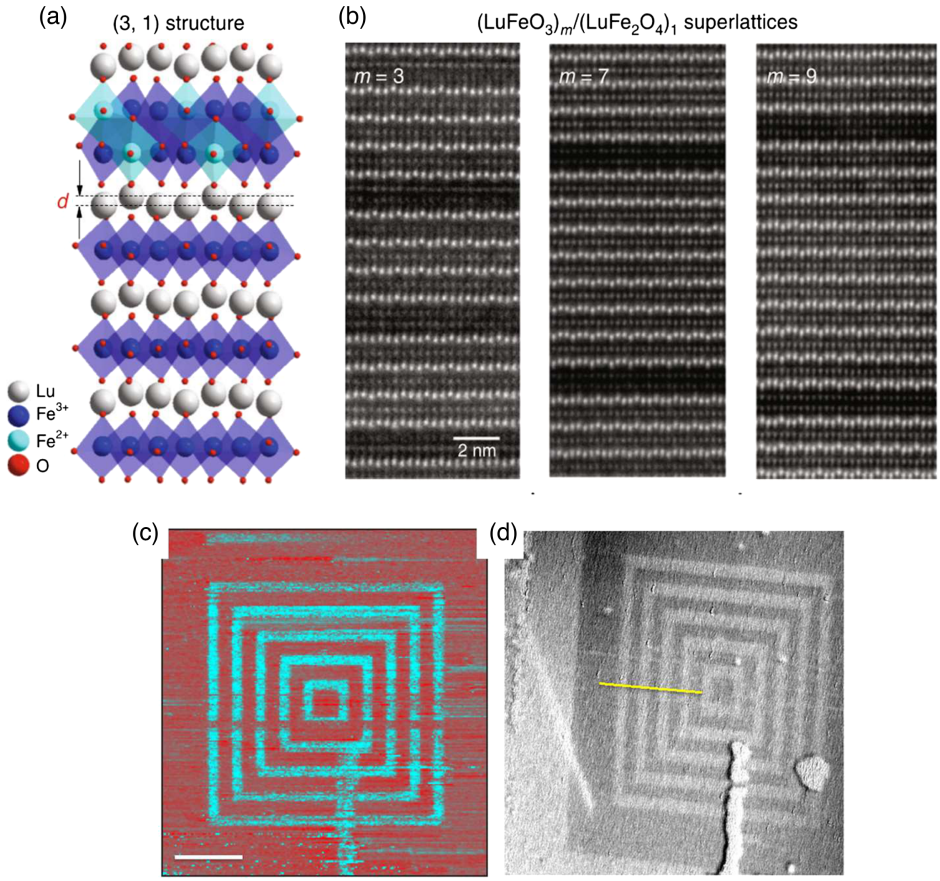


FIG. 16. Epitaxial magnetoelectric superlattices from the improper ferroelectric $LuFeO_3$. (a) Schematic of the crystal structure of a $LuFeO_3/LuFe_2O_4$ superlattice. (b) Atomic resolution images of superlattices with various $LuFeO_3/LuFe_2O_4$ stacking sequences. (c) Piezoforce microscopy image of a $LuFeO_3/LuFe_2O_4$ superlattice showing the box-in-a-box switching of the ferroelectric polarization. (d) The corresponding XMCD-PEEM image at the Fe edge showing the switching of the magnetization state. The scale bar is 3 μm. From Mundy *et al.*, 2016.

In the following we cover these effects for three families of materials, namely, magnetic semiconductors, magnetic oxides, and transition metals. The most impressive effects have been seen in the first two families, albeit mostly at low temperature due to the low $T_C$ of these compounds. Using ionic liquids, large modulations have also been seen at room temperature with ultrathin transition metal films.

### 1. Magnetic semiconductors

Charge-driven magnetoelectric coupling was first explored more than 20 years ago in carrier-mediated ferromagnets such as diluted magnetic semiconductors (DMSs) (Dietl and Ohno, 2014). Experimentally the first demonstration of an electric control of the magnetic state in these systems was in an $(In, Mn)As$ thin film in a field-effect transistor geometry using a polyimide layer as the dielectric. Ohno *et al.* (2000) measured the anomalous Hall effect of the ferromagnet as a function of the applied gate voltage and could thus detect a modulation of the $T_C$ of about 2 K upon applying a voltage of $\pm 125$ V; see Fig. 17. A similar but larger effect was later observed using standard magnetometry in $(Ga, Mn)As$ using $HfO_2$ as the dielectric (Sawicki *et al.*, 2010). Note that the data can be well explained by simulations using the *p-d* Zener model, which is responsible for ferromagnetism in DMSs (Dietl *et al.*, 2000). Similar effects were subsequently reported in other types of DMSs, see Nepal *et al.* (2009) and Wen *et al.* (2013). Not only has $T_C$ been modulated electrically in these systems, but the magnetic anisotropy (Chiba *et al.*, 2008) and the magnetic domain wall motion (Yamanouchi *et al.*, 2006) have been as well. A nonvolatile electric-field transition from a ferromagnetic state (accumulation) to a paramagnetic one (depletion) was demonstrated a few years later when the dielectric gate was replaced by a ferroelectric one (Stolichnov *et al.*, 2008).

### 2. Oxide heterostructures

Because they crystallize in the same perovskite structures as the referenced ferroelectrics [$BaTiO_3$, $Pb(Zr, Ti)O_3$, etc.], magnetic perovskite oxides can be combined with them into epitaxial heterostructures to achieve an electrical control of magnetic properties. As typical carrier-mediated ferromagnets, manganites ($La_{1-x}Sr_xMnO_3$) soon appeared to be natural candidates for magnetoelectric effects. Kanki, Tanaka, and Kawai (2006) evidenced electric-field-induced modifications in the magnetic moment amplitude of a 10 nm $La_{0.85}Ba_{0.15}MnO_3$ channel by conducting XMCD experiments close to the metal-insulator transition temperature using $Pb(Zr, Ti)O_3$ as the ferroelectric gate oxide. This modulation

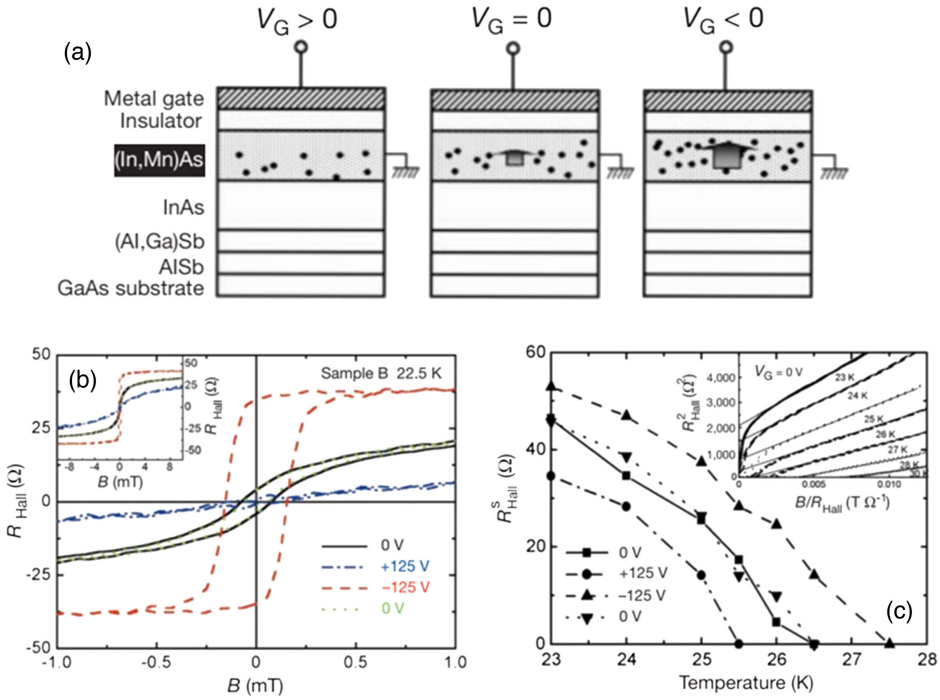


FIG. 17. (a) Field-effect control of the hole-induced ferromagnetism in magnetic semiconductor (In, Mn)As field-effect transistors. The gate voltage $V_G$ applied through the insulator controls the hole concentration in the magnetic semiconductor channel (the filled circles). Negative $V_G$ increases hole concentration, resulting in enhancement of the ferromagnetic interaction among magnetic Mn ions, whereas positive $V_G$ has an opposite effect. The arrow schematically shows the magnitude of the Mn magnetization. (b) Hall effect for different gate voltages. When holes are partially depleted from the channel ($V_G = +125$ V), a paramagnetic response is observed (blue dash-dotted line), whereas a clear hysteresis at low fields (<0.7 mT) appears as holes are accumulated in the channel ($V_G = -125$ V, red dashed line). Two Hall curves measured at $V_G = 0$ V before and after the application of $-125$ V (black solid line and green dotted line, respectively) are virtually identical (i.e., the effect is volatile). Inset: the same curves shown at higher magnetic fields. (c) Temperature dependence of spontaneous Hall resistance $R^S_{\mathrm{Hall}}$ under three different gate biases. $R^S_{\mathrm{Hall}}$ being proportional to the spontaneous magnetization $M_S$ indicates a $\pm 1$ K modulation of $T_C$ upon application of $V_G = \pm 125$ V. $T_C$ is determined using Arrott plots (inset). From Ohno *et al.*, 2000.

was ascribed to changes induced in the carrier density in the channel depending on the remanent ferroelectric polarization direction in the $Pb(Zr, Ti)O_3$ ferroelectric gate as revealed by the resistance dependence. Lu *et al.* (2012) observed a 10% modulation of the magnetization upon polarization reversal in $La_{0.67}Sr_{0.33}MnO_3(10\ \mathrm{nm})/BaTiO_3$ bilayers grown on $SrTiO_3(001)$ substrates. The large change in magnetization, which was inversely proportional to the $La_{0.67}Sr_{0.33}MnO_3$ thickness, was ascribed to the carrier modulation and to the shift in the metal-insulator transition near room temperature.

An electrically induced magnetic transition was identified in $La_{0.8}Sr_{0.2}MnO_3(4\ \mathrm{nm})/Pb(Zr, Ti)O_3$ bilayers (Molegraaf *et al.*, 2009). Important modifications in $T_C$ and the magnetization amplitude at 100 K probed by Kerr magnetometry were reported in this system; see Fig. 18(a). Additional experiments using x-ray absorption near edge spectroscopy revealed the charge-induced change by polarization switching in the valence state of Mn atoms (0.1 electron per Mn atom) in the $La_{0.8}Sr_{0.2}MnO_3$ layer (Vaz *et al.*, 2010). From combined spectroscopic, magnetic, and electric characterizations of this system, Vaz *et al.* concluded that the magnetic spin configuration of $La_{0.8}Sr_{0.2}MnO_3$ at the $Pb(Zr, Ti)O_3$ interface changes from ferromagnetic in the depletion state to *A*-type antiferromagnetic in the accumulation state (increase of hole doping), and that this interface-charge-driven magnetoelectric coupling is at the origin of the effect (Vaz *et al.*, 2011). In the accumulated state, the interface layer consists of strongly depopulated, antibonding $3d$ $e_g$ $3z^2 - r^2$ states, resulting in a weakening of the double-exchange interaction at these orbitals. An antiferromagnetic coupling to the adjacent layers ensures that the $3d$ $e_g$ $x^2 - y^2$ orbitals are energetically privileged, favoring the superexchange interaction and a transition from a ferromagnetic state to an antiferromagnetic one that is consistent with theoretical predictions for related systems (Burton and Tsymbal, 2009). Ma *et al.* (2014) also reported a change by 1 order of magnitude in the in-plane and out-of-plane magnetizations at $La_{0.67}Sr_{0.33}MnO_3/Pb(Zr, Ti)O_3$ interfaces due to the appearance of an antiferromagnetic spin alignment induced by hole doping.

Perhaps the most impressive electric-field modulation of magnetism in $La_{0.7}Sr_{0.3}MnO_3/Pb(Zr, Ti)O_3$ bilayers is from Leufke *et al.* (2013); see Fig. 18(b). The strong correspondence of the polarization versus $E$ and magnetization versus $E$ loops indicates a purely electrostatic doping as the origin of the effect, with a negligible contribution from piezoelectricity and/or electrochemistry (discussed later). Leufke *et al.* (2013) analyzed in detail the dependence of the effect on the poling voltage and on temperature to conclude that phase separation between antiferromagnetic and ferromagnetic

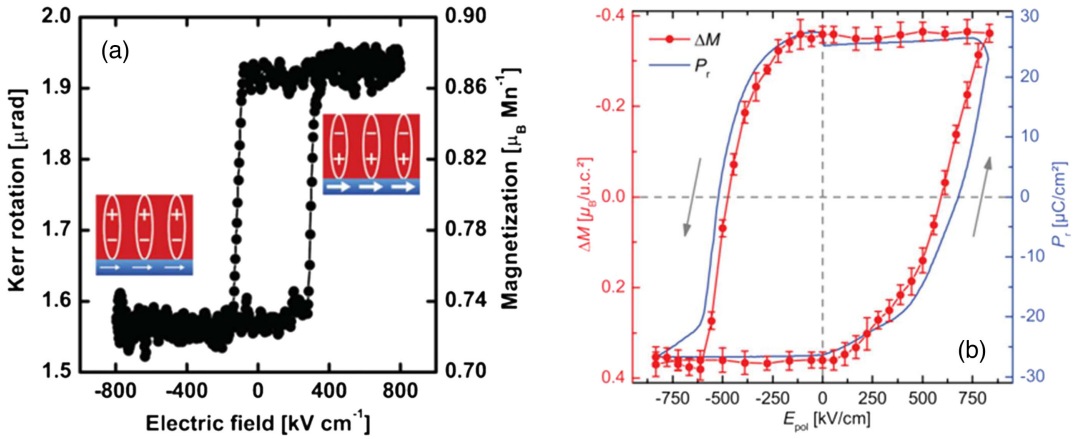


FIG. 18. (a) Magnetoelectric hysteresis curve at 100 K showing the magnetic response of the $Pb(Zr,Ti)O_3/La_{0.8}Sr_{0.2}MnO_3$ system as a function of the applied electric field. The two magnetization values correspond to modulation of the magnetization of the $La_{0.8}Sr_{0.2}MnO_3$ layer. Insets: the magnetic and electric states of the $La_{0.7}Sr_{0.3}MnO_3$ and $Pb(Zr,Ti)O_3$ layers, respectively. The size of the arrow qualitatively indicates the magnetization amplitude. From Molegraaf *et al.*, 2009. (b) Comparison of the electric-field dependence of the remanent ferroelectric polarization $P_r$ and of the magnetic modulation per unit cell area $\Delta M$ measured in a $Pb(Zr,Ti)O_3/La_{0.7}Sr_{0.3}MnO_3$ bilayer. Both curves were measured consecutively at 50 K and 100 Oe. From Leufke *et al.*, 2013.

regions, a common feature of mixed-valence manganites (Tokura and Tomioka, 1999), played a significant role in the observed effects.

In heterostructures combining a ferroelectric such as $Pb(Zr,Ti)O_3$ and a ferromagnet like $La_{0.7}Sr_{0.3}MnO_3$, the influence of the electric field on magnetism may arise from both field-effect and strain-driven effects due to the piezoelectric nature of the ferroelectric. Several studies have evidenced the coexistence of both mechanisms and separated them. Typically the strain-driven effect has an even dependence on the electric field, while charge-driven ones are odd. Since strain effects can extend over large thicknesses into the magnetic film while charge-driven effects are purely interfacial, studying magnetization versus electric-field loops as a function of thickness typically yields a crossover between both types of behavior (Hu, Nan, and Chen, 2011). Preziosi *et al.* (2015) and H. Huang *et al.* (2018) evidenced this phenomenon while also drawing conclusions on the influence of orbital reconstruction effects in the low thickness limit.

Gating of manganites with ionic liquids has also been attempted, leading to striking results. As always with electric double layer systems, but perhaps even more importantly with oxides in which oxygen diffusion can be strong, in such experiments electrostatic effects may be accompanied by electrochemistry (that is, ion migration between the electrolyte and the channel material), and both contributions are difficult to separate (Leighton, 2019; Molinari, Hahn, and Kruk, 2019). Dhoot *et al.* (2009) reported a resistance change approaching 100% and modulations of the metal-insulator transition temperature (corresponding to $T_C$ in these compounds) by over 30 K. Even larger modulations were later found by others in other manganites (Hatano *et al.*, 2013, 2014; Zheng *et al.*, 2018). The results of Molinari, Hahn, and Kruk (2019) correspond to an actual measurement of magnetization under the influence of ionic liquid gating. Working just above room temperature and just below the $T_C$ of an $La_{0.7}Sr_{0.3}MnO_3$ film they were able to modulate magnetization reversibly over tens of cycles with just $\pm 200$ mV (Molinari, Hahn, and Kruk, 2019).

### 3. Transition metal and alloys

To achieve effects at room temperature and in materials that are more compatible with applications, the electric-field effect has been explored on ferromagnets based on transition metals and their alloys. The first report of voltage-controlled magnetism in transition metals was by Weisheit *et al.* (2007), who observed a modulation of about 5% of $H_C$ of FePt ultrathin film at room temperature; see Figs. 19(a) and 19(b). Soon thereafter, the first results on the voltage control of magnetic anisotropy (VCMA) in an all-solid-state system were reported for Fe/MgO (Maruyama *et al.*, 2009) and CoFeB/MgO (Endo *et al.*, 2010); see Figs. 19(c) and 19(d). The electric field was applied across a polyimide layer and a $ZrO_2$ layer, respectively. The mechanism underlying the observed VCMA was investigated theoretically and proposed to be related to changes in the hybridization between O $2p$ states and different Fe $3d$ orbitals (Nakamura *et al.*, 2009, 2010). VCMA was used to induce magnetization reversal and thus to switch a MTJ between parallel and antiparallel states. The application of a short voltage pulse induces the precession of the magnetization, which reverses if the pulse is properly timed.

Accumulating and depleting charge into a ferromagnet is also expected to yield a modulation of its $T_C$, which was realized by Chiba *et al.* (2011) in 0.4 nm Co films using $HfO_2$ as the gate dielectric. Upon applying $\pm 10$ V, they were able to shift $T_C$ by about 12 K, resulting in an electrical switching between ferromagnetism and paramagnetism at around 320 K.

Parallel to these pioneering results, the possibility to use ferroelectricity to control the magnetism of transition metal layers was explored. Research in this direction has been mainly through first-principles calculations, particularly for the $BaTiO_3$/Fe system (Duan, Jaswal, and Tsymbal, 2006; Fechner *et al.*, 2008; Bocher *et al.*, 2012). In particular,

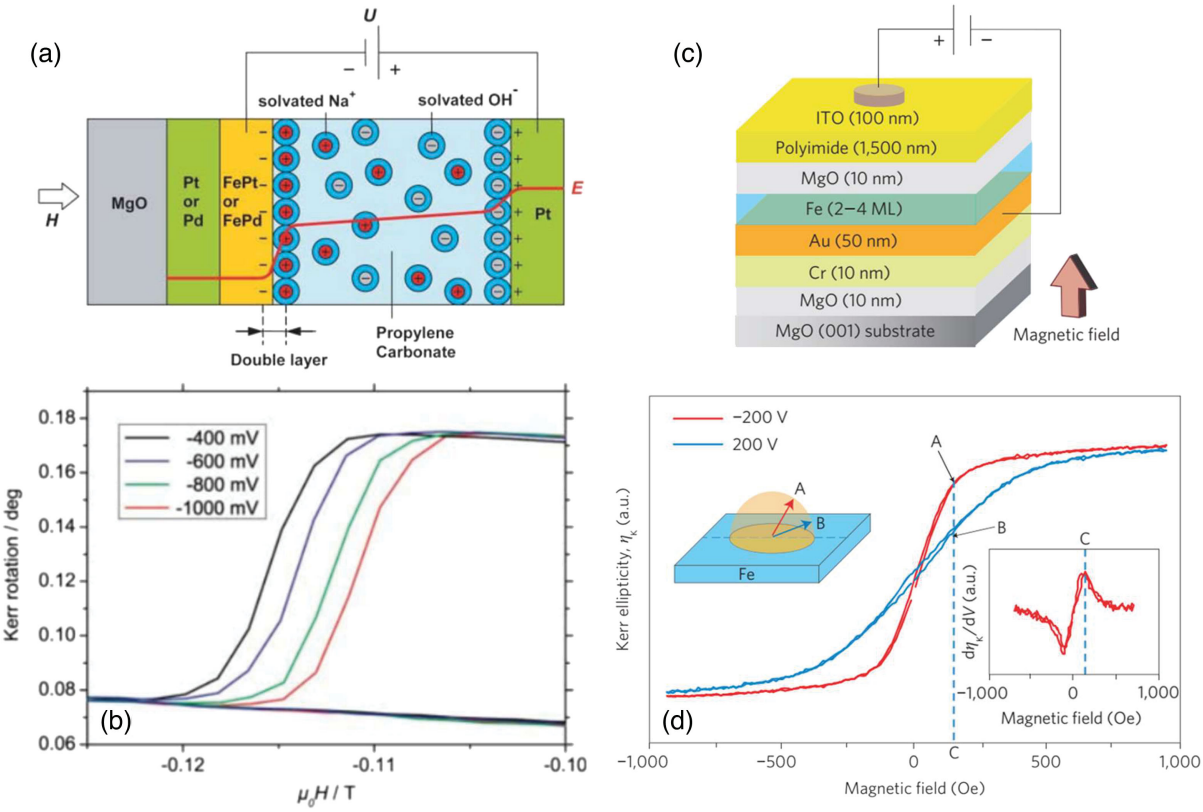


FIG. 19. (a) Schematic of an electrolytic cell containing the FePt or FePd film within an applied magnetic field $H$. The potential profile $E$ due to the applied potential $U$ is indicated by the red line. The potential drop at the Pt electrode side is much lower (compared to that of the sample surface) as a result of the Pt electrode's large surface area. (b) Magnetization switching of the 2-nm-thick FePt film for different $U$ values between the film and the Pt counter electrode. From Weisheit *et al.*, 2007. (c) Schematic of the sample used for a voltage-induced magnetic anisotropy change. (d) Magneto-optical Kerr ellipticity $\eta_k$ for different applied voltages as a function of the applied field. The thickness of the Fe film was 0.48 nm. A significant change in the hysteresis curve indicated a large change in perpendicular anisotropy following application of the bias voltage. Right inset: voltage modulation response of the Kerr ellipticity $d\eta_k/dV$. Left inset: magnetization direction at points $A$ and $B$ in the hysteresis curves. From Maruyama *et al.*, 2009.

ferroelectric switching was predicted to influence the magnetic moment at the interface and the spin polarization near the Fermi energy, which can be exploited in so-called multiferroic tunnel junctions (Garcia *et al.*, 2010; Valencia *et al.*, 2011); see Sec. V.1.2. Using XMCD at the Co $L_{3,2}$ edge, Heidler *et al.* (2016) observed a hysteretic dependence of the Co magnetic moment as a function of electric field in Co/PMN-PT. The data suggested a combination of strain- and charge-induced effects. Mardana, Ducharme, and Adenwalla (2011) combined a Co ultrathin film with a ferroelectric polymer $P$(vinylidene difluoride–FrFE) to achieve nonvolatile electrical control of magnetic coercivity. Subsequent studies reported a hysteretic dependence of coercivity with the electric field in $CoFeB/BaTiO_3$ (Baldrati *et al.*, 2016) and $Fe/BaTiO_3$ (Gorige *et al.*, 2017) and of the anisotropy field in $CoFe/(Ba,Sr)TiO_3$ (Zhou *et al.*, 2015).

The properties of ferromagnetic domains can also be tuned by charge accumulation or depletion. The domain wall velocity was found to strongly depend on the electric field in Co ultrathin films (Chiba and Ono, 2013). Using a meshed gate electrode, Ando *et al.* (2018) were able to achieve magnetic domain writing by electrical gating. The fact that such charge accumulation and depletion effects require ultrathin films is particularly appealing for controlling specific spin textures occurring at such low thickness when the ferromagnet is effectively sandwiched between different layers, leading to inversion symmetry breaking and unleashing the Dzyaloshinskii-Moriya interaction (DMI). Schott *et al.* (2017) exploited this possibility to turn magnetic skyrmion bubbles on and off with an electric field.

Just as for the manganites, the most impressive effects have been obtained using ionic liquid gating. As displayed in Figs. 20(a) and 20(b), a shift in $T_C$ by about 100 K was observed upon applying $\pm 2$V in ultrathin Co films (Shimamura *et al.*, 2012).

Before reviewing 2D magnets in Sec. II.D, we assess the advantages and inconveniences of the approaches for electric-field control of magnetism that we have just discussed, namely, exchange-based magnetoelectric coupling (in single phase materials or in heterostructures involving a room-temperature multiferroic such as $BiFeO_3$), strain-induced control of magnetization, and electric-field effects. All three approaches have evidenced a response at room temperature, although for the first one the choice of materials is limited to $BiFeO_3$ and some hexaferrites with complex unit cells that have not yet been grown as thin films. It is, however, the most straightforward approach to achieve a 180° switching of magnetization. This may also be achieved using strain-based

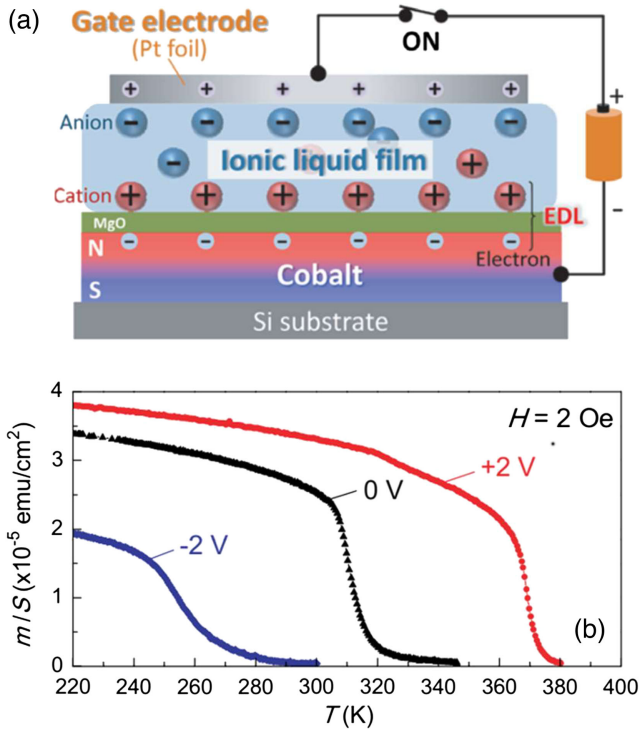


FIG. 20. (a) Sketch of the device for the modulation of the magnetic properties of a Co film. (b) Temperature dependence of the magnetization at $H = 2$ Oe under a gate voltage $V_G = -2, 0,$ and $+2$ V. From Shimamura *et al.*, 2012.

magnetoelectric coupling, but through complex writing protocols and field effect (Fechner *et al.*, 2012), yet this remains to be shown. As a result, the most promising strategy thus far still relies on the use of $BiFeO_3$, although the deterministic nature of the switching is a major issue (Vaz *et al.*, 2022). This emphasizes the need for both new materials, perhaps in the 2D family, and further imaginative schemes for strain- and field-effect-based approaches.

### D. Two-dimensional magnets

Before the discovery of intrinsic magnetism in different 2D materials in 2017, its possibility was disregarded based on the Mermin-Wagner theorem (Mermin and Wagner, 1966), which was formulated for the case of the isotropic Heisenberg model with finite-range interactions. However, the presence of uniaxial anisotropy (such as magnetocrystalline anisotropy caused by spin-orbit coupling) allows for the stabilization of magnetic order in two dimensions (Gong and Zhang, 2019), a possibility that was experimentally confirmed in different van der Waals (vdW) materials.

The first experimental demonstration of 2D magnetism was reported in $Cr_2Ge_2Te_6$ vdW semiconductors down to the bilayer limit with unprecedented control of $T_C$ with low applied magnetic fields (Gong *et al.*, 2017). Another breakthrough experiment demonstrated intrinsic 2D magnetism down to the monolayer limit in insulating exfoliated $CrI_3$ (Huang *et al.*, 2017). These vdW materials showed layer-dependent magnetism due to behavior alternating between ferromagnetic and antiferromagnetic states as the number of layer increases. The third exfoliated material reported to show long-range magnetic order in 2017 was metallic $Fe_3GeTe_2$, which has a higher $T_C$ than the other two materials (Deng *et al.*, 2018; Fei *et al.*, 2018; Tan *et al.*, 2018). Some transition metal dichalcogenides (TMDs), such as $VSe_2$ (Bonilla *et al.*, 2018) and $MnSe_2$ (O'Hara *et al.*, 2018), have also been reported to be magnetic in some of their crystallographic phases. Ising-type magnetic ordering has also been demonstrated in phosphorous-based insulating antiferromagnets, such as in $FePS_3$ (Lee *et al.*, 2016).

These materials form part of more general families of 2D vdW structures. Such a large number of atomically thin vdW magnets show a wide variety of electrical and magnetic properties ranging from ferromagnetic semiconductors or metals to antiferromagnetic insulators. Owing to their 2D character, they are much more sensitive to external stimuli, particularly the electric field, allowing efficient control of their magnetic properties. They can be naturally stacked with a wide range of vdW materials, forming heterostructures with almost ideal interfaces. The electrical control of magnetism in a 2D magnet can occur via different mechanisms such as linear magnetoelectric coupling and electrostatic doping.

The former mechanism requires the material to simultaneously break time-reversal symmetry and inversion symmetry, a condition fulfilled by bilayer $CrI_3$ in the antiferromagnetic ground state, but not by the ferromagnetic phase or the monolayer $CrI_3$, in which inversion symmetry is present. Jiang, Shan, and Mak (2018) measured the magnetoelectric response with magnetic circular dichroism (MCD) and using a dual gate structure to apply an electric field in order to take out the effect of doping. The magnetoelectric coupling was maximal around the spin-flip transition that occurs at ~0.5 T. This made it possible to electrically switch bilayer $CrI_3$ between the antiferromagnetic and ferromagnetic states at a constant magnetic field [close to the spin-flip transition; see Fig. 21(a)].

The control of magnetism is also possible via electrostatic doping in 2D magnets. This mechanism has a benefit in that it does not require the specific symmetry of the linear magnetoelectric coupling and, in addition to bilayer $CrI_3$ (B. Huang *et al.*, 2018; Jiang *et al.*, 2018), it is also present in monolayer $CrI_3$ (Jiang *et al.*, 2018) and in $Cr_2Ge_2Te_6$ (Z. Wang *et al.*, 2018; Verzhbitskiy *et al.*, 2020). In the case of monolayer $CrI_3$ (Jiang *et al.*, 2018), saturation magnetization ($M_S$), $H_C$, and $T_C$ increase (decrease) with hole (electron) doping. In bilayer $CrI_3$, electron doping ($\sim 2.5 \times 10^{13}$ cm$^{-2}$) reduces the spin-flip transition to almost zero magnetic field (Jiang *et al.*, 2018). Although this should enable electrical switching of magnetization at zero field, a magnetic field near the spin-flip transition is required for a fully reversible switch (B. Huang *et al.*, 2018; Jiang *et al.*, 2018). Electrostatic doping using ionic liquid gating has also been reported in multilayer $Cr_2Ge_2Te_6$ (Z. Wang *et al.*, 2018; Verzhbitskiy *et al.*, 2020). Z. Wang *et al.* (2018) used magneto-optical Kerr effect (MOKE) measurements to report that the saturation field ($H_S$) decreases and $M_S$ increases as a function of doping levels (both electron and hole), while $H_C$ and $T_C$ are insensitive to doping. This performance was tentatively attributed to a moment rebalance of the spin-polarized band structure while its Fermi level was tuned. On the contrary,

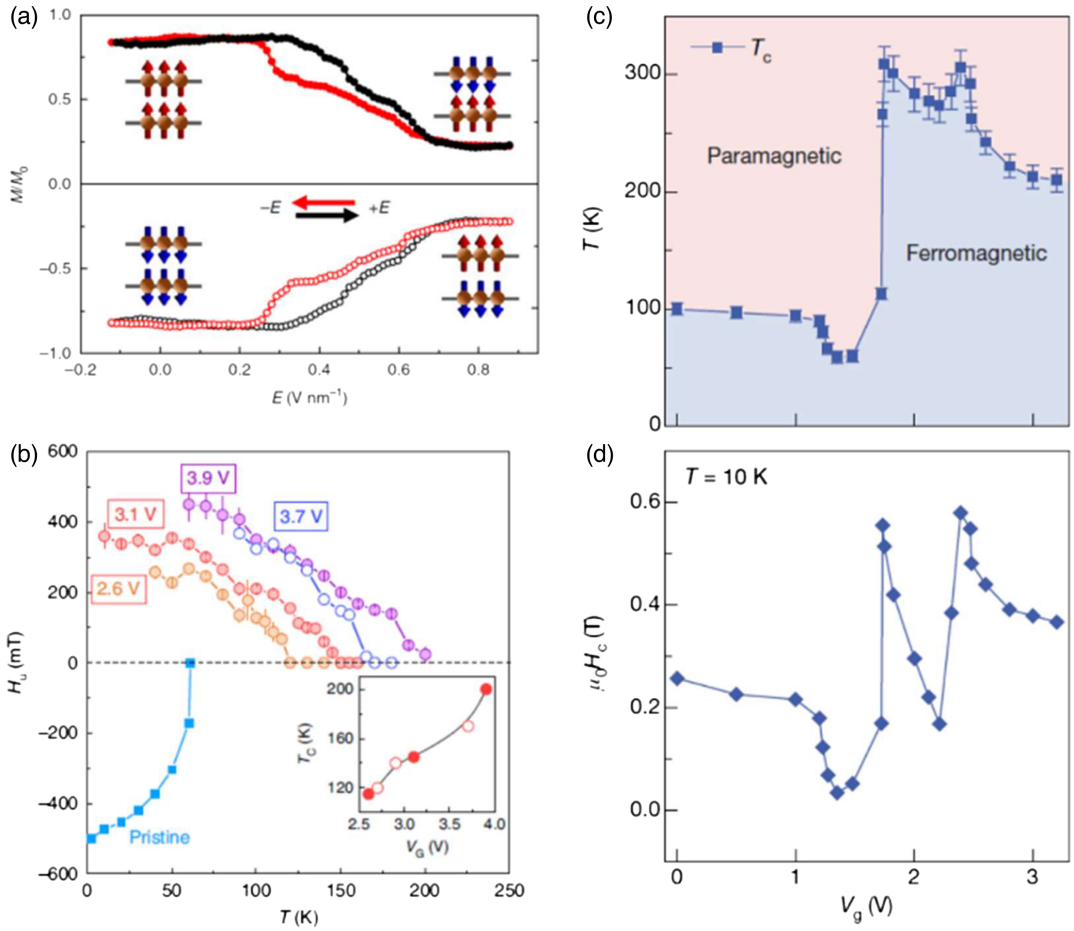


FIG. 21. (a) Normalized magnetization measured by MCD as a function of the applied electric field (trace and retrace) at 4 K and a fixed magnetic field (+0.44 T in the top panel and −0.44 T in the bottom panel), showing the electrical switching of the magnetic order in bilayer $CrI_3$. Insets: the corresponding magnetic states. From Jiang, Shan, and Mak, 2018. (b) Uniaxial magnetic anisotropy field ($H_u = H_s^{\perp} - H_s^{\parallel}$) of multilayer $Cr_2Ge_2Te_6$ as a function of temperature at different gate voltages and in the pristine case. Inset: the dependence of $T_C$ on gate voltage. From Verzhbitskiy *et al.*, 2020. (c) $T_C$ of a trilayer $Fe_3GeTe_2$ as a function of gate voltage. From Deng *et al.*, 2018. (d) $H_C$ of a trilayer $Fe_3GeTe_2$ as a function of gate voltage at 10 K. From Deng *et al.*, 2018.

Verzhbitskiy *et al.* (2020) showed a shift of $T_C$ from ∼61 to up to 200 K when an electron doping of $\sim 4 \times 10^{14}$ cm$^{-2}$ was applied using magnetoresistance measurements. Additionally, the magnetic anisotropy was dramatically changed, moving from perpendicular to in plane; see Fig. 21(b). They attributed the occurrence of this effect to a double-exchange mechanism that was mediated by free carriers, which dominated over the superexchange mechanism of the original insulating state.

A voltage control of magnetism with a completely different origin has been reported in multilayer $CrI_3$. In this material, memristive switching is observed when a large enough voltage is applied such that the two resistive states are coupled to the magnetic phases (Kim *et al.*, 2020). The origin of the effect is a thermally induced mechanism when current flows across $CrI_3$.

Voltage control of magnetism has also been reported in $Fe_3GeTe_2$, which, unlike the previous 2D magnets mentioned in this section, is metallic. Deng *et al.* (2018) applied ionic gating to bring $T_C$ from ∼100 up to ∼300 K in trilayer $Fe_3GeTe_2$ [see Fig. 21(c)], a noteworthy observation since to date no pristine 2D magnet has been ferromagnetic at room temperature. As plotted in Fig. 21(d), $H_C$ roughly follows the variation of $T_C$ with the gate voltage. The large electron doping induced by the ionic gate ($\sim 10^{14}$ cm$^{-2}$ per layer) causes a substantial shift of the electronic bands of $Fe_3GeTe_2$. The large variation in the DOS at the Fermi level leads to appreciable modulation in the ferromagnetism, which is in agreement with the Stoner model for itinerant electrons (Deng *et al.*, 2018; Wang, Chen, and Long, 2020). Finally, metallic ferromagnet $Fe_5GeTe_2$ has been electron doped with protonic gating, which can induce a transition to an antiferromagnetic phase at 2 K (Tan *et al.*, 2021).

### E. Electric-field control of magnetic skyrmions

Magnetic skyrmions are 2D topological solitonic spin textures that can be stabilized in chiral magnets thanks to the DMI, anisotropic interactions existing in the absence of inversion symmetry, either in noncentrosymmetric lattices (Dzyaloshinsky, 1958; Moriya, 1960) or when the breaking of inversion symmetry is due to defects or interfaces (Fert and Levy, 1980; Fert, 1990; Crépieux and Lacroix, 1998). Section III.E is complementary to this section; it describes skyrmions in more detail and discusses how they can be manipulated by electrical currents. Skyrmions have some

similarities with magnetic bubbles, which were used to store data in a nonvolatile memory, popular in the 1970s and 1980s (Malozemoff and Slonczewski, 1979), before being replaced by more advanced technologies such as hard-disk drives and flash memories. However, skyrmion devices have the potential to offer much higher data storage densities than bubble memory due to the smaller size of skyrmions and their stability, which is given by the topological protection. Another difference is the way in which the data are manipulated: while skyrmion devices use spintronic techniques based on charge currents, bubble memory uses magnetic fields to move the bubbles, which does not favor downscaling.

Over the past decade, magnetic skyrmions have been observed in a wide range of materials and heterostructures including metallic MnSi (Mühlbauer *et al.*, 2009; Neubauer *et al.*, 2009) and FeGe (Yu *et al.*, 2011), but also insulating $Cu_2OSeO_3$ (Adams *et al.*, 2012). In insulating skyrmion lattice compounds, the chiral lattice gives rise to a magnetoelectric coupling between electric and magnetic orders, opening a path for electric-field control of magnetic skyrmions, with potentially no Joule-heating dissipation. In single crystal $Cu_2OSeO_3$, it was demonstrated that the electric field can induce a rotation of the skyrmion lattice via this magnetoelectric coupling (White *et al.*, 2014). These giant skyrmion lattice rotations (spanning in a range of 25°) operate via skyrmion distortion, as supported by calculations. However, this skyrmion lattice is restricted to a narrow temperature (54–58 K) and magnetic-field region in $Cu_2OSeO_3$. The electric-field control of the skyrmion phase pocket was revealed by combining magnetic susceptibility and microwave spectroscopy [Fig. 22(a)] (Okamura *et al.*, 2016) and further confirmed using neutron scattering (Kruchkov *et al.*, 2018). Thus, the metastable skyrmion lattice can be created and erased isothermally under electric fields and in a nonvolatile manner (Okamura *et al.*, 2016; White *et al.*, 2018). Using real-space methods such as Lorentz transmission electron microscopy, a skyrmion lattice could be reversibly written and erased under electric-field pulses from a helical spin background in transistor devices based on single crystal $Cu_2OSeO_3$ [Figs. 22(b) and 22(c)] (P. Huang *et al.*, 2018).

Attempts have also been made to stabilize skyrmions in oxide heterostructures [see Matsuno *et al.* (2016) and Vistoli *et al.* (2019)] and to control them with the electric field. We mention the results of L. Wang *et al.* (2018), who reported the observation of skyrmion bubbles in $SrRuO_3/BaTiO_3$ bilayers with a skyrmion density and associated topological Hall effect tunable by ferroelectric polarization; see Fig. 23. Note, however, that reports of skyrmions in $SrRuO_3$ heterostructures and the interpretation of the topological Hall effect are still under intense debate; see Groenendijk *et al.* (2020) and Trier *et al.* (2022).

Novel 2D multiferroic materials were predicted in Co intercalated $MoS_2$ dichalcogenides, with degenerate DMIs in the two ferroelectric states. The chirality of the skyrmions stabilized in such 2D multiferroics can therefore be reversed by electric fields thanks to the magnetoelectric coupling (Shao *et al.*, 2022). When a bilayer vdW heterostructure of $WTe_2/CrCl_3$ was combined with a 2D ferroelectric $CuInP_2S_6$, the electric-field writing and deletion of Néel-type skyrmions was predicted, where an interfacial magnetoelectric coupling involving polarization-induced electronic reconstruction gives rise to nonvolatile control of the DMI (Sun *et al.*, 2021).

While in single phase chiral magnets the skyrmion phase is limited to low temperature, asymmetric multilayer stacks of heavy metals and ferromagnetic layers can give rise to room-temperature skyrmions (Moreau-Luchaire *et al.*, 2016; Woo *et al.*, 2016; Legrand *et al.*, 2017) stabilized by interfacial DMIs (Yang *et al.*, 2015; Belabbes *et al.*, 2016). In multiferroic heterostructures consisting of such asymmetric $[Pt/Co/Ta]_5$ multilayers and a ferroelectric PMN-PT layer, the strain-mediated electric-field control of skyrmions was recently demonstrated (Ba *et al.*, 2021). Observations of electric-field-induced creation, deformation, and annihilation of the skyrmions were corroborated by strain-induced variations of both the magnetic anisotropy and the interfacial DMI. Electromechanical and micromagnetic simulations revealed that applying a voltage between two lateral electrodes in such multiferroic heterostructures can give rise to a transverse strain gradient because of the nonuniform electric-field profile in the piezoelectric material. Owing to the magnetoelastic coupling,

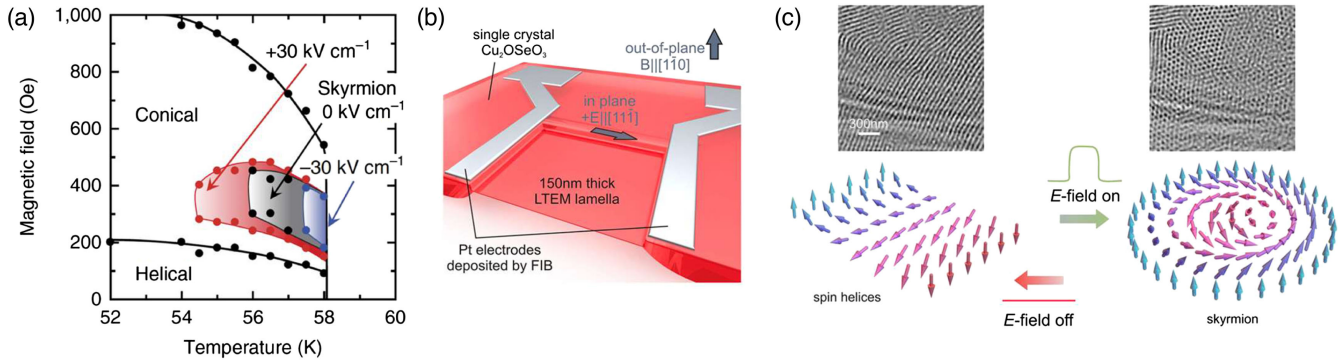


FIG. 22. (a) Electric-field control of the skyrmion phase pocket in single crystal $Cu_2OSeO_3$. Electric and magnetic fields are parallel to the [111] direction of the crystal. From Okamura *et al.*, 2016. (b) Schematic of the single crystal $Cu_2OSeO_3$ sample configuration using patterned Pt electrodes to apply in-plane electric fields of 3.6 V/μm. (c) Reversible electric-field transition between the helical spin state and the skyrmion lattice visualized using Lorentz transmission electron microscopy ($T = 24.7$ K under an out-of-plane magnetic field of 254 Oe). (b),(c) From P. Huang *et al.*, 2018.

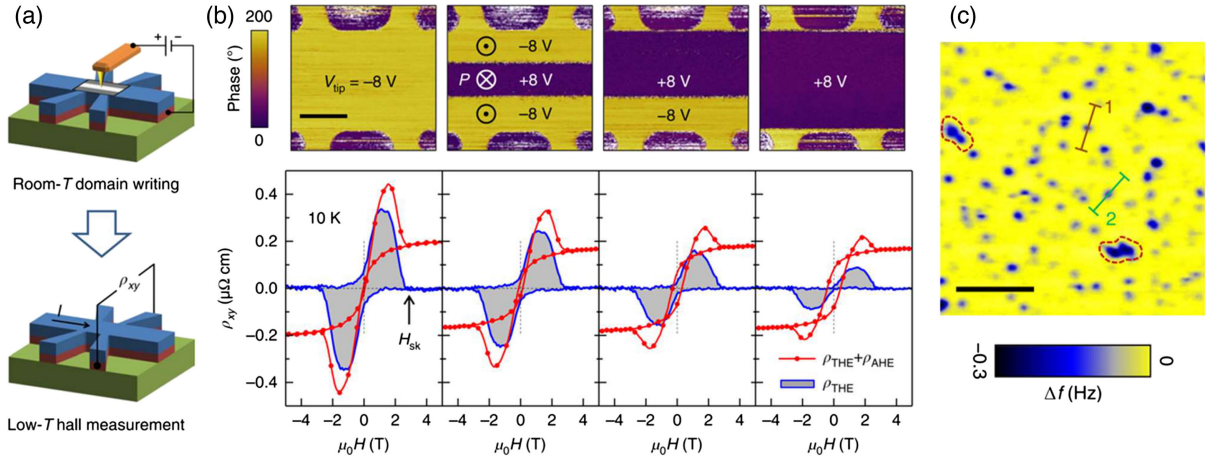


FIG. 23. (a) Schematic diagram of the experimental setup for ferroelectric domain switching using an atomic force microscopy conductive tip and to perform Hall measurements. (b) Piezoresponse force microscopy phase images (top panels) and Hall and extracted topological Hall curves (bottom panels) of a $SrRuO_3/BaTiO_3$ sample for different ferroelectric poling states. The scale bar corresponds to 10 μm. (c) Difference in MFM contrast between images taken at two different magnetic fields. From L. Wang *et al.*, 2018.

this strain gradient can be used to compensate the skyrmion Hall angle and propagate more efficiently skyrmions under STT (Fattouhi *et al.*, 2021).

Writing and deleting individual skyrmions with an electric field was originally demonstrated at a low temperature (7.8 K) using spin-polarized scanning tunneling microscopy on an ultrathin Fe layer on Ir(111) (Hsu *et al.*, 2017). The main mechanism involved was a change of the magnetic exchange interaction with the electric field, leading to either a ferromagnetic ground state (positive electric field) or a skyrmion state (negative electric field). When a CoO/Co/Pt trilayer was used in which large interfacial DMIs were reported and with a Co thickness close to the ferromagnetic-paramagnetic transition at room temperature, micron-size skyrmion bubbles could be reversibly written and erased using an electric field (Schott *et al.*, 2017). These modifications were interpreted by a modulation of the magnetization and anisotropy under an electric field, possibly via changes in the electron density of state of the ultrathin Co layer. In $Ta/FeCoB/TaO_x$ trilayers, a 130% variation of the DMI under voltage could be detected using Brillouin light spectroscopy and magneto-optic Kerr microscopy (Srivastava *et al.*, 2018). These results and the correlated size variations of the skyrmion bubbles were explained by the large sensitivity of the $FeCoB/TaO_x$ Rashba DMI to the electric field. The electric-field creation and directional motion of chiral domain walls and skyrmion bubbles could be achieved in a $SiO_2$/Pt/CoNi/Pt/CoNi/Pt multilayer with a thickness gradient and interfacial DMI (Ma *et al.*, 2019). The $SiO_2$/Pt interface provides a large electric-field-induced magnetic anisotropy change due to the electric quadrupole induction. Recently a femtosecond pulse electric field was predicted to generate a DMI in single ultrathin metallic thin films (Desplat *et al.*, 2021). This mechanism allows the coherent nucleation of skyrmions, as well as other exotic topological defects (antiskyrmions, target skyrmions, etc.), by modifying the properties of the ultrafast electric-field pulse.

As an aside, we note that polar skyrmions and other possible topological objects (polar vortices, center domains, merons, etc.) are now gathering a lot of interest among the ferroelectric community (Wang *et al.*, 2023), as these objects would be smaller than their magnetic counterparts and thus naturally controlled by an electric field (Pereira Gonçalves *et al.*, 2019; Zhou *et al.*, 2022; Zhu *et al.*, 2022). Indeed, polar skyrmions were recently observed in $PbTiO_3/SrTiO_3$ superlattices at room temperature (Das *et al.*, 2019; Han *et al.*, 2022). This field is still in its infancy, and the complex competition between depolarizing fields, strain, and electric-field gradients is currently under investigation. Stabilizing polar chirality in domain walls and bubbles is a prerequisite (Chauleau *et al.*, 2017; Shafer *et al.*, 2018; Fusil *et al.*, 2022), while the underlying mechanisms for this polar chirality have not been clearly identified. Recently the electric analog of the DMI was proposed (Zhao *et al.*, 2021), thereby opening an avenue for the design of topological objects in ferroelectrics and multiferroics.

### F. Dynamics

The dynamics of the antiferromagnetic and ferroelectric states and the coupling between them can be probed in either time-domain- or frequency-domain-based measurements. While the fundamental physics of magnons, electromagnons, and ferroelectromagnons are best studied in frequency-domain measurements, from a more practical perspective, especially in digital electronics, time-domain measurements are more valuable. The emergence of antiferromagnetic spintronics provides another impetus to consider both aspects. There have been some notable reviews of the high frequency dynamics of multiferroics in recent years (Shuvaev, Mukhin, and Pimenov, 2011; Liang *et al.*, 2021). While there have been many papers published on the physics of the polarization switching process in ferroelectrics over 60 years (Merz, 1954; Ishibashi and Takagi, 1971), true time-domain studies are still evolving. In capacitive elements such as a ferroelectric or multiferroic capacitor, the time-domain dynamics of switching of the order parameter is invariably convoluted with the circuit level parameters (and parasitics), which then obfuscate the intrinsic time dynamics. Thus, care is needed to probe the

dynamics in such capacitive elements by reducing resistive losses, as well as circuit level capacitive parasitics.

### 1. Magnonics

In magnonics, spin waves form the fundamental excitation (Chumak *et al.*, 2015; Rezende, 2020). This field has experienced a reemergence over the past decade as interesting discoveries have yielded a breadth of new physics as well as the potential for low-power computing such as magnon logic (Chumak *et al.*, 2015), antiferromagnetic spin wave field-effect transistors (Cheng *et al.*, 2016), and all-magnon transistors based on magnon-magnon scattering with resonant excitation (Chumak, Serga, and Hillebrands, 2014). There are several ways to create magnons (Cornelissen *et al.*, 2015), and spin transport via magnon currents has already been reported in a variety of systems (Althammer, 2021). Although resonant excitations are typically used to study spin waves (Abraha and Tilley, 1996), magnon currents can be excited incoherently by a thermal gradient through the spin Seebeck effect (Uchida *et al.*, 2010) or by the spin accumulation mechanism through the spin Hall effect (SHE), while they can be probed nonlocally with the inverse spin Hall effect (ISHE). Previous research has demonstrated nonlocal spin transport in insulating ferrimagnets (Cornelissen *et al.*, 2015; Giles *et al.*, 2015; Goennenwein *et al.*, 2015; Avci *et al.*, 2020), antiferromagnets (Lebrun *et al.*, 2018; Ross *et al.*, 2020), and ferromagnets (Aguilar-Pujol *et al.*, 2023), with spin transport over exceptionally long distances, electrical field control (C. Liu *et al.*, 2021) and nonvolatile magnetic-field control (Han *et al.*, 2020).

### 2. Electric control of magnons: Ferroelectromagnons

Early work in the 1950s and 1960s (Smolensky and Chupis, 1982) provided the fundamental backbone for the study of coupled spin and charge waves, termed as electromagnons (or, more precisely, ferroelectromagnons) (Baryakthar and Chupis, 1970; Pimenov *et al.*, 2006). In simple terms, ferroelectromagnons are the coupling between spin waves and charge waves. A good example is the case of antiferromagnetic spin waves in prototypical rare-earth ferrites (Abraha and Tilley, 1996) such as $DyFeO_3$. Such antiferromagnetic resonances are typically in the 300–350 GHz range, as a direct consequence of the large antiferromagnetic anisotropy field compared to ferromagnets. Replacing Dy with Bi to create $BiFeO_3$ leads to ferroelectromagnons in the 600–800 GHz range. There have been a few studies of such ferroelectromagnons, particularly using Raman and optical probes (Cazayous *et al.*, 2008; Rovillain *et al.*, 2010; Nagel *et al.*, 2013; Sando *et al.*, 2013; Agbelele *et al.*, 2017). Figure 24 presents Raman experiments from Rovillain *et al.*

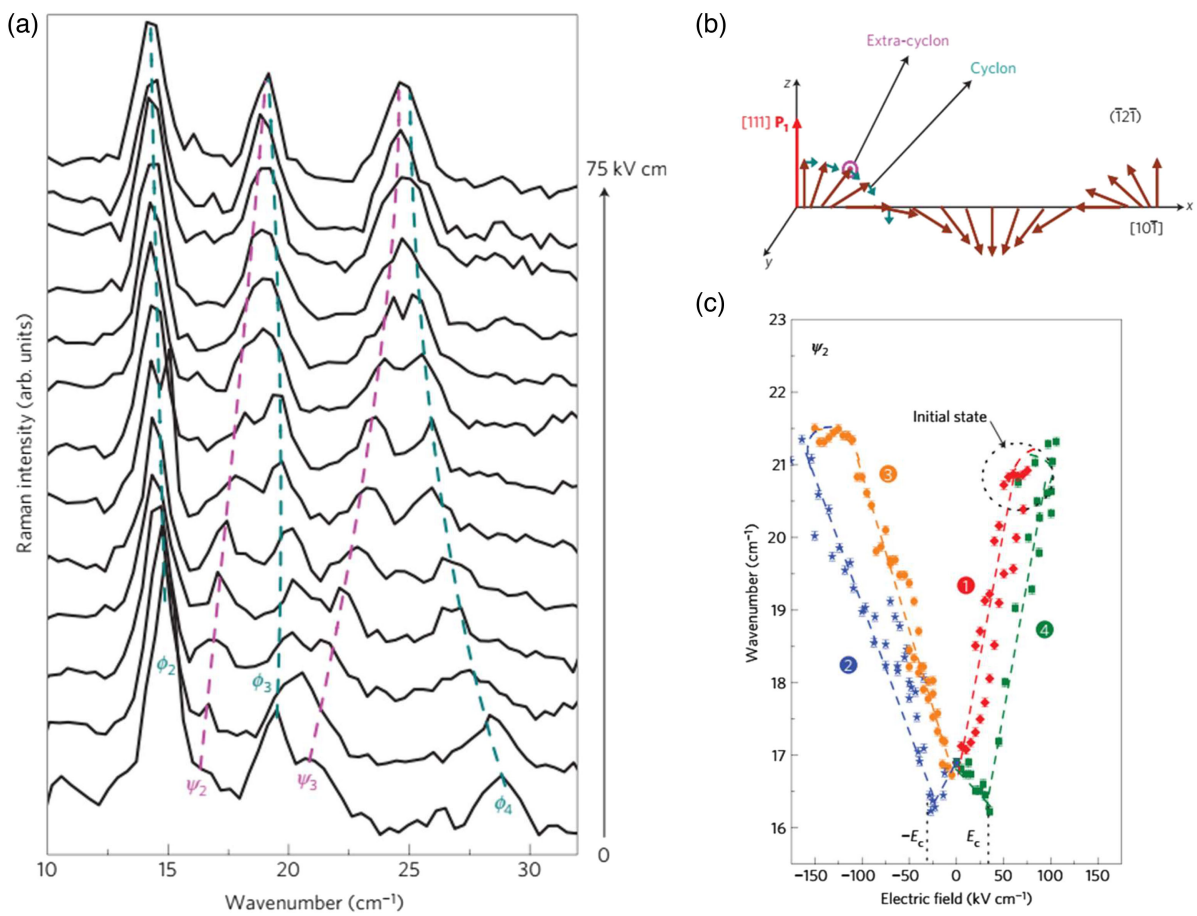


FIG. 24. (a) Raman spectra showing magnon modes (cyclon: $\phi_2$, $\phi_3$, and $\phi_4$; extracyclon: $\psi_2$ and $\psi_3$) in a $BiFeO_3$ single crystal for increasing electric fields. (b) Sketch of the magnon modes in the cycloidal order of $BiFeO_3$. (c) Electric-field dependence of the energy of $\psi_2$ showing a strong and hysteretic modulation. From Rovillain *et al.*, 2010.

(2010) evidencing magnon modes of the cycloidal spin order of a $BiFeO_3$ crystal. Series of modes (cyclon and extracyclon) are present due to zone folding. The energy of the modes can be strongly modulated by electric fields and in a hysteretic fashion.

$BiFeO_3$ provides a good model system to harness the electric-field control of magnons. The ferroelectric and antiferromagnetic domain structures in $BiFeO_3$ exhibit a one-to-one correspondence (Zhao *et al.*, 2006) and deterministic control of magnetic order via manipulation of the ferroelectric state (with applied electric fields) has already been demonstrated (Gross *et al.*, 2017; Haykal *et al.*, 2020). The transport of magnons in $BiFeO_3$ in a nonlocal geometry is shown schematically in Fig. 25. The devices consist of a metal with a large spin-orbit coupling, such as Pt, deposited on the magnet. One strip functions as injector and the other acts as detector. When a charge current $I$ is sent through the injector, the SHE (Hirsch, 1999) generates a transverse spin current; see Sec. III.A.3. A spin accumulation then builds up at the Pt/magnet interface. When its spin orientation is parallel (antiparallel) to the average magnetization, magnons are annihilated (excited), resulting in a nonequilibrium magnon population in the magnet. The nonequilibrium magnons diffuse in the magnet, giving a magnon current that propagates from injector to detector. At the detector, the reciprocal process occurs: magnons interact at the interface, flipping the spins of electrons and creating a spin imbalance in the Pt (Lebrun *et al.*, 2018). Owing to the ISHE, the induced spin current is converted into charge current, which under open-circuit conditions generates a voltage $V$. Figure 25(c) demonstrates a novel manifestation of magnetoelectric coupling in $BiFeO_3$ to manipulate the magnon current (Parsonnet *et al.*, 2022). Nonvolatile, hysteretic, bistable states of magnon current were observed with an applied electric field, indicating that the electric-field-induced switching results in changes to the magnon spin polarization pointing across the channel. Thus, in principle one should be able to sense the magnetic state of the multiferroic using this approach. However, to facilitate magnonic elements operating with a linear response at room temperature, the ideal signal pathway would be input electronic charge signal → electron spins → magnons → electron spins → output charge signal. This will require exploring thermal magnons via both the spin Seebeck effect and the isothermal spin accumulation mechanism.

While much remains to be understood about the fundamentals of magnon transport and its electric-field manipulation, the results of these studies point to a rich frontier of spin dynamics in such multiferroics. Of equal importance is the potential for such approaches to lead to larger inverse spin Hall voltages, perhaps through a thorough search for possible candidate materials (for instance, topological insulators, heavy transition-metal-based complex oxides with an exotic electronic band structure, such as $SrIrO_3$). Specifically, the fact that the antiferromagnetic state of the multiferroic can be directly read out using the ISHE means that a ferromagnetic layer to sense the antiferromagnetic state is not required. This should also help in eliminating the effects of interfacial degradation between the ferromagnet and the multiferroic oxide.

We expect dynamical effects in multiferroics to increase in importance in the coming years, driven by new experimental capabilities such as ultrafast x-ray sources (for example, Linac Coherent Light Source at Stanford Linear Accelerator Center, Stanford University), and the fundamental limits on the dynamics of spin-charge-lattice coupling phenomena

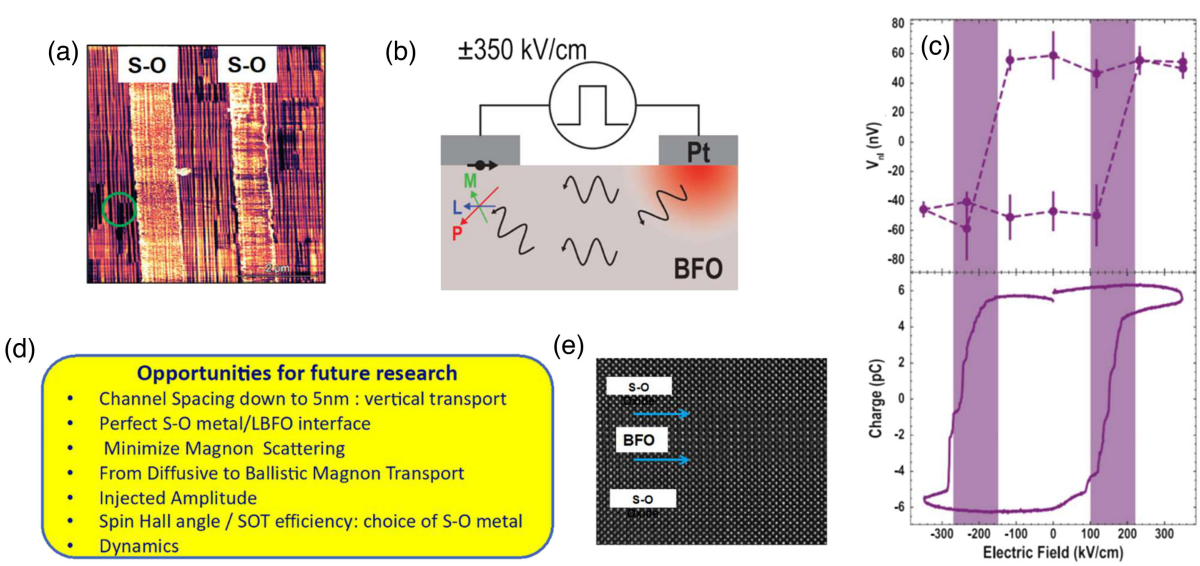


FIG. 25. (a) PFM image of a 100-nm-thick $BiFeO_3$ layer on a $DyScO_3$ substrate illustrating the typical 71° stripe domains. The two broad stripes notated as *S-O* are the metal layers (typically a metal with strong spin-orbit coupling such as Pt) that are used to probe the ISHE and spin Seebeck responses due to the propogation of magnons in the $BiFeO_3$ layer, as illustrated in (b). An electric field applied between these two metal strips enables the ferroelectric polarization state of $BiFeO_3$ to be switched. (c) Top panel: the nonlocal spin Seebeck voltage as a function of dc electric field applied to $BiFeO_3$. Lower panel: the corresponding ferroelectric switching. (d) Summary of some areas of research, specifically a focus on ballistic spin-magnon transport in epitaxial heterostructures such as the one shown in (e). From Parsonnet *et al.*, 2022.

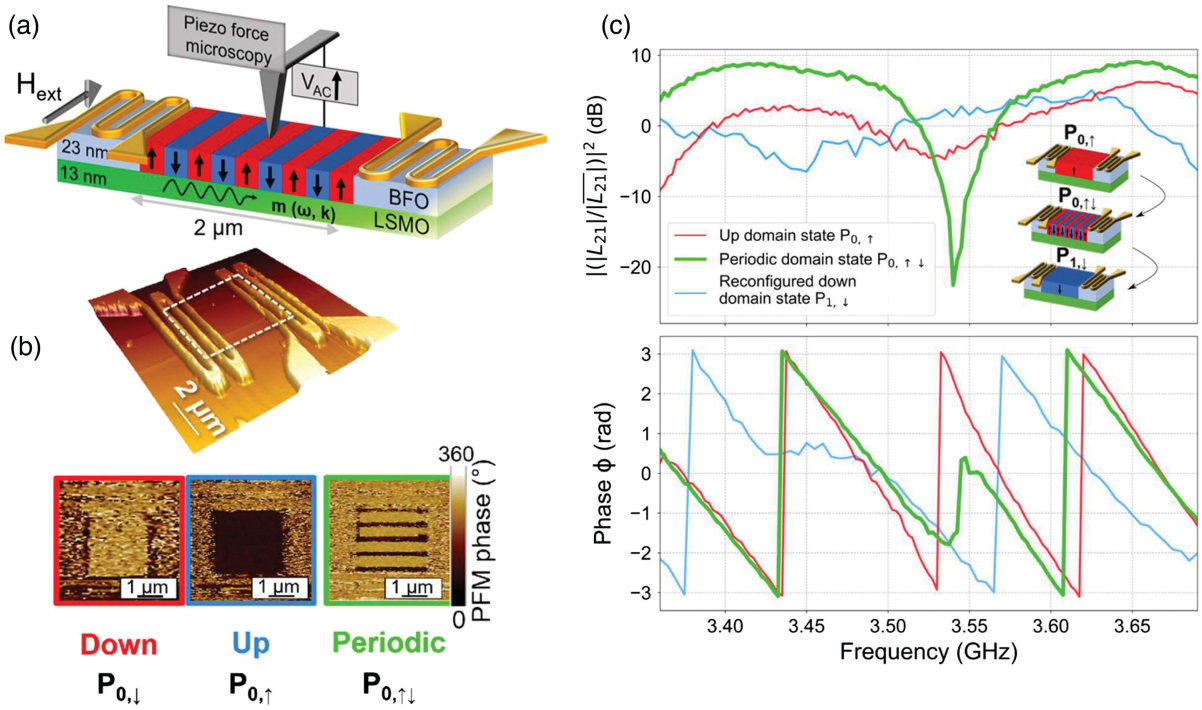


FIG. 26. Voltage-controlled reconfigurable magnonic crystal based on $BiFeO_3/La_{0.7}Sr_{0.3}MnO_3$. (a) Sketch of the setup in which spin waves are injected by an antenna and collected by the other with a 2 μm gap in between. The ferroelectric domains are read and controlled by PFM. (b) 3D view of the actual device and PFM phase images of the gap in three different polarization configurations: down (red), up (blue), and periodic (green) with a period of 500 nm. (c) Frequency dependence of the inductance (top panel) and the phase (bottom panel) showing a 20 dB rejection at 3.54 GHz for the periodically poled configuration (green lines) as well as an accident in the phase. From Merbouche *et al.*, 2021.

to be experimentally established. Theoretical proposals of dynamical multiferroic phenomena, in which a time-dependent polarization induces a magnetization in the reciprocal manner from that in which spin spirals induce polarization (Juraschek *et al.*, 2017), should be validated by careful experiments. At the same time, more work on antiferromagnetic resonance in multiferroics is required; while many studies were carried out in the 1960s and 1970s (Abraha and Tilley, 1996) on conventional antiferromagnets, such measurements with modern multiferroics, which typically have higher resonance frequencies, have been scarce. The recent surge in antiferromagnetic spintronics should be a welcome boost to such studies (Jungwirth *et al.*, 2016; Baltz *et al.*, 2018). In a similar vein, there appears to be a great opportunity for fundamental and applied studies of nonlocal measurements of spin transport and its electric-field manipulation (Lebrun *et al.*, 2018; Parsonnet *et al.*, 2022). We expect such approaches to be of significant scientific and technological interest in the next few years, especially if pathways to enhance the magnitude of the nonlocal spin Hall voltage are discovered.

In addition to static modulations of the exchange bias at $BiFeO_3/La_{0.7}Sr_{0.3}MnO_3$ interfaces, one might as well expect potential modulations of the spin dynamics of $La_{0.7}Sr_{0.3}MnO_3$ by the multiferroic. Merbouche *et al.* (2021) demonstrated that the transmission of spin waves across a 2 μm channel of $La_{0.7}Sr_{0.3}MnO_3$ can be modulated by the domain structure of the adjacent $BiFeO_3$ layer. The 13-nm-thick $La_{0.7}Sr_{0.3}MnO_3$ thin film was optimized on $NdGaO_3(001)$ in order to obtain low Gilbert damping values of the order of $6 \times 10^{-3}$ (Haspot *et al.*, 2022). The spin waves were probed in the Damon-Eshbach configuration by means of propagative spin wave spectroscopy (Merbouche *et al.*, 2021) [Fig. 26(a)]. Using PFM, the out-of-plane polarization of $BiFeO_3$ was electrically controlled in order to define a magnonic crystal structure [Fig. 26(b)]. While the homogeneous up and down states show similar transmission properties, the periodically poled pattern gives rise to a gap in the spin wave transmission at 3.54 GHz with more than 20 dB rejection [Figs. 26(c) and 26(d)]. This constitutes the first example of a nonvolatile electric-field-induced reconfigurable magnonic crystal based on $BiFeO_3$/ferromagnetic metal systems. Indeed, the entire field of antiferromagnetic spintronics and magnonics and electric-field-driven magnonics is worthy of a significantly deeper investigation, again within the perspective of low-energy manipulation of magnons as the principal carriers of information.

### 3. Ultrafast measurements of time-domain dynamics

Despite all of the prior work, switching a ferroelectric state (as well as a multiferroic state) with a voltage as small as 100 mV remains a challenge and a research opportunity. Work thus far with the La-$BiFeO_3$ system points to the possibility of switching timescales below 100 ps if the measurement circuit is fast enough. Since the electric field scales with the dimensions of the ferroelectric, progression toward switching voltages of 100 mV automatically requires either that the

switching field is low or that the switching behavior scales well with thickness. Therefore, it is critical to understand ferroelectric switching behavior in the ultrathin limit (<20 nm). Quantitative studies of the switching dynamics at such a thickness and at timescales of hundreds of picoseconds are still lacking and should be a fruitful area of research, especially on the experimental side. What are the limits to the switching speed of ferroelectrics and multiferroics? There has been speculation that one limit could be the acoustic phonon mode (i.e., the velocity of sound in the material) since the switching of the polar state involves the time-dependent deformation of the lattice, at least in such perovskite-based ferroelectrics. For nominal values of the velocity of sound in such oxides (a few km/s), this would suggest switching time of the order of a few tens of picoseconds. Thus, the role of lattice dynamics during the dipolar switching event needs considerable further work. This is also true of ferroelectrics: the strong coupling between the spontaneous dipole at the lattice immediately suggests that the dipolar switching dynamics in a thin film attached to a substrate will be strongly convoluted by the lattice dynamics. Recent *ab initio* and experimental studies of the switching dynamics of $BiFeO_3$ (Boyn *et al.*, 2017, 2018) indeed point to such a difference, which can be probed by studies of freestanding films compared to a film tethered to a substrate (Shi *et al.*, 2022). This substrate clamping effect on the lattice dynamics can be mitigated by reducing the lateral dimensions of the magnetoelectric element such that it is essentially unclamped (Nagarajan *et al.*, 2003). Measuring at such timescales requires fast electronics (for example, pulse generators with rise times smaller than a few tens of picoseconds and oscilloscopes that can capture the switching transients at commensurate speeds). Thus, it is not surprising that there have been only a few measurements of the polarization switching dynamics approaching such timescales (Li *et al.*, 2004). This is true for both ferroelectrics and multiferroics (Parsonnet *et al.*, 2020), and as we move forward into this interesting field of electric-field-controlled magnetic devices such studies are critically needed.

## III. CONTROL OF MAGNETISM BY CURRENT-INDUCED TORQUE

The main tool for the control of magnetism by current is the spin-transfer mechanism introduced by Berger (1996) and Slonczewski (1996), that is, the transfer of the spin angular momentum and associated magnetization carried by a spin-polarized current (a spin current) to the magnetization of the magnet. This topic has been exhaustively reviewed; see Ralph and Stiles (2008) (for the case in which the spin current is generated by a magnet) and Manchon *et al.* (2019) (for the case in which the spin current is generated by a system with spin-orbit coupling). Here we focus on the main experimental results, highlighting the potential applications of current-induced torques.

### A. Spin currents

We first describe the different types of spin currents and the different ways used to produce them, as summarized in Fig. 27.

#### 1. Spin-polarized current in a magnetic conducting material

The first way to produce a spin current is simply the exploitation of the two-current conduction (Mott, 1936; Fert and Campbell, 1968) in a magnetic (ferromagnetic or

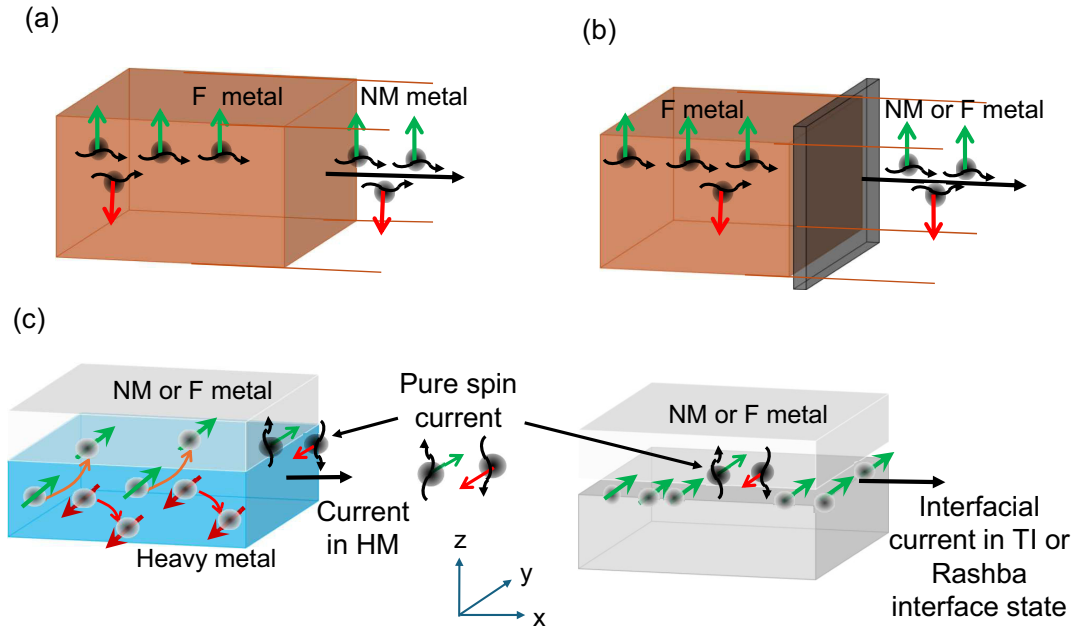


FIG. 27. Spin currents. Spin-polarized currents (a) flowing inside a magnetic ($F$) metal and (b) tunneling from this material. At the interface with a nonmagnetic (NM) metal, the spin polarization extends with an exponential decrease in the range of the spin diffusion length. (c) For current along $x$, emission along $z$ of a pure spin current into a magnetic or nonmagnetic layer by the SHE in a heavy metal (HM) (left panel) and by diffusion from an Edelstein polarization in the surface or interface states of a topological insulator (TI), Dirac semimetal, or Rashba 2DEG (right panel).

ferrimagnetic) material with different currents carried by the electrons having their spin parallel or opposite to the magnetization (spin down and spin up), as represented in Fig. 27(a). We call this type of current a spin-polarized current. At the interface of the magnetic material with a nonmagnetic conductor and for both directions of the current, the spin polarization extends with an exponential decay into the nonmagnetic material at a distance from the interface that is called the spin diffusion length ($\lambda_{sf}$) (Johnson and Silsbee, 1985; Valet and Fert, 1993; Takahashi and Maekawa, 2008).

#### 2. Spin-polarized current tunneling from a magnetic material

A current tunneling from a ferromagnetic or ferrimagnetic material into another material is also spin polarized, as represented in Fig. 27(b), which is exploited in the TMR of the MTJs (Julliere, 1975; Miyazaki and Tezuka, 1995; Moodera *et al.*, 1995; Butler *et al.*, 2001; Mathon and Umerski, 2001). In the approximation of the Julliere model (Julliere, 1975), the spin polarization of the current tunneling from a magnetic material into a nonmagnetic material simply reflects the spin polarization of the density of states at the Fermi level in the magnetic material. However, in the actual situation, the spin polarization of the spin current can also depend on the filtering of different types of wave functions by the material of the tunnel barrier (De Teresa *et al.*, 1999; Mavropoulos, Papanikolaou, and Dederichs, 2000; Butler *et al.*, 2001; Mathon and Umerski, 2001; Oleinik, Tsymbal, and Pettifor, 2001; Zhang and Butler, 2004). Actually, such filtering effects have been exploited to obtain high spin polarizations of the tunneling current and large TMRs Parkin *et al.* (2004) and Yuasa *et al.* (2004).

#### 3. Conversion between charge and spin currents by the spin Hall effect and the spin anomalous Hall effect: Pure spin currents

The SHE of a nonmagnetic material, for example, a heavy metal with large spin-orbit coupling, is related to the spin-orbit-coupling-induced deflection of the electrons of opposite spins in opposite directions (D'yakonov and Perel', 1971; Hirsch, 1999; Kato *et al.*, 2004; Valenzuela and Tinkham, 2006, 2007; Hoffmann, 2013). In the example in Fig. 27(c) with a charge current along $\hat{x}$, the electrons with spins along $\hat{y}$ ($-\hat{y}$) are deflected upward (downward) along $\hat{z}$. This leads to what is called a pure spin current and what can be described as the combination of opposite flows of electrons with opposite spins. In isotropic materials, the SHE is characterized by the spin Hall angle $\theta_{SHE}$. Quantitatively, in an infinite material and for spin-current emission along $+\hat{z}$ generated by a charge current in the $x$-$y$ plane, a charge-current density $J_c$ flowing in the direction of the unit vector $\hat{j}$ emits along $\hat{z}$ a pure spin-current density $J_s$ polarized along

$$\hat{\boldsymbol{\sigma}} = \pm(\hat{\boldsymbol{j}} \times \hat{\boldsymbol{z}}), \tag{1}$$

i.e., $\pm\hat{\boldsymbol{y}}$ for $\hat{\boldsymbol{j}}$ along $\hat{\boldsymbol{x}}$ in Fig. 27(c), depending on the sign of $\theta_{SHE}$. If the charge- and spin-current densities are defined as the respective flows of positive charges $-e$ and unit spins, $J_s$ and $J_c$ are related by $J_s = \theta_{SHE} J_c$. Typical values of $\theta_{SHE}$ are, for example, 0.06 for Pt, 0.15 for Ta, and 0.3 for W (Liu *et al.*, 2012; Pai *et al.*, 2012; Hoffmann, 2013; Rojas-Sánchez *et al.*, 2014).

In an isolated layer, the SHE leads to an accumulation of opposite spin at opposite interfaces. With a conducting layer covering the layer of a heavy metal with the SHE, as represented in the left panel of Fig. 27(c), the accumulation of spin along $+\hat{\boldsymbol{y}}$ (in the figure) diffuses into the top layer, the charge neutrality condition leads to an attraction of spin $-\hat{\boldsymbol{y}}$, and this situation is described as an injection of a pure spin-current density $J_s$ into the neighbor material. The amplitude of the injected spin current depends on the transparency of the interface and also on the possibility of large enough spin absorption (i.e., short enough $\lambda_{sf}$) to limit the spin accumulation in the neighbor material and the resulting repulsion of the injected spins (that is, to prevent reflection of the spin current). In the best conditions, i.e., transparent interface and large enough absorption of the injected spins, the injected spin current keeps approximately its value $\theta_{SHE} J_c$ in the heavy metal.

Spin currents are also generated by current in ferromagnetic or ferrimagnetic materials. Until recently it was supposed that, due to exchange interactions being much stronger than spin-orbit interactions, the transverse component of a spin-orbit-coupling-induced spin current was completely dephased by exchange-induced precessions and its spin polarization was aligned with the magnetization. What remains is the so-called spin anomalous Hall effect (SAHE) with a spin current polarized along the magnetization direction $\hat{\boldsymbol{m}}$ (Taniguchi, Grollier, and Stiles, 2015; Iihama *et al.*, 2018). In an infinite material and for the spin current along $\hat{z}$ generated by a charge current in the $x$-$y$ plane, a charge-current density $J_c$ flowing in the direction of the unit vector $\hat{j}$ emits along $\hat{z}$ a spin-current density $J_s$ polarized along $\hat{m}$ with

$$J_s = \theta_{SAHE}[(\hat{j} \times \hat{m}) \cdot \hat{z}] J_c, \tag{2}$$

where $\theta_{SAHE}$ is the spin anomalous Hall angle.

However, more recent theoretical works by Amin *et al.* (2019), Amin, Haney, and Stiles (2020), and Kim and Lee (2020) showed that the alignment of the spin-orbit-coupling-induced spin current with the magnetization direction is incomplete in most magnetic materials. This gives rise to the coexistence of SAHE-type and SHE-type spin currents. This coexistence was shown in the experiments of Das *et al.* (2017) and was also found in other recent works (Baek, Amin *et al.*, 2018; W. Wang *et al.*, 2019; Liu *et al.*, 2020). In particular, the experiments of Céspedes-Berrocal *et al.* (2021) showed that for GdFeCo ferrimagnetic alloys the $5d$ character of the Gd electrons leads to particularly large currents of SHE and SAHE symmetries coexisting with the respective spin Hall angles $\theta_{SHE} \approx 0.16$ and $\theta_{SAHE} \approx 0.6$.

The generation of a pure spin current from a charge current by the SHE or SAHE can be described as a conversion of a charge current into a spin current. Inversely, in another type of experiment, a spin current injected into a material (say, a heavy metal) can be converted into a charge current in the heavy metal by the ISHE, as expected from Onsager reciprocity (Kimura *et al.*, 2007). Typical examples with the ISHE of Pt can be found in the literature (Hahn *et al.*, 2013;

Hoffmann, 2013; Rojas-Sánchez *et al.*, 2014; Sinova *et al.*, 2015; Sagasta *et al.*, 2016).

#### 4. Conversion between charge and spin current by spin-orbit coupling in surface or interface states

Charge currents flowing in or scattered by surface and interface states can generate spin currents (Amin, Zemen, and Stiles, 2018). Here we describe only the generation of spin currents by the Edelstein effect (EE) in topological surface states or Rashba states (Edelstein, 1990; Zhang *et al.*, 2014; Kondou *et al.*, 2016; Han, Otani, and Maekawa, 2018; Manchon *et al.*, 2019).

Figure 28(a) displays the classical image of the Dirac cone of topological 2D states at the surface or interface of 3D topological insulators or Dirac semimetals (Hasan and Kane, 2010; Pesin and MacDonald, 2012; Rogalev *et al.*, 2017). The corresponding Fermi contour is shown in Fig. 28(b) and is characterized by the locking between spin and momentum represented in the figure. In a similar way, the Rashba interaction generated by spin-orbit coupling and inversion symmetry breaking at surfaces or interfaces (Rashba, 1960; Baek, Amin *et al.*, 2018) leads to the type of dispersion surfaces shown in Fig. 28(c), which gives the two Fermi contours with different radii and opposite spin-momentum locking shown in Fig. 28(d). As represented in Fig. 28(e), a current flowing in a topological surface or interface state generates an overpopulation of spin oriented in a transverse direction with respect to the current and a depletion of the opposite spins. This is the Edelstein spin polarization induced by current in the surface states (Edelstein, 1990). If the topological 2D states are at an interface with a conducting material, the spin accumulation diffuses through the interface and a pure spin-current density $J_s$ with polarization perpendicular to the 2D charge current is injected into the adjacent material (Kondou *et al.*, 2016; Han, Otani, and Maekawa, 2018). For a current flowing in a Rashba two-dimensional electron gas (2DEG), a similar mechanism with a partial compensation of the opposite contributions from the two Fermi contours also leads to a similar production of spin current [Fig. 28(g)]; see Rojas-Sánchez *et al.* (2013), Amin *et al.* (2019), and Manchon *et al.* (2019).

In situations of both topological insulators and Rashba interfaces, the conversion of a 2D charge current into a 3D pure spin current can be characterized by the parameter $q_{\mathrm{ICS}}$

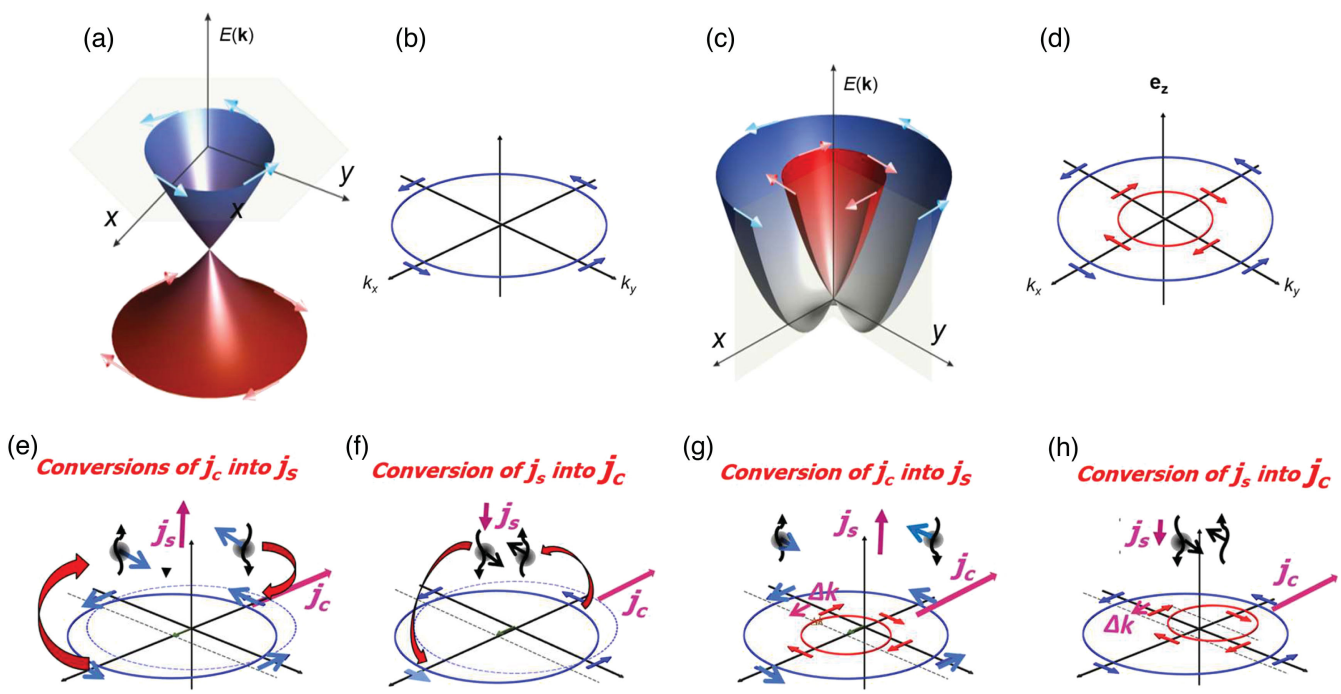


FIG. 28. (a) Sketch of the electronic energy dispersion surfaces in the surface states of a topological insulator (Dirac cone). (b) Fermi contour at constant energy illustrating the spin-momentum locking. At any $k$ position on the contour, the spin is perpendicular to $k$. (c) Electronic dispersion surfaces of a Rashba system. (d) In contrast to the case of topological insulators, here the systems comprises two Fermi contours. On each the spin is locking perpendicular to $k$ for the spins both curling clockwise in one contour and curling counterclockwise in the other contour. (e) Charge-to-spin conversion with a topological insulator. The application of a charge current $J_c$ along $-x$ causes a shift of the Fermi contour and generates an extra population of states with spin along $y$. This generated spin density can then diffuse vertically as a spin current $J_s$. (f) Spin-to-charge conversion with a topological insulator. Spins oriented along $y$ injected into the topological insulator populate states with momentum along $x$ (which is accompanied by the ejection of spins oriented along $-y$ from states with momentum along $-x$), causing an overall shift of the Fermi contour and thus the generation of charge current along $-x$. (g) Charge-to-spin conversion in a Rashba system. The situation is similar to that in (e) except that spin densities with opposite spin polarizations are generated by the injected charge current for the inner and outer contours. However, they do not compensate, yielding the generation of a finite spin density that may diffuse vertically as a spin current. (h) Spin-to-charge conversion in a Rashba system. Again the situation is similar to that in (f), but here the injection of spins causes shifts of the Fermi contours in opposite directions, albeit without a full compensation, which results in the generation of a finite charge current.

(in $m^{-1}$) introduced for topologically protected surfaces by Kondou *et al.* (2016) and relating the 3D spin-current density $J_s^{3D}$ (in $A/m^2$) to the 2D charge-current density $J_c^{2D}$ (in A/m) as follows:

$$J_s^{3D} = q_{ICS} J_c^{2D} \tag{3}$$

with experimental results corresponding to values of $q_{ICS}$ in the $nm^{-1}$ range (Kondou *et al.*, 2016; Khang, Ueda, and Hai, 2018).

The reverse conversion by the inverse Edelstein effect (IEE) can be understood from Figs. 28(f) and 28(h): the injection of a pure spin current into topological or Rashba 2D states leads to an overpopulation of occupied states on one side of the Fermi contour and to a depletion on the other side, that is, to a charge current flowing in the 2D states. In other words, there is a conversion between an injected 3D spin current and a 2D charge current in the 2DEG at the surface or interface. For Rashba Fermi contours, there is only a partial compensation between the two contours and the same type of spin-to-charge conversion exists. In both cases, the conversion of a 3D spin-current density into a 2D charge-current density by the IEE is characterized by a length $\lambda_{IEE} = J_c^{2D}/J_s^{3D}$ with values in the nanometer range or exceeding 10 nm (Rojas-Sánchez *et al.*, 2013, 2016; Shiomi *et al.*, 2014; Isasa *et al.*, 2016; Lesne *et al.*, 2016; Varignon *et al.*, 2018; Vaz *et al.*, 2019; Sanz-Fernández *et al.*, 2020; Pham *et al.*, 2021; Vicente-Arche *et al.*, 2021).

We now compare the spin currents generated by the EE to those produced by the SHE of a heavy metal (Rojas-Sánchez and Fert, 2019). For the SHE, in optimal conditions with transparent enough interfaces, the transferred spin-current density $J_s^{3D}$ is simply related to the charge-current density $J_c^{3D}$ in the SHE layer by the following expression (Liu *et al.*, 2011; Kim *et al.*, 2014):

$$J_s^{3D} = \theta_{SHE}[1 - \mathrm{sech}(t/\lambda_{sf})] J_c^{3D}, \tag{4}$$

where $t$ and $\lambda_{sf}$ are the thickness and the spin diffusion length of a heavy metal. Expressing the current in the heavy metal in terms of a 2D charge-current density $J_c^{2D} = tJ_c^{3D}$, one finds from Eq. (4) that the maximum value of the ratio $J_s^{3D}/J_c^{2D}$ [to be compared to $q_{ICS}$ in Eq. (3)] is obtained for $t \cong 1.5\lambda_{sf}$ and is expressed by $q_{SHE} = 0.38(\theta_{SHE}/\lambda_{sf})$. With typical values of $\theta_{SHE}$ and $\lambda_{sf}$ in the respective ranges of 10% and a few nanometers, one finds values of $q_{SHE}$ smaller than $10^{-1}$ $nm^{-1}$, which is more than 1 order of magnitude below that of the $q_{ICS}$ of the EE in 2DEGs (Rojas-Sánchez and Fert, 2019). Larger spin currents are thus expected from the EE at surface or interface 2DEGs than from the SHE at 3D layers, which is in agreement with the experimental results on switching by SOT that we later discuss.

For the opposite conversion from spin to charge, comparisons between experimental values of the conversion coefficient $\lambda_{IEE}$ for various topological insulators or Rashba surface or interface states and the effective conversion coefficient $\lambda_{SHE} = \theta_{SHE}\lambda_{sf}$ of heavy metals; see Table I of Rojas-Sánchez and Fert (2019). The coefficient $\lambda_{IEE}$ of topological insulator or Rashba surface or interface states can be larger than the effective $\lambda_{SHE}$ of heavy metals by 1 or 2 orders of magnitude.

#### 5. Spin currents in insulating materials

In insulating magnetic materials, spin currents can be carried by magnons (Khitun, Bao, and Wang, 2010; Chumak *et al.*, 2015; Lebrun *et al.*, 2018; Han, Maekawa, and Xie, 2020). Such spin currents carried by magnons in a magnetic insulator layer can be electrically generated by a spin current carried by conduction electrons in a metallic layer via the spin accumulation at the interface. The conversion between metallic spin current and magnon spin current is controlled by the interfacial spin-mixing conductance (Heinrich *et al.*, 2011; Qiu *et al.*, 2013). Typical examples are the direct and inverse conversions between conduction electron spin currents in heavy metals and magnon spin currents in $Y_3Fe_5O_{12}$- (YIG-) based magnetic insulators (Qiu *et al.*, 2013; Shao *et al.*, 2018); see also Sec. II.F.1.

### B. Spin transfer, spin-transfer torques, and magnetization switching by STT

The concept of spin transfer and STT introduced by Berger (1996) and Slonczewski (1996) is illustrated schematically in Fig. 29(a) for the typical case of 3*d* ferromagnetic metals with ferromagnetic layers $F1$ and $F2$ separated by a nonmagnetic layer, either a tunnel barrier such as MgO or a nonmagnetic metal such as Cu. A spin-polarized current is prepared by $F1$ to obtain, in the spacer layer, a spin polarization obliquely oriented with respect to the vertical magnetization of the second magnetic layer $F2$ (the spin polarization in the spacer layer is not simply the polarization of the current inside $F1$, and generally is intermediate between the polarizations of $F1$ and $F2$). When this current enters $F2$, the exchange interactions with the local spins induce precessions of the transverse component of the injected spins around the magnetization axis of $F2$, and the dephasing of these precessions by the distribution of the exchange interactions makes the global transverse polarization disappear. As the exchange interaction is spin conserving, this dephasing corresponds to an absorption of the transverse component of the spin current. The absorption is complete after penetration beyond the so-called spin dephasing length, which is generally of the order of 1 or a few nanometers (or incompletely absorbed if the thickness of the magnetic layer is smaller than the dephasing length). In the first situation of a thick enough layer, if the spin-lattice relaxation by spin-orbit coupling can also be neglected, the total transverse spin component lost by the current is transferred to the total spin of $F2$. This can also be described as a STT acting on $F2$ and given by the following expression as a function of the unit vectors $\hat{m}$ along the magnetization of the magnetic layer and $\hat{\sigma}$ along the spin polarization of the injected current:

$$T_{STT} = \tau_{DL}[\hat{m} \times (\hat{m} \times \hat{\sigma})] + \tau_{FL}(\hat{m} \times \hat{\sigma}). \tag{5}$$

The first and main term, the dampinglike torque, is a direct consequence of the spin-transfer mechanism and the coefficient $\tau_{DL} = (\hbar/2e)J_s^{abs}$ for the torque by spin area can be

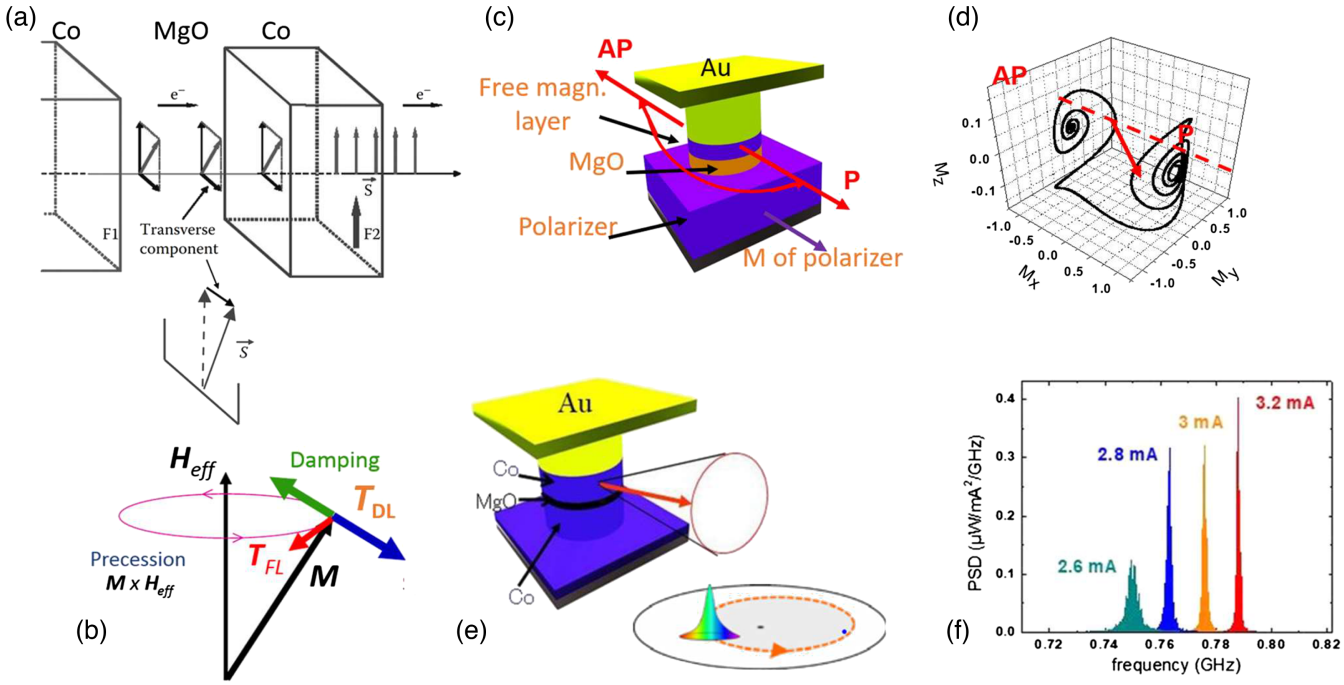


FIG. 29. (a) Concept of spin-transfer torque. A spin-polarized current (prepared by a magnetic material $F1$) is injected through a nonmagnetic layer (tunnel barrier or metal) into the magnetic material $F2$. Inside $F2$, exchange-induced precessions dephase the transverse components of injected spins and lead to a transfer of the transverse component of the injected spin current into $F2$ or, equivalently, to a torque on its magnetization. (b) Schematic of the dampinglike and fieldlike torques on a magnetization $M$ departing from its equilibrium orientation along $H_{\rm eff}$ and precessing around $H_{\rm eff}$ in the situation in which the dampinglike torque is the opposite of the LLG damping torque and enlarges the precessions. (c),(d) Switching by STT: In (d), macrospin simulation of the switching of the device in (c) from parallel (P) to antiparallel (AP) by the STT induced by the injection of a vertical spin current from the polarizer into the free layer. (e) Magnetization dynamics for a device of the type in (c) in the regime in which the STT generates a steady state gyration of the magnetization in the free layer (or a gyration of a magnetic vortex in the free layer; see the inset displaying the vortex core and its trajectory shown as a dashed line). (f) Experimental example of microwave power emission generated by vortex gyration. (a)–(e) Adapted from Fert and Van Dau, 2019. (f) From Dussaux *et al.*, 2010.

directly related to the density of the absorbed spin current $J_s^{\rm abs}$. Figure 29(b) shows that, for the magnetization precessing around its equilibrium direction, the dampinglike torque is in the same direction as the damping torque of the Landau-Lifshitz-Gilbert (LLG) equation and acts to reduce or enhance the damping. For theoretical expressions of the dampinglike torque with different types of injectors and as a function of the interfacial coefficient called spin-mixing conductance, see Stiles and Zangwill (2002) and Barnaś *et al.* (2005). The second term in Eq. (5) is the fieldlike torque, a corrective term generally much smaller than the dampinglike torque, related to the exchange field generated by the injected spin polarization (Zhang, Levy, and Fert, 2002) and to the imaginary part of the spin-mixing conductance (Barnaś *et al.*, 2005).

The first experimental evidence was obtained using either point contacts or pillar-shaped devices [Fig. 29(c)] in which the STT created by the spin-polarized current emitted by the thick reference magnetic layer (polarizer) can switch the magnetization of the thin free magnetic layer between the parallel (P) and antiparallel (AP) orientations of the two layers (Tsoi *et al.*, 1998; Albert *et al.*, 2000; Grollier *et al.*, 2001). A macrospin simulation of the progressively extended precessions and switching of the magnetization of the free layer is also shown in Fig. 29(d). A small switching current is obtained when the coefficient $\alpha$ characterizing the damping torque in the LLG equation and the energy barrier between the P and AP states are small. In a second type of regime in the same device, the STT can be used to generate magnetic excitations in the free layer, steady state precession of the magnetization or gyrations of a magnetic vortex, which leads to ac voltage via TMR or GMR and microwave power emission [Figs. 29(e) and 29(f)].

As far as applications are concerned, the appearance of STT has boosted the development of MRAMs, which are called STT MRAMs for those using STT. Since their first demonstrations in the mid 2000s (Hosomi *et al.*, 2005), STT MRAMs have been frequently described as potential universal memories having arguments to compete with all of the main types of electronic memories. Recently, several major companies started a large production of STT MRAMs (McGrath, 2021; Mearian, 2021). SOT MRAMs, which were based on the SOT discussed in Sec. III.C, have promise to assume prominence, with, in particular, great progress in terms of speed. The second type of interesting application is the spin-torque nano-oscillator in microwave technologies.

### C. Spin-orbit torques and magnetization switching by SOT

#### 1. General metallic magnetic materials

SOTs are the torques induced by the transfer of spins from a spin current $j_s^{3D}$ generated by spin-orbit coupling (Manchon *et al.*, 2019; Shao *et al.*, 2021). Such spin currents can be generated by the SHE of a material of large spin-orbit coupling (such as Pt or Ta), by the SAHE of a ferromagnetic material, or by the EE in topological or Rashba surface or interface states. In the most general case (rotational invariance around the out-of-plane axis), the torque acting on the magnetization of unit vector $\hat{m}$ has the same form as the STT of Eq. (5) and includes dampinglike and fieldlike torques,

$$T_{\mathrm{SOT}} = T_{\mathrm{DL}} + T_{\mathrm{FL}} = \tau_{\mathrm{DL}}[\hat{m} \times (\hat{m} \times \hat{\sigma})] + \tau_{\mathrm{FL}}(\hat{m} \times \hat{\sigma}), \quad (6)$$

where $\hat{\sigma}$ is the unit vector along the polarization of the current injected into the magnetic layer. For both the SHE and the EE and for a current along $\hat{x}$, $\sigma$ is along $+\hat{y}$ or $-\hat{y}$, depending on the sign of $\theta_{\mathrm{SHE}}$ or $q_{\mathrm{ICS}}$ and, for SHE, on the direction of emission (positive or negative). We show in Fig. 30(a) for the SHE [Fig. 30(b) for the EE] an example of the orientation of dampinglike and fieldlike torques where there is out-of-plane magnetization.

The dampinglike torque is generated by the Slonczewski mechanism of transfer of the spin momentum injected into the magnetic material and, as in the STT case, is related to the density of the absorbed spin current. When the spin current is injected from a SHE material, the dampinglike torque is generally predominant and the fieldlike torque is a small corrective term due to exchange interactions between $m$ and the spin accumulation introduced into the magnetic layer (Zhang, Levy, and Fert, 2002). When the spin source is a Rashba polarization at an interface of the magnetic material itself and directly interacting by exchange with its magnetization, the fieldlike torque is generally larger, but the dampinglike torque due to the diffusion of a spin current from the Rashba interfacial polarization can also be large if this spin current is efficiently transferred out of the magnetic layer.

The dampinglike and fieldlike torque (in units of $\mathrm{eV/m^3}$) can be expressed as

$$T_{\mathrm{DL}} = \frac{\hbar}{2e}\xi_{\mathrm{DL}}^{j}\frac{J_c}{t_F}\hat{m} \times (\hat{m} \times \hat{\sigma}), \quad (7)$$

$$T_{\mathrm{FL}} = \frac{\hbar}{2e}\xi_{\mathrm{FL}}^{j}\frac{J_c}{t_F}(\hat{m} \times \hat{\sigma}), \quad (8)$$

where $t_F$ is the thickness of the magnetic layer. The coefficients $\xi_{\mathrm{DL(FL)}}^{j}$ express the efficiencies of the conversion of a charge-current density $J_c$ into the spin-current density $J_s$ transformed into torque. Detailed expressions of $\xi_{\mathrm{DL}}^{j}$ as a function of the conversion coefficients $\theta_{\mathrm{SHE}}$ (for SHE) or $q_{\mathrm{ICS}}$ (for EE), the interfacial transmission coefficients called

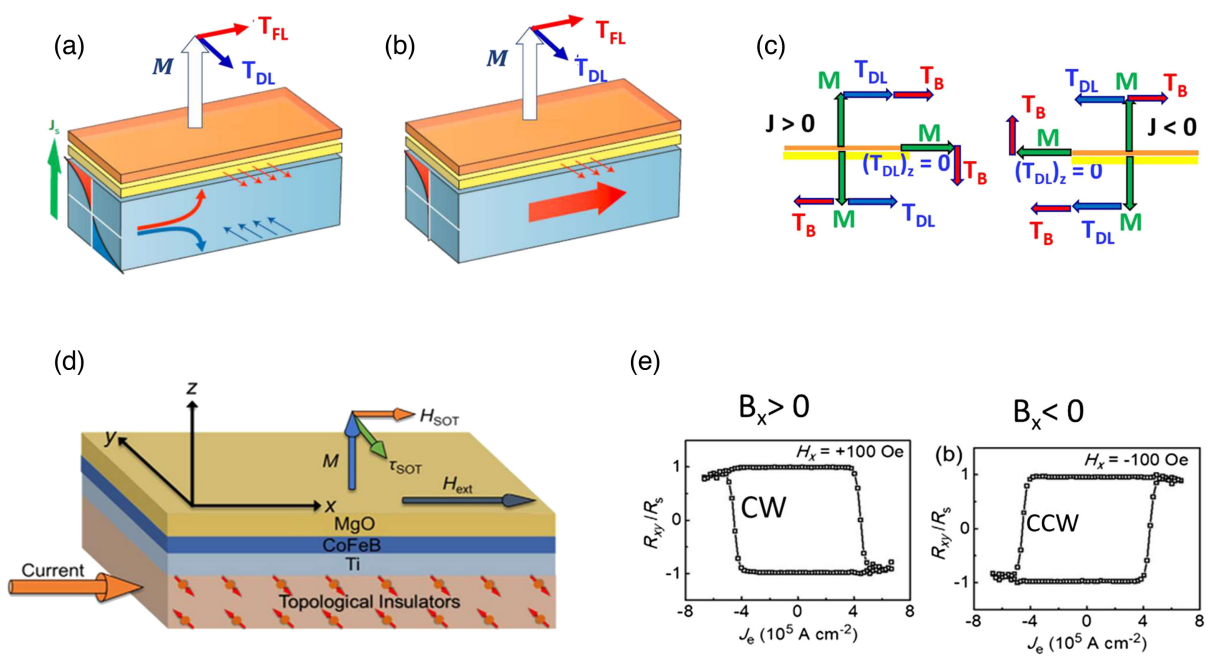


FIG. 30. (a) Dampinglike ($T_{\mathrm{DL}}$) and fieldlike ($T_{\mathrm{FL}}$) SOTs induced by spin currents (polarizations indicated with small arrows) due to SHE in a heavy metal and (b) EE in a Rashba or topological 2DEG. (c) Switching in the macrospin limit is used to illustrate the symmetry of the reversal of perpendicular magnetization under the additive actions of $T_{\mathrm{DL}}$ and torque $T_B$ induced by an applied field along the current direction. Left panel: graphic showing that, for $J > 0$, $T_B$ helps $T_{\mathrm{DL}}$ to reverse $M$ from up to down, especially midway when $M$ is in plane and $T_{\mathrm{DL}} = 0$, regardless of the orientation of $M$ in the plane. Right panel: same applied field with $J < 0$ for a reversal from down to up and a clockwise loop. Reversing the applied field leads to a counterclockwise loop. (d),(e) In the device shown in (d), (e) shows the switching loops of the ferromagnetic CoFeB layer magnetization under the conjugated actions of the spin current generated by the EE in the surface state of the topological insulator $(\mathrm{BiSb})_2\mathrm{Te}_3$ and an applied field $B_x$ in the current direction. The switching loops, which are detected using the anomalous Hall effect, are clockwise for $B_x > 0$ or counterclockwise for $B_x < 0$. From Wu *et al.*, 2019.

spin-mixing conductances, and the spin diffusion lengths $\lambda_{sf}$ in the different layers can be found in several publications (Pai *et al.*, 2015; Seung *et al.*, 2017; Manchon *et al.*, 2019). In the case of spin emitted by SHE from a heavy metal and generating a torque in another material, the efficiency coefficient $\xi^j_{DL}$ can be seen as an effective $\theta_{SHE}$ characterizing the finally transferred spin current. Its maximum value for optimal transmission is the intrinsic $\theta_{SHE}$ of the heavy metal. When 2D surface or interface states of a layer generate spin currents from 2D charge currents, the usual simplified picture is that of a layer with only SHE and a uniformly distributed effective $\theta_{SHE}$ taking into account, approximately, both the bulk and surface effects. In this situation, $\xi^j_{DL}$ can be larger than 1, as it is observed with efficient spin emission by Rahba or topological surface or interface states. The expressions are more complex for $\xi^j_{FL}$ as they also depend on the exchange interaction between spin accumulation and magnetization.

Alternatively, the SOT of Eqs. (7) and (8) can be rewritten in terms of SOT-induced effective fields $B_{DL}$ and $B_{FL}$ inducing the dampinglike and fieldlike torques on the magnetization,

$$T_{DL,FL} = m \times B_{DL,FL}. \tag{9}$$

As pointed out, the expressions of SOT Eqs. (7) and (8) are for rotational invariance around the out-of-plane axis, that is, for the most frequent situation where the spin source is a polycrystal. A material of lower symmetry for the spin source leads to more complex expressions of SOT (Garello *et al.*, 2013). An experimental example of the complex symmetry of dampinglike torque is given by the SOT generated by $WTe_2$, in which the surface crystal structure has only one mirror symmetry and no twofold rotational invariance (MacNeill *et al.*, 2017). Another example of low-symmetry SOT was given by L. Liu *et al.* (2021). They showed that the symmetry at the $L1_1$-ordered interface of a CuPt/CoPt epitaxial bilayer gives rise to out-of-plane SOT and makes it possible to switch the out-of-plane magnetization of CoPt in zero applied field with a threefold angular dependence of the switching.

#### 2. Magnetization switching by SOT

The realization of current-induced magnetization switching by SOT is a promising direction for the development of SOT MRAMs and the relay to the STT MRAMs in production today. In particular, the high speed of the switching of layers with perpendicular magnetic anisotropy (PMA) by the dampinglike torque is especially appealing. This is the type of switching that we describe and discuss in the main part of this section.

Experimental examples of switching of magnetic layers with PMA by SOT are displayed in Fig. 30(e) in both situations of spin current induced by the SHE in a heavy metal and the EE in the surface states of a topological insulator. The schematics in Figs. 30(a) and 30(b) indicate the spin polarization of the spin currents injected into the top magnetic layer by the SHE in heavy metal [Fig. 30(a)] or the EE in 2DEG [Fig. 30(b)] and the orientation of the SOTs [from Eqs. (7) and (8)] acting on a vertical magnetization. The dampinglike torque does not break the symmetry between the up and down states, and the switching between these states is only possible by adding an applied field along the current direction, as can be understood in the macrospin model of Fig. 30(c). With a positive current and an applied field $B_x > 0$, the additive actions of the dampinglike torque and field-induced torque allow the magnetization to switch from up to down because the field-induced torque is nonzero when the SOT is zero at midway from up and down. The demand for an in-plane field can be justified more generally by symmetry arguments for systems with rotational symmetry around the axis perpendicular to the layers (Manchon *et al.*, 2019). SOT switching of PMA layers in the presence of an applied field is also the usual observation when the switching process is by nucleation and extension of domains with opposing magnetization (Baumgartner *et al.*, 2017; Figueiredo-Prestes *et al.*, 2021).

In the experimental examples of Figs. 30(d) and 30(e) (topological insulator as the source of SOT) and Figs. 31(c)–31(f) (heavy metal as the source of SOT), an in-plane field along the current direction is necessary to switch the magnetization and leads to either clockwise or counterclockwise magnetization cycles, depending on the direction of the applied field with respect to the current direction. Similar behavior is also found when the magnetic layer is a magnetic insulator in which the spin current emitted by the SHE or EE cannot flow but can be transmitted by magnetic excitations into the insulator. There have been recent examples employing thulium iron garnet (TmIG) films (Qiu *et al.*, 2013; Avci *et al.*, 2017; Figueiredo-Prestes *et al.*, 2021).

Another conclusion can be derived from the comparison between SOT or switching experiments with the SHE in heavy metals and the EE in 2D states of topological insulators, Dirac semimetals, or Rashba interfaces. As discussed (Rojas-Sánchez and Fert, 2019), the conversion between charge and spin current is generally more efficient by 1 or 2 orders of magnitude when using the EE in 2D states than with the SHE of 3D states. This result is confirmed by a direct comparison of the SOT efficiencies and writing powers in experiments of torque and magnetization switching.

In Table II, which was adapted from Ding *et al.* (2021), we present a selection of experimental results at room temperature on the SOT efficiency coefficient $\xi^j_{DL}$ and the writing power $\rho_{WP}$ in different systems (heavy metal, metallic oxides, topological insulators, Dirac semimetals, and Rashba interfaces) for the production of the spin current. The efficiency is derived from experiments with SOT and switching with different magnetic materials. The writing power $\rho_{WP} = [(1+s)/\xi^j_{DL}]^2\rho_{SOC}$, where $s$ is the ratio of the shunting current to the switching current and $\rho_{SOC}$ is the resistivity of the spin-orbit coupling material, indicates that a total energy $\rho_{WP}(J_c)^2$ is needed for the transfer into the magnet of a flux of spins equal to the flux of electrons in $J_c$ (Zhu and Buhrman, 2019; Ding *et al.*, 2021). It is an essential element to probe the potential of a SOT material or magnetic materials system for devices, for example, the SOT MRAM type; see Sec. V.A.1.

For the SHE of heavy metals, although all the determinations have not been always obtained in the same conditions, there is a good convergence of the results for a given heavy metal. We present the typical data for three heavy metals: Pt, $\beta$-W, and AuPt. The stronger efficiency of the metallic oxide

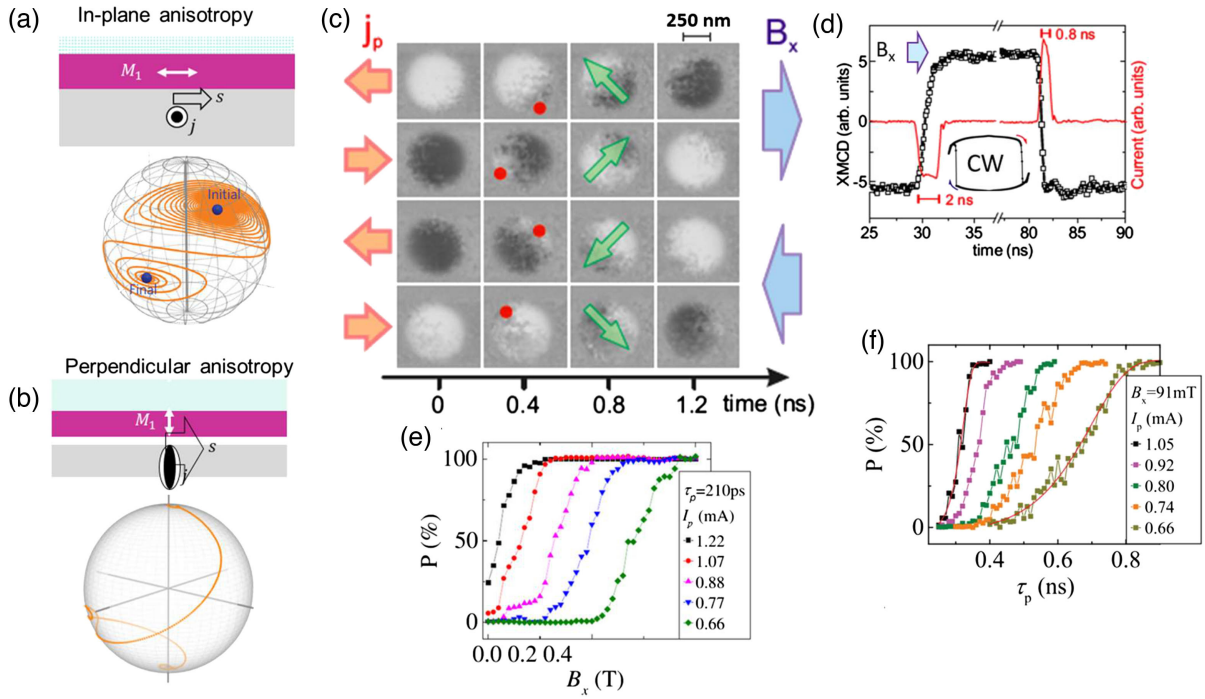


FIG. 31. Symmetry and dynamics of the switching of a magnetic layer with PMA by SOT. Macrospin simulations of the switching by SOT of (a) in-plane and (b) out-of-plane magnetizations. Courtesy of P. Gambardella. For in-plane magnetization, the SOT progressively enlarges precessions of the magnetization around its initial orientation to finally reverse it. The long incubation time (successive precessions) leads to long switching times. For the PMA in (b), the action of SOT is immediate and can lead to much shorter switching times around or below 1 ns. (c) Switching of a ferromagnetic layer with PMA in the process of nucleation and extension of domains where snapshots of x-ray magnetic dichroism images of a dot of Pt/Co/MgO with PMA during the reversal of its magnetization by the SOT is induced by current pulses in Pt. Adapted from Baumgartner *et al.*, 2017. With an applied field along $x$ ($-x$), the SOT induces a reversal from up (down) to down (up) for positive current and from down (up) to up (down) for negative current, as in the magnetization loops. The nucleation of a reversed domain starts on the edges at a point (the dot) where the combination of the applied field and the DMI favors this nucleation. (d) Time trace of the average out-of-plane magnetization (squares) during current injection (line) derived from the images in (c). Successive pulse amplitudes of $-3.1\times10^8$, $+4.4\times10^8$ A/cm$^2$, and $B_x = 0.11$ T. From Manchon *et al.*, 2019. (e) Switching probability $P$ of a square of a Pt(3 nm)/Co(0.6 nm)/AlO$_x$ layer as a function of $B_x$ at different current amplitudes of pulses of 210 ps and (f) as a function of pulse length at a fixed field of 91 mT and varying current amplitudes. From Garello *et al.*, 2014.

TABLE II. Comparison of the SOT efficiencies and writing powers [at room temperature except for $LaAlO_3/SrTiO_3$ (LAO/STO)] obtained in a selection of spin-orbit coupling materials (heavy metals, metallic oxides, topological insulators, Dirac semimetals, and Rashba 2DEGs). Compared to a heavy metal, the strong efficiency of the metallic oxide $SrIrO_3$ expresses the combination of the bulk SHE and interfacial EE [its writing power has been estimated from the transport data on $SrIrO_3$/CoTb given by H. Wang, Meng *et al.* (2019)]. The strong efficiency and low energy consumption for $Bi_{0.9}Sb_{0.1}$, if confirmed, is promising for devices. The 2DEG Rashba system $LaAlO_3/SrTiO_3$ cannot be characterized by a 3D resistivity and a writing power in terms of 3D resistivity. A general conclusion is that, with respect to heavy metals, $\xi^j_{DL}$ can be larger by 2 orders of magnitude or more in materials with spin-orbit coupling in surface or interface states (and the writing power can be much smaller too). A majority of these results are from Zhu and Buhrman (2019). Adapted from Ding *et al.*, 2021.

| Spin-orbit coupling material | | Resistivity $\rho_{SOC}(\times10^{-4}\ \Omega\,\mathrm{cm})$ | Current ratio $s$ | SOT efficiency $\xi^j_{DL}$ | Writing power $\left(\frac{1+s}{\xi^j_{DL}}\right)^2$ $\rho_{SOC}(\times10^{-4}\ \Omega\,\mathrm{cm})$ | Reference |
|---|---|---|---|---|---|---|
| Heavy metal | $Au_{25}Pt_{75}$ | 0.83 | 0.255 | 0.35 | 10.68 | Zhu and Buhrman (2019) |
| | Pt | 0.20 | 0.061 | 0.055 | 74.5 | Zhu and Buhrman (2019) |
| | $\beta$-W | 3.0 | 0.923 | 0.33 | 102 | Zhu and Buhrman (2019) |
| Oxides (metallic) | $SrIrO_3$ | 12 | 1.8 | 1.1 | 31.8 | H. Wang, Meng *et al.* (2019) |
| Topological insulator | $Bi_{0.9}Sb_{0.1}$ | 4.0 | 1.2 | 52 | 0.007 | Khang, Ueda, and Hai (2018) |
| | $Bi_xSe_{1-x}$ | 130 | 40 | 18.6 | 632 | Zhu and Buhrman (2019) |
| | $(Bi,Se)_2Te_3$ | 40.20 | 12.37 | 0.4 | 44900 | Zhu and Buhrman (2019) |
| Topological Dirac semimetal | $\alpha$-Sn | 0.81 | 0.119 | 6.15 | 0.027 | Ding *et al.* (2021) |
| Rashba 2DEG | LAO/STO | | | 1.8 | | H. Yang *et al.* (2019) |

$SrIrO_3$ reflects the combination of the SHE in the layer and the EE from surface states of $SrIrO_3$, as in other systems with $SrTiO_3$. For topological insulators, there is a large dispersion of experimental results, due mainly to the difficulty of the separation between the 2D (EE) and 3D (SHE) contributions and to the variety of more or less valid techniques that have been used to derive the SOT. Publishing a large table of largely dispersed data is not necessary, and we selected only four systems. We have included the attractive result obtained on $Bi_{0.9}Sb_{0.1}$ by Khang, Ueda, and Hai (2018). This result has drawn much attention. However, it needs to be confirmed by other groups to be realistically promising for applications. In spite of the dispersion of the results, it turns out that, for the efficiency and also for low-power consumption, 2D systems (topological insulators and Dirac semimetals) perform better than the usual heavy metals by 2 orders of magnitude or more. For applications, other aspects must be accounted for. For example, the advantage of $Bi_{0.9}Sb_{0.1}$ in terms of efficiency at low power offset by the disadvantage of a preparation by molecular beam epitaxy (MBE), a nontypical technology in spintronic devices, and the requested in-plane field [there are, however, some recent reports on BiSb grown by sputtering; see T. Fan *et al.* (2020)]. In contrast, $\alpha$-Sn is somewhat below in terms of efficiency and is low power but has the advantage of fabrication by sputtering.

The requirement of an in-plane applied field to switch an out-of-plane magnetization by SOT in the conditions of Eqs. (7) and (8) (i.e., in the general situation of samples of rotational invariance around the out-of-plane axis) is a disadvantage for devices based on SOT and PMA layers. However, an important advantage of the reversal of PMA layers by SOT is its much faster dynamics in comparison with what can be obtained by SOT with in-plane magnetizations or STT, as we now discuss.

In Figs. 31(a) and 31(b), we show the macrospin simulations of switching by SOT of in-plane [Fig. 31(a)] and out-of-plane [Fig. 31(b)] magnetizations. With initial in-plane magnetization, the SOT progressively enlarges precessions of the magnetization around its initial orientation to finally reverse it, as was also the process for switching by STT in Fig. 29(d). This long incubation time leads to switching times of a few nanoseconds or longer. As shown in Fig. 31(b) for PMA in the same macrospin picture, the action of SOT is immediate and can lead to short switching times below 1 ns. Analytic expressions as well as macrospin simulations reproduce not only the short switching times in the nanosecond range but also several other features related to symmetry, such as the requirement of an in-plane field $B_x$ and the dependence of the switching current on the anisotropy field and $B_x$ (Lee *et al.*, 2013). For a realistic interpretation of experiments on samples larger than the width of a domain, macrospin models are no longer realistic and it is necessary to consider mechanisms related to the nucleation and extension of domains of opposing out-of-plane magnetizations. However, even in this nucleation-extension regime, the SOT switching of PMA layers is also short. This is the case in Fig. 31(c) (Baumgartner *et al.*, 2017), which shows snapshots of x-ray magnetic dichroism images of a dot of Pt/Co/MgO with PMA during the reversal of its magnetization by current pulses in Pt by SOT. The nucleation of the reversed domain starts on the edges at a point (in red) where the combination of the applied field and the DMI favors this nucleation.

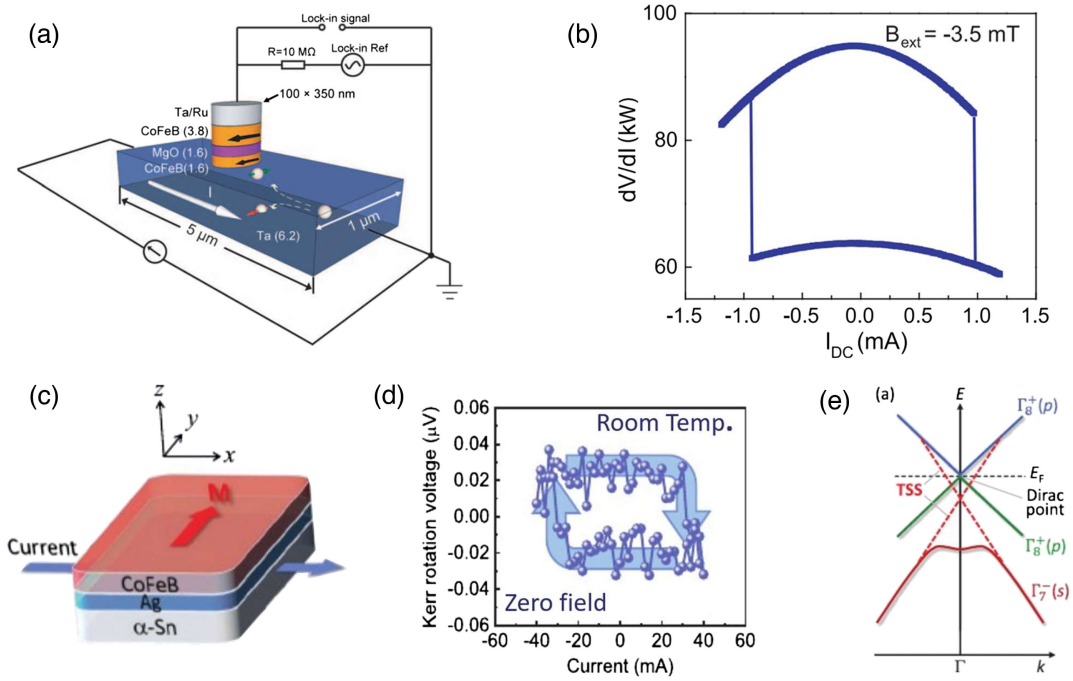


FIG. 32. Current-induced switching of in-plane magnetization of a CoFeB layer by SOT generated from SHE in a Ta layer, with (a) an experimental device and (b) a switching loop at room temperature detected by TMR in a CoFeB/MgO/CoFeB MTJ. From Liu *et al.*, 2012. (c) Current-induced switching of the in-plane magnetization of a CoFeB layer generated by the EE in the surface states of the Dirac semimetal $\alpha$-Sn in a $\alpha$-Sn/Ag/CoFeB trilayer , (d) switching loop at zero field and room temperature detected by MOKE, and (e) band structure and Dirac cone of $\alpha$-Sn. (c)–(e) From Ding *et al.*, 2021.

In addition, as again expected from symmetry, in an applied field along $x$ ($-x$) the SOT induces a reversal from up (down) to down (up) for a positive current and from down (up) to up (down) for a negative current. As shown in Figs. 31(d)–31(f), some of the reversals occur in less than 1 ns. Figures 31(e) and 31(f) show that the probability of switching increases with the amplitude of the in-plane field, as well as with the amplitude and duration of the current pulses.

Experimental examples of switching of in-plane magnetization by SOT are also displayed in Fig. 32, with SOT induced by either the SHE of the heavy metal Ta in Figs. 32(a) and 32(b) or the EE in the topological surface states of the Dirac semimetal $\alpha$-Sn in Figs. 32(c) and 32(d). As previously pointed out and as illustrated in Figs. 31(a) and 31(b) in a macrospin picture, the disadvantage of in-plane magnetizations by SOT is a long incubation time during progressively enlarging precessions. The resulting slow dynamics compared to layers with PMA makes the latter the most promising SOT-based devices. However, for some types of applications, the advantage of in-plane magnetism is the possibility of switching by SOT in a zero applied field, as illustrated in Figs. 32(c) and 32(d) for the switching by SOT generated by the EE in the interface states of $\alpha$-Sn.

#### 3. Magnetization switching of single magnetic layers by SOT

Most of the previously described experiments are performed with bilayers including a magnetic layer and a layer with large spin-orbit coupling (heavy metals or materials having Rashba or topological surface states). The bilayer structure breaks the inversion symmetry, which is the condition for current-induced torque on a magnetic layer in a heterostructure. Additionally, the spin-orbit coupling of the nonmagnetic layer is used to generate the spin current for the SOT. However, switching by SOT of a single magnetic layer can also be obtained if the magnetic layer itself has a large spin-orbit coupling generating spin currents (for example, the spin-orbit coupling of the $5d$ band of rare-earth elements or Pt magnetic alloys) and, in addition, no inversion symmetry. The absence of inversion symmetry can be obtained with a noncentrosymmetric crystal structure (L. Liu *et al.*, 2021) by introducing a composition gradient along the out-of-plane axis (Yu *et al.*, 2019; Bekele *et al.*, 2021; Céspedes-Berrocal *et al.*, 2021; Zheng *et al.*, 2021) or with nonsymmetric interfaces (Céspedes-Berrocal *et al.*, 2021).

As examples of electrical switching of a single magnetic layer with a noncentrosymmetric crystal structure, we have the antiferromagnetic CuMnAs (Wadley *et al.*, 2018) and $Mn_2Au$ (Bodnar *et al.*, 2018). In these cases, the antiferromagnetic order and the particular crystal structure result in staggered SOT in each sublattice, leading to current-induced switching of the Néel vector. This effect has been shown to be deterministic and multilevel, with the potential for embedded memory-logic applications (Olejník *et al.*, 2017).

We can also cite the pioneering results of Miron *et al.* (2010) on a Co layer between Pt and MgO. The perpendicular switching could be ascribed either to the SHE of Pt or to the Rashba effect induced at the interfaces of Co with Pt and MgO. In the second case, it would correspond to the switching of a single Co layer thanks to its asymmetric interfaces with Pt and MgO.

#### 4. Field-free switching by SOT

Since applying an in-plane field $B_x$ to reverse a perpendicular magnetization by SOT is an important disadvantage for the development of applications, several approaches have been developed to solve the problem. The first one is to introduce additional magnetic stripes to provide a dipole field or an exchange-induced effective field (Fukami *et al.*, 2016; Lau *et al.*, 2016; Zhao, Smith *et al.*, 2020). An effective $B_x$ can also be created by an in-plane exchange-bias field provided by an antiferromagnet (Fukami *et al.*, 2016; Oh *et al.*, 2016; van den Brink *et al.*, 2016).

An interesting solution was proposed by M. Wang *et al.* (2018) by combining the STT and SOT to achieve the field-free and low-power switching of the out-of-plane magnetized free layer of a MTJ.

Finally, field-free switching has also been obtained in single crystal structures by going out of the rotational invariance of the standard polycrystalline structures. L. Liu *et al.* (2021) achieved field-free switching with $L1_1$-ordered CuPt/CoPt bilayers in which the low-symmetry point group $3m1$ generates a SOT depending on the relative orientation of current and crystal axes and leads to field-free switching for some of these orientations. By tuning the composition of the CoPt layer, Liu *et al.* (2022) were able to achieve self-switching, which is also field free due to the low symmetry at the Co platelet/Pt interfaces present in the CoPt alloy.

#### 5. Current-induced magnetization switching of insulating magnetic material

As described in Secs. II.F.1 and III.A.5, the injection of a spin current into a magnetic insulator can be achieved by interfacial conversion of a spin current carried by electrons in a metallic layer into a spin current carried by magnons in the magnetic insulator. The resulting torques on the magnetization obey the same symmetry rules as were previously described for magnetic metals in Sec. III.C.1. A typical example is the switching of the out-of-plane magnetization of TmIG in W/TmIG bilayers by the spin current initially induced by the SHE in W (Shao *et al.*, 2018). Just as for PMA metallic layers in Sec. III.C.2, the switching is induced by the combination of SOT and the in-plane magnetic field.

### D. Current-induced motion of domain walls

The study of the current-induced motion of domain walls (DWs) (Berger, 1984; Freitas and Berger, 1985) [accelerated by the proposition of DW-based racetrack memory by Parkin, Hayashi, and Thomas (2008)] has been a field of intense research in recent years. Important progress came from the prediction by Thiaville *et al.* (2012) that DWs of a Néel type can be stabilized with the DMI and moved at high velocities by a current. Most recent studies have been developed on this type of DW.

Figure 33(a) displays a schematic of the DMI at an interface between a magnetic metal and a nonmagnetic heavy metal, $H_{\mathrm{DMI}} = (S_1 \times S_2) \cdot D_{12}$. In a magnetic layer with PMA, the

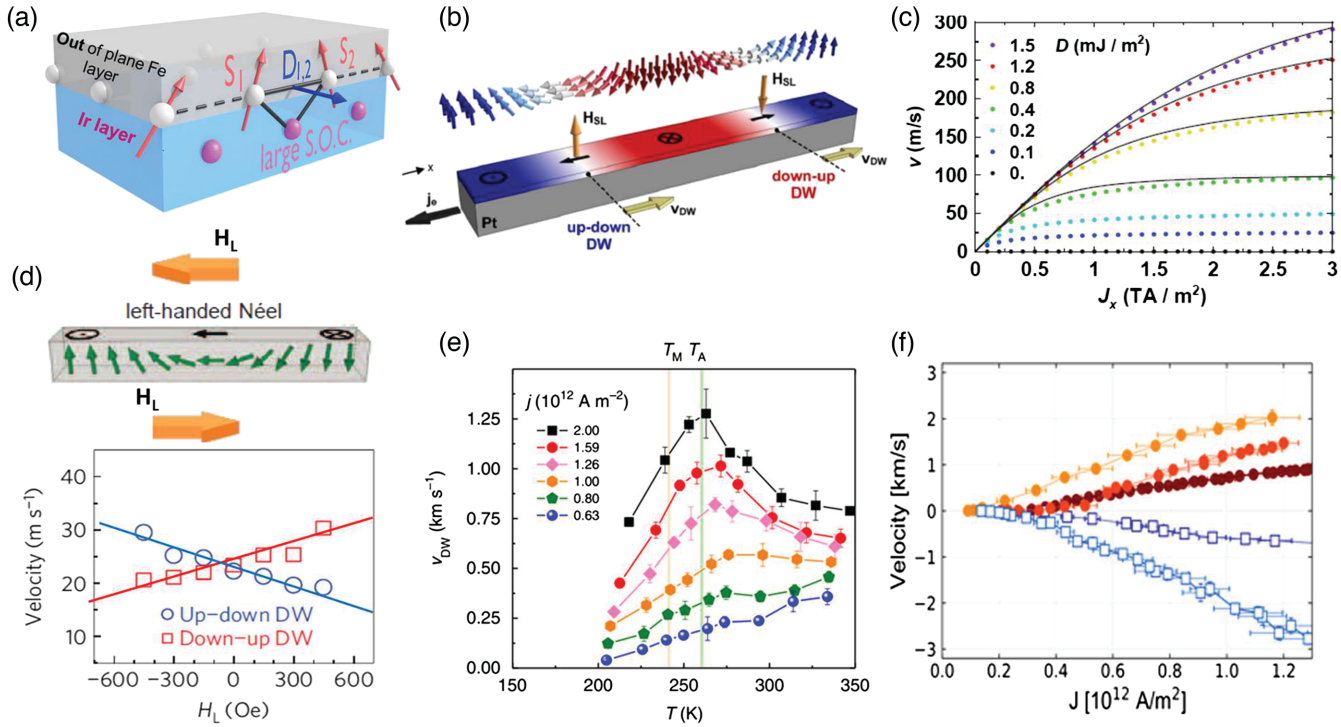


FIG. 33. (a) Illustration of the DMI induced by spin-orbit coupling and the breaking of inversion symmetry at the interface between a magnetic layer and a heavy metal. (b) Illustration of a left-handed chiral DW in Pt/CoFe/MgO. The effective field $H_{SL}$ induced by SHE in Pt moves adjacent up-down and up-down DWs in the same direction against electron flow $j_e$. Adapted from Emori *et al.*, 2013. (c) Velocity of chiral DWs vs current density for several DMI values. From Thiaville *et al.*, 2012. (d) Top panel: schematic showing that an applied in-plane field $H_L$ along the current axis can help the DMI (top arrow) or compete with it (bottom arrow) for the formation of a chiral Néel DW. Adapted from Emori *et al.*, 2013. Bottom panel: dependence of the DW velocity on the sign and magnitude of the applied field along the current axis. Adapted from Emori *et al.*, 2013. (e) SOT-induced velocity of Néel DWs as a function of temperature in the vicinity of the compensation temperatures $T_M$ (blue vertical line) and $T_A$ (green vertical line) for a ferrimagnetic $Co_{44}Gd_{56}$ layer on Pt. From Caretta *et al.*, 2018. (f) STT-induced velocities, up to about 3 km/s, for Néel DWs as a function of temperature near the compensation temperature of $Mn_{4-x}Ni_xN$ films. From Ghosh *et al.*, 2021.

DMI favors a given direction of rotation when one goes from $S_1$ to $S_2$ and leads to the chiral Néel DWs described by Thiaville *et al.* (2012) and presented in Fig. 33(b). When one moves from left to right in the figure, the rotation of the spins is counterclockwise in both DWs and the directions of the central spins are opposite in the up-down and down-up DWs. Thiaville *et al.* (2012) showed that such chiral DWs created by the DMI can be moved at high velocity by the SOT induced by the SHE in the heavy metal layer below or above the magnetic layer. Figure 33(c) displays a typical calculated variation of the velocity as a function of the magnitude of the DMI.

One of the first experimental indications of the influence of spin-orbit coupling effects on the current-induced motion of DW came from the experiments of Moore *et al.* (2008) and Miron *et al.* (2011), who proposed that the current-induced DW motion observed in Pt/Co/MgO and not in symmetric Pt/Co/Pt was due to the fieldlike torque generated by Rashba interactions. The 2012 prediction of Thiaville *et al.* (2012) on the conjugated effects of the DMI and SOT was confirmed by the experimental papers of Emori *et al.* (2013) and Ryu *et al.* (2013). The role of the DMI was tested by looking at the variation of the velocity when the in-plane magnetic field is applied along the axis of the current. As shown in Fig. 33(d), an in-plane field $H_L$ depending on its orientation along the current axis helps the DMI in the stabilization of the down-up left-handed Néel DW or competes with it. What is expected is an increase (decrease) of the velocity of the down-up (up-down) DW, as observed in the experimental results in the bottom of Fig. 33(d). Another test was based on the knowledge that Pt and Ta present opposite signs of the SHE. Emori *et al.* (2013) compared the DW velocities in Pt/CoFe/MgO and Ta/CoFe/MgO, and the observed opposing velocities confirmed that the origin of the current-induced motion is the spin current generated by the SHE and the resulting torque on the DW.

Most efforts since 2013 have been devoted to improving the potential of current-induced motion of chiral DWs for applications with two main objectives: higher velocities with smaller current and thinner DW width to reduce the bit size in nanodevices. Figure 33(e) shows an example of a noteworthy result obtained in $Pt/Gd_{44}Co_{56}/TaO_x$ films for temperatures close to the angular compensation temperature $T_A$ of the ferrimagnet $Gd_{44}Co_{56}$, at which there is a compensation of the angular momenta of the antiferromagnetically aligned Gd and Co (Caretta *et al.*, 2018). At this temperature and near it, the precessional regime of the dynamics is strongly reduced, which gives an immediate motion and high velocities, as shown in Fig. 33(e), with velocities exceeding 1 km/s. In addition, as the magnetic compensation temperature $T_M$ is close to $T_A$, the magnetization is small in this temperature range, what reduces the stray field interactions and the width of the DW.

Other directions have been explored to obtain large velocities in the absence of SOT by exploiting STT in magnetic materials of strongly spin-polarized conduction and small magnetization, as with $Mn_4N$ grown epitaxially on $SrTiO_3$ and velocities above 1 km/s (Gushi *et al.*, 2019). Doping $Mn_4N$ with Ni led to velocities close to 3 km/s for a sample of small magnetization in the vicinity of the magnetic compensation. Because the current spin polarization is related to the spin on the Mn(I) site, the sign of the velocity changes when the global spin of the alloy becomes the opposite of the Mn(I) spin at the Ni concentration for compensation, as shown in Fig. 33(f) (Ghosh *et al.*, 2021).

### E. Current-induced motion of magnetic skyrmions

A magnetic skyrmion is a local whirl of the spin configuration in a magnetic material, a type of topological spin structure that was referred to in Sec. II.E. As shown in Fig. 34(a) for a Néel skyrmion in a magnetic layer with out-of-plane magnetization, the spins inside the skyrmion rotate progressively with a fixed chirality, for example, from the up direction at one edge to the down direction in the center and then to up direction again on the other edge. The type of nontrivial topology characterizing the skyrmions was introduced by Skyrme (1961) in nuclear physics as topological solitons in the nuclear field. In the case of skyrmions in magnetic materials (Bogdanov and Yablonskii, 1989; Bogdanov and Hubert, 1994; Rößler, Bogdanov, and Pfleiderer, 2006), the spin configuration is generally determined by chiral interactions of the DMI type and, consequently, skyrmions can be found in noncentrosymmetric lattices in which they were first observed using neutron scattering (Mühlbauer *et al.*, 2009) or Lorentz microscopy (X. Z. Yu *et al.*, 2010). Skyrmions could later be found in systems with the DMI induced by inversion symmetry breaking at interfaces (Fert, 1990) and were first observed in spin-polarized scanning tunneling microscopy experiments on Fe monolayers grown on Ir (Heinze *et al.*, 2011). The nontrivial topology of the spin configuration of skyrmions ensures that it cannot be twisted continuously to result in a trivial magnetic configuration. This can be described as a topological protection. To be more precise, the skyrmions can form a skyrmion lattice that is the DMI-induced ground state of the spin system (Rößler, Bogdanov, and Pfleiderer, 2006; X. Z. Yu *et al.*, 2010; Heinze *et al.*, 2011) or can exist as individual skyrmions that can be described as metastable local spin configurations stabilized by their topological protection (Soumyanarayanan *et al.*, 2016; Fert, Reyren, and Cros, 2017).

For the specific property of electrical control of magnetism discussed in our review, the crucial property of the skyrmions is their solitonic nature: they can be electrically moved as particles, and this possibility is at the basis of many applications. The first experimental results of motion were obtained for skyrmions in a noncentrosymmetric lattice with a combination of neutron scattering and Hall effect measurements (Schulz *et al.*, 2012) and real-space Lorentz TEM images of skyrmion lattices in FeGe in which the motion of the skyrmions is induced by electrical currents or gradients of the magnetic field or temperature (X. Z. Yu *et al.*, 2012). The current-induced motion of the skyrmions can be described as being due to STT (Fert, Cros, and Sampaio, 2013; Iwasaki, Mochizuki, and Nagaosa, 2013; Sampaio *et al.*, 2013; Fert, Reyren, and Cros, 2017) or, alternatively, in terms of the emergent electromagnetic field generated by the skyrmion spin texture (Everschor *et al.*, 2011; Schulz *et al.*, 2012). Most applications that have been proposed are based on the current-induced motion, fusion,

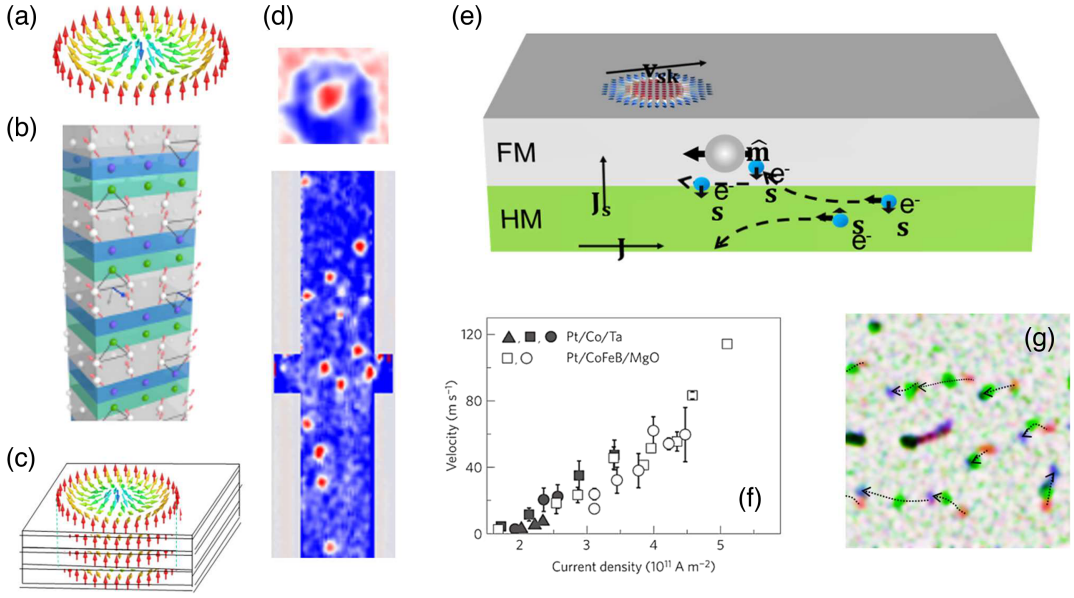


FIG. 34. Current-induced motion of magnetic skyrmions. (a) Spin configuration in a Néel skyrmion. (b) Multilayer with an additive DMI at the top and bottom interfaces of the Co layers. (c) Column of coupled skyrmions in a multilayer with interfacial DMIs. (d) Magnetic force microscopy images of skyrmions in a multilayer of the type shown in (b). (a)–(d) From Maccariello *et al.*, 2018. (e) Motion of skyrmions driven by the SOT induced by the SHE in the heavy metal below the magnetic layer. (f) SHE-induced skyrmion velocity as a function of current density in two types of multilayers. From Woo *et al.*, 2016. (g) Snapshots of the SOT-driven motion of skyrmions in a |Ta10|Pt8|(Co1.4|Ru1.2|Pt0.6) × 3|Pt2.4 multilayer induced by $7 \times 10^{11}$ A/m$^2$ pulses of 12 ns. Courtesy of N. Reyren.

or annihilation of such individual skyrmions, with the best known being the racetrack memory based on the current-induced motion of trains of individual skyrmions.

The most recently studied systems for application are skyrmions induced by the DMI at the interface of a thin enough magnetic layer with a heavy metal (Pt, etc.) or an oxide (MgO, etc.); see Fig. 34(b). As a small skyrmion in a single thin layer can be destabilized by thermal fluctuations at room temperature, a convenient and classical structure is a multilayer such as that displayed in Fig. 34(b) with an additive interfacial DMI for Co between Pt and Ir (Fert, Reyren, and Cros, 2017). A small ferromagnetic interaction between Pt/Co/Ir trilayers couples the skyrmions of successive trilayers, which leads to columnar skyrmions of the type represented in Fig. 34(c). Typical magnetic force microscopy images are displayed in Fig. 34(d).

After the presentation of the current-induced motion of the DW in Sec. III.D, the simplest way to understand the current-induced motion of a skyrmion is to consider it as a couple of DWs: up and down from one edge to the center and down and up from the center to the other side. In agreement with what was found for DWs, an efficient way to move the skyrmions is by the SOT generated by SHE in the heavy metals below or above, as represented in Fig. 34(e), or due to the EE at the interfaces of the magnetic layer (Soumyanarayanan *et al.*, 2016; Fert, Reyren, and Cros, 2017). A general feature of the current-induced motion of skyrmions is the coexistence of a longitudinal motion (i.e., along the direction of the current) and a transverse motion (the so-called skyrmion Hall effect) generated by gyrotropic forces related to the topology of the skyrmion. The direction of the longitudinal motion depends on both the chirality of the skyrmion and the spin polarization of the injected current (the motion is typically in the direction of the charge current for the DMI at the Pt/Co interface and the SHE of Pt). The transverse deflection of the skyrmion, left or right, depends on the spin polarization at the center of the skyrmion. Experimental results on the velocities obtained by SOT are presented in Fig. 34(f). An almost linear variation of the velocity with the current density starts only after a creep regime in which, due to the pinning by defects, the skyrmions either do not move or move at only a low velocity, while the skyrmion Hall angle is small. Above a critical current, the velocity increases linearly, as expected from theory (Hrabec *et al.*, 2018), and in Fig. 34(f) it reaches values of around 100 m/s. However, with this type of multilayer generally fabricated by sputtering, the scattering and pinning by defects have significant effects even in the quasilinear regime, which usually leads to the type of nonuniform motions illustrated by Fig. 34(g). A current challenge is obtaining skyrmions in materials with fewer defects, single crystal layers or 2D vdW magnets (see Sec. III.F). Another challenge is the suppression of the transverse motion, and promising results have been obtained with antiferromagnetically coupled skyrmions in successive layers (Dohi *et al.*, 2019; Legrand *et al.*, 2020).

### F. Control of magnetism by current-induced torques in 2D magnets

As for the 3D magnets, the magnetization of 2D magnets can be controlled and manipulated by current-induced torques (STT or SOT). However, the SOT plays a more important role in the case of 2D magnets for the following reason: because the Mermin-Wagner theorem rules out magnetic ordering for isotropic systems of Heisenberg spins (Mermin and Wagner, 1966), magnetically ordered materials exist in two dimensions only if they can escape from the Mermin-Wagner theorem thanks to large magnetic anisotropies induced by the large spin-orbit interactions of elements such as Te, I, and Bi (Gong and Zhang, 2019). In addition, because interfaces play a particularly important role in the properties of 2D materials, the generation of spin current at interfaces by interfacial Rashba interactions and the EE can be particularly relevant in heterostructures of 2D magnets (vdW heterostructures).

The first example of magnetization control by SOT shown in Fig. 35(a) is the switching of the out-of-plane magnetized 2D ferromagnet $Fe_3GeTe_2$ by the spin current generated by the SHE of Pt deposited on a metallic $Fe_3GeTe_2$ layer (Alghamdi *et al.*, 2019; X. Wang *et al.*, 2019). As in the switching of PMA of 3D magnets by SOT in Sec. III.C.2, an applied field along the current direction is required to switch the magnetization of $Fe_3GeTe_2$. Either clockwise [Fig. 35(b)] or counterclockwise [Fig. 35(c)] loops are observed, depending on the direction of the applied field. Similar switching of 2D magnets with PMA have also been obtained with semiconducting $Cr_2Ge_2Te_6$ in combination with Ta or Pt (Lohmann *et al.*, 2019; Gupta *et al.*, 2020; Ostwal, Shen, and Appenzeller, 2020). For possible future application to SOT MRAM devices, we compare the current densities and in-plane fields required for SOT switching in 3D and 2D magnetic materials. Figure 35(d), from Ostwal, Shen, and Appenzeller (2020), compares the experimental data of a bilayer of 3D or 2D magnetic materials with heavy metals or topological insulators. A smaller switching current density is required for $Ta/Cr_2Ge_2Te_6$, an order of magnitude below the density for the classical Ta/CoFeB system, with the disadvantage of the 3D CoFeB compared to a 2D magnet coming mainly from the useless large current shunting in the metallic CoFeB layer. The current density required for $Ta/Cr_2Ge_2Te_6$ is even smaller than for a bilayer of Ta and the magnetic insulator TmIG. Concerning the required in-plane field, the values are similar for 2D and 3D magnetic materials. However, the bottleneck of 2D magnets for applications is still the required low temperature, even if some recent experiments have shown that, in some 2D magnets, the ordering temperature can be raised above room temperature, as has already been achieved for $Fe_3GeTe_2$ grown on $Bi_2Te_3$ (Wang *et al.*, 2020) or with electrostatic doping (Deng *et al.*, 2018).

In the previously described examples with switching of 2D magnets by SOT, the sources of spin current are 3D heavy metals. Alternatively, both the magnetic layer and the spin source can be 2D materials forming a vdW heterostructure with spin currents generated at their interface. Dolui *et al.* (2020) developed a first-principles quantum model for transport in vdW heterostructures ($TaSe_2/CrI_3$ bilayer) in which, at equilibrium, there is an antiferromagnetic coupling between the two $CrI_3$ layers. They found that a current flowing in the 2DEG at the interface between $TaSe_2$ and the bottom $CrI_3$ layer [see Fig. 35(e)] can switch by SOT the magnetization of this bottom layer to induce a ferromagnetic $CrI_3$ bilayer. An

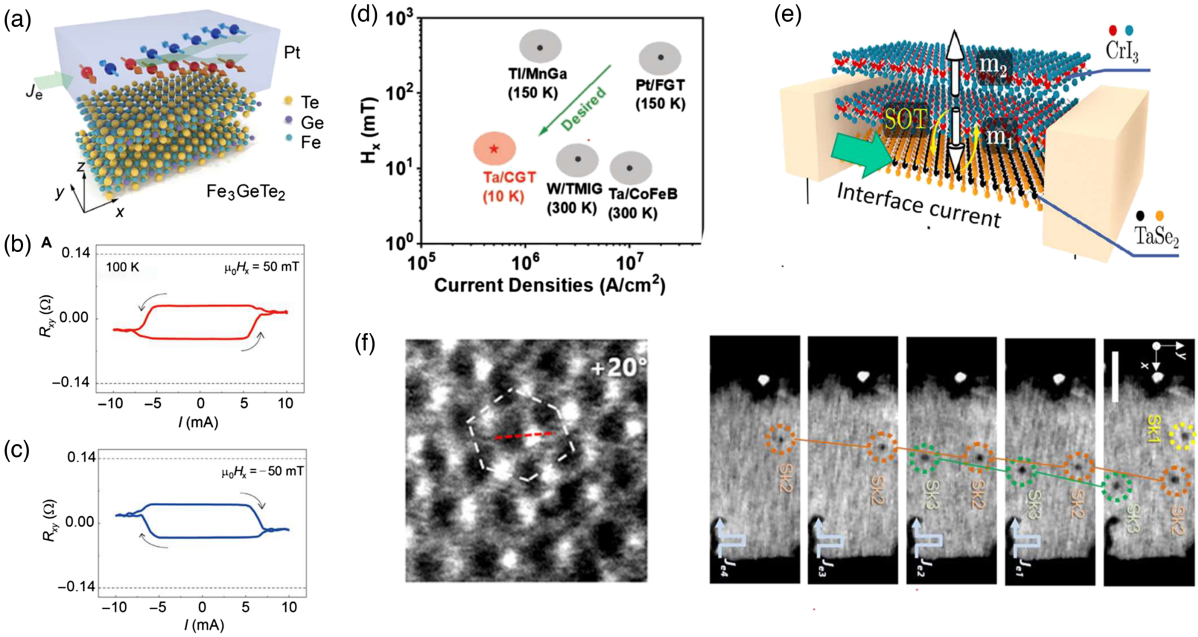


FIG. 35. Control of magnetism by currents in 2D magnets. (a) Illustration of a $Fe_3GeTe_2$/Pt bilayer. From X. Wang *et al.*, 2019. SOT switching of the bilayer displayed in (a) in the presence of a (b) positive or (c) negative in-plane field along the current direction. From X. Wang *et al.*, 2019. (d) Comparison of the current densities and in-plane fields required for SOT switching in devices based on 3D magnets (CoFeB, MnGa, and TmIG) and 2D magnets ($Fe_3GeTe_2$ and $Cr_2Ge_2Te_6$), with the best results found for Ta/$Cr_2Ge_2Te_6$. From Ostwal, Shen, and Appenzeller, 2020. (e) Schematic view of a $CrI_3$ bilayer/$TaSe_2$ heterostructure in which the SOT induced by the interfacial current can drive the relative orientation of the magnetizations of the two $CrI_3$ layers from parallel to antiparallel. From Dolui *et al.*, 2020. (f) Lorentz microscopy images of skyrmions in a $Fe_3GeTe_2$ film with oxidized interfaces and current-induced motion of the skyrmions. From Park *et al.*, 2021.

experimental demonstration of a magnetization switching by SOT in an all-vdW heterostructure was recently reported for $WTe_2/Fe_3GeTe_2$ by two different groups (Kao *et al.*, 2022; Shin *et al.*, 2022).

The last point on current-induced magnetization control in 2D magnets is the manipulation of skyrmions. The only example we know of is presented in Fig. 35(f) and shows the motion of skyrmions in $Fe_3GeTe_2$ foils. Magnetic skyrmions in 2D magnets have been observed by several groups (Han *et al.*, 2019; B. Ding *et al.*, 2020; Wu *et al.*, 2020; Park *et al.*, 2021), with the skyrmions in Fig. 35(f) Néel skyrmions generated by an interfacial DMI at the oxidized interfaces of $Fe_3GeTe_2$ (in the first approximation, interfaces between $Fe_3GeTe_2$ and oxidized $Fe_3GeTe_2$). The results in Fig. 35(f) are promising, as the motion seems less affected by defects and more uniform than in the usual sputtered multilayers of magnetic and heavy metals. Many points remain to be understood for skyrmions in 2D magnets, such as the exact mechanism inducing the motion (STT or SOT).

## IV. COMBINED USE OF ELECTRIC FIELDS AND CURRENT-INDUCED TORQUES

In Sec. III, we reviewed the control of magnetization by current-induced torques, a field with a large potential for applications in MRAM technology. One of the major drawbacks of using current-induced torques is the energy dissipation associated with the high current densities required for the switching. In this regard, the use of an electric field (voltage) to assist the current-induced torque is of extreme interest to lower the energy consumption of MRAM technology.

The electric field can modulate different ingredients in a current-induced torque system. One of them is the free layer storing the nonvolatile information, whose magnetic anisotropy can be controlled with the application of voltage (the VCMA effect reviewed in Sec. II.C.3). Another ingredient is the electric-field control of the spin-charge interconversion, the mechanism at the core of SOTs, which is reviewed in Sec. IV.A. It has recently been shown that such electric control can also be performed through ferroelectricity, as reviewed in Sec. IV.B. Finally, examples in which the electric field is used to assist switching in STT and SOT systems are reviewed in Sec. IV.C.

### A. Electric-field control of spin-charge interconversion

Currently, the most widely used way to create spin currents without the use of a ferromagnet is with charge-to-spin-current conversion effects in systems with high spin-orbit coupling such as the SHE (see Sec. III.A.3) or the EE in interfaces with Rashba coupling and surface states of topological insulators (see Sec. III.A.4). Conversely, spin currents can be detected with spin-to-charge-current conversion from the corresponding inverse effects. Since the conversions fulfill Onsager reciprocity, we use the term spin-charge interconversion here to refer to both the direct and inverse conversions. In this section, we review the various possibilities for electrical

control of such spin-charge interconversion, which can open the path to new functionalities for future energy-efficient electronic devices.

The first observation for the SHE controlled by an electric field was reported in GaAs. In this material, the different valleys in the band structure have different spin-orbit coupling properties. Okamoto *et al.* (2014) excited spin-polarized electrons at the valley Γ with circularly polarized light and applied an electric field to induce an electrical intervalley transition in the conduction band from valley Γ to $L$, which showed larger spin-orbit coupling [Fig. 36(a)]. The $\theta_{\mathrm{SHE}}$ determined by the generated transverse voltage ($V_{\mathrm{SH}}$) in a GaAs Hall bar [inset in Fig. 36(b)] could be tuned from 0.0005 to 0.02 by the electric field [Fig. 36(b)].

The SHE in a heavy metal has also been tuned by voltage using a ionic liquid gate on ultrathin Pt. Dushenko *et al.* (2018) showed that the resistivity of Pt could be tuned by gating [Fig. 36(c)]. They used the spin-pumping technique from an adjacent YIG layer to inject a spin current and measure the transverse charge current to quantify the SHE in Pt [Fig. 36(d)]. Since the $\theta_{\mathrm{SHE}}$ in Pt depends on its resistivity, a clear gate dependence was observed for the thinnest Pt films [Fig. 36(e)]. This experiment allowed Dushenko *et al.* (2018) to reach the dirty regime of the SHE in Pt.

Spin-charge interconversion has been intensively studied in topological insulators due to the spin-momentum locking present in their Dirac-cone-type surface states. Its efficiency is in principle independent of the Fermi level position within the Dirac cone (Zhang and Fert, 2016). Indeed, H. Wang, Kally *et al.* (2019) did not observe any gate dependence of the spin-charge interconversion efficiency in epitaxial $Cr_{0.08}(Bi_xSb_{1-x})_{1.92}Te_3$ thin films measured by spin pumping. However, the carrier density of the surface states is tunable with electric gating (Yang *et al.*, 2014), and the output signal can therefore also be tuned (Burkov and Hawthorn, 2010). For instance, Tian *et al.* (2021) observed in $Bi_2Te_2Se$ a modulation of the spin signal measured by spin potentiometry with the back gate voltage due to the gate tunability of its resistance. Voerman *et al.* (2019) also observed a tuning of the spin signal with the back gate voltage when measuring $BiSbTeSe_2$ combined with graphene using a nonlocal spin-valve technique, although the origin remains elusive. In general, one must be aware that experiments involving topological insulators have the additional complication that bulk is hardly an ideal insulator. Therefore, it can contribute to transport and be a potential source of spin-charge interconversion via the SHE.

Graphene is a Dirac semimetal in which the Fermi level can be easily tuned with an applied gate, therefore allowing its transport properties to be controlled (Novoselov *et al.*, 2004). While graphene is a highly effective material for long-distance spin transport (Tombros *et al.*, 2007) due to its weak intrinsic spin-orbit coupling and negligible hyperfine interaction, it is not a preferred material for spin-charge interconversion for the same reason. Nevertheless, a small but measurable spin-charge interconversion was reported in pristine graphene

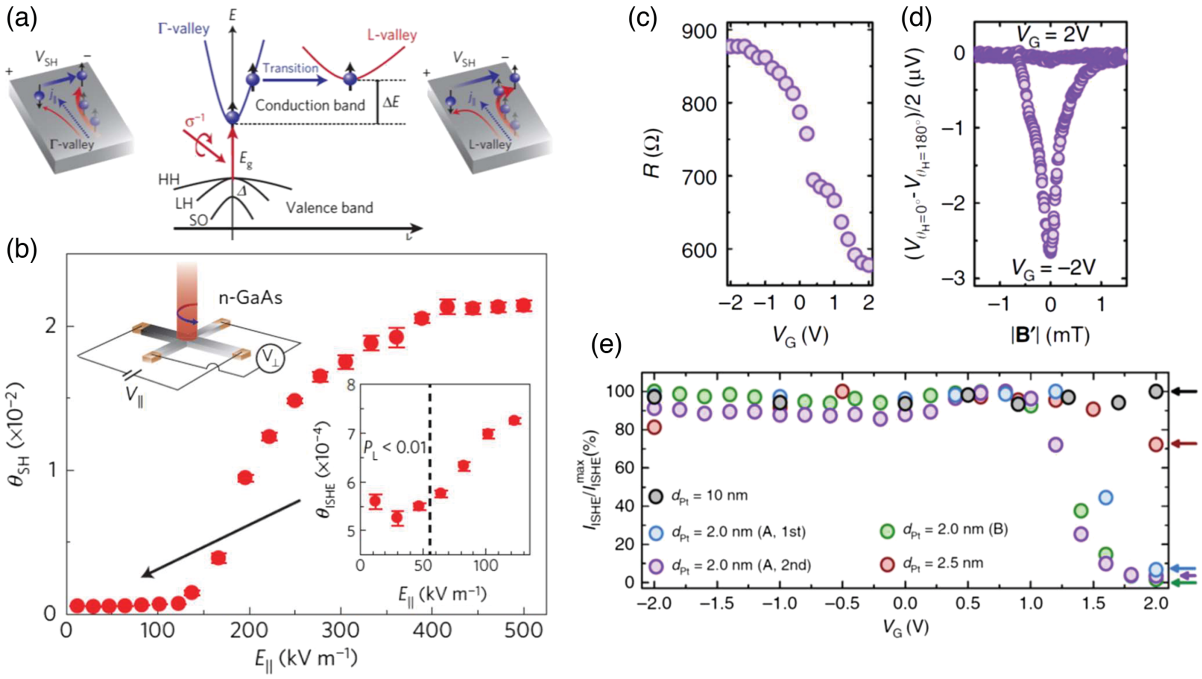


FIG. 36. Electric control of spin-charge interconversion effects in different systems. (a) GaAs band structures and spin-polarized electrons generated by circularly polarized light absorption. A high electric field induces the transition of the spin-polarized electrons from the Γ valley to the satellite $L$ valley, where part of its $p$ character provides a larger effective spin-orbit coupling. Sketches at the left and right show the optically induced SHE for the Γ valley and $L$ valley, respectively; the SHE is larger in the latter. (b) Electric-field dependence of the $\theta_{\mathrm{SHE}}$ in GaAs. Right inset: enlargement at low field. Left inset: measurement configuration of the optically induced SHE. (a),(b) From Okamoto *et al.*, 2014. (c) Resistance as a function of gate voltage $V_G$ for a 2-nm-thick Pt on YIG. (d) Output voltage detected during spin pumping at the same sample for $V_G = 2$ and $-2$ V. (e) Normalized spin-to-charge output current as a function of $V_G$ for different Pt thicknesses. (c)–(e) From Dushenko *et al.*, 2018.

using spin-pumping techniques from an adjacent YIG layer, although the origin of the effect, the SHE (Ohshima *et al.*, 2014; Dushenko *et al.*, 2016) or the EE (Mendes *et al.*, 2015), was a source of controversy. Dushenko *et al.* (2016) measured the spin-charge interconversion as a function of the gate with an ionic liquid and observed a sign change of the spin-charge interconversion signal when the carrier type was tuned from electrons to holes. Such a sign change with the carrier polarity is a result of symmetry (Milletarì *et al.*, 2017). The small spin-charge interconversion efficiency in graphene can be greatly enhanced by inducing spin-orbit coupling by proximity with a TMD, which gives rise to a spin texture with both an out-of-plane and a helical in-plane component. Theoretical calculations predicted a large SHE (Garcia, Cummings, and Roche, 2017) and EE (Offidani *et al.*, 2017; Garcia *et al.*, 2018) in graphene/TMD vdW heterostructures, in which both effects can be modulated by tuning the Fermi energy of the system, changing sign with the carrier polarity. While the SHE gives rise to a spin current and spin accumulation with spins pointing out of plane when a current is applied in the proximitized graphene [the red arrows in Fig. 37(a)], the EE generates a nonequilibrium spin density with spins pointing in plane [the blue arrow in Fig. 37(a)]. Using a nonlocal spin-valve technique that allows the direction of the generated spins to be distinguished [Fig. 37(a)], a large SHE was first experimentally confirmed in graphene/$MoS_2$ (Safeer *et al.*, 2019) and followed by the simultaneous observation of the SHE and EE in graphene/$WS_2$ (Ghiasi *et al.*, 2019; Benítez *et al.*, 2020). In particular, Benítez *et al.* (2020) experimentally confirmed the predicted sign change of the SHE (below ~200 K) and the EE (up to room temperature) with carrier concentration, which is tuned by gating the graphene [Fig. 37(b)]. A gate dependence of the EE in the proximitized graphene has also been reported for $WS_2$ (Ghiasi *et al.*, 2019), $TaS_2$ (Li *et al.*, 2020), $(Bi,Sb)_2Te_3$ (Khokhriakov *et al.*, 2020), and $MoTe_2$ (Hoque *et al.*, 2021). A large variation of the SHE with an applied gate has also been observed in graphene/$WSe_2$, with an unprecedented spin-charge interconversion efficiency (Herling *et al.*, 2020).

A different system of much interest for spin-charge interconversion involves 2DEGs that occur at interfaces of oxide heterostructures. A primary example is the 2DEG present in the $SrTiO_3/LaAlO_3$ system (Ohtomo and Hwang, 2004). Using spin pumping [Fig. 37(c)], Lesne *et al.* (2016) observed spin-charge interconversion with in-plane spins originating from the EE in $SrTiO_3/LaAlO_3$, thereby showing a large efficiency. A strong gate tunability associated with the band structure of the 2DEG allows the sign of the spin-charge

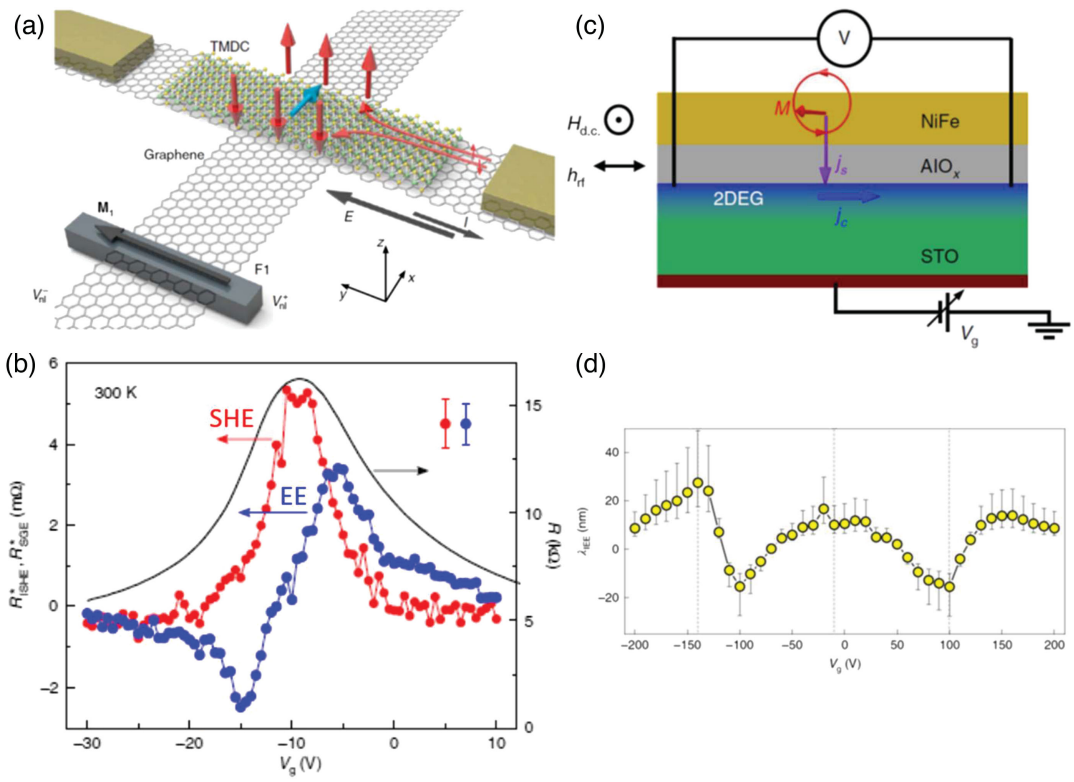


FIG. 37. (a) Sketch of the nonlocal spin-valve concept for spin-charge interconversion measurement in a graphene/TMD vdW heterostructure. A current $I$ along the graphene/TMD arm ($y$ axis) generates a nonequilibrium spin density due to the EE with spins along $x$ (blue arrow) and a spin accumulation with spins out of plane (along $z$) due to the SHE with opposite orientation at opposite edges of the graphene/TMD arm (red arrows). The induced spins diffuse in graphene toward the ferromagnetic electrode $F1$ and are detected by measuring $V_{nl}^F = V_{nl}^+ - V_{nl}^-$. The EE and SHE contributions to $V_{nl}^F$ are separated via spin precession by applying an external magnetic field along $z$ and $x$, respectively. (b) Spin-charge interconversion signals for the SHE (red line) and the EE (blue line) as a function of $V_G$. The sheet resistance of graphene vs $V_G$ is also plotted to show the charge neutrality point. (a),(b) From Benítez *et al.*, 2020. (c) Sketch of the spin-pumping experiment to quantify spin-charge interconversion in a $SrTiO_3/AlO_x$ 2DEG. (d) Gate dependence of the Edelstein length $\lambda_{IEE}$ of a $SrTiO_3/AlO_x$ 2DEG at 15 K. (c),(d) From Vaz *et al.*, 2019.

interconversion to be changed. A different gate dependence in the same system has been reported at room temperature (Song *et al.*, 2017). A more dramatic modulation of the EE by gate voltage was subsequently obtained in the 2DEG present in a $SrTiO_3/AlO_x$ interface (Vaz *et al.*, 2019), where the spin-charge interconversion efficiency parameter ($\lambda_{IEE}$) changes sign several times with gate voltage [Fig. 37(d)]. The evolution of this parameter with gate and its large value can be explained by the different contributions of the electronic bands involved, which have different properties ranging from Rashba-like splitting to topological avoided crossings. Spin-charge interconversion with spins out of plane originating from the SHE has also been observed in the 2DEG at the $SrTiO_3/LaAlO_3$ interface using a nonlocal double Hall bar setup (Jin *et al.*, 2017; Trier *et al.*, 2020). The gate control achieved is also attributed to the complex band structure of the 2DEG (Trier *et al.*, 2020). An electric-field control of charge-to-spin conversion has also been reported through unidirectional magnetoresistance measurements in $SrTiO_3$-based 2DEGs (Choe *et al.*, 2019; Vaz *et al.*, 2020) and in chiral tellurium crystals (Calavalle *et al.*, 2022).

### B. Ferroelectric control of spin-charge interconversion

As polar materials, ferroelectrics are a natural place to look to engineer Rashba spin-orbit coupling. In addition, their ability to accumulate and deplete charge (depending on the polarization direction) into adjacent materials induces electric fields (over the Thomas-Fermi screening length) whose amplitude and even sign may be switched; see Fig. 38(a). If the adjacent material possesses a sizable spin-orbit coupling, this may generate a region prone to displaying a Rashba spin-orbit coupling tunable electrically, and in a nonvolatile way. In the most simple case, the chirality of the spin contours would be reversed upon switching polarization, as sketched in Fig. 38(b). Injecting a spin current into such a system would then lead to the generation of a charge current whose sign will be set by the ferroelectric polarization direction [Fig. 38(c)] (Noël *et al.*, 2020). The operating device would thus be equivalent to that of a Rashba system combined with a ferromagnet in which magnetization switching would yield a produced charge current with a positive or negative sign, with the notable difference that here the sign of the output current is caused by switching a ferroelectric with an electric field rather than by switching a ferromagnet with a magnetic field (or spin torque). According to Manipatruni, Nikonov, and Young (2018), this is typically 1000 times more energy efficient. The operation of such a ferroelectric spin-orbit (FESO) device would require a regular ferroelectric rather than a multiferroic as in MESO devices, thereby circumventing the scarcity of such materials.

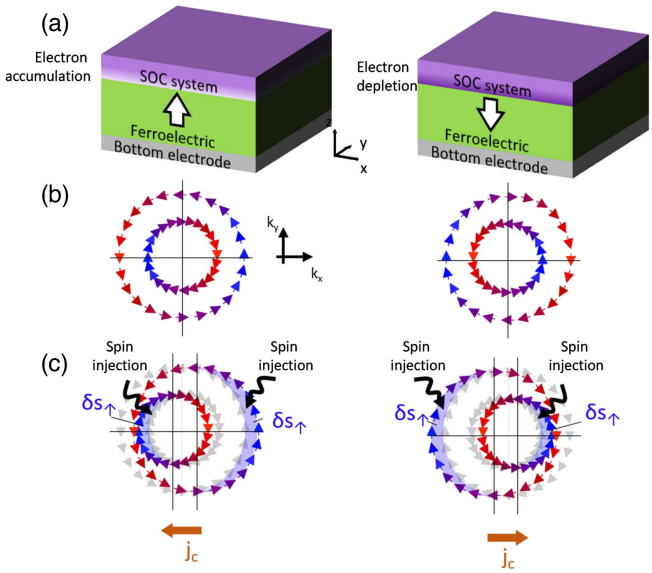


FIG. 38. (a) Sketch of an interfacial ferroelectric Rashba system in which the ferroelectric accumulates or depletes the carrier into an adjacent layer with large spin-orbit coupling (top layer), thus generating a Rashba state at the interface. (b) Spin contours in the Rashba states. The chirality is reversed upon switching the ferroelectric polarization direction. (c) Ferroelectric control of the IEE. From Noël *et al.*, 2020.

Perhaps the first system in which the combination of ferroelectricity and Rashba spin-orbit coupling was considered is GeTe (Di Sante *et al.*, 2013). This compound is the best known member of the family of ferroelectric Rashba semiconductors (FERSCs) (Picozzi, 2014). GeTe has a ferroelectric $T_C$ of about 700 K in which Ge and Te are displaced along the [111] direction from their ideal rocksalt sites (Pawley *et al.*, 1966). Its band gap is only ~0.6 eV (Park *et al.*, 2008), which led to difficulties in showing polarization switching that finally came through piezoresponse force microscopy experiments (Kolobov *et al.*, 2014). GeTe displays a giant Rashba splitting of $\alpha_R \sim 5$ eV Å owing to several factors, namely, the presence of heavy atoms with large spin-orbit coupling, a narrow gap, and the same orbital character of the valence and conduction bands. The electronic structure evidencing Rashba-split bands was first reported by Liebmann *et al.* (2016), who used ARPES and spin-polarized photoemission. Soon thereafter, two papers reported the dependence of the bands spin texture with ferroelectric polarization direction (Krempaský *et al.*, 2018; Rinaldi *et al.*, 2018). While Rinaldi *et al.* (2018) reported different spin textures for separate samples with up or down ferroelectric polarization tuned by the surface termination, Krempaský *et al.* (2018) applied an electric field *in situ* to detect this change.

The ability to control spin textures by ferroelectricity triggered studies on the influence of ferroelectric on spin-charge interconversion. Zhang *et al.* (2020) found that the spin Hall conductivity could be strongly tuned by ferroelectricity. Experimentally, Varotto *et al.* (2021) made a major advance in the integration of GeTe into spin-orbitronic devices. They not only provided evidence for ferroelectric switching from electric measurements but also showed that the amplitude and sign of spin-charge interconversion efficiency (of an amplitude comparable to that of Pt) changed with polarization switching at room temperature; see Fig. 39. This paves the way toward advanced devices based on FERSCs. We note that the related material SnTe has also been predicted to be a FERSC (Plekhanov *et al.*, 2014; Wang, Gopal *et al.*, 2020).

The low band gap of GeTe leads to the search for more insulating FERSCs in the traditional ferroelectric family:

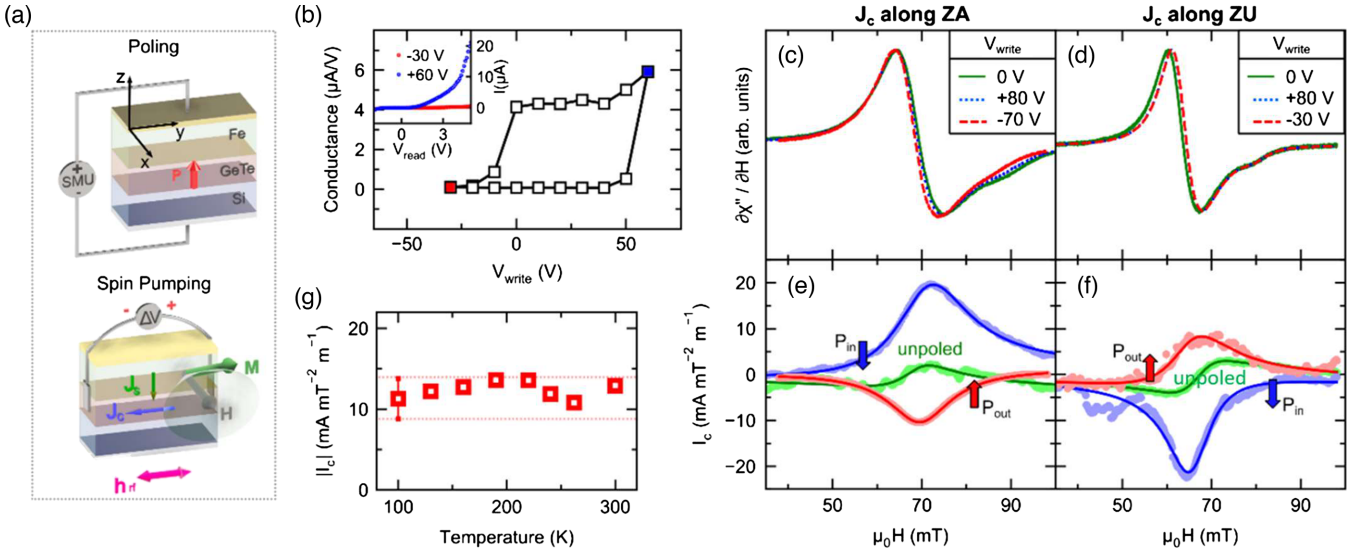


FIG. 39. Ferroelectric control of the spin-charge interconversion in GeTe investigated by spin pumping ferromagnetic resonance (FMR). (a) Setup for the study of the ferroelectric switching of the spin-charge interconversion in GeTe. Top: electrical circuit for ferroelectric switching monitored by resistance changes. Bottom: sketch of the contacts used to measure the lateral voltage proportional to the charge-current production in the same experiment. Negative (positive) voltage pulses were applied by a source-measure unit (SMU) to set the ferroelectric polarization direction ($P_{\rm in}$ or $P_{\rm out}$). (b) Hysteresis loop of the conductance vs $V_{\rm write}$ of a Au(3 nm)/Fe(20 nm)/GeTe(15 nm)/Si sample. Inset: *I-V* curves of the heterostructure after the application of two saturating voltage pulses at $V_{\rm write} = -30$ and $+60$ V. (c),(d) FMR spectra and (e),(f) normalized current production at 300 K for the slab oriented along the *ZA* and *ZU* directions vs ferroelectric polarization. The dashed curves correspond to $P_{\rm in}(V_{\rm write} < 0)$ and the dotted curves correspond to $P_{\rm out}(V_{\rm write} > 0)$. The spin-pumping peak is positive (negative) for $P_{\rm in}$ and negative (positive) for $P_{\rm out}$. The green curves in (e) and (f) refer to the pristine (unpoled) states. The relatively small amplitude of the spin-pumping signal in the unpoled state is associated with a multidomain ferroelectric configuration. (g) Temperature dependence of the charge current production. From Varotto *et al.*, 2021.

perovskite oxides. This includes $BiAlO_3$ (da Silveira, Barone, and Picozzi, 2016), $PbTiO_3$ (Arras *et al.*, 2019; Gosteau *et al.*, 2021), $BiInO_3$ (Tao and Tsymbal, 2018), strained $KTaO_3$ (Tao and Wang, 2016), and strained $SrBiO_3$ (Varignon, Santamaria, and Bibes, 2019). In $SrBiO_3$, in particular, ferroelectric polarization switching was predicted to lead to a reversal of the spin chirality of the Rashba state at the conduction band minimum (Varignon, Santamaria, and Bibes, 2019). Djani *et al.* (2019), however, argued that the pseudocubic perovskite oxide family is possibly not the best family to achieve a ferroelectrically tunable Rashba state, because in most cases the tunable Rashba state will not be present at the valence band minimum or the conduction band maximum but rather in other bands. They proposed that Aurivillius phases such as $Bi_2WO_6$ are more promising in this respect. Perovskite halides have also been proposed as FERSCs (Stroppa *et al.*, 2014; Isarov *et al.*, 2017), as well as perovskite nitrides (Zhao, Chen *et al.*, 2020). Outside of the perovskite family, an electrically reversible spin texture has also been proposed for $HfO_2$ (Tao *et al.*, 2017). However, to date there have not been any experimental demonstrations of a Rashba state in most of these compounds, let alone of the possibility to tune it through ferroelectricity.

Electrically tunable Rashba states at interfaces between a ferroelectric and a material with large spin-orbit coupling has also been explored. Mirhosseini *et al.* (2010) predicted a Rashba state at the interface between $BaTiO_3$ and an ultrathin film of Bi, with a modest dependence on polarization direction. This system was later explored experimentally, and a spin splitting was observed (Lutz *et al.*, 2017). A fully switchable, giant Rashba coefficient was predicted in oxide heterostructures combining $BaTiO_3$ with $BaRuO_3$, $BaIrO_3$, or $BaOsO_3$ (Zhong *et al.*, 2015) and in $BiInO_3/PbTiO_3$ heterostructures (Y. Song *et al.*, 2019).

Experimentally, interfacial systems have been used to achieve a ferroelectric control of spin-charge interconversion. A noteworthy result from Fang *et al.* (2020) is reported in Figs. 40(c) and 40(d). Working with a $La_{0.7}Sr_{0.3}MnO_3/PbZr_{0.2}Ti_{0.8}O_3/Pt$ heterostructure, they injected a spin-polarized current from $La_{0.7}Sr_{0.3}MnO_3$ by tunneling through the thin (5 nm) $PbZr_{0.2}Ti_{0.8}O_3$ ferroelectric layer; this current is converted into a charge current through the ISHE by the Pt. Depending on the ferroelectric polarization direction, the sign of the ISHE signal may be reversed. These experiments were reported at low temperature only, due to the low spin polarization of $La_{0.7}Sr_{0.3}MnO_3$ at higher temperatures (Garcia *et al.*, 2004), but could probably be extended to room temperature by replacing $La_{0.7}Sr_{0.3}MnO_3$ with another material.

The large IEE reported for $SrTiO_3$ 2DEGs (Chauleau *et al.*, 2016; Lesne *et al.*, 2016; Vaz *et al.*, 2019) makes them an appealing system for ferroelectric control of spin-charge interconversion. This is all the more true because $SrTiO_3$ is on the verge of ferroelectricity: $^{18}O$ substitution for $^{16}O$ (Itoh *et al.*, 1999), minute Ca substitution for Sr (Bednorz and Müller, 1984), epitaxial strain (Haeni *et al.*, 2004), the application of femtosecond light pulses (Nova *et al.*, 2019), and the application of a large electric field (Hemberger *et al.*, 1995; Sidoruk *et al.*, 2016; Manaka, Nozaki, and Miura,

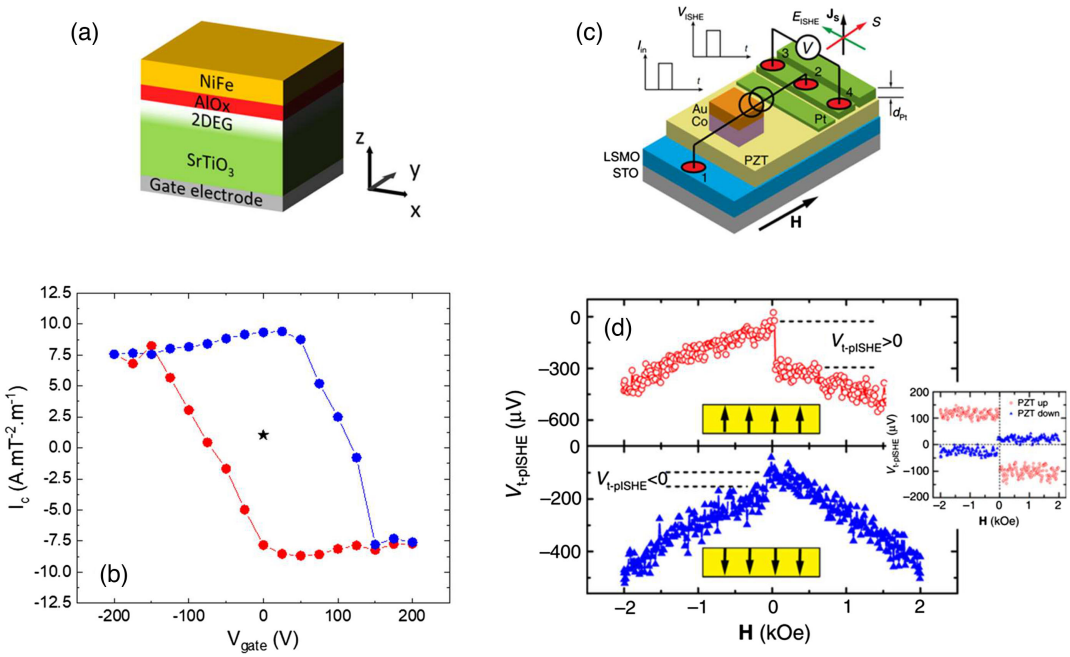


FIG. 40. (a) Sketch of the sample for detecting the ferroelectric control of the IEE. (b) Gate voltage dependence of the current produced by spin-charge interconversion through the IEE in $NiFe/AlO_x/SrTiO_3$ heterostructures after application of a large electric field to $SrTiO_3$ to induce a ferroelectriclike state $T = 7$ K. From Noël *et al.*, 2020. (c) Schematic illustrations of tunneling pulsed ISHE measurements in the ISHE type based on a $La_{0.7}Sr_{0.3}MnO_3/Pb(Zr,Ti)O_3/Pt$ stack. (d) The injected pulsed tunneling current ($I_e$) generates a flow of pulsed spin-current ($J_S$) in the Pt metal, which produces a transverse pulsed ISHE voltage ($V_{t\text{-pISHE}}$) at $T = 10$ K. From Fang *et al.*, 2020.

2017) all induce a ferroelectric (or ferroelectriclike) state in spin-orbit coupling.

Figures 40(a) and 40(b) present spin-charge interconversion experiments in $SrTiO_3$ 2DEGs formed by the deposition of a thin Al layer after application of a large electric field (of 5–10 kV/cm). The produced charge current displays a strong hysteretic dependence on the applied gate voltage that is reminiscent of the ferroelectric loops observed in this system (Noël *et al.*, 2020). It is noteworthy that two different remanent states with opposing produced current signs are obtained, as sketched in Fig. 38(c). This strong gate dependence and sign change is likely connected with the multiorbital nature of the 2DEG electronic structure, with competing bands having different effective Rashba coefficients. Also important is the large spin-charge interconversion figure of merit in this system, with $\lambda_{\mathrm{IEE}} \sim 30$ nm.

Finally, we mention several recent predictions of ferroelectric Rashba systems in 2D or monolayer materials. This includes $Ag_2Te$ monolayers (Alam *et al.*, 2012), $MX_2$ monolayers ($M =$ Mo or W; $X =$ S, Se, or Te) (Bruyer *et al.*, 2016), and $WO_2Cl_2$ (Ai *et al.*, 2019).

### C. Electric control of STT and SOT

Starting with STT-based devices, Wang *et al.* (2012) and Wang and Chien (2013) first reported the combined effect of VCMA and STT in a MTJ with PMA consisting of a $CoFeB/MgO/CoFeB$ stack; see Fig. 41(a). In such a MTJ, $H_C$ of the free CoFeB layer shows a dramatic change under different bias voltages due to the VCMA [Fig. 41(b)]. By applying consecutive negative pulses with alternating amplitude, the free CoFeB layer is reversibly switched as it is monitored with low-voltage TMR measurements [Fig. 41(c)]. The explanation of the unipolar switching is sketched in Fig. 41(d). On the whole, the strong reduction of $H_C$ at negative voltage allows the STT switching to occur at a current density of $\sim 10^4\ \mathrm{A\,cm^{-2}}$, much smaller than the expected value of $\sim 10^6\ \mathrm{A\,cm^{-2}}$. Using also the combination of VCMA and STT and the same MTJ type, Kanai *et al.* (2014) applied a switching scheme with two voltage pulses: whereas the first pulse induced magnetization precession by the electric-field effect on magnetic anisotropy (see Sec. II.C.3), the second pulse stablilized the magnetization direction by STT. This way, a faster and more reliable switching can be obtained. Theoretical simulations showed that, when combining an $E$ field and STT with a single pulse in this system, a deterministic switching was achieved with a current density above $\sim 5 \times 10^5\ \mathrm{A\,cm^{-2}}$, leading to a decrease in the power consumption by 2 orders of magnitude compared to the switching by STT only (Zhang, Zhang *et al.*, 2015; Zhang *et al.*, 2016).

Once the interest of the community shifted from STT to SOT, so did the possibility of combining the effect of the $E$ field with SOT through the $E$ field control of spin-charge interconversion. Using the prototypical $Pt/Co/Al_2O_3$ stack for SOT, Liu, Lim, and Urazhdin (2014) observed the modulation of the fieldlike torque with an $E$ field caused by the enhancement of the interfacial Rashba effect. A modulation of interfacial spin-orbit fields by directly applying an $E$ field was confirmed in the $Fe/GaAs(100)$ interface by Chen *et al.* (2018).

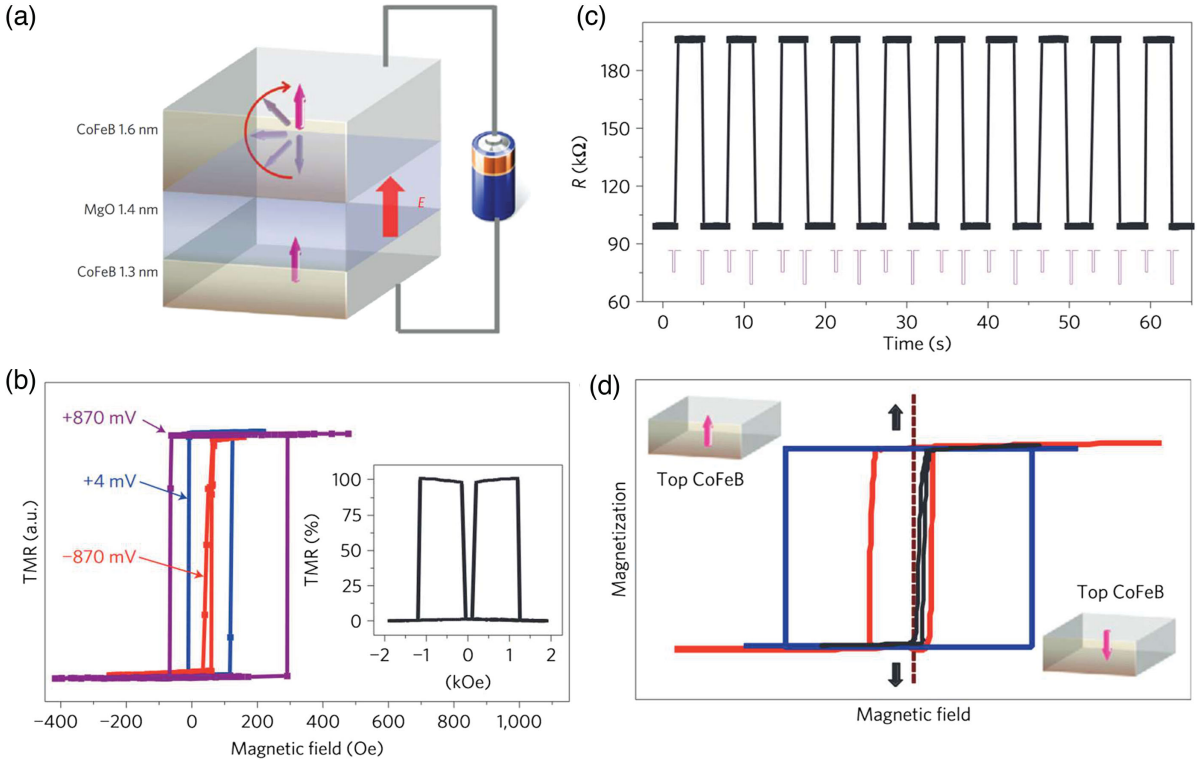


FIG. 41. Electric control of STT. (a) Sketch of a perpendicularly magnetized MTJ and the effect of the electric field through a voltage to the free CoFeB layer. (b) Normalized minor loops of the TMR curve at different applied bias values. Inset: full TMR curve measured at low bias. (c) Unipolar switching of the MTJ using a series of negative pulses (schematically shown in purple at the bottom) with alternating amplitudes of −0.9 and −1.5 V. A constant biasing magnetic field ($H_{\mathrm{bias}}$) of 55 Oe was applied in favor of the antiparallel state at −0.9 V. (d) Sketch of the hysteresis loops of the top CoFeB layer showing the unipolar switching process: magnetization down → up switching at $V = V_1$ (red) through STT with a greatly reduced energy barrier; magnetization up → down switching at $V = V_2$ (black) using another negative electric field, where $|V_2| > |V_1|$. The loop for $V = 0$ is shown in blue. The vertical dotted line represents the position of the constant $H_{\mathrm{bias}}$. The moment of the bottom CoFeB is fixed pointing down. From Wang *et al.*, 2012.

Although in these cases the $E$ field directly affects the spin-charge interconversion, in general it influences the spin-charge interconversion in a more indirect way (for instance, through oxygen ion migration). By replacing $Al_2O_3$ with $GdO_x$, a nonvolatile voltage control of the oxidation state in the $Co/GdO_x$ interface was achieved, leading not only to the expected decrease in the magnetic anisotropy of Co but also to an enhancement of the dampinglike torque, although the later origin could not be addressed (Emori *et al.*, 2014). With this same system, Mishra *et al.* (2019) observed a change not only in the magnitude but also in the direction of the SOT, which they attributed to the transport of oxygen ions ($O^{2-}$) modifying the interfacial Rashba SOT at the Pt/Co interface. In a similar stack $Pt/Co/HfO_x$ using ionic liquid gating, Yan *et al.* (2016) reported the modulation of the dampinglike torque, in this case attributed to the variation of the spin transparency of the Pt/Co interface with the $E$ field. Also using $HfO_x$ as a gate insulator, Hirai *et al.* (2020) studied the voltage control of SOT in an in-plane magnetized $Pd/Co/Pd/HfO_x$ stack in which $O^{2-}$ migration at the top Co/Pd interface is at the origin of the modulation of both the dampinglike and the fieldlike torque through different mechanisms. Using oxygen-incorporated Pt in a stack, $Pt(O)/FeNi/SiO_2$, where the dampinglike torque is claimed to arise from the Pt(O)/FeNi interfacial spin-orbit coupling, An *et al.* (2018) achieved a voltage control of such SOT through reversible migration of $O^{2-}$ toward or away from that interface. Another indirect way in which an $E$ field can modulate the spin-charge interconversion is through strain, which has also been shown by Filianina *et al.* (2020) to influence the SOT in perpendicularly magnetized W/CoFeB/MgO stacks grown on piezoelectric PMN-PT through a combination of spin-orbit coupling, crystal symmetry, and orbital polarization. Moving from metals to more exotic systems such as topological insulators, the $E$ field can change the Fermi level position within the gap of the material. Fan *et al.* (2016) reported $E$-field control of SOT in a single layer of Cr-doped $(Bi, Se)_2Te_3$, a magnetically doped topological insulator. By voltage gating the topological insulator, the SOT strength can be modulated up to a factor of 4 and was attributed to the variation of the carrier density of the topologically protected surface states, which are the source of the spin-charge interconversion.

A second possibility is that the $E$ field directly controls the VCMA, which is the case reported by Inokuchi *et al.* (2017), where the switching current is reduced up to 3.6 times in in-plane magnetized Ta/CoFeB/MgO/CoFeB/Ru/CoFe/IrMn stacks by changing the control voltage from −1.0 to +1.0 V; see Fig. 42. In many recent works, though, the $E$-field effect has been shown to modulate both the VCMA and the spin-charge interconversion. For example, Xu and Chien (2021)

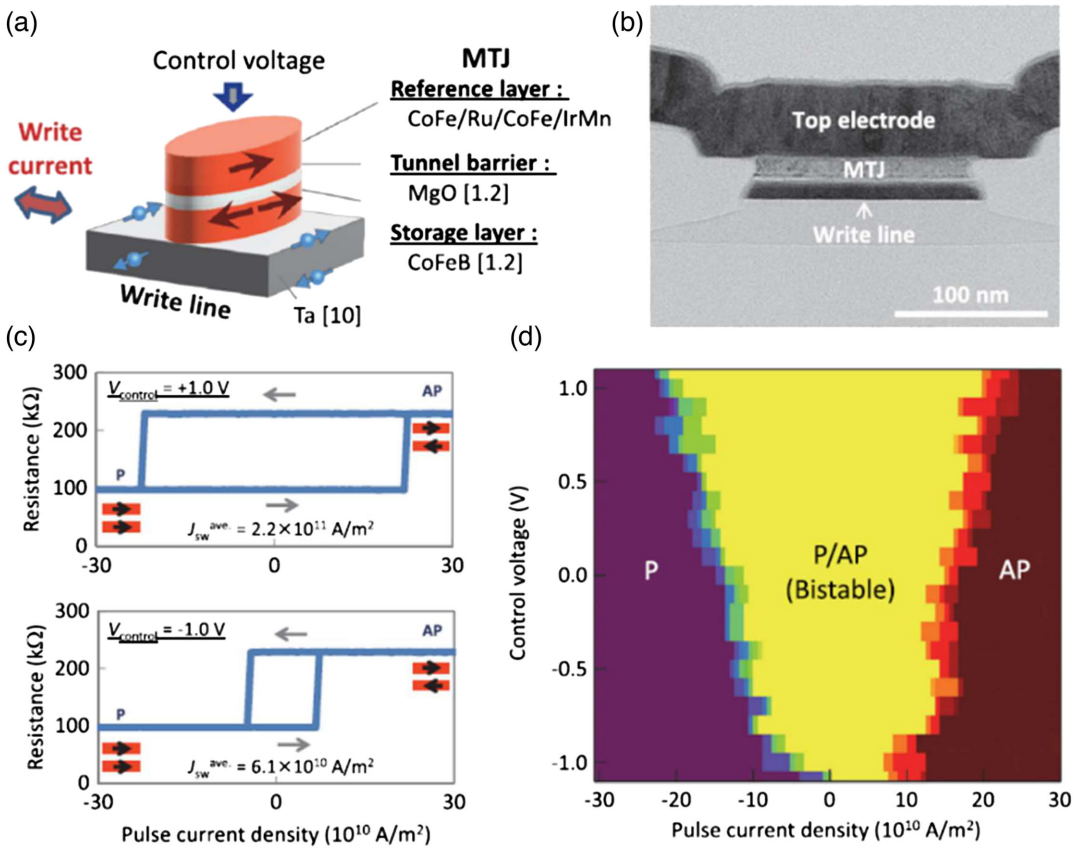


FIG. 42. Electrical control of SOT. (a) Sketch and (b) cross section TEM image of the device, a single MTJ consisting of Ta/CoFeB/MgO/CoFeB/Ru/CoFe/IrMn fabricated on a thermally oxidized Si wafer. (c) MTJ resistance as a function of the write pulse current density while applying a control voltage pulse of +1.0 V (top panel) and −1.0 V (bottom panel). The width of both the write current pulse and the control voltage pulse was 50 ns. No $H_{\mathrm{bias}}$ was applied during the measurement. (d) Switching phase diagram obtained by taking the resistance-write pulse current density curves. From Inokuchi *et al.*, 2017.

reported an efficient voltage control of SOT in a W/CoFeB/MgO stack with PMA that arises from both a decrease in $H_{\mathrm{C}}$ of the ferromagnet and an increase in the dampinglike torque efficiency. In contrast, using perpendicularly magnetized IrMn/CoFeB/MgO stacks, Li *et al.* (2021) observed that, while VCMA helps to reduce the switching current, the dampinglike torque decreases with applied voltage, thereby becoming detrimental for the switching current reduction.

SOTs produced by spin-charge interconversion were also shown to be tunable by ferroelectricity. In Pt/CoNiCo/Pt/PMN-PT heterostructures, by switching the in-plane ferroelectric polarization of the PMN-PT substrate, the chirality of the current-induced magnetization switching curves is reversed (Cai *et al.*, 2017). The ferroelectric polarization has been argued to generate an additional, switchable SOT in the CoNiCo.

## V. DEVICES

### A. Spintronic devices for logic and memory based on electrical control of magnetism

#### 1. From toggle MRAM to SOT MRAM

With the currently growing demand for big-data storage and processing, a highly efficient and low-power processing of large data becomes a major challenge that is difficult to overcome with conventional electronic components. The separation of memory and processor units in conventional von Neumann architectures causes long memory access latency, limited memory bandwidth, and large power dissipation known as the memory wall and the power wall (Wulf and McKee, 1995; Kuroda, 2002; Nam *et al.*, 2003; Guo *et al.*, 2021). Therefore, to break this bottleneck, processing in memory has reignited great interest and is stimulated by the development of nonvolatile memories such as spintronic MRAM and MESO devices. STT MRAMs, which have been in production by major electronic companies for only a few years, have already begun to contribute to a reduction of the large energy consumption and significant contribution to global warming by all of the information and communication technologies (about 10% of the worldwide electricity production today, with a value of about 20% expected in 2030); see Fig. 4 (Jones, 2018).

A road map for spintronic logic and memory devices is displayed in Fig. 43. In almost all MRAMs, the memory is associated with the relative orientations of the magnetization in the free layer and the reference layer of a MTJ, and the main differences are in the writing process. Toggle MRAM (Engel *et al.*, 2005), which has been on the market since 2006, is written using the magnetic field generated by currents in additional lines. The increase of the critical switching field

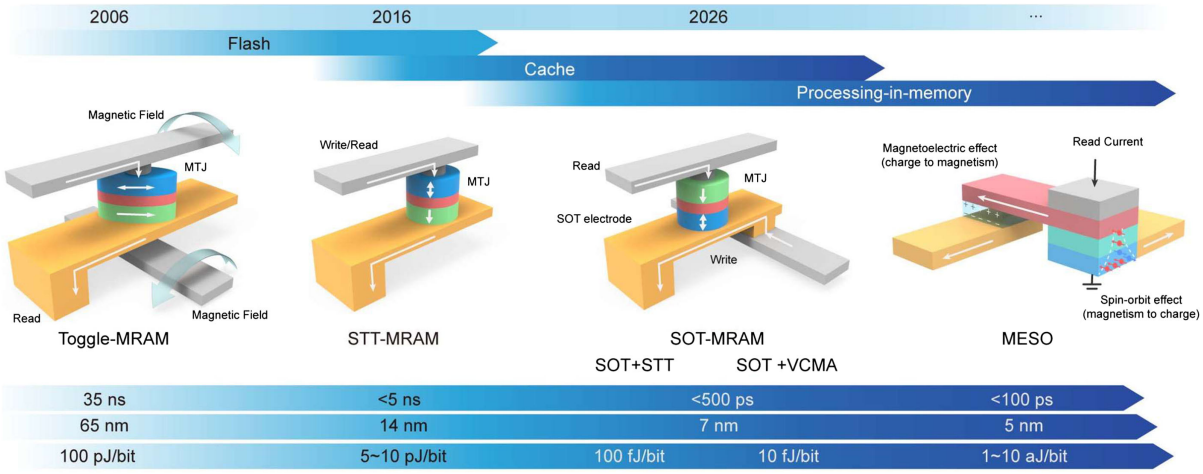


FIG. 43. Road map for spintronic logic and memory devices and advances to higher write speed, smaller size, and lower power dissipation in areas of processing in memory ranging from toggle MRAM, on the market since 2006, to STT MRAM, which is in production today, and the SOT MRAM or MESO devices expected in the coming generations. Adapted from Guo *et al.*, 2021.

with downsizing of toogle MRAM and the resulting increase of driving currents degrades the power consumption performance at small sizes. However, owing mainly to their radiation hardness and wide temperature range, toggle MRAM has been extensively adopted in certain technologies for avionics, space, and defense.

The memory of a STT MRAM is written using the action of the STT generated by a vertical current in the structure, as discussed in Sec. III.B. The magnetizations can be in plane, in the form of in-plane magnetic anisotropy (IMA), or out of plane, in the form of PMA. IMA requires a shape anisotropy (an ellipse or rectangle) to generate an easy axis of magnetization and the resulting thermal stability. However, at small sizes the shape anisotropy is not large enough to provide sufficient thermal stability. Consequently, STT MRAMs with PMA are better adapted to downsizing and low dissipation (Guo *et al.*, 2021). This is the type of STT MRAM in development today by the electronic industry. STT MRAMs are of high interest to replace embedded flash and DRAM memories. In addition, with technology nodes of STT MRAM scaling down to 10 nm and write speeds reaching the nanosecond range, they also have a possible interest to replace the relatively large static random-access memory (SRAM) in logic circuits (processing in memory).

The promising MRAMs for the next generation are SOT MRAMs with writing by SOT (dampinglike torque). As described in Sec. III.C.2, the advantage of the SOT with PMA is the timescale for switching and writing, which can be in the nanoscale range or shorter. Both heavy metals (Pt, Ta, W, etc.) and 2DEGs at Rashba interfaces or surface-interface states of topological insulators or Dirac semimetals have been tested as the spin source. As discussed in Sec. III.C.2, the generation of spin current by 2DEGs can be more efficient than with heavy metals, at least if the shunting by the magnetic layers or the bulk part of the spin-orbit coupling material can be controlled. Growth by MBE can give interfaces of better quality but sputtering ($\alpha$-Sn) has also led to good results.

However, with PMA a difficulty for switching by SOT is the generation of the needed in-plane field. In Sec. III.C.4, we described how field-free switching can be achieved by exchange-bias coupling with an antiferromagnetic material, by combining SOT with STT, etc. Recently it was theoretically and experimentally demonstrated that the combination of SOT and STT enables subnanosecond ultrafast and low-power magnetization switching through a proper timing scheme (Z. Wang *et al.*, 2019; Cai *et al.*, 2021).

Another solution is SOT with VCMA in which a voltage pulse changes the interfacial magnetic anisotropy (Yoda *et al.*, 2016; Inokuchi *et al.*, 2017; Peng *et al.*, 2019). The reorientation of the magnetization and fieldlike torque induces precessions between the two stable magnetization states and allows the magnetic switching. In addition, with no current through the MTJ, this solution is of interest for dissipation reduction. Recently, Grimaldi *et al.* (2020) showed that the combination of SOT, STT, and VCMA leads to reproducible subnanosecond switching with a narrow distribution of the switching times. The study was performed in a perpendicularly magnetized MTJ (with a top-pinned CoFeB/MgO/CoFeB free layer) deposited on a $\beta$-phase W current line by simultaneously applying a bias in the MTJ and a current in the W line (Grimaldi *et al.*, 2020). Such a combination reaches an energy efficiency comparable to that of STT, with the main advantage of SOT for switching in the subnanosecond range (Krizakova *et al.*, 2021). Finally, spintronic reconfigurable logic gates based on SOT and VCMA have also been proposed and tested for several types of logic operations (Baek, Park *et al.*, 2018).

Other efforts were devoted to the introduction of concepts of two-terminal devices having advantages over the three-terminal device displayed in Fig. 43 in terms of downscaling the structure. An example of a two-terminal SOT MRAM using an in-plane current not only to write using the SOT induced by the SHE of Pt but also to read using in-plane current and GMR was reported by Avci *et al.* (2021). A comparison between the properties of current volatile devices (DRAM and SRAM) and perpendicular STT MRAM and SOT MRAM is presented in Table III.

TABLE III. Comparison of the properties of volatile memory technologies and perpendicular STT (pSTT) MRAM and SOT MRAM at advanced CMOS technology modes (7 and 5 nm). The numbers for SRAM and DRAM are for current technologies, and those for STT MRAM [in the pSTT 35 nm write error rate (WER) column] and SOT MRAM are extrapolated to optimized devices. Adapted from Dieny *et al.*, 2020.

| | Volatile | | | | Nonvolatile | |
|---|---|---|---|---|---|---|
| | DRAM 10× | HP SRAM 5 nm | HD SRAM 5 nm | HD SRAM 7 nm | pSTT 35 nm WER | SOT 35 nm |
| Technology/node | 10× | 5 nm | 5 nm | 7 nm | 5 nm | 5 nm |
| Write energy/bit (fJ) | 89 | 19 | 76 | 70 | <500/375 | 75 |
| Read energy/bit (fJ) | 58 | 17 | 55 | 50 | 60/52 | 15 |
| Write latency (ns) | 10 | >1 | 2.75 | 2.5 | >10/7.5 | 1.2 |
| Read latency (ns) | 10 | >1 | 2.5 | 2.2 | 3.5/3.5 | 1 |
| Cell size ($\mu m^2$) | 0.0026 | 0.034 | 0.0267 | 0.0422 | 0.014/0.009 | 0.0282 |

We end this section by pointing out that MRAMs are commercial products that are entering the consumer electronics market. For instance, Sony's CXD5605 Global Positioning System receiver uses an 8 MB MRAM chip manufactured by Samsung (28 nm node) and is used in Huawei's GT2 smartwatch. Another example is Ambiq's Apollo, a system on a chip for the Internet of things that uses one 2 MB and one 1 MB MRAM chips (Coughlin and Handy, 2021). A much larger market may open for MRAM if it can be scaled beyond 22 nm, which is believed to be the limit for embedded flash memories (LaPedus, 2023).

### 2. Multiferroic junctions

Parallel to MTJs, another type of tunnel device consisting of an ultrathin ferroelectric layer sandwiched between two metallic electrodes (Esaki, Laibowitz, and Stiles, 1971) was investigated more (Tsymbal and Kohlstedt, 2006; Garcia *et al.*, 2009). In such ferroelectric tunnel junctions, the reversal of the ferroelectric polarization by an external electric field can produce a large change in the tunnel transmission due to electrostatic effects (if there is any asymmetry between the two interfaces) (Zhuravlev *et al.*, 2005), an effect called tunnel electroresistance (Chanthbouala *et al.*, 2012a; Garcia and Bibes, 2014; Wen and Wu, 2020). Merging ferroelectricity and MTJs in so-called multiferroic tunnel junctions consisting of a ferroelectric tunnel barrier sandwiched by two ferromagnetic electrodes gives rise to a four-resistance state memory due to the combined tunnel electroresistance and TMR effects related to the two ferroic orders.

The existence of a four-state memory was first experimentally reported using a multiferroic (ferroelectric and ferromagnetic) tunnel barrier of $La_{0.1}Bi_{0.9}MnO_3$ sandwiched between $La_{0.7}Sr_{0.3}MnO_3$ and Au electrodes (Gajek *et al.*, 2007). Resorting to pure ferroelectric and ferromagnetic materials is probably more adequate for this type of multiferroic devices, as it should in principle allow room-temperature operation (high ordering temperature in traditional ferroelectric materials), as well as a more efficient magnetic decoupling between the barrier and the magnetic electrode. In addition, interfacial magnetoelectric coupling between the ferroelectric tunnel barrier and the ferromagnetic electrode can be detected by measuring the variations of TMR induced by ferroelectric polarization reversal. For instance, large interfacial magnetoelectric coupling was predicted as a result of a modification of the bonding at the $Fe/BaTiO_3$ interface, with sizable changes of the Fe- and Ti-induced magnetic moments when the ferroelectric polarization is reversed (Duan, Jaswal, and Tsymbal, 2006). Experiments using $Fe/BaTiO_3(1.2\ nm)/La_{0.7}Sr_{0.3}MnO_3$ tunnel junctions confirmed these predictions with large changes of the TMR of up to 450%, depending on the ferroelectric polarization state of the tunnel barrier [Fig. 44(a)] (Garcia *et al.*, 2010). The TMR is high (low) when the $BaTiO_3$ polarization points toward Fe ($La_{0.7}Sr_{0.3}MnO_3$), which is in agreement with electric-field-induced modifications of the spin polarization at the $Fe/BaTiO_3$ interface (Bocher *et al.*, 2012). Thus, the electric-field control of the polarization of the ferroelectric tunnel barrier provides a way to control the spin polarization in a nonvolatile way and with low energy.

Radaelli *et al.* (2014) demonstrated that ferroelectric polarization reversal at the $Fe/BaTiO_3$ interface controls the magnetic interaction of the interfacial ultrathin FeO, thereby suggesting an alternative scenario for the large changes of TMR reported in $Fe/BaTiO_3/La_{0.7}Sr_{0.3}MnO_3$: when the ferroelectric polarization points toward Fe, ferromagnetism in FeO promotes a significant spin polarization, while when it points away from Fe antiferromagnetism in FeO results in a low effective spin polarization. Later it was shown that the sign of the TMR can even be reversed by switching the ferroelectric polarization in $Co/PbZr_{0.2}Ti_{0.8}O_3(3.2\ nm)/La_{0.7}Sr_{0.3}MnO_3$ tunnel junctions (Pantel *et al.*, 2012). Although the TMR is not large in these particular devices, its relative variation with the ferroelectric polarization reaches −230%. The ferroelectric tunnel junction can be used not only as a simple binary nonvolatile resistive memory encoded by the two saturated states of polarization but also as a memristor related to the presence of multiple nonuniform configurations of ferroelectric domains (Chanthbouala *et al.*, 2012b). Consequently, a multilevel state of tunnel magnetoresistance (varying from −3% to −30%) was reported for $Co/PbTiO_3(4.8\ nm)/La_{0.7}Sr_{0.3}MnO_3$ junctions upon progressively tuning the ferroelectric domain population under voltage pulses [Fig. 44(b)] (Luo *et al.*, 2018).

In some cases, ferroelectric polarization reversal can even trigger interfacial phase transitions, as was suggested for $La_{0.7}Sr_{0.3}MnO_3/La_{0.5}Ca_{0.5}MnO_3(0.8\ nm)/BaTiO_3/La_{0.7}Sr_{0.3}MnO_3$ (Yin *et al.*, 2013). The polarization-induced metal-insulator phase transition in $La_{0.5}Ca_{0.5}MnO_3$ is accompanied by a ferromagnetic-antiferromagnetic transition, giving rise to a change of the TMR from about 100% when the ferroelectric polarization points toward $La_{0.5}Ca_{0.5}MnO_3$ (ferromagnetic state) to nearly zero when it points away from $La_{0.5}Ca_{0.5}MnO_3$ (antiferromagnetic state). Therefore, driving

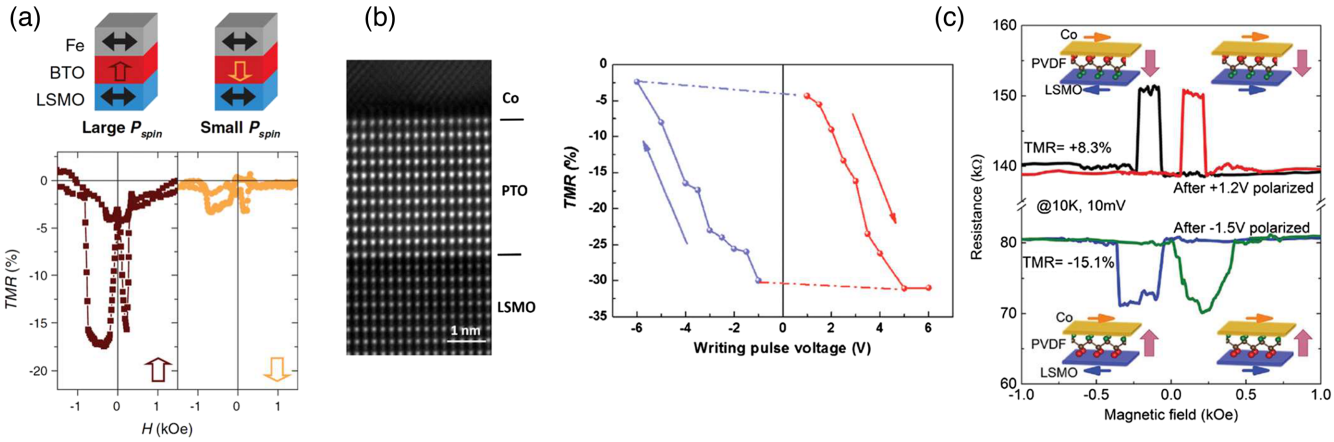


FIG. 44. (a) Ferroelectric control of the TMR in $Fe/BaTiO_3/La_{0.7}Sr_{0.3}MnO_3$ tunnel junctions. Top images: orientation of the ferroelectric polarization of the tunnel barrier, which controls the spin polarization at the $Fe/BaTiO_3$ interface. Bottom panel: TMR (4.2 K, 50 mV) for both polarization states after $\pm 1$ V, 1 s pulses. From Garcia *et al.*, 2010. (b) Left panel: annular dark field scanning transmission microscopy cross section image of the $Co/PbTiO_3/La_{0.7}Sr_{0.3}MnO_3$ junction. Right panel: hysteretic dependence of the TMR (10 K, 10 mV) with the polarization state of $PbTiO_3$ controlled using various pulse voltages (50 μs). From Luo *et al.*, 2018. (c) TMR of a $Co/PVDF/La_{0.6}Sr_{0.4}MnO_3$ junction (10 K, 10 mV) after the PVDF is polarized downward (+1.2 V) and upward (−1.5 V). From Liang *et al.*, 2016.

an interfacial magnetic phase transition with the ferroelectric polarization of the tunnel barrier is an efficient way to control the spin polarization of the tunnel current. More recently it was shown that spin reconstructions at the interfaces of a $La_{0.7}Sr_{0.3}MnO_3/BaTiO_3/La_{0.7}Sr_{0.3}MnO_3$ multiferroic tunnel junction result in a spin filtering effect that can be turned on and off by reversing the ferroelectric polarization (Tornos *et al.*, 2019). This tunable spin filter enables a giant electrical modulation of the TMR of between 10% and 1000%. Alternatively, multiferroic tunnel junctions including an organic ferroelectric barrier of PVDF were investigated. Note that the TMR of these $Co/PVDF/La_{0.6}Sr_{0.4}MnO_3$ junctions changes its sign when the ferroelectric polarization is reversed [Fig. 44(c)], which is interpreted by a change of sign of the spin polarization at the Co/PVDF interface (Liang *et al.*, 2016).

As all of the aforementioned experiments on multiferroic tunnel junctions use an epitaxial oxide perovskite of $La_{0.7}Sr_{0.3}MnO_3$ as a bottom electrode, a sizable tunnel magnetoresistance is limited to low temperature (Yin *et al.*, 2011; Pawlak *et al.*, 2022), which restricts their potential for applications. Other material combinations including transition metals and their alloys and new ferroelectric materials ($HfO_x$, 2D ferroelectrics, etc.) should be investigated thoroughly to develop efficient ferroelectric control of spin polarization at room temperature. In this vein, first-principles calculations performed on vdW multiferroic tunnel junctions combining 2D ferroelectric $In_2Se_3$ and ferromagnetic $Fe_nGeTe_2$ have recently predicted multiple resistance states with sizable TMR and tunnel electroresistance, together with low resistance-area products ($<1\ \Omega\,\mu m^2$) (Su *et al.*, 2021).

### 3. Magnetoelectric memories

The MRAM outperforms other nonvolatile memory technologies in terms of reading and writing speed and endurance. However, writing the magnetic states using either STT or SOT requires high current densities, which limits the scalability of these devices. Therefore, several schemes of magnetoelectric RAMs (MeRAMs) involving electric-field control of magnetization rather than current-based control were proposed in the late 2000s.

One of them consisted of applying an electric field across the antiferromagnetic magnetoelectric $Cr_2O_3$ during a cooling step through its Néel temperature, to tune the exchange bias onto an adjacent Co/Pt multilayer of an MRAM (Chen *et al.*, 2006). A simpler concept proposed by Bibes and Barthélémy (2008) consisted of using an antiferromagnetic and ferroelectric multiferroic (such as $BiFeO_3$) exchange coupled to one of the ferromagnetic layers of a spin valve. In this three-terminal device, the electric field applied across the multiferroic thin film switches the ferroelectric polarization and the antiferromagnetic order via the magnetoelectric coupling (Zhao *et al.*, 2006; Lebeugle *et al.*, 2008). Switching of the antiferromagnetic multiferroic modifies the exchange coupling to the ferromagnetic layer and ideally reverses its direction by 180° at zero magnetic field. This magnetization reversal is then probed electrically by the two-terminal current-perpendicular-to-plane GMR. Allibe *et al.* (2009) experimentally explored this concept, reduced the leakage of the multiferroic $BiFeO_3$ film while preserving the exchange bias to a metallic ferromagnet, and demonstrated the first electric-field control of the GMR in $Co/Cu/CoFeB/BiFeO_3$ magnetoelectric devices, although the effect was not reversible (Allibe, Deranlot, and Bibes, 2012). By optimizing the quality of the $BiFeO_3$ multiferroic thin films and using an in-plane geometry for the switching of polarization, Heron *et al.* (2014) demonstrated, in a two-step process for the switching of polarization, a deterministic switching of ferromagnetism and detected a hysteretic variation of the resistance of a $Pt/Co_{0.9}Fe_{0.1}/Cu/Co_{0.9}Fe_{0.1}$ spin valve as a function of the voltage applied to the $BiFeO_3$ [Fig. 45(a)]; see also Fig. 13.

Another approach proposed by Pertsev and Kohlstedt (2009) consisted of using strain resulting from the voltage

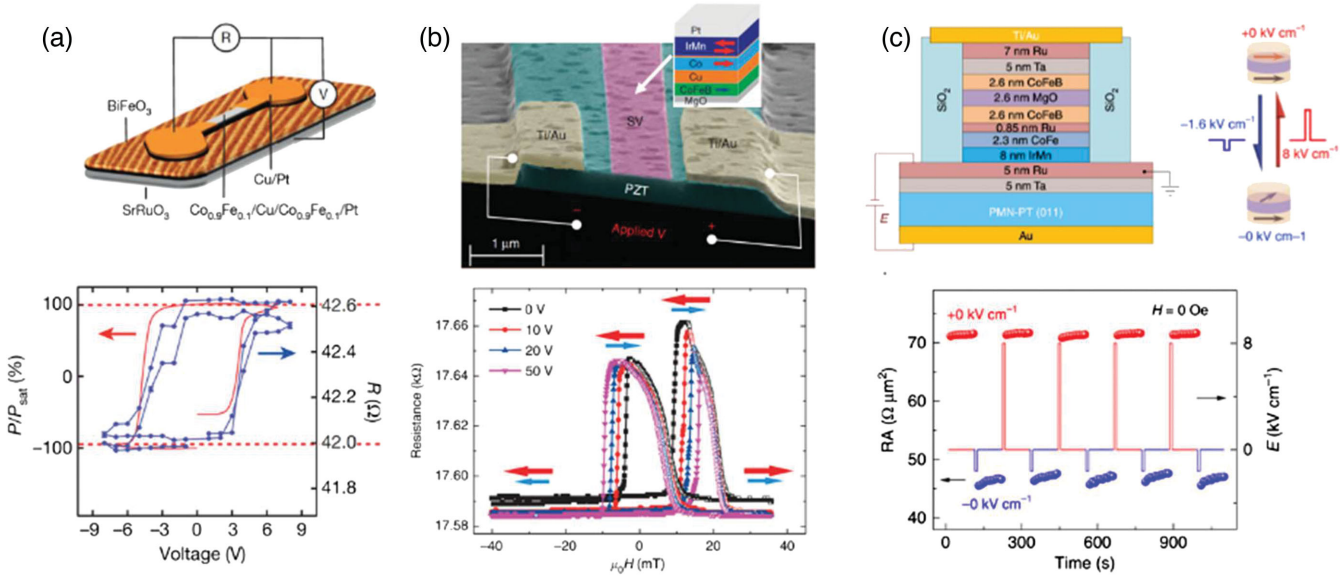


FIG. 45. (a) Top image: schematic of a magnetoelectric device consisting of a $Co_{0.9}Fe_{0.1}/Cu/Co_{0.9}Fe_{0.1}$ spin valve on $BiFeO_3$. Bottom panel: two $R(V)$ loops under zero magnetic field along with a ferroelectric loop (red line) from a neighboring device. From Heron *et al.*, 2014. (b) Top image: Sketch of the spin-valve (SV) stack and cross section of the device measured using scanning electron microscopy. Bottom panel: GMR loops with different applied voltages, which start with a depolarized state of the $Pb(Zr, Ti)O_3$ layer. From Lei *et al.*, 2013. (c) Top image: schematic of the MTJ device structure deposited on PNM-PT. Bottom panel: repeatable bistable remanent resistance states modulated by 8 and $-1.6$ kV cm$^{-1}$ electric-field pulses in the absence of a bias magnetic field. RA is the resistance-area product. From Chen *et al.*, 2019.

applied across the piezoelectric ferroelectric to control the magnetization direction of a magnetostrictive electrode of a MTJ. Using phase simulations, Hu *et al.* (2011) further extended the concept of a strain-mediated MeRAM and simulated low write energy (0.16 fJ/bit) together with potentially high memory density (88 Gbyte in.$^{-2}$) on MRAMs composed of magnetostrictive Ni coupled to relaxor lead magnesium niobate–lead titanate. Lei *et al.* (2013) demonstrated that voltage-driven strain effects from a $Pb(Zr, Ti)O_3$ gate can be used to pin the domain wall propagation in a magnetostrictive CoFeB magnetic wire. The resulting $H_C$ change of this free CoFeB magnetic layer is then probed using the modifications of the GMR of IrMn/Co/Cu/CoFeB as a function of voltage [Fig. 45(b)]. The butterfly hysteretic voltage loop of the propagation magnetic field of the CoFeB layer is correlated with capacitance versus voltage hysteresis loops of the $Pb(Zr, Ti)O_3$, supporting the belief that strain-driven magnetoelectric effects are controlling the spintronic device.

The same kind of geometry was used to control the GMR of Co/Cu/Fe spin valves on $BaTiO_3$ single crystals (Savitha Pillai *et al.*, 2015). Using IrMn/CoFeB/$AlO_x$/CoFeB MTJ on PMN-PT, Li *et al.* (2014) demonstrated a volatile 90° rotation of the free CoFeB layer by applying a vertical electric field to the (011) ferroelectric substrate, which resulted in modifications of the TMR under the electric field. A similar volatile strain-mediated MeRAM was then proposed with CoFeB/MgO/CoFeB MTJs on PNM-PT using a local gating scheme (Zhao *et al.*, 2016). More recently Chen *et al.* (2019) demonstrated a large (55%), reversible, and nonvolatile change of the TMR of CoFeB/MgO/CoFeB on PNM-PT without need for a magnetic field [Fig. 45(c)]. This was achieved with an electric-field-induced remanent magnetization rotation of 90° of the CoFeB top free layer via strain-mediated magnetoelectric coupling [Fig. 45(c)]. Using a similar stack but combining two pairs of in-plane electrodes on the ferroelectric [Fig. 46(a)], Chen, Zhao *et al.* (2019) later demonstrated the full control of the IMA of the CoFeB free layer by the electric-field-induced in-plane strain [Fig. 46(b)]. By combining voltage sequences to the different gate electrodes, they achieved a complete nonvolatile 180° rotation of the free magnetic layer accompanied by 200% resistance contrast without an external magnetic field [Fig. 46(c)].

#### 4. MESO devices

In 2019, Intel proposed a new concept of logic device called MESO (Manipatruni *et al.*, 2019) that they argued could result in 10 to 30 times higher efficiency and 5 times higher logic density compared to CMOS. MESO is expected to strongly reduce power consumption for computation by harnessing ferroic materials that have embedded nonvolatility and by relying on a voltage rather than a current to switch the ferroic order parameter (Nikonov and Young, 2015; Manipatruni, Nikonov, and Young, 2018). A sketch of MESO is shown in Fig. 47. The core of MESO is a ferromagnetic element whose magnetization is switched thanks to a magnetoelectric element at the input. The output comprises a spin-orbit element that converts a spin current injected into it from the ferromagnet into a charge current (through the ISHE or the IEE), allowing the information stored by the magnetization state in the ferromagnet to be read. MESO is a logic-in-memory concept and individual MESO elements are concatenable; i.e., the output line of one element can be used as the input line of the next one. This is possible because MESO operates with and

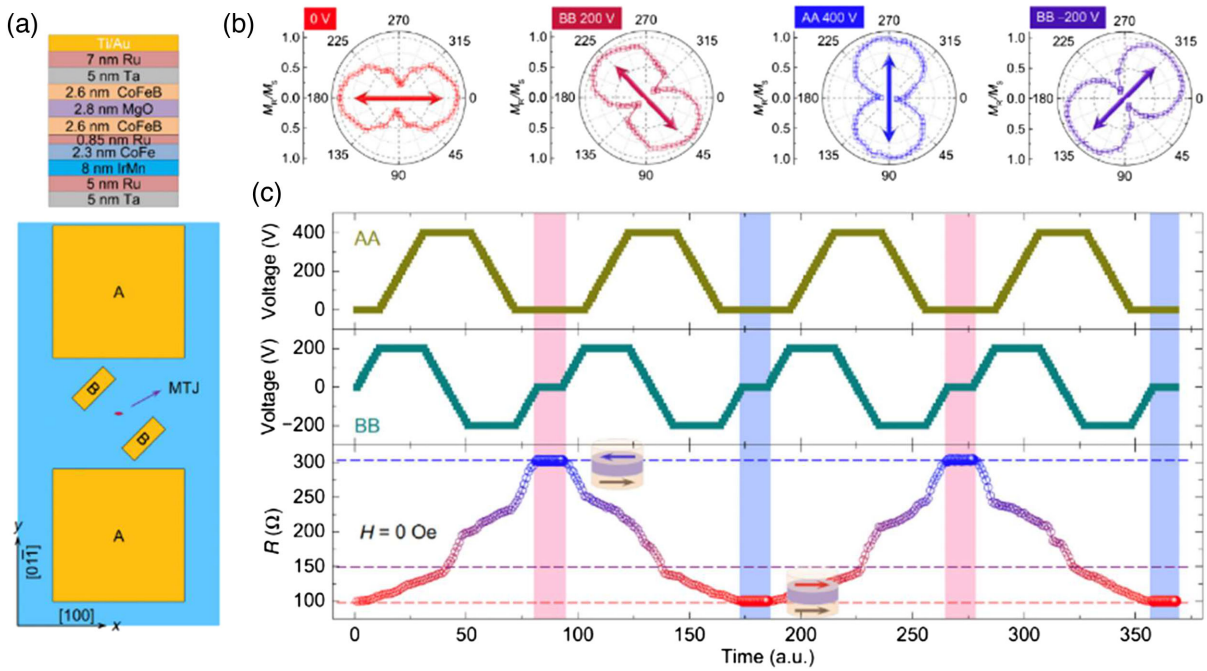


FIG. 46. (a) Detailed structure of the MTJ and schematic top view of a sample structure with two pairs of *AA* and *BB* electrodes. The major axis of the elliptical device was along the $x$ axis. The pinning direction of the MTJ was along the [100] direction of the PMN-PT substrate ($+x$ axis). (b) Polar curves of the angular-dependent $M_R/M_S$ of a CoFeB layer with the applied voltages 0 V, *BB* 200 V, *AA* 400 V, and *BB* −200 V. The [100] direction of the PMN-PT substrate corresponds to 0. The double-headed arrows indicate the direction of the magnetic easy axis. (c) Dependence of the resistance of the tunnel junction on voltage synergistically applied to the *AA* and *BB* electrode pairs at $H = 0$ Oe. The reversible resistance switching between high- and low-resistance states corresponds to the antiparallel and parallel magnetization configurations of the MTJ, as illustrated in the insets, which indicate the 180° magnetization switching of the free layer driven by voltage. From Chen, Zhao *et al.*, 2019.

generates bipolar currents (with positive or negative signs), unlike CMOS devices. For MESO-based architectures to benefit from concatenation, the SO module must generate an output voltage of at least 100 mV, while the ME module must switch with 100 mV or less. To satisfy both these conditions is extremely challenging. In particular, the scarcity of multiferroic materials practically imposes the use of $BiFeO_3$ (or slightly modified or doped versions of it) for the ME module. For the SO module to generate >100 mV, the SO element must possess not only a high spin-charge interconversion efficiency but also a high resistance (Pham *et al.*, 2020).

Efforts toward a first proof-of-concept MESO have involved optimizing devices (Pham *et al.*, 2016, 2020; Groen *et al.*, 2021) with a T-shaped geometry. A prototype combining $BiFeO_3$, CoFe, and Pt was recently presented (Vaz *et al.*, 2022, 2024); see Fig. 48. As visible in Fig. 48(b), the output resistance of the Pt element displays two different levels depending on the magnetization of the CoFe ferromagnetic element. Applying a voltage to the ME element [Fig. 48(c)] switches the magnetization of the CoFe, which results in two different output voltage levels in the Pt [Fig. 48(d)].

### B. Spin-torque nano-oscillators and spin diodes

Spin-torque nano-oscillators (STNOs) based on today's standard MTJs can be used in two ways, as illustrated in Figs. 49(a) and 49(b). They can be efficient nanoscale rf emitters, as described in Sec. III.B, and they can also act as spin diodes, that is, nanoscale transducers from rf to dc in which an input rf signal, rf field, or rf spin torque induces magnetization oscillations that are in turn converted into a dc voltage via a magnetoresistive effect (Tulapurkar *et al.*, 2005). Recent advances have led to active developments of communication and signal processing systems exploiting the frequency tunability, the nanoscale size, and the multifunctionality of the

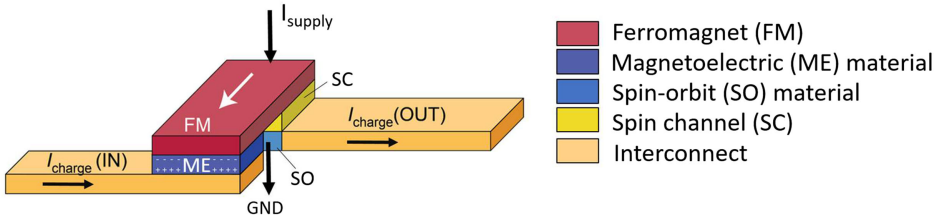


FIG. 47. Sketch of a MESO device. Adapted from Manipatruni *et al.*, 2019.

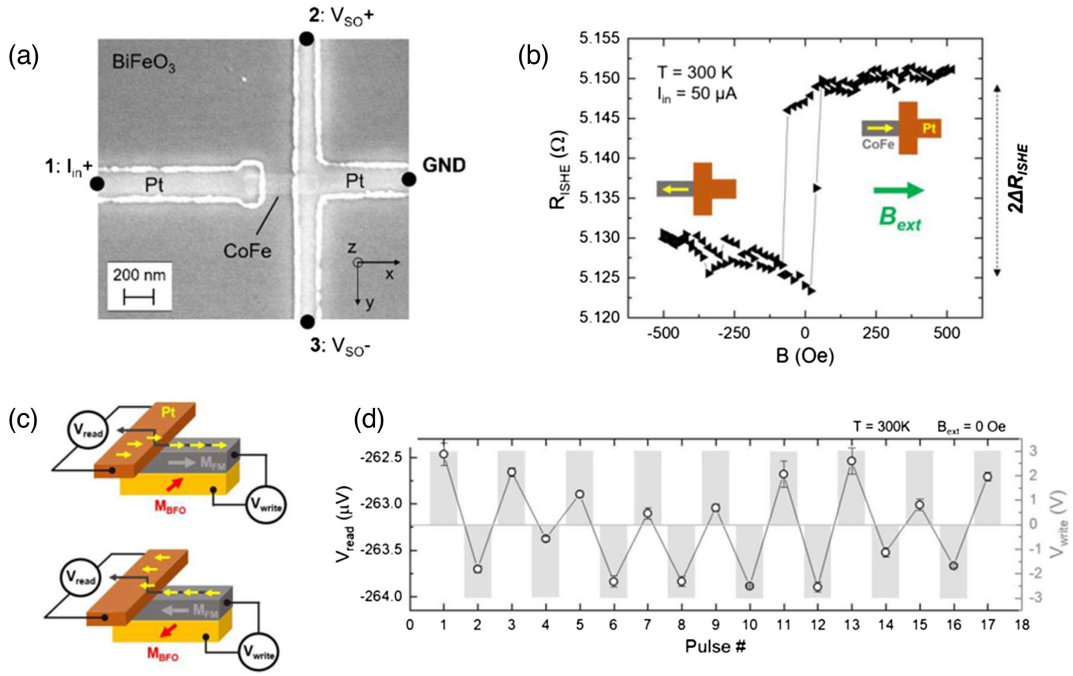


FIG. 48. (a) Scanning electron microscope image of the SO module device region. The CoFe element dimensions are $500 \times 100 \times 2.5\ \mathrm{nm}^3$ (length, width, and thickness). An applied charge current $I_{\mathrm{in}}$ between contact 1 and ground becomes spin-polarized and is injected in the T-shaped Pt structure through a $100 \times 100\ \mathrm{nm}^2$ junction. Owing to the ISHE, an output voltage $V_{\mathrm{read}} = V_{\mathrm{SO+}} - V_{\mathrm{SO-}}$ is detected between contacts 2 and 3. (b) Output signal of the SO module, obtained from the transverse resistance $\mathrm{R}_{\mathrm{ISHE}} = V_{\mathrm{read}}/I_{\mathrm{in}}$ as a function of an external magnetic field $B_{\mathrm{ext}}$. The two magnetization states of the CoFe element, with an amplitude of $2\Delta R_{\mathrm{ISHE}}$, are depicted in the insets by the yellow arrows. (c) Sketch for the full MESO operation at room temperature, without any external magnetic field applied, shown in (d). Voltage pulses $V_{\mathrm{write}}$ drives $\mathrm{BiFeO_3}$ magnetization ($M_{\mathrm{BFO}}$) switching and the subsequent magnetization reversal of the ferromagnetic element $M_{\mathrm{FM}}$ . $M_{\mathrm{FM}}$ is electrically read through the ISHE in the Pt element. (d) The output signal $V_{\mathrm{read}}$ changes by ~1.5 μV for $V_{\mathrm{write}} = \pm 3$ V, reflecting opposite $M_{\mathrm{FM}}$ orientations. After each pulse, the magnetization state is read three times (at intervals of 1 s) and averaged. From Vaz *et al.*, 2022.

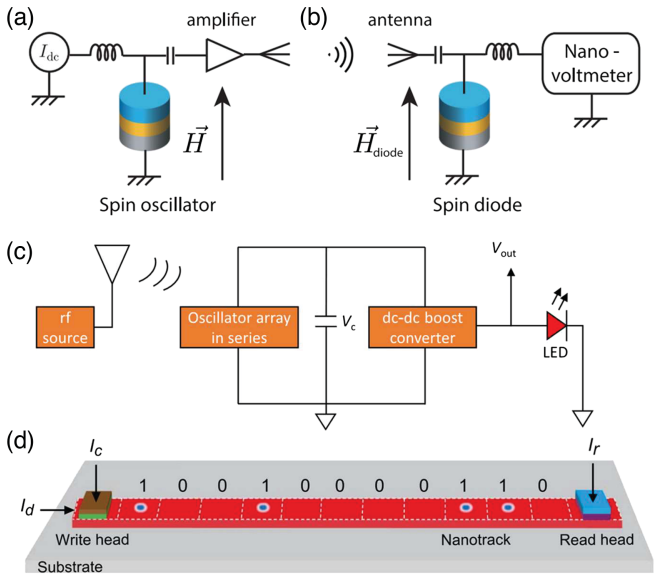


FIG. 49. Applications of STNOs. Schematics of STNOs functioning as (a) spin oscillator for rf emission and (b) spin diode for conversion from rf to dc. From Marković *et al.*, 2020. (c) Schematic of circuit with arrays of eight spin diodes used for energy harvesting and lightning the light-emitting diode (LED) on the right. From Sharma *et al.*, 2021. (d) Schematic of a skyrmion-based racetrack memory. From Kang *et al.*, 2016.

STNO (Chen *et al.*, 2016; Fang *et al.*, 2016; Jenkins *et al.*, 2016; Tarequzzaman *et al.*, 2018; Finocchio *et al.*, 2021; Goto *et al.*, 2021). The rf detection bandwidths of MTJ-based spin-diode devices make them comparable or even better in performance than the semiconductor Schottky diode. One strategy is based on a resonant passive approach with sensitivity approaching 1000 V/W (Fang *et al.*, 2016), a conversion efficiency larger than state-of-the art Schottky diodes. The sensitivity can be further amplified through dc spin-transfer effects (Jenkins *et al.*, 2016) or spin bolometer effects reaching sensitivity up $4.4 \times 10^6$ V/W in the subgigahertz region (Goto *et al.*, 2021). Another strategy has been to harness magnetic configurations showing a larger susceptibility (Tarequzzaman *et al.*, 2018) and/or nonlinear response (Fang *et al.*, 2019) that results in the broadband rectification effect for up to a few gigahertz. This is an important feature for their use in energy harvesting (Fang *et al.*, 2019; Sharma *et al.*, 2021), as illustrated in Fig. 49(c). Note also that the development of arrays of nanoscale STNOs in which the emission by a given STNO can be detected by other STNOs (Jarollahi *et al.*, 2014; Marković *et al.*, 2020), an interesting result for the design of circuits and chips based on STNO communication via microwave. A promising development is the exploitation of such arrays of STNOs in the formulation of spintronic neural networks (Talatchian *et al.*, 2020; Leroux *et al.*, 2021).

### C. Devices based on skyrmions and DWs

Many devices harnessing magnetic skyrmions have been proposed over the past decade. The best known, which is illustrated in Fig. 49(d), is the skyrmion racetrack memory (Fert, Cros, and Sampaio, 2013; Fert, Reyren, and Cros, 2017; Everschor-Sitte *et al.*, 2018) based on the same principle as the racetrack memory with magnetic domain walls proposed by Parkin and Yang (2015). The information can be encoded by a sequence of individual skyrmions that can be moved along a magnetic track between the write head (injector) where the skyrmions are injected and the read head (detector) where they are detected [Fig. 49(d)]. The diameter of the skyrmions can be as small of 10 nm or less and, in addition, can be compressed by decreasing the track width (Fert, Reyren, and Cros, 2017). As the spacing between neighboring skyrmions on a track can be of the order of the skyrmion diameter, one can expect a higher density with skyrmions than with DWs in a racetrack memory (Yang *et al.*, 2021).

The most convenient way to put the skyrmions into motion is the SOT generated by the SHE in a heavy metal layer (Fert, Cros, and Sampaio, 2013; Fert, Reyren, and Cros, 2017; Everschor-Sitte *et al.*, 2018). Velocities up to the order of 100 m/s can be obtained with realistic current densities. The lateral component of the velocity (the skyrmion Hall effect) can be suppressed by working with coupled skyrmions in antiferromagnetic arrangements of layers (Legrand *et al.*, 2020). It can also be obtained in sufficiently narrow tracks when the repulsion by the edges keeps the skyrmion in the center of the track. Another advantage of skyrmions is that their motion by spin torques will be similar on straight tracks or on curved ones as they are guided by the confinement from the edges, whereas the motion of the DWs will be affected on curved parts of the racetrack because the torques will act differently in the wall at the inner and outer parts of the track.

The skyrmions can be injected on the track by current pulses through nanocontacts or also deleted by opposite pulses (Finizio *et al.*, 2019; Yang *et al.*, 2021). They can be detected at the read head by sensing the change of Hall voltage induced by the skyrmion (the anomalous Hall effect or the topological Hall effect) (Maccariello *et al.*, 2018) through the TMR of a tunnel junction deposited on the track or by transport effects specifically associated with the topological nature of skyrmions, for example, noncollinear magnetoresistance. Note that this concept of a skyrmion racetrack can be easily transformed and adapted to become a nanoscale voltage gate skyrmion transistor. This new function was proposed by Zhang, Zhou *et al.* (2015), who added a gate in a given part of the track in order to locally modify through the application of an electric field the magnetic properties of the magnetic media, which are the PMA or the DMI and thus control the passing or not of a skyrmion equivalent of the "on-off" switch of a transistor.

Finally, note that skyrmions have been proposed not only for the conventional storage of information in racetrack memories but also to implement reservoir computing models in recursive neural networks of neuromorphic computers (Yang *et al.*, 2021).

In addition to devices based only on skyrmions, the transformation of skyrmions into domain walls and vice versa on tracks of varying width has been proposed for concepts pertaining to logic gates in conventional computing (Zhang, Ezawa, and Zhou, 2015). Another application of skyrmions is the magnonic crystal based on a periodic and reconfigurable arrangement of skyrmions (Roldán-Molina, Nunez, and Fernández-Rossier, 2016).

## VI. PERSPECTIVES

There is increasing evidence for electric-field control of the magnetization direction at room temperature, with the voltage required to accomplish this dropping down to 0.5 V. To get to an attojoule switch, it is critical to reduce these switching voltages even further (100 mV and below) in conjunction with a switching charge density of $\sim 10\ \mu C/cm^2$. How robust can this be, especially with respect to the repeated cycling of the electric and magnetic states? In this regard, as in the field of ferroelectric thin films (Fernandez *et al.*, 2022) for memory applications, it appears that we need to increase the focus on the nature of the ferromagnet and its interface to the multiferroic. Prior experience with ferroelectric capacitors has shown that a conducting oxide contact yields a robust capacitor. In a similar vein, we expect an oxide ferromagnet to form a more robust contact to the oxide multiferroic or piezoelectric. Thus, there is an urgent need to discover and interface an oxide ferromagnet that couples magnetically to the multiferroic at room temperature. A template for this is already available from the work on $La_{0.7}Sr_{0.3}MnO_3/BiFeO_3$ interfaces, which display robust electric-field control of the magnetization direction, albeit at 100 K. Can double perovskites such as $Sr_2(Fe,Mo)O_6$ (Kobayashi *et al.*, 1998; Bibes *et al.*, 2003) and $Sr_2(Cr,Re)O_6$ (Geprägs *et al.*, 2009) be possible alternatives to the $La_{0.7}Sr_{0.3}MnO_3$ system? In the same vein, it is important to discover more room-temperature multiferroics so that one can explore multiple pathways to use these novel functionalities. Computational discovery platforms such as the materials genomics approach driven by machine learning pathways (Jain *et al.*, 2018) should be particularly valuable in this endeavor. The confluence of crystal chemistry, computational discovery, and atomically precise synthesis is a potent combination that has already been shown to lead to unexpected phenomena (Ramesh and Schlom, 2019).

In this sense, tremendous progress has been made in understanding chemistry-structure-property relationships and in engineering specific atomic architectures, so an era of "multiferroic materials by design" is already under way. In particular, targeted functionalities, such as large magnetization and polarization and even exotic polarization topologies, are now within reach. For magnetoelectric devices to be technologically competitive will therefore require precise growth of ultrathin films guided by theoretical studies to exactly define the chemical compositions needed to optimize the polarization and coercive field. This will require an improved fundamental understanding, which can be facilitated by improved first- and second-principles methods. Even with such a low-field-switching breakthrough, scale-up and integration, in particular, compatibility with existing silicon processing methods, and integration with the appropriate peripheral electronics are key challenges.

The recent discovery of polar vortices and skyrmions in ferroelectric superlattices presents another tantalizing opportunity to create analogous, coupled spin-charge textures out of multiferroics such as $BiFeO_3$ (Yadav *et al.*, 2016; Das *et al.*, 2019; Chauleau *et al.*, 2020). This could present a unique pathway to overcome the antiferromagnetic ground state through such curling patterns as spin-dipolar patterns, as illustrated for the case of polar vortices and skyrmions in $PbTiO_3/SrTiO_3$ superlattices (Das *et al.*, 2019). A first set of studies have been carried out to explore the possibility of forming polar textures in the $BiFeO_3$ system (Chauleau *et al.*, 2020). Imposing electrostatic boundary conditions by interfacing to a lattice matched, nonpolar La-$BiFeO_3$ layer, however, leads to the formation of an array of 109° domains as well as stabilization of an antipolar structure in the $BiFeO_3$ layer (Mundy *et al.*, 2022). These results seem to suggest that, while the idea of imposing electrostatic boundary conditions does work in a general sense, the consequences are governed more by the structural details, particularly the octahedral tilts, which are a key component of the crystal structure of $BiFeO_3$. The rather surprising outcome of the formation of the antipolar structure can be rationalized through the fact that the electrostatic energy is more than sufficient to raise the free energy of the polar phase above that of the antipolar phase. Indeed, this seems to be a hallmark of the $BiFeO_3$ system, where a number of phases are within close proximity in energy scale to the ground state (Diéguez *et al.*, 2011).

An aspect that would benefit from a detailed crystal-chemistry-based phase equilibrium study is the stabilization of metastable phases; for example, one could be looking for polytypoids (phases that have the same crystal structure but a different chemical-stacking sequence, for example, Y-Si-Al-O-N or the polytypes in SiC) (Thompson, Korgul, and Hendry, 1983) of the $BiFeO_3$ composition or chemically distinct derivatives thereof. Two examples of this could be (i) based on the hexagonal Ba*M*-type layered ferrites (Kimura, 2012) and (ii) the Ruddelsen-Popper-type perovskites or the Aurivillius-type phases (Lee and Lee, 2017). This magnetoelectric behavior has been demonstrated in hexagonal ferrites (Kimura, 2012). Further, chemically substituted Aurivillius phases have been known to exhibit magnetoelectric behavior, although the magnetic state is not a robust ground state (more like a spin glass) (Smolensky and Chupis, 1982). On this note, it is prudent to start with ferrimagnets (such as layered hexaferrites) and attempt to induce a robust ferroelectric state in them through chemical substitution or epitaxy. Charge ordering transitions, such as the Vervey transition in $Fe_3O_4$, were thought to lead to breaking inversion symmetry (Ikeda *et al.*, 2005); demonstrating a robust magnetoelectric effect in such systems should be a focus for research in the coming years. 2D materials represent many opportunities for magnetoelectricity, either by combining 2D magnets with 2D ferroelectrics (Wu, 2021) or by designing 2D multiferroic materials (Song *et al.*, 2022). A possible route to reach efficient control of magnetization with an electric field at room temperature is also using hybrid magnetoelectric multiferroics, with superlattices made of ferroelectric and ferromagnetic materials. Combining strain-driven improper ferroelectrics with ferrites is an interesting material choice to achieve this goal.

What are the limits on the length scales of the spin-charge coupling? For example, can we manipulate the spin state of a single ion using an electric field? Recent work in this direction not only is poised to impact the fundamental physics of spin-orbit coupling and its coherent manipulation with an electric field but also has the potential to impact the field of quantum computing in which all of the operations are carried out using an electric field (J. Liu *et al.*, 2021).

We expect dynamical effects in multiferroics to increase in importance in the coming years, driven by new experimental capabilities such as ultrafast x-ray sources (Dhillon *et al.*, 2017), and we expect that fundamental limits on the dynamics of spin-charge-lattice coupling phenomena will be established. Theoretical proposals of dynamical multiferroic phenomena in which a time-dependent polarization induces a magnetization in the reciprocal manner from that in which spin spirals induce polarization (Juraschek *et al.*, 2017) should be validated by careful experiments. At the same time, more work on antiferromagnetic resonance in multiferroics is required. While many studies were carried out in the 1960s (Abraha and Tilley, 1996) and 1970s on conventional antiferromagnets, activity with modern multiferroics, which typically have higher resonance frequencies [∼700 GHz in $BiFeO_3$ (Cazayous *et al.*, 2008; Rovillain *et al.*, 2010; Talbayev *et al.*, 2011) compared to ∼350 GHz in other perovskite orthoferrites (Abraha and Tilley, 1996)], has been scarce.

The field of multiferroics and magnetoelectrics is poised to make further significant breakthroughs, and we hope that this review will inspire additional research on this interesting class of materials and their applications. While scientific interest in the field is beyond question, our community needs to identify market niches and enable pathways to products so that multiferroics will go beyond being an "area to watch" and address contemporary technological challenges. To achieve this, a shift in focus from fundamental materials discoveries to translational research and development will be needed, similar to what occurred in the field of GaN-based light-emitting diodes two decades ago. The complexity of oxide-based materials systems raises particular additional challenges, as we have seen with colossal magnetoresistive manganites, making the active engagement of applied physicists and device engineers early in the research and development process even more essential. In this vein, the recent engagement of large microelectronic companies in the field of multiferroics (Manipatruni *et al.*, 2019) is particularly encouraging. While basic research in multiferroics is vibrant, the field would benefit from an injection of focused programs that address the transition to devices, in particular, scale-up and integration issues. In Table IV we list some of the most pressing challenges for the field.

For the control of magnetism by current-induced torques, advances have been fast approaching in recent years, especially on the manipulation of magnetization by SOT (Shao *et al.*, 2021). The market entry of high-performance components of the SOT MRAM type can be expected soon, first at the cache level and later in processing-in-memory structures, as described in Sec. V.A.1. Some final questions must be solved, related to the field-free switching of perpendicularly magnetized layers by SOT (see Sec. III.C.4), the combined use

TABLE IV. Challenges for the science and technology of the electrical control of magnetism by electric field and current-induced torques.

| Science | Technology |
|---|---|
| • Room-temperature multiferroics with robust coupling between magnetism and ferroelectricity and high remanent magnetic moment | • Thermal stability of ferroelectric and magnetic order parameters, as well as robust coupling between them, in 10 nm length scales at room temperature |
| • New magnetoelectric coupling mechanisms, and understanding and approaching the limits of such phenomena. | • Reducing the voltage required for ferroelectric or magnetoelectric switching to ∼100 mV |
| • Quantitative measurements of magnetoelectric and multiferroic coupling at 10 nm length scales | • Attojoule switch: designing proper ferroelectric multiferroics with small but stable spontaneous polarizations of ∼1–5 $\mu C/cm^2$ |
| • Reaching the theoretical Landauer limit for switching $[kT(\ln 2)]$ would be desirable and will require significant effort | • Integration and scale-up of synthetic approaches to enable manufacturing would be valuable |
| • Atomic-scale design and layer-by-layer growth to discover and synthesize new multiferroics | • Speeding up the development of SOT MRAMs, SOT and STT MRAMs, SOT and VCMA MRAMs, and devices integrating logic and memory functions |
| • Understanding the limits, controlling and exploiting the dynamics | • Development of logic and memory devices combining ferroelectric and ferromagnetic materials (for example, MESO and FESO) |
| • Are there convergences between multiferroics and other correlated electron materials and phenomena? | • Development of STNO-based devices for the harvesting of ambient rf energy |
| • Search for materials with efficient spin-charge interconversion by the SHE or the IEE at room temperature | • Developments of STNO-based devices for neuromorphic computing |
| • Better control of Rashba interfaces and surfaces or interfaces of topological insulators or Dirac semimetals | • Development of racetrack memories based on DW or skyrmions |
| • Mastering a simple and efficient way for field-free switching of perpendicular magnetization by SOT | • Development of an application of skyrmions for logic and memory devices as well as for elements for neuromorphic computing |
| • Better understanding and control of the nucleation and current-induced motion of skyrmions | • Development of an application of arrangements of skyrmions in magnonic devices |
| • Mastering the synchronization of large assemblies of STNOs for additive outputs | • Development of high-speed light-induced SOT MRAMs |
| • Developing reliable methods to raise the ordering temperature of 2D magnets well above room temperature | |
| • Exploring the advantages for spin-orbitronics coming from the combination of spin-orbit coupling and broken inversion symmetry in 2D magnets or at interfaces of vdW heterostructures | |
| • Extension of experiments of magnetization switching by SOT to magnetic insulators | |
| • Better understanding the generation of light-induced spin currents for their exploitation for current-induced torques | |
| • Better understanding light-induced terahertz emission from magnetic materials and multilayers | |
| • Exploring the potential of pure orbital currents for the control of magnetization in the emerging field of orbitronics | |

of electric-field- and current-induced torques in VCMA devices (see Sec. IV.C), or the combined use of magnetoelectric effects and spin-charge interconversion in MESO devices (see Sec. V.A.4). Although the results of Fig. 48 demonstrate the feasibility of MESO, much work is needed to increase the output voltage difference. In particular, it appears that optimizing the output signal based on heavy metals such as Pt or Ta will not be enough owing to their low resistivity. Rather, working with 2D systems such as 2DEGs, surface states of topological insulators, and graphene/TMD vdW heterostructures is a more promising route owing to their large spin-charge interconversion efficiency ($\lambda_{IEE}$ or $\lambda_{SHE}$), as well as their high resistivity (Pham *et al.*, 2020). In parallel, in the field of neuromorphic computing several concepts of nanoscale neuron or synapse components based on SOT have recently been successfully tested, and their development as devices by the electronic industry can be expected in the next decade.

Although the next generation of devices will probably use heavy metals as the source of spin current, better performances can be expected in the second stage, again by the use of 2DEGs at the surface of topological insulators or Dirac semimetals and at Rashba interfaces, as well as from the introduction of 2D materials. Some results on topological insulators and Dirac semimetals are promising (see Table II), but their integration into devices could be a long process requiring better control of the interplay between bulk and surface-interface contributions to the production of spin current and improvements in the fabrication-integration processes. On the fundamental research side, advances can come from the use of magnetic materials other than transition metals and associated alloys (Co, CoFeB, etc.) or alloys combining rare-earth and transition metals (TbFe, etc.). In these classical magnetic materials, the conduction is by *s* and *d* electrons, and mainly by *s* electrons that do not have spin-orbit coupling. Recently record DW velocities were obtained in magnetic alloys with *p* carriers as nitrides of Mn (Ghosh *et al.*, 2021). Other types of magnetic materials with *p* conduction could be explored, as in the case of TMDs. The use of antiferromagnets as the magnetic material is another promising direction, with the advantage of having no net magnetization, which makes them insensitive to spurious magnetic fields and thus robust as

memory elements, while they can be written by current-induced torques (or electric fields).

Recent years have also seen demonstrations of the noteworthy properties of 2D materials, particularly 2D magnets, as described in Secs. II.D and III.F. The control of magnetism in layered magnets with an electric field has much potential since atomically thick materials can be more sensitive to an electric field than normal thin films, with the additional advantage of obtaining almost ideal interfaces when one stacks them with other vdW materials (such as the aforementioned 2D materials with efficient spin-charge interconversion mentioned). Regarding voltage control of the magnetism present in these atomically thick materials, some attempts have been made (Jiang *et al.*, 2019; T. Song *et al.*, 2019) to integrate the voltage-induced switching of the magnetic order of $CrI_3$ (see Sec. II.D) in a device that shows nonvolatility and could be an alternative in MRAM applications. Regarding current-induced torques, the performance of 2D-magnet-based devices requires small current densities and small applied fields [a comparison between the potential of 3D and 2D magnets for switching by SOT is given in Fig. 35(d)], although the small electrical signal for reading the magnetic state of the semiconducting 2D magnet (based on spin Hall magnetoresistance) will need to be improved. To date the obvious drawback of 2D magnets is their ordering temperature, which is generally below room temperature. However, recent work has shown that this temperature in some systems can be raised by a proximity effect with another 2D material (Wang *et al.*, 2020) or by electric fields (Deng *et al.*, 2018). If this possibility becomes more likely, the 2D magnets will also become promising materials for the electrical control of magnetization.

Another emerging direction for the current-induced control of magnetization is the possibility of exploiting orbital currents that carry orbital angular momentum rather than the usual spin currents carrying the intrinsic angular momentum. They can be generated by the orbital Hall effect, which is expected to be larger than the SHE, even in transition metals with weak spin-orbit coupling (Tanaka *et al.*, 2008; Jo, Go, and Lee, 2018; Salemi and Oppeneer, 2022). Indeed, recent experiments have confirmed the presence of the orbital Hall effect in 3*d* transition metals: Ti (Choi *et al.*, 2023) and Cr (Lyalin *et al.*, 2023) by MOKE and Mn (Sala *et al.*, 2023) by Hanle magnetoresistance. Likewise, the orbital equivalent of the EE (the orbital Edelstein effect) is predicted to generate a current-induced orbital magnetization (Levitov, Nazarov, and Eliashberg, 1985; Yoda, Yokoyama, and Murakami, 2015; Go *et al.*, 2017; Salemi *et al.*, 2019; Johansson *et al.*, 2021). The orbital currents generated in a nonmagnetic material could efficiently exert a torque when injected into a ferromagnet. For this to occur, spin-orbit coupling is needed to convert the orbit current into a spin current. For this purpose, one could use a middle layer with strong spin-orbit coupling between the nonmagnetic metal and the ferromagnet (S. Ding *et al.*, 2020; Hayashi *et al.*, 2023) or could directly use a ferromagnet with strong spin-orbit coupling (Lee *et al.*, 2021). This new field of research, called orbitronics, might open the door to a plethora of materials and interfaces, not previously considered because of their lack of spin-orbit coupling, to be used to achieve large current-induced torques. Recently, light-induced orbit currents have also been used for efficient terahertz emission (Seifert *et al.*, 2023; Xu *et al.*, 2023).

Finally, although this review has been devoted to the control of magnetization by electric-field and electrical currents, it is probable that we will soon see an interplay of these well-performing electrical controls and additional controls by light move in the direction of faster speeds and better energy efficiency. The most recent experiments showed that the magnetization of a magnetic layer can be controlled by an ultrashort laser pulse. The magnetization can be switched with a single nonpolarized laser pulse in specific ferrimagnetic materials such as GdCo, GdFeCo (Stanciu *et al.*, 2007), and Tb/Co multilayers (Avilés-Félix *et al.*, 2020). Moreover, a large variety of materials (ferrimagnetic, ferromagnetic, synthetic antiferromagnets, granular media, etc.) can also be switched using circularly polarized laser pulses (Lambert *et al.*, 2014). Those types of all-optical switching effects could be applied, for example, to switch the magnetization of one layer in a MTJ stack to change the magnetic state of an MRAM in which one of the electrodes is made with one of these ferrimagnetic materials. More recently, however, it was demonstrated that the out-of-plane magnetization of a standard ferromagnetic layer (such as Co, Co/Ni, or Co/Pt) can be electronically switched via the transmission of the spin-polarized current generated by a light pulse on a GdFeCo layer (without switching the magnetization of GdFeCo) (Remy *et al.*, 2020). This hybrid approach, which combines the generation of a spin-polarized ultrashort current pulse by light in a first magnetic layer and the switching of a second magnetic layer by spin-current injection, could be used for the writing of MRAMs based on the optimized materials of today. In any case, using direct or indirect control of magnetization by light, it turns out that future generations of ultrafast devices will probably combine the well-performing electrical controls that we described in this review with direct or indirect controls by light.

## ACKNOWLEDGMENTS

We have written this review on behalf of many collaborators, co-workers, students, and postdoctoral researchers worldwide and acknowledge their intellectual participation and contribution. The rapid pace of development in this field means that it is impossible to acknowledge and cite each of them independently. We encourage the interested reader to refer to the articles cited in this review and to reach out to us if we can be of further assistance. We thank Frédéric Nguyen Van Dau for proofreading the article and making many valuable suggestions to improve it. Our work would not have been possible without the sustained support of federal and industrial funding agencies. In particular, we acknowledge the support by Intel Corporation through the "FEINMAN" Intel Science Technology Center. R. R. acknowledges the sustained support of the U.S. Department of Energy, Basic Energy Sciences Office; the Semiconductor Research Corporation's JUMP Initiative; the National Science Foundation, specifically, the MRSEC program; and the Army Research Office. A. F. acknowledges the support of the Universidad del País Vasco as a distinguished researcher. M. B. acknowledges support from the European Research Council through AdG Grant

No. 833973 "FRESCO," the French Agence Nationale de la Recherche project "CONTRABASS," and the M-ERA.NET project "SWIPE." F. C. acknowledges the support of the Spanish MCIN/AEI and ERDF "A way of making Europe" (Project No. PID2021-122511OB-I00 and Maria de Maeztu Units of Excellence Programme No. CEX2020-001038-M), from the European Union H2020 program under the Marie Skłodowska-Curie Actions (Grant Agreement No. 955671-SPEAR), and from the "Valleytronics" Intel Science Technology Center. V. G. acknowledges support from the French Agence Nationale de la Recherche (ANR) through the project TATOO (Project No. ANR-21-CE09-0033) and the European Union's Horizon 2020 research and innovation program under Grant Agreement No. 964931 (TSAR).

## REFERENCES

Abraha, K., and D. R. Tilley, 1996, "Theory of far infrared properties of magnetic surfaces, films and superlattices," Surf. Sci. Rep. **24**, 129–222.

Adams, T., A. Chacon, M. Wagner, A. Bauer, G. Brandl, B. Pedersen, H. Berger, P. Lemmens, and C. Pfleiderer, 2012, "Long-Wavelength Helimagnetic Order and Skyrmion Lattice Phase in $Cu_2OSeO_3$," Phys. Rev. Lett. **108**, 237204.

Agbelele, A., *et al.*, 2017, "Strain and magnetic field induced spin-structure transitions in multiferroic $BiFeO_3$," Adv. Mater. **29**, 1602327.

Aguilar-Pujol, M. X., S. Catalano, C. González-Orellana, W. Skowroński, J. M. Gomez-Perez, M. Ilyn, C. Rogero, M. Gobbi, L. E. Hueso, and F. Casanova, 2023, "Magnon currents excited by the spin Seebeck effect in ferromagnetic EuS thin films," Phys. Rev. B **108**, 224420.

Ahn, C. H., J.-M. Triscone, and J. Mannhart, 2003, "Electric field effect in correlated oxide systems," Nature (London) **424**, 1015–1018.

Ai, H., X. Ma, X. Shao, W. Li, and M. Zhao, 2019, "Reversible out-of-plane spin texture in a two-dimensional ferroelectric material for persistent spin helix," Phys. Rev. Mater. **3**, 054407.

Alam, S., *et al.*, 2012, "Theory and the experimental confirmation of the local electronic structure of the multiferroic $PbVO_3$, a new member of $PbTiO_3$ family, studied by x-ray near edge absorption structure: I," J. Phys. Soc. Jpn. **81**, 074709.

Albert, F. J., J. A. Katine, R. A. Buhrman, and D. C. Ralph, 2000, "Spin-polarized current switching of a Co thin film nanomagnet," Appl. Phys. Lett. **77**, 3809–3811.

Alghamdi, M., M. Lohmann, J. Li, P. R. Jothi, Q. Shao, M. Aldosary, T. Su, B. P. T. Fokwa, and J. Shi, 2019, "Highly efficient spin-orbit torque and switching of layered ferromagnet $Fe_3GeTe_2$," Nano Lett. **19**, 4400–4405.

Allibe, J., C. Deranlot, and M. Bibes, 2012, "Room temperature electrical manipulation of giant magnetoresistance in spin valves exchange-biased with $BiFeO_3$," Nano Lett. **12**, 1141.

Allibe, J., I. C. Infante, S. Fusil, K. Bouzehouane, E. Jacquet, C. Deranlot, M. Bibes, and A. Barthélémy, 2009, "Coengineering of ferroelectric and exchange bias properties in $BiFeO_3$ based heterostructures," Appl. Phys. Lett. **95**, 182503.

Althammer, M., 2021, "All-electrical magnon transport experiments in magnetically ordered insulators," Phys. Status Solidi RRL **15**, 2100130.

Amin, V. P., P. M. Haney, and M. D. Stiles, 2020, "Interfacial spin-orbit torques," J. Appl. Phys. **128**, 151101.

Amin, V. P., J. Li, M. D. Stiles, and P. M. Haney, 2019, "Intrinsic spin currents in ferromagnets," Phys. Rev. B **99**, 220405.

Amin, V. P., J. Zemen, and M. D. Stiles, 2018, "Interface-Generated Spin Currents," Phys. Rev. Lett. **121**, 136805.

An, H., T. Ohno, Y. Kanno, Y. Kageyama, Y. Monnai, H. Maki, J. Shi, and K. Ando, 2018, "Current-induced magnetization switching using an electrically insulating spin-torque generator," Sci. Adv. **4**, eaar2250.

Ando, F., M. Ishibashi, T. Koyama, Y. Shiota, T. Moriyama, D. Chiba, and T. Ono, 2018, "Magnetic domain writing defined by electrical gating in Pt/Co film," Appl. Phys. Lett. **113**, 252402.

Arima, T., A. Tokunaga, T. Goto, H. Kimura, Y. Noda, and Y. Tokura, 2006, "Collinear to Spiral Spin Transformation without Changing the Modulation Wavelength upon Ferroelectric Transition in $Tb_{(1-x)}Dy_x MnO_3$," Phys. Rev. Lett. **96**, 097202.

Arras, R., J. Gosteau, H. J. Zhao, C. Paillard, Y. Yang, and L. Bellaiche, 2019, "Rashba-like spin-orbit and strain effects in tetragonal $PbTiO_3$," Phys. Rev. B **100**, 174415.

Atou, T., H. Chiba, K. Ohoyama, Y. Yamaguchi, and Y. Syono, 1999, "Structure determination of ferromagnetic perovskite $BiMnO_3$," J. Solid State Chem. **145**, 639–642.

Avci, C. O., C.-H. Lambert, G. Sala, and P. Gambardella, 2021, "A two-terminal spin valve device controlled by spin-orbit torques with enhanced giant magnetoresistance," Appl. Phys. Lett. **119**, 032406.

Avci, C. O., A. Quindeau, C.-F. Pai, M. Mann, L. Caretta, A. S. Tang, M. C. Onbasli, C. A. Ross, and G. S. D. Beach, 2017, "Current-induced switching in a magnetic insulator," Nat. Mater. **16**, 309–314.

Avci, C. O., E. Rosenberg, M. Huang, J. Bauer, C. A. Ross, and G. S. D. Beach, 2020, "Nonlocal Detection of Out-of-Plane Magnetization in a Magnetic Insulator by Thermal Spin Drag," Phys. Rev. Lett. **124**, 027701.

Avilés-Félix, L., *et al.*, 2020, "Single-shot all-optical switching of magnetization in Tb/Co multilayer-based electrodes," Sci. Rep. **10**, 5211.

Ba, Y., *et al.*, 2021, "Electric-field control of skyrmions in multiferroic heterostructure via magnetoelectric coupling," Nat. Commun. **12**, 322.

Baek, S. C., K.-W. Park, D.-S. Kil, Y. Jang, J. Park, K.-J. Lee, and B.-G. Park, 2018, "Complementary logic operation based on electric-field controlled spin-orbit torques," Nat. Electron. **1**, 398–403.

Baek, S.-h. C., V. P. Amin, Y. W. Oh, G. Go, S. J. Lee, G. H. Lee, K. J. Kim, M. D. Stiles, B. G. Park, and K. J. Lee, 2018, "Spin currents and spin-orbit torques in ferromagnetic trilayers," Nat. Mater. **17**, 509–513.

Bai, F., J. Wang, M. Wuttig, J. Li, N. Wang, A. P. Pyatakov, A. K. Zvezdin, L. E. Cross, and D. Viehland, 2005, "Destruction of spin cycloid in $(111)_c$-oriented $BiFeO_3$ thin films by epitiaxial constraint: Enhanced polarization and release of latent magnetization," Appl. Phys. Lett. **86**, 032511.

Baibich, M. N., J. M. Broto, A. Fert, F. N. Van Dau, F. Petroff, P. Etienne, G. Creuzet, A. Friederich, and J. Chazelas, 1988, "Giant Magnetoresistance of (001)Fe/(001)Cr Magnetic Superlattices," Phys. Rev. Lett. **61**, 2472–2475.

Baldrati, L., C. Rinaldi, A. Manuzzi, M. Asa, L. Aballe, M. Foerster, N. Biškup, M. Varela, M. Cantoni, and R. Bertacco, 2016, "Electrical switching of magnetization in the artificial multiferroic $CoFeB/BaTiO_3$," Adv. Electron. Mater. **2**, 1600085.

Ball, P., 2012, "Computer engineering: Feeling the heat," Nature (London) **492**, 174–176.

Baltz, V., A. Manchon, M. Tsoi, T. Moriyama, T. Ono, and Y. Tserkovnyak, 2018, "Antiferromagnetic spintronics," Rev. Mod. Phys. **90**, 015005.

Barnaś, J., A. Fert, M. Gmitra, I. Weymann, and V. K. Dugaev, 2005, "From giant magnetoresistance to current-induced switching by spin transfer," Phys. Rev. B **72**, 024426.

Baryakthar, V. G., and I. E. Chupis, 1970, "Quantum theory of oscillations in a ferroelectric ferromagnet," Sov. Phys. Solid State **11**, 2628.

Batoo, K. M., S. Bhardwaj, G. K. Bhargava, and M. Singh, 2021, *Ferrites and Multiferroics: Fundamentals to Applications* (Springer, New York).

Baumgartner, M., *et al.*, 2017, "Spatially and time-resolved magnetization dynamics driven by spin-orbit torques," Nat. Nanotechnol. **12**, 980–986.

Béa, H., M. Bibes, F. Ott, B. Dupé, X.-H. Zhu, S. Petit, S. Fusil, C. Deranlot, K. Bouzehouane, and A. Barthélémy, 2008, "Mechanisms of Exchange Bias with Multiferroic $BiFeO_3$ Epitaxial Thin Films," Phys. Rev. Lett. **100**, 017204.

Béa, H., M. Bibes, S. Petit, J. Kreisel, and A. Barthélémy, 2007, "Structural distortion and magnetism of $BiFeO_3$ epitaxial thin films: A Raman spectroscopy and neutron diffraction study," Philos. Mag. Lett. **87**, 165–174.

Béa, H., S. Fusil, K. Bouzehouane, M. Bibes, M. Sirena, G. Herranz, E. Jacquet, J.-P. Contour, and A. Barthélémy, 2006, "Ferroelectricity down to at least 2 nm in multiferroic $BiFeO_3$ epitaxial thin films," Jpn. J. Appl. Phys. **45**, L187–L189.

Béa, H., *et al.*, 2005, "Influence of parasitic phases on the properties of $BiFeO_3$ epitaxial thin films," Appl. Phys. Lett. **87**, 072508.

Béa, H., *et al.*, 2006, "Tunnel magnetoresistance and robust room temperature exchange bias with multiferroic $BiFeO_3$ epitaxial thin films," Appl. Phys. Lett. **89**, 242114.

Bednorz, J. G., and K. A. Müller, 1984, "$Sr_{1-x}Ca_xTiO_3$: An *XY* Quantum Ferroelectric with Transition to Randomness," Phys. Rev. Lett. **52**, 2289–2292.

Bekele, Z. A., X. Liu, Y. Cao, and K. Wang, 2021, "High-efficiency spin-orbit torque switching using a single heavy-metal alloy with opposite spin Hall angles," Adv. Electron. Mater. **7**, 2000793.

Belabbes, A., G. Bihlmayer, F. Bechstedt, S. Blügel, and A. Manchon, 2016, "Hund's Rule-Driven Dzyaloshinskii-Moriya Interaction at 3*d*–5*d* Interfaces," Phys. Rev. Lett. **117**, 247202.

Belik, A. A., *et al.*, 2007, "Origin of the monoclinic-to-monoclinic phase transition and evidence for the centrosymmetric crystal structure of $BiMnO_3$," J. Am. Chem. Soc. **129**, 971–977.

Benítez, L. A., W. Savero Torres, J. F. Sierra, M. Timmermans, J. H. Garcia, S. Roche, M. V. Costache, and S. O. Valenzuela, 2020, "Tunable room-temperature spin galvanic and spin Hall effects in van der Waals heterostructures," Nat. Mater. **19**, 170–175.

Berger, L., 1984, "Exchange interaction between ferromagnetic domain wall and electric current in very thin metallic films," J. Appl. Phys. **55**, 1954–1956.

Berger, L., 1996, "Emission of spin waves by a magnetic multilayer traversed by a current," Phys. Rev. B **54**, 9353–9358.

Bhattacharjee, S., D. Rahmedov, D. Wang, J. Íñiguez, and Bellaiche, L., 2014, "Ultrafast Switching of the Electric Polarization and Magnetic Chirality in $BiFeO_3$ by an Electric Field," Phys. Rev. Lett. **112**, 147601.

Bibes, M., and A. Barthélémy, 2008, "Towards a magnetoelectric memory," Nat. Mater. **7**, 425–426.

Bibes, M., *et al.*, 2003, "Tunnel magnetoresistance in nanojunctions based on $Sr_2FeMoO_6$," Appl. Phys. Lett. **83**, 2629–2631.

Bihler, C., *et al.*, 2008, "$Ga_{1-x}Mn_xAs$/piezoelectric actuator hybrids: A model system for magnetoelastic magnetization manipulation," Phys. Rev. B **78**, 045203.

Binasch, G., P. Grünberg, F. Saurenbach, and W. Zinn, 1989, "Enhanced magnetoresistance in layered magnetic structures with antiferromagnetic interlayer exchange," Phys. Rev. B **39**, 4828(R)–4830(R).

Bocher, L., A. Gloter, A. Crassous, V. Garcia, K. March, A. Zobelli, and S. Valencia, 2012, "Atomic and electronic structure of the $BaTiO_3$/Fe interface in multiferroic tunnel junctions," Nano Lett. **12**, 376–382.

Bodnar, S. Yu., L. Šmejkal, I. Turek, T. Jungwirth, O. Gomonay, J. Sinova, A. A. Sapozhnik, H.-J. Elmers, M. Kläui, and M. Jourdan, 2018, "Writing and reading antiferromagnetic $Mn_2Au$ by Néel spin-orbit torques and large anisotropic magnetoresistance," Nat. Commun. **9**, 348.

Bogdanov, A., and A. Hubert, 1994, "Thermodynamically stable magnetic vortex states in magnetic crystals," J. Magn. Magn. Mater. **138**, 255–269.

Bogdanov, A. N., and D. A. Yablonskii, 1989, "Thermodynamically stable 'vortices' in magnetically ordered crystals: The mixed state of magnets," Sov. Phys. JETP **68**, 101, http://www.jetp.ras.ru/cgi-bin/dn/e_068_01_0101.pdf.

Bokov, V. A., I. E. Myl'nikova, S. A. Kizhaev, M. F. Bryzhina, and N. A. Grigoryan, 1966, "Structure and magnetic properties of $BiMnO_3$," Sov. Phys. Solid State **7**, 2993.

Bonilla, M., S. Kolekar, Y. Ma, H. C. Diaz, V. Kalappattil, R. Das, T. Eggers, H. R. Gutierrez, M.-H. Phan, and M. Batzill, 2018, "Strong room-temperature ferromagnetism in $VSe_2$ monolayers on van der Waals substrates," Nat. Nanotechnol. **13**, 289–293.

Borders, W. A., A. Z. Pervaiz, S. Fukami, K. Y. Camsari, H. Ohno, and S. Datta, 2019, "Integer factorization using stochastic magnetic tunnel junctions," Nature (London) **573**, 390–393.

Bousquet, E., M. Dawber, N. Stucki, C. Lichtensteiger, P. Hermet, S. Gariglio, J.-M. Triscone, and P. Ghosez, 2008, "Improper ferroelectricity in perovskite oxide artificial superlatices," Nature (London) **452**, 732–736.

Boyn, S., A. Chanthbouala, S. Girod, C. Carrétéro, A. Barthélémy, M. Bibes, J. Grollier, S. Fusil, and V. Garcia, 2018, "Real-time switching dynamics of ferroelectric tunnel junctions under single-shot voltage pulses," Appl. Phys. Lett. **113**, 232902.

Boyn, S., *et al.*, 2017, "Learning through ferroelectric domain dynamics in solid-state synapses," Nat. Commun. **8**, 14736.

Bruyer, E., D. Di Sante, P. Barone, A. Stroppa, M.-H. Whangbo, and S. Picozzi, 2016, "Possibility of combining ferroelectricity and Rashba-like spin splitting in monolayers of the 1*T*-type transition-metal dichalcogenides $MX_2$ ($M$ = Mo, W; $X$ = S, Se, Te)," Phys. Rev. B **94**, 195402.

Burkov, A. A., and D. G. Hawthorn, 2010, "Spin and Charge Transport on the Surface of a Topological Insulator," Phys. Rev. Lett. **105**, 066802.

Burton, J. D., and E. Y. Tsymbal, 2009, "Prediction of electrically induced magnetic reconstruction at the manganite/ferroelectric interface," Phys. Rev. B **80**, 174406.

Butler, W. H., X.-G. Zhang, T. C. Schulthess, and J. M. MacLaren, 2001, "Spin-dependent tunneling conductance of Fe|MgO|Fe sandwiches," Phys. Rev. B **63**, 054416.

Cai, K., *et al.*, 2017, "Electric field control of deterministic current-induced magnetization switching in a hybrid ferromagnetic/ferroelectric structure," Nat. Mater. **16**, 712–716.

Cai, W., *et al.*, 2021, "Sub-ns field-free switching in perpendicular magnetic tunnel junctions by the interplay of spin transfer and orbit torques," IEEE Electron Device Lett. **42**, 704–707.

Calavalle, F., *et al.*, 2022, "Gate-tuneable and chirality-dependent charge-to-spin conversion in tellurium nanowires," Nat. Mater. **21**, 526.

Cano, A., D. Meier, and M. Trassin, 2021, *Multiferroics: Fundamentals and Applications* (De Gruyter, Berlin).

Caretta, L., *et al.*, 2018, "Fast current-driven domain walls and small skyrmions in a compensated ferrimagnet," Nat. Nanotechnol. **13**, 1154–1160.

Catalan, G., and J. F. Scott, 2009, "Physics and applications of bismuth ferrite," Adv. Mater. **21**, 2463–2485.

Cazayous, M., Y. Gallais, A. Sacuto, R. de Sousa, D. Lebeugle, and D. Colson, 2008, "Possible Observation of Cycloidal Electromagnons in $BiFeO_3$," Phys. Rev. Lett. **101**, 037601.

Céspedes-Berrocal, D., *et al.*, 2021, "Current-induced spin torques on single GdFeCo magnetic layers," Adv. Mater. **33**, 2007047.

Chai, Y. S., S. Kwon, S. H. Chun, I. Kim, B.-G. Jeon, K. H. Kim, and S. Lee, 2014, "Electrical control of large magnetization reversal in a helimagnet," Nat. Commun. **5**, 4208.

Chandra, P., M. Dawber, P. B. Littlewood, and J. F. Scott, 2004, "Scaling of the coercive field with thickness in thin-film ferroelectrics," Ferroelectrics **313**, 7–13.

Chanthbouala, A., *et al.*, 2012a, "Solid-state memories based on ferroelectric tunnel junctions," Nat. Nanotechnol. **7**, 101–104.

Chanthbouala, A., *et al.*, 2012b, "A ferroelectric memristor," Nat. Mater. **11**, 860–864.

Chauleau, J.-Y., M. Boselli, S. Gariglio, R. Weil, G. de Loubens, J.-M. Triscone, and M. Viret, 2016, "Efficient spin-to-charge conversion in the 2D electron liquid at the LAO/STO interface," Europhys. Lett. **116**, 17006.

Chauleau, J.-Y., E. Haltz, C. Carrétéro, S. Fusil, and M. Viret, 2017, "Multi-stimuli manipulation of antiferromagnetic domains assessed by second-harmonic imaging," Nat. Mater. **16**, 803–807.

Chauleau, J.-Y., *et al.*, 2020, "Electric and antiferromagnetic chiral textures at multiferroic domain walls," Nat. Mater. **19**, 386–390.

Chen, A., Y. Zhao, Y. Wen, L. Pan, P. Li, and X.-X. Zhang, 2019, "Full voltage manipulation of the resistance of a magnetic tunnel junction," Sci. Adv. **5**, eaay5141.

Chen, A., *et al.*, 2019, "Giant nonvolatile manipulation of magnetoresistance in magnetic tunnel junctions by electric fields via magnetoelectric coupling," Nat. Commun. **10**, 243.

Chen, L., M. Gmitra, M. Vogel, R. Islinger, M. Kronseder, D. Schuh, D. Bougeard, J. Fabian, D. Weiss, and C. H. Back, 2018, "Electric-field control of interfacial spin-orbit fields," Nat. Electron. **1**, 350–355.

Chen, T., R. K. Dumas, A. Eklund, P. K. Muduli, A. Houshang, A. A. Awad, P. Durrenfeld, B. G. Malm, A. Rusu, and J. Akerman, 2016, "Spin-torque and spin-Hall nano-oscillators," Proc. IEEE **104**, 1919–1945.

Chen, X., A. Hochstrat, P. Borisov, and W. Kleemann, 2006, "Magnetoelectric exchange bias systems in spintronics," Appl. Phys. Lett. **89**, 202508.

Cheng, R., M. W. Daniels, J.-G. Zhu, and D. Xiao, 2016, "Antiferromagnetic spin wave field-effect transistor," Sci. Rep. **6**, 24223.

Cherifi, R. O., *et al.*, 2014, "Electric-field control of magnetic order above room temperature," Nat. Mater. **13**, 345–351.

Chiba, D., S. Fukami, K. Shimamura, N. Ishiwata, K. Kobayashi, and T. Ono, 2011, "Electrical control of the ferromagnetic phase transition in cobalt at room temperature," Nat. Mater. **10**, 853–856.

Chiba, D., and T. Ono, 2013, "Control of magnetism in Co by an electric field," J. Phys. D **46**, 213001.

Chiba, D., M. Sawicki, Y. Nishitani, Y. Nakatani, F. Matsukura, and H. Ohno, 2008, "Magnetization vector manipulation by electric fields," Nature (London) **455**, 515–518.

Choe, D., *et al.*, 2019, "Gate-tunable giant nonreciprocal charge transport in noncentrosymmetric oxide interfaces," Nat. Commun. **10**, 4510.

Choi, Y.-G., D. Jo, K.-H. Ko, D. Go, K.-H. Kim, H. G. Park, C. Kim, B.-C. Min, G.-M. Choi, and H.-W. Lee, 2023, "Observation of the orbital Hall effect in a light metal Ti," Nature (London)**619**, 52.

Chu, Y. H., *et al.*, 2007, "Ferroelectric size effects in multiferroic $BiFeO_3$ thin films," Appl. Phys. Lett. **90**, 252906.

Chu, Y. H., *et al.*, 2008, "Low voltage performance of epitaxial $BiFeO_3$ films on Si substrates through lanthanum substitution," Appl. Phys. Lett. **92**, 102909.

Chumak, A. V., A. A. Serga, and B. Hillebrands, 2014, "Magnon transistor for all-magnon data processing," Nat. Commun. **5**, 4700.

Chumak, A. V., V. I. Vasyuchka, A. A. Serga, and B. Hillebrands, 2015, "Magnon spintronics," Nat. Phys. **11**, 453–461.

Chun, S. H., *et al.*, 2012, "Electric Field Control of Nonvolatile Four-State Magnetization at Room Temperature," Phys. Rev. Lett. **108**, 177201.

Cornelissen, L. J., J. Liu, R. A. Duine, J. B. Youssef, and B. J. van Wees, 2015, "Long-distance transport of magnon spin information in a magnetic insulator at room temperature," Nat. Phys. **11**, 1022–1026.

Coughlin, T., and J. Handy, 2021, "Dynamic trends in nonvolatile memory technologies," https://www.snia.org/sites/default/files/PM-Summit/2021/snia-pm-cs-summit-Coughlin-Handy-Dynamic-Trends-2021.pdf.

Cowley, R. A., S. N. Gvasaliya, S. G. Lushnikov, B. Roessli, and G. M. Rotaru, 2011, "Relaxing with relaxors: A review of relaxor ferroelectrics," Adv. Phys. **60**, 229–327.

Cox, P. A., and P. A. Cox, 1995, *Transition Metal Oxides: An Introduction to Their Electronic Structure and Properties*, International Series of Monographs on Chemistry (Oxford University Press, Oxford).

Crépieux, A., and C. Lacroix, 1998, "Dzyaloshinsky-Moriya interactions induced by symmetry breaking at a surface," J. Magn. Magn. Mater. **182**, 341–349.

Marković, D., N. Leroux, A. Mizrahi, J. Trastoy, V. Cros, P. Bortolotti, L. Martins, A. Jenkins, R. Ferreira, and J. Grollier, 2020, "Detection of the Microwave Emission from a Spin-Torque Oscillator by a Spin Diode," Phys. Rev. Appl. **13**, 044050.

Das, H., A. L. Wysocki, Y. Geng, W. Wu, and C. J. Fennie, 2014, "Bulk magnetoelectricity in the hexagonal manganites and ferrites," Nat. Commun. **5**, 2998.

Das, K. S., W. Y. Schoemaker, B. J. van Wees, and I. J. Vera-Marun, 2017, "Spin injection and detection via the anomalous spin Hall effect of a ferromagnetic metal," Phys. Rev. B **96**, 220408.

Das, S., *et al.*, 2019, "Observation of room-temperature polar skyrmions," Nature (London) **568**, 368–372.

da Silveira, L. G. D., P. Barone, and S. Picozzi, 2016, "Rashba-Dresselhaus spin-splitting in the bulk ferroelectric oxide $BiAlO_3$," Phys. Rev. B **93**, 245159.

Daumont, C., *et al.*, 2012, "Strain dependence of polarization and piezoelectric response in epitaxial $BiFeO_3$ thin films," J. Phys. Condens. Matter **24**, 162202.

De Luca, G. M., D. Preziosi, F. Chiarella, R. Di Capua, S. Gariglio, S. Lettieri, and M. Salluzzo, 2013, "Ferromagnetism and ferroelectricity in epitaxial $BiMnO_3$ ultra-thin films," Appl. Phys. Lett. **103**, 062902.

Deng, Y., *et al.*, 2018, "Gate-tunable room-temperature ferromagnetism in two-dimensional $Fe_3GeTe_2$," Nature (London) **563**, 94–99.

Dennard, R. H., F. H. Gaensslen, H.-N. Yu, V. L. Rideout, E. Bassous, and A. R. Leblanc, 1974, "Design of ion-implanted

MOSFET's with very small physical dimensions," IEEE J. Solid-State Circuits **9**, 256–268.

Desplat, L., S. Meyer, J. Bouaziz, P. M. Buhl, S. Lounis, B. Dupé, and P.-A. Hervieux, 2021, "Mechanism for ultrafast electric-field driven skyrmion nucleation," Phys. Rev. B **104**, L060409.

De Teresa, J. M., A. Barthélémy, A. Fert, J. P. Contour, F. Montaigne, and P. Seneor, 1999, "Role of metal-oxide interface in determining the spin polarization of magnetic tunnel junctions," Science **286**, 507–509.

Dhillon, S. S., *et al.*, 2017, "The 2017 terahertz science and technology roadmap," J. Phys. D **50**, 043001.

Dhoot, A. S., C. Israel, X. Moya, N. D. Mathur, and R. H. Friend, 2009, "Large Electric Field Effect in Electrolyte-Gated Manganites," Phys. Rev. Lett. **102**, 136402.

Diéguez, O., O. E. González-Vázquez, J. C. Wojdeł, and J. Íñiguez, 2011, "First-principles predictions of low-energy phases of multiferroic $BiFeO_3$," Phys. Rev. B **83**, 094105.

Diéguez, O., and J. Íñiguez, 2015, "Epitaxial phases of $BiMnO_3$ from first principles," Phys. Rev. B **91**, 184113.

Dieny, B., *et al.*, 2020, "Opportunities and challenges for spintronics in the microelectronics industry," Nat. Electron. **3**, 446–459.

Dietl, T., and H. Ohno, 2014, "Dilute ferromagnetic semiconductors: Physics and spintronic structures," Rev. Mod. Phys. **86**, 187–251.

Dietl, T., H. Ohno, F. Matsukura, D. Ferrand, and J. Cibert, 2000, "Zener model description of ferromagnetism in zinc-blende magnetic semiconductors," Science **287**, 1019–1022.

Ding, B., Z. Li, G. Xu, H. Li, Z. Hou, E. Liu, X. Xi, F. Xu, Y. Yao, and W. Wang, 2020, "Observation of magnetic skyrmion bubbles in a van der Waals ferromagnet $Fe_3GeTe_2$," Nano Lett. **20**, 868–873.

Ding, J., *et al.*, 2021, "Switching of a magnet by spin-orbit torque from a topological Dirac semimetal," Adv. Mater. **33**, 2005909.

Ding, L. J., K. L. Yao, and H. H. Fu, 2011, "Spin-lattice coupling driven ferroelectric transition in one-dimensional organic quantum magnets," J. Mater. Chem. **21**, 449–455.

Ding, S., *et al.*, 2020, "Harnessing Orbital-to-Spin Conversion of Interfacial Orbital Currents for Efficient Spin-Orbit Torques," Phys. Rev. Lett. **125**, 177201.

Di Sante, D., P. Barone, R. Bertacco, and S. Picozzi, 2013, "Electric control of the giant Rashba effect in bulk GeTe," Adv. Mater. **25**, 509–513.

Djani, H., A. C. Garcia-Castro, W.-Y. Tong, P. Barone, E. Bousquet, S. Picozzi, and P. Ghosez, 2019, "Rationalizing and engineering Rashba spin-splitting in ferroelectric oxides," npj Quantum Mater. **4**, 1–6.

Dohi, T., S. DuttaGupta, S. Fukami, and H. Ohno, 2019, "Formation and current-induced motion of synthetic antiferromagnetic skyrmion bubbles," Nat. Commun. **10**, 5153.

Dolui, K., M. D. Petrović, K. Zollner, P. Plecháč, J. Fabian, B. Nikolić, and K. Proximity, 2020, "Spin-orbit torque on a two-dimensional magnet within van der Waals heterostructure: Current-driven antiferromagnet-to-ferromagnet reversible nonequilibrium phase transition in bilayer $CrI_3$," Nano Lett. **20**, 2288–2295.

Dong, S., J.-M. Liu, S.-W. Cheong, and Z. Ren, 2015, "Multiferroic materials and magnetoelectric physics: Symmetry, entanglement, excitation, and topology," Adv. Phys. **64**, 519–626.

Duan, C.-G., S. S. Jaswal, and E. Y. Tsymbal, 2006, "Predicted Magnetoelectric Effect in $Fe/BaTiO_3$ Multilayers: Ferroelectric Control of Magnetism," Phys. Rev. Lett. **97**, 047201.

Dushenko, S., H. Ago, K. Kawahara, T. Tsuda, S. Kuwabata, T. Takenobu, T. Shinjo, Y. Ando, and M. Shiraishi, 2016, "Gate-Tunable Spin-Charge Conversion and the Role of Spin-Orbit Interaction in Graphene," Phys. Rev. Lett. **116**, 166102.

Dushenko, S., M. Hokazono, K. Nakamura, Y. Ando, T. Shinjo, and M. Shiraishi, 2018, "Tunable inverse spin Hall effect in nanometer-thick platinum films by ionic gating," Nat. Commun. **9**, 3118.

Dussaux, A., *et al.*, 2010, "Large microwave generation from current-driven magnetic vortex oscillators in magnetic tunnel junctions," Nat. Commun. **1**, 8.

D'yakonov, M., and V. Perel', 1971, "Possibility of orienting electron spins with current," JETP Lett. **13**, 657–660.

Dzyaloshinsky, I. A, 1958, "Thermodynamic theory of 'weak' ferromagnetism of antiferromagnetics," J. Phys. Chem. Solids **4**, 241–255.

Eckert, J. P., 1953, "A survey of digital computer memory systems," Proc. IRE **41**, 1393–1406.

Edelstein, V. M., 1990, "Spin polarization of conduction electrons induced by electric current in two-dimensional asymmetric electron systems," Solid State Commun. **73**, 233–235.

Ederer, C., and N. A. Spaldin, 2005, "Weak ferromagnetism and magnetoelectric coupling in bismuth ferrite," Phys. Rev. B **71**, 060401.

Eerenstein, W., N. D. Mathur, and J. F. Scott, 2006, "Multiferroic and magnetoelectric materials," Nature (London) **442**, 759–765.

Eerenstein, W., M. Wiora, J. L. Prieto, J. F. Scott, and N. D. Mathur, 2007, "Giant sharp and persistent converse magnetoelectric effects in multiferroic epitaxial heterostructures," Nat. Mater. **6**, 348–351.

Ellsworth, M. J., L. A. Campbell, R. E. Simons, M. K. Iyengar, R. R. Schmidt, and R. C. Chu, 2008, "The evolution of water cooling for IBM large server systems: Back to the future," in *Proceedings of the 11th Intersociety Conference on Thermal and Thermomechanical Phenomena in Electronic Systems, Orlando, 2008* (IEEE, New York), pp. 266–274, 10.1109/ITHERM.2008.4544279.

Emori, S., U. Bauer, S.-M. Ahn, E. Martinez, and G. S. D. Beach, 2013, "Current-driven dynamics of chiral ferromagnetic domain walls," Nat. Mater. **12**, 611–616.

Emori, S., U. Bauer, S. Woo, and G. S. D. Beach, 2014, "Large voltage-induced modification of spin-orbit torques in $Pt/Co/GdO_x$," Appl. Phys. Lett. **105**, 222401.

Endo, M., S. Kanai, S. Ikeda, F. Matsukura, and H. Ohno, 2010, "Electric-field effects on thickness dependent magnetic anisotropy of sputtered $MgO/Co_{40}Fe_{40}B_{20}/Ta$ structures," Appl. Phys. Lett. **96**, 212503.

Engel, B. N., *et al.*, 2005, "A 4-Mb toggle MRAM based on a novel bit and switching method," IEEE Trans. Magn. **41**, 132–136.

Esaki, L., R. B. Laibowitz, and P. J. Stiles, 1971, "Polar switch," IBM Tech. Discl. Bull. **13**, 2161.

Everschor, K., M. Garst, R. A. Duine, and A. Rosch, 2011, "Current-induced rotational torques in the skyrmion lattice phase of chiral magnets," Phys. Rev. B **84**, 064401.

Everschor-Sitte, K., J. Masell, R. M. Reeve, and M. Kläui, 2018, "Perspective: Magnetic skyrmions—Overview of recent progress in an active research field," J. Appl. Phys. **124**, 240901.

Fan, S., *et al.*, 2020, "Site-specific spectroscopic measurement of spin and charge in $(LuFeO_3)_m/(LuFe_2O_4)_1$ multiferroic superlattices," Nat. Commun. **11**, 5582.

Fan, T., M. Tobah, T. Shirokura, N. H. D. Khang, and P. N. Hai, 2020, "Crystal growth and characterization of topological insulator BiSb thin films by sputtering deposition on sapphire substrates," Jpn. J. Appl. Phys. **59**, 063001.

Fan, Y., *et al.*, 2016, "Electric-field control of spin-orbit torque in a magnetically doped topological insulator," Nat. Nanotechnol. **11**, 352–359.

Fang, B., *et al.*, 2016, "Giant spin-torque diode sensitivity in the absence of bias magnetic field," Nat. Commun. **7**, 11259.

Fang, B., *et al.*, 2019, "Experimental Demonstration of Spintronic Broadband Microwave Detectors and Their Capability for Powering Nanodevices," Phys. Rev. Appl. **11**, 014022.

Fang, M., *et al.*, 2020, "Tuning the interfacial spin-orbit coupling with ferroelectricity," Nat. Commun. **11**, 2627.

Fattouhi, M., F. García-Sánchez, R. Yanes, V. Raposo, E. Martínez, and L. Lopez-Diaz, 2021, "Electric Field Control of the Skyrmion Hall Effect in Piezoelectric-Magnetic Devices," Phys. Rev. Appl. **16**, 044035.

Fechner, M., I. V. Maznichenko, S. Ostanin, A. Ernst, J. Henk, P. Bruno, and I. Mertig, 2008, "Magnetic phase transition in two-phase multiferroics predicted from first principles," Phys. Rev. B **78**, 212406.

Fechner, M., P. Zahn, S. Ostanin, M. Bibes, and I. Mertig, 2012, "Switching Magnetization by 180° with an Electric Field," Phys. Rev. Lett. **108**, 197206.

Fei, Z., *et al.*, 2018, "Two-dimensional itinerant ferromagnetism in atomically thin $Fe_3GeTe_2$," Nat. Mater. **17**, 778–782.

Feng, Z., H. Yan, and Z. Liu, 2019, "Electric-field control of magnetic order: From FeRh to topological antiferromagnetic spintronics," Adv. Electron. Mater. **5**, 1800466.

Ferain, I., C. A. Colinge, and J.-P. Colinge, 2011, "Multigate transistors as the future of classical metal-oxide-semiconductor field-effect transistors," Nature (London) **479**, 310–316.

Fernandez, A., M. Acharya, H.-G. Lee, J. Schimpf, Y. Jiang, D. Lou, Z. Tian, and L. W. Martin, 2022, "Thin-film ferroelectrics," Adv. Mater. **34**, 2108841.

Fert, A., 1990, "Magnetic and transport properties of metallic multilayers," Mater. Sci. Forum **59–60**, 439–480.

Fert, A., and I. A. Campbell, 1968, "Two-Current Conduction in Nickel," Phys. Rev. Lett. **21**, 1190–1192.

Fert, A., and I. A. Campbell, 1971, "Transport properties of ferromagnetic transition metals," J. Phys. (Paris), Colloq. **32**, C1-46–C1-50.

Fert, A., and I. A. Campbell, 1976, "Electrical resistivity of ferromagnetic nickel and iron based alloys," J. Phys. F **6**, 849–871.

Fert, A., V. Cros, and J. Sampaio, 2013, "Skyrmions on the track," Nat. Nanotechnol. **8**, 152–156.

Fert, A., and P. M. Levy, 1980, "Role of Anisotropic Exchange Interactions in Determining the Properties of Spin-Glasses," Phys. Rev. Lett. **44**, 1538–1541.

Fert, A., N. Reyren, and V. Cros, 2017, "Magnetic skyrmions: Advances in physics and potential applications," Nat. Rev. Mater. **2**, 17031.

Fert, A., and F. N. Van Dau, 2019, "Spintronics, from giant magnetoresistance to magnetic skyrmions and topological insulators," C.R. Phys. **20**, 817–831.

Fiebig, M., 2005, "Revival of the magnetoelectric effect," J. Phys. D **38**, R123–R152.

Fiebig, M., C. Degenhardt, and R. V. Pisarev, 2002, "Magnetic phase diagram of $HoMnO_3$," J. Appl. Phys. **91**, 8867.

Fiebig, M., T. Lottermoser, D. Meier, and M. Trassin, 2016, "The evolution of multiferroics," Nat. Rev. Mater. **1**, 16046.

Fiebig, M., Th. Lottermoser, and R. V. Pisarev, 2003, "Spin-rotation phenomena and magnetic phase diagrams of hexagonal $RMnO_3$," J. Appl. Phys. **93**, 8194–8196.

Figueiredo-Prestes, N., *et al.*, 2021, "Magnetization switching and deterministic nucleation in Co/Ni multilayered disks induced by spin-orbit torques," Appl. Phys. Lett. **119**, 032410.

Filianina, M., J.-P. Hanke, K. Lee, D.-S. Han, S. Jaiswal, A. Rajan, G. Jakob, Y. Mokrousov, and M. Kläui, 2020, "Electric-Field Control of Spin-Orbit Torques in Perpendicularly Magnetized W/CoFeB/MgO Films," Phys. Rev. Lett. **124**, 217701.

Fina, I., and J. Fontcuberta, 2020, "Strain and voltage control of magnetic and electric properties of FeRh films," J. Phys. D **53**, 023002.

Finizio, S., K. Zeissler, S. Wintz, S. Mayr, T. Weßels, A. J. Huxtable, G. Burnell, C. H. Marrows, and J. Raabe, 2019, "Deterministic field-free skyrmion nucleation at a nanoengineered injector device," Nano Lett. **19**, 7246–7255.

Finocchio, G., R. Tomasello, B. Fang, A. Giordano, V. Puliafito, M. Carpentieri, and Z. Zeng, 2021, "Perspectives on spintronic diodes," Appl. Phys. Lett. **118**, 160502.

Freitas, P. P., and L. Berger, 1985, "Observation of *s-d* exchange force between domain walls and electric current in very thin Permalloy films," J. Appl. Phys. **57**, 1266–1269.

Fukami, S., C. Zhang, S. DuttaGupta, A. Kurenkov, and H. Ohno, 2016, "Magnetization switching by spin-orbit torque in an antiferromagnet-ferromagnet bilayer system," Nat. Mater. **15**, 535–541.

Fusil, S., V. Garcia, A. Barthélémy, and M. Bibes, 2014, "Magnetoelectric devices for spintronics," Annu. Rev. Mater. Res. **44**, 91–116.

Fusil, S., *et al.*, 2022, "Polar chirality in $BiFeO_3$ emerging from a peculiar domain wall sequence," Adv. Electron. Mater. **8**, 2101155.

Gajek, M., M. Bibes, S. Fusil, K. Bouzehouane, J. Fontcuberta, A. Barthélémy, and A. Fert, 2007, "Tunnel junctions with multiferroic barriers," Nat. Mater. **6**, 296–302.

Garcia, J. H., A. W. Cummings, and S. Roche, 2017, "Spin Hall effect and weak antilocalization in graphene/transition metal dichalcogenide heterostructures," Nano Lett. **17**, 5078–5083.

Garcia, J. H., M. Vila, A. W. Cummings, and S. Roche, 2018, "Spin transport in graphene/transition metal dichalcogenide heterostructures," Chem. Soc. Rev. **47**, 3359–3379.

Garcia, V., and M. Bibes, 2014, "Ferroelectric tunnel junctions for information storage and processing," Nat. Commun. **5**, 4289.

Garcia, V., M. Bibes, A. Barthélémy, M. Bowen, E. Jacquet, J.-P. Contour, and A. Fert, 2004, "Temperature dependence of the interfacial spin polarization of $La_{2/3}Sr_{1/3}MnO_3$," Phys. Rev. B **69**, 052403.

Garcia, V., S. Fusil, K. Bouzehouane, S. Enouz-Vedrenne, N. D. Mathur, A. Barthélémy, and M. Bibes, 2009, "Giant tunnel electroresistance for non-destructive readout of ferroelectric states," Nature (London) **460**, 81–84.

Garcia, V., *et al.*, 2010, "Ferroelectric control of spin polarization," Science **327**, 1106–1110.

García-Fernández, P., J. C. Wojdeł, J. Íñiguez, and J. Junquera, 2016, "Second-principles method for materials simulations including electron and lattice degrees of freedom," Phys. Rev. B **93**, 195137.

Garello, K., C. O. Avci, I. M. Miron, M. Baumgartner, A. Ghosh, S. Auffret, O. Boulle, G. Gaudin, and P. Gambardella, 2014, "Ultrafast magnetization switching by spin-orbit torques," Appl. Phys. Lett. **105**, 212402.

Garello, K., I. M. Miron, C. O. Avci, F. Freimuth, Y. Mokrousov, S. Blügel, S. Auffret, O. Boulle, G. Gaudin, and P. Gambardella, 2013, "Symmetry and magnitude of spin-orbit torques in ferromagnetic heterostructures," Nat. Nanotechnol. **8**, 587–593.

Geprägs, S., A. Brandlmaier, M. Opel, R. Gross, and S. T. B. Goennenwein, 2010, "Electric field controlled manipulation of the magnetization in $Ni/BaTiO_3$ hybrid structures," Appl. Phys. Lett. **96**, 142509.

Geprägs, S., F. D. Czeschka, M. Opel, S. T. B. Goennenwein, W. Yu, W. Mader, and R. Gross, 2009, "Epitaxial growth and magnetic

properties of $Sr_2CrReO_6$ thin films," J. Magn. Magn. Mater. **321**, 2001–2004.

Ghiasi, T. S., A. A. Kaverzin, P. J. Blah, and B. J. van Wees, 2019, "Charge-to-spin conversion by the Rashba-Edelstein effect in two-dimensional van der Waals heterostructures up to room temperature," Nano Lett. **19**, 5959–5966.

Ghidini, M., R. Pellicelli, J. L. Prieto, X. Moya, J. Soussi, J. Briscoe, S. Dunn, and N. D. Mathur, 2013, "Non-volatile electrically-driven repeatable magnetization reversal with no applied magnetic field," Nat. Commun. **4**, 1453.

Ghosh, S., *et al.*, 2021, "Current-driven domain wall dynamics in ferrimagnetic nickel-doped $Mn_4N$ films: Very large domain wall velocities and reversal of motion direction across the magnetic compensation point," Nano Lett. **21**, 2580–2587.

Giles, B. L., Z. Yang, J. S. Jamison, and R. C. Myers, 2015, "Long-range pure magnon spin diffusion observed in a nonlocal spin-Seebeck geometry," Phys. Rev. B **92**, 224415.

Giovannetti, G., S. Kumar, A. Stroppa, J. van den Brink, and S. Picozzi, 2009, "Multiferroicity in TTF-CA Organic Molecular Crystals Predicted through *Ab Initio* Calculations," Phys. Rev. Lett. **103**, 266401.

Go, D., J.-P. Hanke, P. M. Buhl, F. Freimuth, G. Bihlmayer, H.-W. Lee, Y. Mokrousov, and S. Blügel, 2017, "Toward surface orbitronics: Giant orbital magnetism from the orbital Rashba effect at the surface of $sp$-metals," Sci. Rep. **7**, 46742.

Goennenwein, S. T. B., R. Schlitz, M. Pernpeintner, K. Ganzhorn, M. Althammer, R. Gross, and H. Huebl, 2015, "Non-local magnetoresistance in YIG/Pt nanostructures," Appl. Phys. Lett. **107**, 172405.

Gong, C., and X. Zhang, 2019, "Two-dimensional magnetic crystals and emergent heterostructure devices," Science, **363**, eaav4450.

Gong, C., *et al.*, 2017, "Discovery of intrinsic ferromagnetism in two-dimensional van der Waals crystals," Nature (London) **546**, 265–269.

Gorige, V., A. Swain, K. Komatsu, M. Itoh, and T. Taniyama, 2017, "Magnetization reversal in $Fe/BaTiO_3(110)$ heterostructured multiferroics," Phys. Status Solidi RRL **11**, 1700294.

Gosteau, J., R. Arras, P. Chen, H. J. Zhao, C. Paillard, and L. Bellaiche, 2021, "Spin-orbit effects in ferroelectric $PbTiO_3$ under tensile strain," Phys. Rev. B **103**, 024416.

Goto, M., *et al.*, 2021, "Uncooled sub-GHz spin bolometer driven by auto-oscillation," Nat. Commun. **12**, 536.

Goto, T., T. Kimura, G. Lawes, A. P. Ramirez, and Y. Tokura, 2004, "Ferroelectricity and Giant Magnetocapacitance in Perovskite Rare-Earth Manganites," Phys. Rev. Lett. **92**, 257201.

Grimaldi, E., V. Krizakova, G. Sala, F. Yasin, S. Couet, G. Sankar Kar, K. Garello, and P. Gambardella, 2020, "Single-shot dynamics of spin-orbit torque and spin transfer torque switching in three-terminal magnetic tunnel junctions," Nat. Nanotechnol. **15**, 111–117.

Groen, I., V. T. Pham, N. Leo, A. Marty, L. E. Hueso, and F. Casanova, 2021, "Disentangling Spin, Anomalous, and Planar Hall Effects in Ferromagnet–Heavy-Metal Nanostructures," Phys. Rev. Appl. **15**, 044010.

Groenendijk, D. J., *et al.*, 2020, "Berry phase engineering at oxide interfaces," Phys. Rev. Res. **2**, 023404.

Grollier, J., V. Cros, A. Hamzic, J. M. George, H. Jaffrès, A. Fert, G. Faini, J. Ben Youssef, and H. Legall, 2001, "Spin-polarized current induced switching in Co/Cu/Co pillars," Appl. Phys. Lett. **78**, 3663–3665.

Gross, I., *et al.*, 2017, "Real-space imaging of non-collinear antiferromagnetic order with a single-spin magnetometer," Nature (London) **549**, 252–256.

Gruner, M. E., E. Hoffmann, and P. Entel, 2003, "Instability of the rhodium magnetic moment as the origin of the metamagnetic phase transition in $\alpha$-FeRh," Phys. Rev. B **67**, 064415.

Guo, Z., J. Yin, Y. Bai, D. Zhu, K. Shi, G. Wang, K. Cao, and W. Zhao, 2021, "Spintronics for energy-efficient computing: An overview and outlook," Proc. IEEE **109**, 1398–1417.

Gupta, V., *et al.*, 2020, "Manipulation of the van der Waals magnet $Cr_2Ge_2Te_6$ by spin-orbit torques," Nano Lett. **20**, 7482–7488.

Gushi, T., *et al.*, 2019, "Large current driven domain wall mobility and gate tuning of coercivity in ferrimagnetic $Mn_4N$ thin films," Nano Lett. **19**, 8716–8723.

Haeni, J. H., *et al.*, 2004, "Room-temperature ferroelectricity in strained $SrTiO_3$," Nature (London) **430**, 758–761.

Hahn, C., G. de Loubens, O. Klein, M. Viret, V. V. Naletov, and J. Ben Youssef, 2013, "Comparative measurements of inverse spin Hall effects and magnetoresistance in YIG/Pt and YIG/Ta," Phys. Rev. B **87**, 174417.

Han, J., P. Zhang, Z. Bi, Y. Fan, T. S. Safi, J. Xiang, J. Finley, L. Fu, R. Cheng, and L. Liu, 2020, "Birefringence-like spin transport via linearly polarized antiferromagnetic magnons," Nat. Nanotechnol. **15**, 563–568.

Han, L., *et al.*, 2022, "High-density switchable skyrmion-like polar nanodomains integrated on silicon," Nature (London) **603**, 63–67.

Han, M.-G., J. A. Garlow, Y. Liu, H. Zhang, J. Li, D. DiMarzio, M. W. Knight, C. Petrovic, D. Jariwala, and Y. Zhu, 2019, "Topological magnetic-spin textures in two-dimensional van der Waals $Cr_2Ge_2Te_6$," Nano Lett. **19**, 7859–7865.

Han, W., S. Maekawa, and X.-C. Xie, 2020, "Spin current as a probe of quantum materials," Nat. Mater. **19**, 139–152.

Han, W., YoshiChika Otani, and Sadamichi Maekawa, 2018, "Quantum materials for spin and charge conversion," npj Quantum Mater. **3**, 27.

Hasan, M. Z., and C. L. Kane, 2010, "Colloquium: Topological insulators," Rev. Mod. Phys. **82**, 3045–3067.

Haspot, V., P. Noël, J.-P. Attané, L. Vila, M. Bibes, A. Anane, and A. Barthélémy, 2022, "Temperature dependence of the Gilbert damping of $La_{0.7}Sr_{0.3}MnO_3$ thin films," Phys. Rev. Mater. **6**, 024406.

Hatano, T., Y. Ogimoto, N. Ogawa, M. Nakano, S. Ono, Y. Tomioka, K. Miyano, Y. Iwasa, and Y. Tokura, 2013, "Gate control of electronic phases in a quarter-filled manganite," Sci. Rep. **3**, 2904.

Hatano, T., Z. Sheng, M. Nakamura, M. Nakano, M. Kawasaki, Y. Iwasa, and Y. Tokura, 2014, "Gate control of percolative conduction in strongly correlated manganite films," Adv. Mater. **26**, 2874–2877.

Hayashi, H., D. Jo, D. Go, T. Gao, S. Haku, Y. Mokrousov, H.-W. Lee, and K. Ando, 2023, "Observation of long-range orbital transport and giant orbital torque," Commun. Phys. **6**, 32.

Haykal, A., *et al.*, 2020, "Antiferromagnetic textures in $BiFeO_3$ controlled by strain and electric field," Nat. Commun. **11**, 1704.

He, X., Y. Wang, N. Wu, A. N. Caruso, E. Vescovo, K. D. Belashchenko, P. A. Dowben, and C. Binek, 2010, "Robust isothermal electric control of exchange bias at room temperature," Nat. Mater. **9**, 579.

Heidler, J., *et al.*, 2016, "Magnetoelectroelastic control of magnetism in an artificial multiferroic," Phys. Rev. B **94**, 014401.

Heinrich, B., C. Burrowes, E. Montoya, B. Kardasz, E. Girt, Y.-Y. Song, Y. Sun, and M. Wu, 2011, "Spin Pumping at the Magnetic Insulator (YIG)/Normal Metal (Au) Interfaces," Phys. Rev. Lett. **107**, 066604.

Heinze, S., K. von Bergmann, M. Menzel, J. Brede, A. Kubetzka, R. Wiesendanger, G. Bihlmayer, and S. Blügel, 2011, "Spontaneous

atomic-scale magnetic skyrmion lattice in two dimensions," Nat. Phys. **7**, 713–718.

Hemberger, J., P. Lunkenheimer, R. Viana, R. Böhmer, and A. Loidl, 1995, "Electric-field-dependent dielectric constant and nonlinear susceptibility in $SrTiO_3$," Phys. Rev. B **52**, 13159–13162.

Herling, F., C. K. Safeer, J. Ingla-Aynés, N. Ontoso, L. E. Hueso, and F. Casanova, 2020, "Gate tunability of highly efficient spin-to-charge conversion by spin Hall effect in graphene proximitized with $WSe_2$," APL Mater. **8**, 071103.

Heron, J. T., D. G. Schlom, and R. Ramesh, 2014, "Electric field control of magnetism using $BiFeO_3$-based heterostructures," Appl. Phys. Rev. **1**, 021303.

Heron, J. T., *et al.*, 2014, "Deterministic switching of ferromagnetism at room temperature using an electric field," Nature (London) **516**, 370–373.

Hill, N. A., 2000, "Why are there so few magnetic ferroelectrics?," J. Phys. Chem. B **104**, 6694–6709.

Hirai, T., Y. Hibino, K. Hasegawa, M. Kohda, T. Koyama, and D. Chiba, 2020, "Voltage control of spin-orbit torque in $Pd/Co/Pd/HfO_x$," Appl. Phys. Express **13**, 123005.

Hirsch, J. E., 1999, "Spin Hall Effect," Phys. Rev. Lett. **83**, 1834–1837.

Hoffmann, A., 2013, "Spin Hall effects in metals," IEEE Trans. Magn. **49**, 5172–5193.

Hoque, A. M., D. Khokhriakov, K. Zollner, B. Zhao, B. Karpiak, J. Fabian, and S. P. Dash, 2021, "All-electrical creation and control of spin-galvanic signal in graphene and molybdenum ditelluride heterostructures at room temperature," Commun. Phys. **4**, 1–9.

Hosomi, M., *et al.*, 2005, "A novel nonvolatile memory with spin torque transfer magnetization switching: Spin-ram," in *Proceedings of the IEEE International Electron Devices Meeting, Tempe, 2005* (IEEE, New York), pp. 459–462, 10.1109/IEDM.2005.1609379.

Hrabec, A., V. Křižáková, S. Pizzini, J. Sampaio, A. Thiaville, S. Rohart, and J. Vogel, 2018, "Velocity Enhancement by Synchronization of Magnetic Domain Walls," Phys. Rev. Lett. **120**, 227204.

Hsu, P.-J., A. Kubetzka, A. Finco, N. Romming, K. von Bergmann, and R. Wiesendanger, 2017, "Electric-field-driven switching of individual magnetic skyrmions," Nat. Nanotechnol. **12**, 123–126.

Hu, J.-M., Z. Li, L.-Q. Chen, and C.-W. Nan, 2011, "High-density magnetoresistive random access memory operating at ultralow voltage at room temperature," Nat. Commun. **2**, 553.

Hu, J.-M., C.-W. Nan, and L.-Q. Chen, 2011, "Size-dependent electric voltage controlled magnetic anisotropy in multiferroic heterostructures: Interface-charge and strain comediated magnetoelectric coupling," Phys. Rev. B **83**, 134408.

Huang, B., *et al.*, 2017, "Layer-dependent ferromagnetism in a van der Waals crystal down to the monolayer limit," Nature (London) **546**, 270–273.

Huang, B., *et al.*, 2018, "Electrical control of 2D magnetism in bilayer $CrI_3$," Nat. Nanotechnol. **13**, 544–548.

Huang, H., *et al.*, 2018, "Distinguishing charge and strain coupling in ultrathin $(001)$-$La_{0.7}Sr_{0.3}MnO_3$/PMN-PT heterostructures," Appl. Phys. Lett. **113**, 262901.

Huang, P., M. Cantoni, A. Kruchkov, J. Rajeswari, A. Magrez, F. Carbone, and H. M. Rønnow, 2018, "*In situ* electric field skyrmion creation in magnetoelectric $Cu_2OSeO_3$," Nano Lett. **18**, 5167–5171.

Huang, Y.-L., *et al.*, 2020, "Manipulating magnetoelectric energy landscape in multiferroics," Nat. Commun. **11**, 2836.

Huang, Z. J., Y. Cao, Y. Y. Sun, Y. Y. Xue, and C. W. Chu, 1997, "Coupling between the ferroelectric and antiferromagnetic orders in $YMnO_3$," Phys. Rev. B **56**, 2623–2626.

Hur, N., I. K. Jeong, M. F. Hundley, S. B. Kim, and S.-W. Cheong, 2009, "Giant magnetoelectric effect in multiferroic $HoMnO_3$ with a high ferroelectric transition temperature," Phys. Rev. B **79**, 134120.

Ichinose, T., D. Miura, and H. Naganuma, 2021, "High-quality sputtered $BiFeO_3$ for ultrathin epitaxial films," ACS Appl. Electron. Mater. **3**, 4836–4848.

Ihlefeld, J. F., *et al.*, 2007, "Adsorption-controlled molecular-beam epitaxial growth of $BiFeO_3$," Appl. Phys. Lett. **91**, 071922.

Iihama, S., T. Taniguchi, K. Yakushiji, A. Fukushima, Y. Shiota, S. Tsunegi, R. Hiramatsu, S. Yuasa, Y. Suzuki, and H. Kubota, 2018, "Spin-transfer torque induced by the spin anomalous Hall effect," Nat. Electron. **1**, 120–123.

Ikeda, N., *et al.*, 2005, "Ferroelectricity from iron valence ordering in the charge-frustrated system $LuFe_2O_4$," Nature (London) **436**, 1136–1138.

Imada, M., A. Fujimori, and Y. Tokura, 1998, "Metal-insulator transitions," Rev. Mod. Phys. **70**, 225.

Inokuchi, T., *et al.*, 2017, "Improved read disturb and write error rates in voltage-control spintronics memory (VoCSM) by controlling energy barrier height," Appl. Phys. Lett. **110**, 252404.

Isarov, M., L. Z. Tan, M. I. Bodnarchuk, M. V. Kovalenko, A. M. Rappe, and E. Lifshitz, 2017, "Rashba effect in a single colloidal $CsPbBr_3$ perovskite nanocrystal detected by magneto-optical measurements," Nano Lett. **17**, 5020–5026.

Isasa, M., *et al.*, 2016, "Origin of inverse Rashba-Edelstein effect detected at the Cu/Bi interface using lateral spin valves," Phys. Rev. B **93**, 014420.

Ishibashi, Y., and Y. Takagi, 1971, "Note on ferroelectric domain switching," J. Phys. Soc. Jpn. **31**, 506–510.

Itoh, M., R. Wang, Y. Inaguma, T. Yamaguchi, Y.-J. Shan, and T. Nakamura, 1999, "Ferroelectricity Induced by Oxygen Isotope Exchange in Strontium Titanate Perovskite," Phys. Rev. Lett. **82**, 3540.

Iwasaki, J., M. Mochizuki, and N. Nagaosa, 2013, "Current-induced skyrmion dynamics in constricted geometries," Nat. Nanotechnol. **8**, 742–747.

Jain, A., *et al.*, 2018, "The Materials Project: Accelerating materials design through theory-driven data and tools," in *Handbook of Materials Modeling: Methods: Theory and Modeling*, edited by W. Andreoni and S. Yip (Springer International Publishing, Cham, Switzerland), pp. 1–34.

Jarollahi, H., N. Onizawa, V. Gripon, N. Sakimura, T. Sugibayashi, T. Endoh, H. Ohno, T. Hanyu, and W. J. Gross, 2014, "A nonvolatile associative memory-based context-driven search engine using 90 nm CMOS/MTJ-hybrid logic-in-memory architecture," IEEE J. Emerg. Sel. Top. Circuits Syst. **4**, 460–474.

Jeen, H., G. Singh-Bhalla, P. R. Mickel, K. Voigt, C. Morien, S. Tongay, A. F. Hebard, and A. Biswas, 2011, "Growth and characterization of multiferroic $BiMnO_3$ thin films," J. Appl. Phys. **109**, 074104.

Jenkins, A. S., *et al.*, 2016, "Spin-torque resonant expulsion of the vortex core for an efficient radiofrequency detection scheme," Nat. Nanotechnol. **11**, 360–364.

Jeong, Y. K., J.-H. Lee, S.-J. Ahn, and H. M. Jang, 2012, "Epitaxially constrained hexagonal ferroelectricity and canted triangular spin order in $LuFeO_3$ thin films," Chem. Mater. **24**, 2426–2428.

Jiang, S., L. Li, Z. Wang, K. F. Mak, and J. Shan, 2018, "Controlling magnetism in 2D $CrI_3$ by electrostatic doping," Nat. Nanotechnol. **13**, 549–553.

Jiang, S., L. Li, Z. Wang, J. Shan, and K. F. Mak, 2019, "Spin tunnel field-effect transistors based on two-dimensional van der Waals heterostructures," Nat. Electron. **2**, 159–163.

Jiang, S., J. Shan, and K. F. Mak, 2018, "Electric-field switching of two-dimensional van der Waals magnets," Nat. Mater. **17**, 406–410.

Jin, M.-J., *et al.*, 2017, "Nonlocal spin diffusion driven by giant spin Hall effect at oxide heterointerfaces," Nano Lett. **17**, 36–43.

Jo, D., D. Go, and H.-W. Lee, 2018, "Gigantic intrinsic orbital Hall effects in weakly spin-orbit coupled metals," Phys. Rev. B **98**, 214405.

Johansson, A., B. Göbel, J. Henk, M. Bibes, and I. Mertig, 2021, "Spin and orbital Edelstein effects in a two-dimensional electron gas: Theory and application to $SrTiO_3$ interfaces," Phys. Rev. Res. **3**, 013275.

Johnson, M., and R. H. Silsbee, 1985, "Interfacial Charge-Spin Coupling: Injection and Detection of Spin Magnetization in Metals," Phys. Rev. Lett. **55**, 1790–1793.

Jones, N., 2018, "How to stop data centres from gobbling up the world's electricity," Nature (London) **561**, 163–166.

Julliere, M., 1975, "Tunneling between ferromagnetic films," Phys. Lett. **54A**, 225–226.

Jungwirth, T., X. Marti, P. Wadley, and J. Wunderlich, 2016, "Antiferromagnetic spintronics," Nat. Nanotechnol. **11**, 231–241.

Juraschek, D. M., M. Fechner, A. V. Balatsky, and N. A. Spaldin, 2017, "Dynamical multiferroicity," Phys. Rev. Mater. **1**, 014401.

Kagawa, F., S. Horiuchi, M. Tokunaga, J. Fujioka, and Y. Tokura, 2010, "Ferroelectricity in a one-dimensional organic quantum magnet," Nat. Phys. **6**, 169–172.

Kanai, S., Y. Nakatani, M. Yamanouchi, S. Ikeda, H. Sato, F. Matsukura, and H. Ohno, 2014, "Magnetization switching in a CoFeB/MgO magnetic tunnel junction by combining spin-transfer torque and electric field-effect," Appl. Phys. Lett. **104**, 212406.

Kang, W., Y. Huang, X. Zhang, Y. Zhou, and W. Zhao, 2016, "Skyrmion-electronics: An overview and outlook," Proc. IEEE **104**, 2040–2061.

Kanki, T., H. Tanaka, and T. Kawai, 2006, "Electric control of room temperature ferromagnetism in a $Pb(Zr_{0.2}Ti_{0.8})O_3/La_{0.85}Ba_{0.15}MnO_3$ field-effect transistor," Appl. Phys. Lett. **89**, 242506.

Kao, I.-H., *et al.*, 2022, "Deterministic switching of a perpendicularly polarized magnet using unconventional spin-orbit torques in $WTe_2$," Nat. Mater. **21**, 1029–1034.

Karpinsky, D. V., *et al.*, 2017, "Thermodynamic potential and phase diagram for multiferroic bismuth ferrite ($BiFeO_3$)," npj Comput. Mater. **3**, 1–10.

Kato, Y. K., R. C. Myers, A. C. Gossard, and D. D. Awschalom, 2004, "Observation of the spin Hall effect in semiconductors," Science **306**, 1910–1913.

Katsura, H., N. Nagaosa, and A. V. Balatsky, 2005, "Spin Current and Magnetoelectric Effect in Noncollinear Magnets," Phys. Rev. Lett. **95**, 057205.

Ke, X., P. P. Zhang, S. H. Baek, J. Zarestky, W. Tian, and C. B. Eom, 2010, "Magnetic structure of epitaxial multiferroic $BiFeO_3$ films with engineered ferroelectric domains," Phys. Rev. B **82**, 134448.

Kenzelmann, M., A. B. Harris, S. Jonas, C. Broholm, J. Schefer, S. B. Kim, C. L. Zhang, S.-W. Cheong, O. P. Vajk, and J. W. Lynn, 2005, "Magnetic Inversion Symmetry Breaking and Ferroelectricity in $TbMnO_3$," Phys. Rev. Lett. **95**, 087206.

Khan, H. N., D. A. Hounshell, and E. R. H. Fuchs, 2018, "Science and research policy at the end of Moore's law," Nat. Electron. **1**, 14–21.

Khang, N. H. D., Y. Ueda, and P. N. Hai, 2018, "A conductive topological insulator with large spin Hall effect for ultralow power spin-orbit torque switching," Nat. Mater. **17**, 808–813.

Khitun, A., M. Bao, and K. L. Wang, 2010, "Magnonic logic circuits," J. Phys. D **43**, 264005.

Khokhriakov, D., A. M. Hoque, B. Karpiak, and S. P. Dash, 2020, "Gate-tunable spin-galvanic effect in graphene-topological insulator van der Waals heterostructures at room temperature," Nat. Commun. **11**, 3657.

Kim, H. H., S. Jiang, B. Yang, S. Zhong, S. Tian, C. Li, H. Lei, J. Shan, K. F. Mak, and A. W. Tsen, 2020, "Magneto-memristive switching in a 2D layer antiferromagnet," Adv. Mater. **32**, 1905433.

Kim, J., J. Sinha, S. Mitani, M. Hayashi, S. Takahashi, S. Maekawa, M. Yamanouchi, and H. Ohno, 2014, "Anomalous temperature dependence of current-induced torques in CoFeB/MgO heterostructures with Ta-based underlayers," Phys. Rev. B **89**, 174424.

Kim, K.-W., and K.-J. Lee, 2020, "Generalized Spin Drift-Diffusion Formalism in the Presence of Spin-Orbit Interaction of Ferromagnets," Phys. Rev. Lett. **125**, 207205.

Kimura, T., 2012, "Magnetoelectric hexaferrites," Annu. Rev. Condens. Matter Phys. **3**, 93–110.

Kimura, T., T. Goto, H. Shintani, K. Ishizaka, T. Arima, and Y. Tokura, 2003, "Magnetic control of ferroelectric polarization," Nature (London) **426**, 55–58.

Kimura, T., S. Kawamoto, I. Yamada, M. Azuma, M. Takano, and Y. Tokura, 2003, "Magnetocapacitance effect in multiferroic $BiMnO_3$," Phys. Rev. B **67**, 180401.

Kimura, T., G. Lawes, T. Goto, Y. Tokura, and A. P. Ramirez, 2005, "Magnetoelectric phase diagrams of orthorhombic $RMnO_3$ ($R$ = Gd, Tb, and Dy)," Phys. Rev. B **71**, 224425.

Kimura, T., G. Lawes, and A. P. Ramirez, 2005, "Electric Polarization Rotation in a Hexaferrite with Long-Wavelength Magnetic Structures," Phys. Rev. Lett. **94**, 137201.

Kimura, T., Y. Otani, T. Sato, S. Takahashi, and S. Maekawa, 2007, "Room-Temperature Reversible Spin Hall Effect," Phys. Rev. Lett. **98**, 156601.

Kiselev, S. V., R. P. Ozerov, and G. S. Zhdanov, 1963, "Detection of magnetic order in ferroelectric $BiFeO_3$ by neutron diffraction," Sov. Phys. Dokl. **7**, 742.

Kobayashi, K.-I., T. Kimura, H. Sawada, K. Terakura, and Y. Tokura, 1998, "Room-temperature magnetoresistance in an oxide material with an ordered double-perovskite structure," Nature (London) **395**, 677–680.

Kocsis, V., *et al.*, 2019, "Magnetization-polarization cross-control near room temperature in hexaferrite single crystals," Nat. Commun. **10**, 1247.

Kolobov, A. V., D. J. Kim, A. Giussani, P. Fons, J. Tominaga, R. Calarco, and A. Gruverman, 2014, "Ferroelectric switching in epitaxial GeTe films," APL Mater. **2**, 066101.

Kondou, K., R. Yoshimi, A. Tsukazaki, Y. Fukuma, J. Matsuno, K. S. Takahashi, M. Kawasaki, Y. Tokura, and Y. Otani, 2016, "Fermi-level-dependent charge-to-spin current conversion by Dirac surface states of topological insulators," Nat. Phys. **12**, 1027.

Kouvel, J. S., and C. C. Hartelius, 1962, "Anomalous magnetic moments and transformations in the ordered alloy FeRh," J. Appl. Phys. **33**, 1343–1344.

Krempaský, J., *et al.*, 2018, "Operando Imaging of All-Electric Spin Texture Manipulation in Ferroelectric and Multiferroic Rashba Semiconductors," Phys. Rev. X **8**, 021067.

Krizakova, V., E. Grimaldi, K. Garello, G. Sala, S. Couet, G. S. Kar, and P. Gambardella, 2021, "Interplay of Voltage Control of Magnetic Anisotropy, Spin-Transfer Torque, and Heat in the Spin-Orbit-Torque Switching of Three-Terminal Magnetic Tunnel Junctions," Phys. Rev. Appl. **15**, 054055.

Kruchkov, A. J., J. S. White, M. Bartkowiak, I. Živković, A. Magrez, and H. M. Rønnow, 2018, "Direct electric field control of the skyrmion phase in a magnetoelectric insulator," Sci. Rep. **8**, 10466.

Kuhn, K. J., 2012, "Considerations for ultimate CMOS scaling," IEEE Trans. Electron Devices **59**, 1813–1828.

Kuroda, T., 2002, "Low-power, high-speed CMOS VLSI design," in *Proceedings of the IEEE International Conference on Computer Design: VLSI in Computers and Processors, Freiberg, Germany, 2002* (IEEE, New York), pp. 310–315.

Lagerwall, S. T., and I. Dahl, 1984, "Ferroelectric liquid crystals," Mol. Cryst. Liq. Cryst. **114**, 151–187.

Lahtinen, T. H. E., K. J. A. Franke, and S. van Dijken, 2012, "Electric-field control of magnetic domain wall motion and local magnetization reversal," Sci. Rep. **2**, 258.

Lahtinen, T. H. E., J. O. Tuomi, and S. van Dijken, 2011, "Pattern transfer and electric-field-induced magnetic domain formation in multiferroic heterostructures," Adv. Mater. **23**, 3187–3191.

Lambert, C.-H., *et al.*, 2014, "All-optical control of ferromagnetic thin films and nanostructures," Science **345**, 1337–1340.

LaPedus, M., 2023, "Embedded flash scaling limits," https://semiengineering.com/embedded-flash-scaling-limits/ (accessed January 21, 2023).

Lau, Y.-C., D. Betto, K. Rode, J. M. D. Coey, and P. Stamenov, 2016, "Spin-orbit torque switching without an external field using interlayer exchange coupling," Nat. Nanotechnol. **11**, 758–762.

Lebeugle, D., D. Colson, A. Forget, and M. Viret, 2007, "Very large spontaneous electric polarization in $BiFeO_3$ single crystals at room temperature and its evolution under cycling fields," Appl. Phys. Lett. **91**, 022907.

Lebeugle, D., D. Colson, A. Forget, M. Viret, A. M. Bataille, and A. Gukasov, 2008, "Electric-Field-Induced Spin Flop in $BiFeO_3$ Single Crystals at Room Temperature," Phys. Rev. Lett. **100**, 227602.

Lebrun, R., A. Ross, S. A. Bender, A. Qaiumzadeh, L. Baldrati, J. Cramer, A. Brataas, R. A. Duine, and M. Kläui, 2018, "Tunable long-distance spin transport in a crystalline antiferromagnetic iron oxide," Nature (London) **561**, 222–225.

Lee, D., and H. N. Lee, 2017, "Controlling oxygen mobility in ruddlesden-popper oxides," Materials **10**, 368.

Lee, D., *et al.*, 2021, "Orbital torque in magnetic bilayers," Nat. Commun. **12**, 6710.

Lee, J.-U., S. Lee, J. H. Ryoo, S. Kang, T. Y. Kim, P. Kim, C.-H. Park, J.-G. Park, and H. Cheong, 2016, "Ising-type magnetic ordering in atomically thin $FePS_3$," Nano Lett. **16**, 7433–7438.

Lee, K.-S., S.-W. Lee, B.-C. Min, and K.-J. Lee, 2013, "Threshold current for switching of a perpendicular magnetic layer induced by spin Hall effect," Appl. Phys. Lett. **102**, 112410.

Lee, Y., *et al.*, 2015, "Large resistivity modulation in mixed-phase metallic systems," Nat. Commun. **6**, 5959.

Legrand, W., D. Maccariello, F. Ajejas, S. Collin, A. Vecchiola, K. Bouzehouane, N. Reyren, V. Cros, and A. Fert, 2020, "Room-temperature stabilization of antiferromagnetic skyrmions in synthetic antiferromagnets," Nat. Mater. **19**, 34–42.

Legrand, W., D. Maccariello, N. Reyren, K. Garcia, C. Moutafis, C. Moreau-Luchaire, S. Collin, K. Bouzehouane, V. Cros, and A. Fert, 2017, "Room-temperature current-induced generation and motion of sub–100 nm skyrmions," Nano Lett. **17**, 2703–2712.

Lei, N., *et al.*, 2013, "Strain-controlled magnetic domain wall propagation in hybrid piezoelectric/ferromagnetic structures," Nat. Commun. **4**, 1378.

Leighton, C., 2019, "Electrolyte-based ionic control of functional oxides," Nat. Mater. **18**, 13–18.

Leroux, N., D. Marković, E. Martin, T. Petrisor, D. Querlioz, A. Mizrahi, and J. Grollier, 2021, "Radio-Frequency Multiply-and-Accumulate Operations with Spintronic Synapses," Phys. Rev. Appl. **15**, 034067.

Lesne, E., Y. Fu, S. Oyarzun, J. C. Rojas-Sánchez, D. C. Vaz, H. Naganuma, and G. Sicoli, 2016, "Highly efficient and tunable spin-to-charge conversion through Rashba coupling at oxide interfaces," Nat. Mater. **15**, 1261.

Leufke, P. M., R. Kruk, R. A. Brand, and H. Hahn, 2013, "*In situ* magnetometry studies of magnetoelectric LSMO/PZT heterostructures," Phys. Rev. B **87**, 094416.

Levitov, L. S., Yu. V. Nazarov, and G. M. Eliashberg, 1985, "Magnetoelectric effects in conductors with mirror isomer symmetry," Sov. Phys. JETP **61**, 133.

Li, J., B. Nagaraj, H. Liang, W. Cao, Chi. H. Lee, and R. Ramesh, 2004, "Ultrafast polarization switching in thin-film ferroelectrics," Appl. Phys. Lett. **84**, 1174–1176.

Li, L., *et al.*, 2020, "Gate-tunable reversible Rashba-Edelstein effect in a few-layer graphene/2H-$TaS_2$ heterostructure at room temperature," ACS Nano **14**, 5251–5259.

Li, M., H. Tan, and W. Duan, 2020, "Hexagonal rare-earth manganites and ferrites: A review of improper ferroelectricity, magnetoelectric coupling, and unusual domain walls," Phys. Chem. Chem. Phys. **22**, 14415–14432.

Li, P., A. Chen, D. Li, Y. Zhao, S. Zhang, L. Yang, Y. Liu, M. Zhu, H. Zhang, and X. Han, 2014, "Electric field manipulation of magnetization rotation and tunneling magnetoresistance of magnetic tunnel junctions at room temperature," Adv. Mater. **26**, 4320–4325.

Li, W., S. Peng, J. Lu, H. Wu, X. Li, D. Xiong, Y. Zhang, Y. Zhang, K. L. Wang, and W. Zhao, 2021, "Experimental demonstration of voltage-gated spin-orbit torque switching in an antiferromagnet/ferromagnet structure," Phys. Rev. B **103**, 094436.

Liang, S., *et al.*, 2016, "Ferroelectric control of organic/ferromagnetic spinterface," Adv. Mater. **28**, 10204–10210.

Liang, X., *et al.*, 2021, "Roadmap on magnetoelectric materials and devices," IEEE Trans. Magn. **57**, 1–57.

Liebmann, M., *et al.*, 2016, "Giant Rashba-type spin splitting in ferroelectric GeTe(111)," Adv. Mater. **28**, 560–565.

Lines, M. E., and A. M. Glass, 2001, *Principles and Applications of Ferroelectrics and Related Materials* Oxford Classic Texts in the Physical Sciences (Oxford University Press, Oxford).

Liu, C., *et al.*, 2021, "Electric field control of magnon spin currents in an antiferromagnetic insulator," Sci. Adv. **7**, eabg1669.

Liu, J., V. V. Laguta, K. Inzani, W. Huang, S. Das, R. Chatterjee, E. Sheridan, S. M. Griffin, A. Ardavan, and R. Ramesh, 2021, "Coherent electric field manipulation of $Fe^{3+}$ spins in $PbTiO_3$," Sci. Adv. **7**, eabf8103.

Liu, L., T. Moriyama, D. C. Ralph, and R. A. Buhrman, 2011, "Spin-Torque Ferromagnetic Resonance Induced by the Spin Hall Effect," Phys. Rev. Lett. **106**, 036601.

Liu, L., C.-F. Pai, Y. Li, H. W. Tseng, D. C. Ralph, and R. A. Buhrman, 2012, "Spin-torque switching with the giant spin Hall effect of tantalum," Science **336**, 555–558.

Liu, L., *et al.*, 2020, "Electrical switching of perpendicular magnetization in a single ferromagnetic layer," Phys. Rev. B **101**, 220402.

Liu, L., *et al.*, 2021, "Symmetry-dependent field-free switching of perpendicular magnetization," Nat. Nanotechnol. **16**, 277–282.

Liu, L., *et al.*, 2022, "Current-induced self-switching of perpendicular magnetization in CoPt single layer," Nat. Commun. **13**, 3539.

Liu, R. H., W. L. Lim, and S. Urazhdin, 2014, "Control of current-induced spin-orbit effects in a ferromagnetic heterostructure by electric field," Phys. Rev. B **89**, 220409.

Liu, S., I. Grinberg, and A. M. Rappe, 2013, "Development of a bond-valence based interatomic potential for $BiFeO_3$ for accurate

molecular dynamics simulations," J. Phys. Condens. Matter **25**, 102202.

Liu, S., I. Grinberg, and A. M. Rappe, 2016, "Intrinsic ferroelectric switching from first principles," Nature (London) **534**, 360–363.

Liu, Z. Q., *et al.*, 2016, "Full Electroresistance Modulation in a Mixed-Phase Metallic Alloy," Phys. Rev. Lett. **116**, 097203.

Lohmann, M., *et al.*, 2019, "Probing magnetism in insulating $Cr_2Ge_2Te_6$ by induced anomalous Hall effect in Pt," Nano Lett. **19**, 2397–2403.

Lorenz, B., 2021, "Hexagonal manganites," in *Multiferroics: Fundamentals and Applications*, edited by A. Cano, D. Meier, and M. Trassin (De Gruyter, Berlin).

Lorenz, B., A. P. Litvinchuk, M. M. Gospodinov, and C. W. Chu, 2004, "Field-Induced Reentrant Novel Phase and a Ferroelectric-Magnetic Order Coupling in $HoMnO_3$," Phys. Rev. Lett. **92**, 087204.

Lorenz, B., Y. Q. Wang, Y. Y. Sun, and C. W. Chu, 2004, "Large magnetodielectric effects in orthorhombic $HoMnO_3$ and $YMnO_3$," Phys. Rev. B **70**, 212412.

Lou, J., M. Liu, D. Reed, Y. Ren, and N. X. Sun, 2009, "Giant electric field tuning of magnetism in novel multiferroic FeGaB/lead zinc niobate–lead titanate (PZN-PT) heterostructures," Adv. Mater. **21**, 4711–4715.

Lu, C., M. Wu, L. Lin, and J.-M. Liu, 2019, "Single-phase multiferroics: New materials, phenomena, and physics," Natl. Sci. Rev. **6**, 653–668.

Lu, H., *et al.*, 2012, "Electric modulation of magnetization at the $BaTiO_3/La_{0.67}Sr_{0.33}MnO_3$ interfaces," Appl. Phys. Lett. **100**, 232904.

Lunkenheimer, P., *et al.*, 2012, "Multiferroicity in an organic charge-transfer salt that is suggestive of electric-dipole-driven magnetism," Nat. Mater. **11**, 755–758.

Luo, Z.-D., G. Apachitei, M.-M. Yang, J. J. P. Peters, A. M. Sanchez, and M. Alexe, 2018, "Bi-ferroic memristive properties of multiferroic tunnel junctions," Appl. Phys. Lett. **112**, 102905.

Lutz, P., T. Figgemeier, Z. M. A. El-Fattah, H. Bentmann, and F. Reinert, 2017, "Large Spin Splitting and Interfacial States in a $Bi/BaTiO_3(001))$ Rashba Ferroelectric Heterostructure," Phys. Rev. Appl. **7**, 044011.

Lyalin, I., S. Alikhah, M. Berritta, P. M. Oppeneer, and R. K. Kawakami, 2023, "Magneto-Optical Detection of the Orbital Hall Effect in Chromium, Phys. Rev. Lett. **131**, 156702.

Ma, C., X. Zhang, J. Xia, M. Ezawa, W. Jiang, T. Ono, S. N. Piramanayagam, A. Morisako, Y. Zhou, and X. Liu, 2019, "Electric field-induced creation and directional motion of domain walls and skyrmion bubbles," Nano Lett. **19**, 353–361.

Ma, X., A. Kumar, S. Dussan, H. Zhai, F. Fang, H. B. Zhao, J. F. Scott, R. S. Katiyar, and G. Lüpke, 2014, "Charge control of antiferromagnetism at $PbZr_{0.52}Ti_{0.48}O_3/La_{0.67}Sr_{0.33}MnO_3$ interface," Appl. Phys. Lett. **104**, 132905.

Maccariello, D., W. Legrand, N. Reyren, K. Garcia, K. Bouzehouane, S. Collin, V. Cros, and A. Fert, 2018, "Electrical detection of single magnetic skyrmions in metallic multilayers at room temperature," Nat. Nanotechnol. **13**, 233–237.

MacNeill, D., G. M. Stiehl, M. H. D. Guimaraes, R. A. Buhrman, J. Park, and D. C. Ralph, 2017, "Control of spin-orbit torques through crystal symmetry in $WTe_2$/ferromagnet bilayers," Nat. Phys. **13**, 300–305.

Maksymovych, P., *et al.*, 2012, "Ultrathin limit and dead-layer effects in local polarization switching of $BiFeO_3$," Phys. Rev. B **85**, 014119.

Malozemoff, A. P., and J. C. Slonczewski, 1979, *Magnetic Domain Walls in Bubble Materials: Advances in Materials and Device Research* (Academic Press, New York).

Manaka, H., H. Nozaki, and Y. Miura, 2017, "Microscopic observation of ferroelectric domains in $SrTiO_3$ using birefringence imaging techniques under high electric fields," J. Phys. Soc. Jpn. **86**, 114702.

Manchon, A., J. Železný, I. M. Miron, T. Jungwirth, J. Sinova, A. Thiaville, K. Garello, and P. Gambardella, 2019, "Current-induced spin-orbit torques in ferromagnetic and antiferromagnetic systems," Rev. Mod. Phys. **91**, 035004.

Manipatruni, S., D. E. Nikonov, C.-C. Lin, T. A. Gosavi, H. Liu, B. Prasad, Y.-L. Huang, E. Bonturim, R. Ramesh, and I. A. Young, 2019, "Scalable energy-efficient magnetoelectric spin-orbit logic," Nature (London) **565**, 35–42.

Manipatruni, S., D. E. Nikonov, and I. A. Young, 2018, "Beyond CMOS computing with spin and polarization," Nat. Phys. **14**, 338–343.

Mardana, A., S. Ducharme, and S. Adenwalla, 2011, "Ferroelectric control of magnetic anisotropy," Nano Lett. **11**, 3862–3867.

Martin, L. W., Y.-H. Chu, M. B. Holcomb, M. Huijben, P. Yu, S.-J. Han, D. Lee, S. X. Wang, and R. Ramesh, 2008, "Nanoscale control of exchange bias with $BiFeO_3$ thin films," Nano Lett. **8**, 2050–2055.

Maruyama, T., *et al.*, 2009, "Large voltage-induced magnetic anisotropy change in a few atomic layers of iron," Nat. Nanotechnol. **4**, 158–161.

Mathon, J., and A. Umerski, 2001, "Theory of tunneling magnetoresistance of an epitaxial $Fe/MgO/Fe(001)$ junction," Phys. Rev. B **63**, 220403.

Matsuno, J., N. Ogawa, K. Yasuda, F. Kagawa, W. Koshibae, N. Nagaosa, Y. Tokura, and M. Kawasaki, 2016, "Interface-driven topological Hall effect in $SrRuO_3$-$SrIrO_3$ bilayer," Sci. Adv. **2**, e1600304.

Mavropoulos, Ph., N. Papanikolaou, and P. H. Dederichs, 2000, "Complex Band Structure and Tunneling through Ferromagnet/Insulator/Ferromagnet Junctions," Phys. Rev. Lett. **85**, 1088–1091.

McGrath, D., 2021, "Intel says FinFET-based embedded MRAM is production-ready," https://www.eetimes.com/intel-says-finfet-based-embedded-mram-is-production-ready/ (accessed August 27, 2021).

Mearian, L., 2021, "Everspin ships first ST-MRAM memory with 500× performance of flash," https://www.computerworld.com/article/2493603/everspin-ships-first-st-mram-memory-with-500x-performance-of-flash.html (accessed August 27, 2021).

Mendes, J. B. S., O. Alves Santos, L. M. Meireles, R. G. Lacerda, L. H. Vilela-Leão, F. L. A. Machado, R. L. Rodríguez-Suárez, A. Azevedo, and S. M. Rezende, 2015, "Spin-Current to Charge-Current Conversion and Magnetoresistance in a Hybrid Structure of Graphene and Yttrium Iron Garnet," Phys. Rev. Lett. **115**, 226601.

Merbouche, H., *et al.*, 2021, "Voltage-controlled reconfigurable magnonic crystal at the sub-micrometer scale," ACS Nano **15**, 9775–9781.

Mermin, N. D., and H. Wagner, 1966, "Absence of Ferromagnetism or Antiferromagnetism in One- or Two-Dimensional Isotropic Heisenberg Models," Phys. Rev. Lett. **17**, 1133–1136.

Merz, W. J., 1954, "Domain formation and domain wall motions in ferroelectric $BaTiO_3$ single crystals," Phys. Rev. **95**, 690–698.

Meyer, R. B., 1977, "Ferroelectric liquid crystals: A review," Mol. Cryst. Liq. Cryst. **40**, 33–48.

Milletarì, M., M. Offidani, A. Ferreira, and R. Raimondi, 2017, "Covariant Conservation Laws and the Spin Hall Effect in Dirac-Rashba Systems," Phys. Rev. Lett. **119**, 246801.

Mirhosseini, H., I. V. Maznichenko, S. Abdelouahed, S. Ostanin, A. Ernst, I. Mertig, and J. Henk, 2010, "Toward a ferroelectric control of Rashba spin-orbit coupling: Bi on $BaTiO_3(001)$ from first principles," Phys. Rev. B **81**, 073406.

Miron, I. M., G. Gaudin, S. Auffret, B. Rodmacq, A. Schuhl, S. Pizzini, J. Vogel, and P. Gambardella, 2010, "Current-driven spin torque induced by the Rashba effect in a ferromagnetic metal layer," Nat. Mater. **9**, 230–234.

Miron, I. M., *et al.*, 2011, "Fast current-induced domain-wall motion controlled by the Rashba effect," Nat. Mater. **10**, 419–423.

Mishra, R., F. Mahfouzi, D. Kumar, K. Cai, M. Chen, X. Qiu, N. Kioussis, and H. Yang, 2019, "Electric-field control of spin accumulation direction for spin-orbit torques," Nat. Commun. **10**, 248.

Miyazaki, T., and N. Tezuka, 1995, "Giant magnetic tunneling effect in $Fe/Al_2O_3/Fe$ junction," J. Magn. Magn. Mater. **139**, L231–L234.

Molegraaf, H. J. A., J. Hoffman, C. A. F. Vaz, and S. Gariglio, 2009, "Magnetoelectric effects in complex oxides with competing ground states," Adv. Mater. **21**, 3470.

Molinari, A., H. Hahn, and R. Kruk, 2019, "Voltage-control of magnetism in all-solid-state and solid/liquid magnetoelectric composites," Adv. Mater. **31**, 1806662.

Moodera, J. S., L. R. Kinder, T. M. Wong, and R. Meservey, 1995, "Large Magnetoresistance at Room Temperature in Ferromagnetic Thin Film Tunnel Junctions," Phys. Rev. Lett. **74**, 3273–3276.

Moore, G. E., 1968, "Cramming more components onto integrated circuits," IEEE Solid-State Circuits Soc. Newsl. **38**, 114.

Moore, T. A., I. M. Miron, G. Gaudin, G. Serret, S. Auffret, B. Rodmacq, A. Schuhl, S. Pizzini, J. Vogel, and M. Bonfim, 2008, "High domain wall velocities induced by current in ultrathin $Pt/Co/AlO_x$ wires with perpendicular magnetic anisotropy," Appl. Phys. Lett. **93**, 262504.

Moreau-Luchaire, C., *et al.*, 2016, "Additive interfacial chiral interaction in multilayers for stabilization of small individual skyrmions at room temperature," Nat. Nanotechnol. **11**, 444–448.

Moreira dos Santos, A., A. K. Cheetham, T. Atou, Y. Syono, Y. Yamaguchi, K. Ohoyama, H. Chiba, and C. N. R. Rao, 2002, "Orbital ordering as the determinant for ferromagnetism in biferroic $BiMnO_3$," Phys. Rev. B **66**, 064425.

Moriya, T., 1960, "Anisotropic superexchange interaction and weak ferromagnetism," Phys. Rev. **120**, 91–98.

Moruzzi, V. L., and P. M. Marcus, 1992, "Antiferromagnetic-ferromagnetic transition in FeRh," Phys. Rev. B **46**, 2864–2873.

Mott, N. F., 1936, "The electrical conductivity of transition metals," Proc. R. Soc. A **153**, 699–717.

Mühlbauer, S., B. Binz, F. Jonietz, C. Pfleiderer, A. Rosch, A. Neubauer, R. Georgii, and P. Böni, 2009, "Skyrmion lattice in a chiral magnet," Science **323**, 915–919.

Mundy, J. A., *et al.*, 2016, "Atomically engineered ferroic layers yield a room-temperature magnetoelectric multiferroic," Nature (London) **537**, 523–527.

Mundy, J. A., *et al.*, 2022, "Liberating a hidden antiferroelectric phase with interfacial electrostatic engineering," Sci. Adv. **8**, eabg5860.

Nagarajan, V., A. Roytburd, A. Stanishevsky, S. Prasertchoung, T. Zhao, L. Chen, J. Melngailis, O. Auciello, and R. Ramesh, 2003, "Dynamics of ferroelastic domains in ferroelectric thin films," Nat. Mater. **2**, 43–47.

Nagel, U., R. S. Fishman, T. Katuwal, H. Engelkamp, D. Talbayev, H. T. Yi, S.-W. Cheong, and T. Rõõm, 2013, "Terahertz Spectroscopy of Spin Waves in Multiferroic $BiFeO_3$ in High Magnetic Fields," Phys. Rev. Lett. **110**, 257201.

Nakamura, K., T. Akiyama, T. Ito, M. Weinert, and A. J. Freeman, 2010, "Role of an interfacial FeO layer in the electric-field-driven switching of magnetocrystalline anisotropy at the Fe/MgO interface," Phys. Rev. B **81**, 220409.

Nakamura, K., R. Shimabukuro, Y. Fujiwara, T. Akiyama, T. Ito, and A. J. Freeman, 2009, "Giant Modification of the Magnetocrystalline Anisotropy in Transition-Metal Monolayers by an External Electric Field," Phys. Rev. Lett. **102**, 187201.

Nam, Sung Kim, T. Austin, D. Blaauw, T. Mudge, K. Flautner, S. Hu Jie, M. J. Irwin, M. Kandemir, and V. Narayanan, 2003, "Leakage current: Moore's law meets static power," Computer **36**, 68–75.

Nan, T., *et al.*, 2020, "Electric-field control of spin dynamics during magnetic phase transitions," Sci. Adv. **6**, eabd2613.

Neaton, J. B., C. Ederer, U. V. Waghmare, N. A. Spaldin, and K. M. Rabe, 2005, "First-principles study of spontaneous polarization in multiferroic $BiFeO_3$," Phys. Rev. B **71**, 014113.

Nepal, N., M. O. Luen, J. M. Zavada, S. M. Bedair, P. Frajtag, and N. A. El-Masry, 2009, "Electric field control of room temperature ferromagnetism in III-N dilute magnetic semiconductor films," Appl. Phys. Lett. **94**, 132505.

Neubauer, A., C. Pfleiderer, B. Binz, A. Rosch, R. Ritz, P. G. Niklowitz, and P. Böni, 2009, "Topological Hall Effect in the *A* Phase of MnSi," Phys. Rev. Lett. **102**, 186602.

Nikonov, D. E., and I. A. Young, 2015, "Benchmarking of beyond-CMOS exploratory devices for logic integrated circuits," IEEE J. Explor. Solid-State Comput. Devices Circuits **1**, 3–11.

Ning, S., A. Kumar, K. Klyukin, E. Cho, J. H. Kim, T. Su, H.-S. Kim, J. M. LeBeau, B. Yildiz, and C. A. Ross, 2021, "An antisite defect mechanism for room temperature ferroelectricity in orthoferrites," Nat. Commun. **12**, 4298.

Niranjan, M. K., J. D. Burton, J. P. Velev, S. S. Jaswal, and E. Y Tsymbal, 2009, "Magnetoelectric effect at the $SrRuO_3/BaTiO_3$ (001) interface: An *ab initio* study," Appl. Phys. Lett. **95**, 052501.

Noël, P., *et al.*, 2020, "Non-volatile electric control of spin-charge conversion in a $SrTiO_3$ Rashba system," Nature (London) **580**, 483–486.

Nova, T. F., A. S. Disa, M. Fechner, and A. Cavalleri, 2019, "Metastable ferroelectricity in optically strained $SrTiO_3$," Science **364**, 1075–1079.

Novoselov, K. S., A. K. Geim, S. V. Morozov, D. Jiang, Y. Zhang, S. V. Dubonos, I. V. Grigorieva, and A. A. Firsov, 2004, "Electric field effect in atomically thin carbon films," Science **306**, 666–669.

Offidani, M., M. Milletarì, R. Raimondi, and A. Ferreira, 2017, "Optimal Charge-to-Spin Conversion in Graphene on Transition-Metal Dichalcogenides," Phys. Rev. Lett. **119**, 196801.

Oh, Y.-W., *et al.*, 2016, "Field-free switching of perpendicular magnetization through spin-orbit torque in antiferromagnet/ferromagnet/oxide structures," Nat. Nanotechnol. **11**, 878–884.

O'Hara, D. J., *et al.*, 2018, "Room temperature intrinsic ferromagnetism in epitaxial manganese selenide films in the monolayer limit," Nano Lett. **18**, 3125–3131.

Ohno, H., D. Chiba, F. Matsukura, T. Omiya, E. Abe, T. Dietl, Y. Ohno, and K. Ohtani, 2000, "Electric-field control of ferromagnetism," Nature (London) **408**, 944.

Ohshima, R., A. Sakai, Y. Ando, T. Shinjo, K. Kawahara, H. Ago, and M. Shiraishi, 2014, "Observation of spin-charge conversion in chemical-vapor-deposition-grown single-layer graphene," Appl. Phys. Lett. **105**, 162410.

Ohtomo, A., and H. Y. Hwang, 2004, "A high-mobility electron gas at the $LaAlO_3/SrTiO_3$ heterointerface," Nature (London) **427**, 423–426.

Okamoto, N., H. Kurebayashi, T. Trypiniotis, I. Farrer, D. A. Ritchie, E. Saitoh, J. Sinova, J. Mašek, T. Jungwirth, and C. H. W. Barnes,

2014, "Electric control of the spin Hall effect by intervalley transitions," Nat. Mater. **13**, 932–937.

Okamura, Y., F. Kagawa, S. Seki, and Y. Tokura, 2016, "Transition to and from the skyrmion lattice phase by electric fields in a magnetoelectric compound," Nat. Commun. **7**, 12669.

Okumura, K., T. Ishikura, M. Soda, T. Asaka, H. Nakamura, Y. Wakabayashi, and T. Kimura, 2011, "Magnetism and magnetoelectricity of a *U*-type hexaferrite $Sr_4Co_2Fe_{36}O_{60}$," Appl. Phys. Lett. **98**, 212504.

Oleinik, I. I., E. Y. Tsymbal, and D. G. Pettifor, 2001, "Atomic and electronic structure of $Co/SrTiO_3/Co$ magnetic tunnel junctions," Phys. Rev. B **65**, 020401(R).

Olejník, K., *et al.*, 2017, "Antiferromagnetic CuMnAs multi-level memory cell with microelectronic compatibility," Nat. Commun. **8**, 15434.

Ostwal, V., T. Shen, and J. Appenzeller, 2020, "Efficient spin-orbit torque switching of the semiconducting van der Waals ferromagnet $Cr_2Ge_2Te_6$," Adv. Mater. **32**, 1906021.

Ovchinnikov, I. V., and K. L. Wang, 2009, "Theory of electric-field-controlled surface ferromagnetic transition in metals," Phys. Rev. B **79**, 020402.

Pai, C.-F., L. Liu, Y. Li, H. W. Tseng, D. C. Ralph, and R. A. Buhrman, 2012, "Spin transfer torque devices utilizing the giant spin Hall effect of tungsten," Appl. Phys. Lett. **101**, 122404.

Pai, C.-F., Y. Ou, L. H. Vilela-Leão, D. C. Ralph, and R. A. Buhrman, 2015, "Dependence of the efficiency of spin Hall torque on the transparency of Pt/ferromagnetic layer interfaces," Phys. Rev. B **92**, 064426.

Pantel, D., S. Goetze, D. Hesse, and M. Alexe, 2012, "Reversible electrical switching of spin polarization in multiferroic tunnel junctions," Nat. Mater. **11**, 289–293.

Paredes, S., Y. Madhour, G. Schlottig, C. L. Ong, and T. Brunschwiler, 2014, "(Invited) Wafer-level integration of embedded cooling approaches," ECS Trans. **64**, 253–265.

Park, J.-W., *et al.*, 2008, "Optical properties of $(GeTe, Sb_3Te_3)$ pseudobinary thin films studied with spectroscopic ellipsometry," Appl. Phys. Lett. **93**, 021914.

Park, T.-E., *et al.*, 2021, "Néel-type skyrmions and their current-induced motion in van der Waals ferromagnet-based heterostructures," Phys. Rev. B **103**, 104410.

Parkin, S., and S.-H. Yang, 2015, "Memory on the racetrack," Nat. Nanotechnol. **10**, 195–198.

Parkin, S. S. P., M. Hayashi, and L. Thomas, 2008, "Magnetic domain-wall racetrack memory," Science **320**, 190.

Parkin, S. S. P., C. Kaiser, A. Panchula, P. M. Rice, B. Hughes, M. Samant, and S.-H. Yang, 2004, "Giant tunnelling magnetoresistance at room temperature with $MgO(100)$ tunnel barriers," Nat. Mater. **3**, 862–867.

Parsonnet, E., Y.-L. Huang, T. Gosavi, A. Qualls, D. Nikonov, C.-C. Lin, I. Young, J. Bokor, L. W. Martin, and R. Ramesh, 2020, "Toward Intrinsic Ferroelectric Switching in Multiferroic $BiFeO_3$," Phys. Rev. Lett. **125**, 067601.

Parsonnet, E., *et al.*, 2022, "Nonvolatile Electric Field Control of Thermal Magnons in the Absence of an Applied Magnetic Field," Phys. Rev. Lett. **129**, 087601.

Patterson, D., and J. Hennessy, 2017, "A new golden age for computer architecture: Domain-specific hardware/software co-design, enhanced security, open instruction sets, and agile chip development," in *Proceedings of the 2018 ACM/IEEE 45th Annual International Symposium on Computer Architecture (ISCA), Los Angeles, 2018* (IEEE, New York), pp. 27–29.

Pawlak, J., W. Skowroński, A. Żywczak, and M. Przybylski, 2022, "Room-temperature multiferroicity and magnetization dynamics in Fe/BTO/LSMO tunnel junction," Adv. Electron. Mater. **8**, 2100574.

Pawley, G. S., W. Cochran, R. A. Cowley, and G. Dolling, 1966, "Diatomic Ferroelectrics," Phys. Rev. Lett. **17**, 753–755.

Peng, S. Z., J. Q. Lu, W. X. Li, L. Z. Wang, H. Zhang, X. Li, K. L. Wang, and W. S. Zhao, 2019, "Field-free switching of perpendicular magnetization through voltage-gated spin-orbit torque," in *Proceedings of the 2019 IEEE International Electron Devices Meeting (IEDM), San Francisco, 2019* (IEEE, New York), pp. 28.6.1–28.6.4.

Pereira Gonçalves, M. A., C. Escorihuela-Sayalero, P. Garca-Fernández, J. Junquera, and J. Íñiguez, 2019, "Theoretical guidelines to create and tune electric skyrmion bubbles," Sci. Adv. **5**, eaau7023.

Pertsev, N. A., 2008, "Giant magnetoelectric effect via strain-induced spin reorientation transitions in ferromagnetic films," Phys. Rev. B **78**, 212102 2008.

Pertsev, N. A., and H. Kohlstedt, 2009, "Magnetic tunnel junction on a ferroelectric substrate," Appl. Phys. Lett. **95**, 163503.

Pesin, D., and A. H. MacDonald, 2012, "Spintronics and pseudo-spintronics in graphene and topological insulators," Nat. Mater. **11**, 409–416.

Pham, V. T., L. Vila, G. Zahnd, A. Marty, W. Savero-Torres, M. Jamet, and J.-P. Attané, 2016, "Ferromagnetic/nonmagnetic nanostructures for the electrical measurement of the spin Hall effect," Nano Lett. **16**, 6755–6760.

Pham, V. T., H. Yang, W. Y. Choi, A. Marty, I. Groen, A. Chuvilin, F. S. Bergeret, L. E. Hueso, I. V. Tokatly, and F. Casanova, 2021, "Large spin-charge interconversion induced by interfacial spin-orbit coupling in a highly conducting all-metallic system," Phys. Rev. B **104**, 184410.

Pham, V. T., *et al.*, 2020, "Spin-orbit magnetic state readout in scaled ferromagnetic/heavy metal nanostructures," Nat. Electron. **3**, 309–315.

Phillips, L. C., *et al.*, 2015, "Local electrical control of magnetic order and orientation by ferroelastic domain arrangements just above room temperature," Sci. Rep. **5**, 10026.

Picozzi, S., 2014, "Ferroelectric Rashba semiconductors as a novel class of multifunctional materials," Front. Phys. **2**, 10.

Pimenov, A., A. A. Mukhin, V. Yu. Ivanov, V. D. Travkin, A. M. Balbashov, and A. Loidl, "Possible evidence for electromagnons in multiferroic manganites," Nat. Phys. **2**, 97–100 2006.

Plekhanov, E., P. Barone, D. Di Sante, and S. Picozzi, 2014, "Engineering relativistic effects in ferroelectric SnTe," Phys. Rev. B **90**, 161108.

Prasad, B., *et al.*, 2020, "Ultralow voltage manipulation of ferromagnetism," Adv. Mater. **32**, 2001943.

Preziosi, D., M. Alexe, D. Hesse, and M. Salluzzo, 2015, "Electric-Field Control of the Orbital Occupancy and Magnetic Moment of a Transition-Metal Oxide," Phys. Rev. Lett. **115**, 157401.

Pyatakov, A. P., and A. K. Zvezdin, 2012, "Magnetoelectric and multiferroic media," Phys. Usp. **55**, 557.

Qin, W., D. Jasion, X. Chen, M. Wuttig, and S. Ren, 2014, "Charge-transfer magnetoelectrics of polymeric multiferroics," ACS Nano **8**, 3671–3677.

Qin, W., B. Xu, and S. Ren, 2015, "An organic approach for nanostructured multiferroics," Nanoscale **7**, 9122–9132.

Qiu, Z., K. Ando, K. Uchida, Y. Kajiwara, R. Takahashi, H. Nakayama, T. An, Y. Fujikawa, and E. Saitoh, 2013, "Spin mixing

conductance at a well-controlled platinum/yttrium iron garnet interface," Appl. Phys. Lett. **103**, 092404.

Rabe, K. M., C. H. Ahn, and J.-M. Triscone, 2007, Eds., *Physics of Ferroelectrics: A Modern Perspective*, Topics in Applied Physics (Springer, Berlin).

Rabe, K. M., and U. V. Waghmare, 1995, "Localized basis for effective lattice Hamiltonians: Lattice Wannier functions," Phys. Rev. B **52**, 13236–13246.

Radaelli, G., *et al.*, 2014, "Electric control of magnetism at the Fe/$BaTiO_3$ interface," Nat. Commun. **5**, 3404.

Rahmedov, D., D. Wang, J. Íñiguez, and L. Bellaiche, 2012, "Magnetic Cycloid of $BiFeO_3$ from Atomistic Simulations," Phys. Rev. Lett. **109**, 037207.

Ralph, D. C., and M. D. Stiles, 2008, "Spin transfer torques," J. Magn. Magn. Mater. **320**, 1190–1216.

Ramazanoglu, M., M. Laver, W. Ratcliff, S. M. Watson, W. C. Chen, A. Jackson, K. Kothapalli, S. Lee, S.-W. Cheong, and V. Kiryukhin, 2011, "Local Weak Ferromagnetism in Single-Crystalline Ferroelectric $BiFeO_3$," Phys. Rev. Lett. **107**, 207206.

Ramesh, R., and D. G. Schlom, 2019, "Creating emergent phenomena in oxide superlattices," Nat. Rev. Mater. **4**, 257–268.

Ramesh, R., and N. A. Spaldin, 2007, "Multiferroics: Progress and prospects in thin films," Nat. Mater. **6**, 21–29.

Rana, D. S., I. Kawayama, K. Mavani, K. Takahashi, H. Murakami, and M. Tonouchi, 2009, "Understanding the nature of ultrafast polarization dynamics of ferroelectric memory in the multiferroic $BiFeO_3$," Adv. Mater. **21**, 2881–2885.

Rashba, E. I., 1960, "Properties of semiconductors with an extremum loop. I. Cyclotron and combinational resonance in a magnetic field perpendicular to the plane of the loop," Sov. Phys. Solid State **2**, 1109.

Remy, Q., J. Igarashi, S. Iihama, G. Malinowski, M. Hehn, J. Gorchon, J. Hohlfeld, S. Fukami, H. Ohno, and S. Mangin, 2020, "Energy efficient control of ultrafast spin current to induce single femtosecond pulse switching of a ferromagnet," Adv. Sci. Lett. **7**, 2001996.

Ren, S., and M. Wuttig, 2012, "Organic exciton multiferroics," Adv. Mater. **24**, 724–727.

Rezende, S. M., 2020 *Fundamentals of Magnonics*, Lecture Notes in Physics Vol. 969 (Springer International Publishing, Cham, Switzerland).

Rinaldi, C., *et al.*, 2018, "Ferroelectric control of the spin texture in GeTe," Nano Lett. **18**, 2751–2758.

Rogalev, V. A., *et al.*, 2017, "Double band inversion in $\alpha$-Sn: Appearance of topological surface states and the role of orbital composition," Phys. Rev. B **95**, 161117.

Rojas-Sánchez, J. C., L. Vila, G. Desfonds, S. Gambarelli, J. P. Attané, J. M. De Teresa, C. Magén, and A. Fert, 2013, "Spin-to-charge conversion using Rashba coupling at the interface between non-magnetic materials," Nat. Commun. **4**, 2944.

Rojas-Sánchez, J.-C., and A. Fert, 2019, "Compared Efficiencies of Conversions between Charge and Spin Current by Spin-Orbit Interactions in Two- and Three-Dimensional Systems," Phys. Rev. Appl. **11**, 054049.

Rojas-Sánchez, J.-C., N. Reyren, P. Laczkowski, W. Savero, J.-P. Attané, C. Deranlot, M. Jamet, J.-M. George, L. Vila, and H. Jaffrès, 2014, "Spin Pumping and Inverse Spin Hall Effect in Platinum: The Essential Role of Spin-Memory Loss at Metallic Interfaces," Phys. Rev. Lett. **112**, 106602.

Rojas-Sánchez, J.-C., *et al.*, 2016, "Spin to Charge Conversion at Room Temperature by Spin Pumping into a New Type of Topological Insulator: $\alpha$-Sn Films," Phys. Rev. Lett. **116**, 096602.

Roldán-Molina, A., A. S. Nunez, and J. Fernández-Rossier, 2016, "Topological spin waves in the atomic-scale magnetic skyrmion crystal," New J. Phys. **18**, 045015.

Ross, A., *et al.*, 2020, "Propagation length of antiferromagnetic magnons governed by domain configurations," Nano Lett. **20**, 306–313.

Rößler, U. K., A. N. Bogdanov, and C. Pfleiderer, 2006, "Spontaneous skyrmion ground states in magnetic metals," Nature (London) **442**, 797–801.

Rovillain, P., R. de Sousa, Y. Gallais, A. Sacuto, M. A. Méasson, D. Colson, A. Forget, M. Bibes, A. Barthélémy, and M. Cazayous, 2010, "Electric-field control of spin waves at room temperature in multiferroic $BiFeO_3$," Nat. Mater. **9**, 975–979.

Ryu, K.-S., L. Thomas, S.-H. Yang, and S. Parkin, 2013, "Chiral spin torque at magnetic domain walls," Nat. Nanotechnol. **8**, 527–533.

Safeer, C. K., J. Ingla-Aynés, F. Herling, J. H. Garcia, M. Vila, N. Ontoso, M. R. Calvo, S. Roche, L. E. Hueso, and F. Casanova, 2019, "Room-temperature spin Hall effect in graphene/$MoS_2$ van der Waals heterostructures," Nano Lett. **19**, 1074–1082.

Sagasta, E., Y. Omori, M. Isasa, M. Gradhand, L. E. Hueso, Y. Niimi, Y. Otani, and F. Casanova, 2016, "Tuning the spin Hall effect of Pt from the moderately dirty to the superclean regime," Phys. Rev. B **94**, 060412.

Sahoo, S., S. Polisetty, C.-G. Duan, S. S. Jaswal, E. Y. Tsymbal, and C. Binek, 2007, "Ferroelectric control of magnetism in $BaTiO_3$/Fe heterostructures via interface strain coupling," Phys. Rev. B **76**, 092108.

Sala, G., H. Wang, W. Legrand, and P. Gambardella, 2023, "Orbital Hanle Magnetoresistance in a 3*d* Transition Metal," Phys. Rev. Lett. **131**, 156703.

Salahuddin, S., K. Ni, and S. Datta, 2018, "The era of hyper-scaling in electronics," Nat. Electron. **1**, 442–450.

Salemi, L., M. Berritta, A. K. Nandy, and P. M. Oppeneer, 2019, "Orbitally dominated Rashba-Edelstein effect in noncentrosymmetric antiferromagnets," Nat. Commun. **10**, 5381.

Salemi, L., and P. M. Oppeneer, 2022, "First-principles theory of intrinsic spin and orbital Hall and Nernst effects in metallic monoatomic crystals," Phys. Rev. Mater. **6**, 095001.

Sampaio, J., V. Cros, S. Rohart, A. Thiaville, and A. Fert, 2013, "Nucleation, stability and current-induced motion of isolated magnetic skyrmions in nanostructures," Nat. Nanotechnol. **8**, 839–844.

Sando, D., A. Barthélémy, and M. Bibes, 2014, "$BiFeO_3$ Epitaxial thin films and devices: Past, present and future," J. Phys. Condens. Matter **26**, 473201.

Sando, D., *et al.*, 2013, "Crafting the magnonic and spintronic response of $BiFeO_3$ films by epitaxial strain," Nat. Mater. **12**, 641–646.

Sanz-Fernández, C., V. T. Pham, E. Sagasta, L. E. Hueso, I. V. Tokatly, F. Casanova, and F. S. Bergeret, 2020, "Quantification of interfacial spin-charge conversion in hybrid devices with a metal/insulator interface," Appl. Phys. Lett. **117**, 142405.

Savitha Pillai, S., H. Kojima, M. Itoh, and T. Taniyama, 2015, "Lateral electric-field control of giant magnetoresistance in Co/Cu/Fe/$BaTiO_3$ multiferroic heterostructure," Appl. Phys. Lett. **107**, 072903.

Sawicki, M., D. Chiba, A. Korbecka, Y. Nishitani, J. A. Majewski, F. Matsukura, T. Dietl, and H. Ohno, 2010, "Experimental probing of the interplay between ferromagnetism and localization in (Ga, Mn)As," Nat. Phys. **6**, 22–25.

Schmid, H., 1994, "Multi-ferroic magnetoelectrics," Ferroelectrics **162**, 317–338.

Schott, M., A. Bernand-Mantel, L. Ranno, S. Pizzini, and J. Vogel, 2017, "The skyrmion switch: Turning magnetic skyrmion bubbles on and off with an electric field," Nano Lett. **17**, 3006.

Schulz, T., R. Ritz, A. Bauer, M. Halder, M. Wagner, C. Franz, C. Pfleiderer, K. Everschor, M. Garst, and A. Rosch, 2012, "Emergent electrodynamics of skyrmions in a chiral magnet," Nat. Phys. **8**, 301–304.

Seifert, T. S., D. Go, H. Hayashi, R. Rouzegar, F. Freimuth, K. Ando, Y. Mokrousov, and T. Kampfrath, 2023, "Time-domain observation of ballistic orbital-angular-momentum currents with giant relaxation length in tungsten," Nat. Nanotechnol. **18**, 1132–1138.

Sergienko, I. A., and E. Dagotto, 2006, "Role of the Dzyaloshinskii-Moriya interaction in multiferroic perovskites," Phys. Rev. B **73**, 094434.

Serrate, D., J. M. D. Teresa, and M. R. Ibarra, 2007, "Double perovskites with ferromagnetism above room temperature," J. Phys. Condens. Matter **19**, 023201.

Seshadri, R., and N. A. Hill, 2001, "Visualizing the role of Bi 6*s* 'lone pairs' in the off-center distortion in ferromagnetic $BiMnO_3$," Chem. Mater. **13**, 2892–2899.

Seung, Ham W., S. Kim, D.-H. Kim, K.-J. Kim, T. Okuno, H. Yoshikawa, A. Tsukamoto, T. Moriyama, and T. Ono, 2017, "Temperature dependence of spin-orbit effective fields in Pt/GdFeCo bilayers," Appl. Phys. Lett. **110**, 242405.

Shafer, P., *et al.*, 2018, "Emergent chirality in the electric polarization texture of titanate superlattices," Proc. Natl. Acad. Sci. U.S.A. **115**, 915–920.

Shannon, R. D., and C. T. Prewitt, 1969, "Effective ionic radii in oxides and fluorides," Acta Crystallogr. Sect. B **25**, 925–946.

Shao, Q., *et al.*, 2018, "Role of dimensional crossover on spin-orbit torque efficiency in magnetic insulator thin films," Nat. Commun. **9**, 3612.

Shao, Q., *et al.*, 2021, "Roadmap of spin-orbit torques," IEEE Trans. Magn. **57**, 1–39.

Shao, Z., J. Liang, Q. Cui, M. Chshiev, A. Fert, T. Zhou, and H. Yang, 2022, "Multiferroic materials based on transition-metal dichalcogenides: Potential platform for reversible control of Dzyaloshinskii-Moriya interaction and skyrmion via electric field," Phys. Rev. B **105**, 174404.

Sharma, R., R. Mishra, T. Ngo, Y.-X. Guo, S. Fukami, H. Sato, H. Ohno, and H. Yang, 2021, "Electrically connected spin-torque oscillators array for 2.4 GHz WiFi band transmission and energy harvesting," Nat. Commun. **12**, 2924.

Shi, Q., *et al.*, 2022, "The role of lattice dynamics in ferroelectric switching," Nat. Commun. **13**, 1110.

Shimamura, K., D. Chiba, S. Ono, S. Fukami, N. Ishiwata, M. Kawaguchi, K. Kobayashi, and T. Ono, 2012, "Electrical control of Curie temperature in cobalt using an ionic liquid film," Appl. Phys. Lett. **100**, 122402.

Shin, I., *et al.*, 2022, "Spin-orbit torque switching in an all–van der Waals heterostructure," Adv. Mater. **34**, 2101730.

Shiomi, Y., K. Nomura, Y. Kajiwara, K. Eto, M. Novak, K. Segawa, Y. Ando, and E. Saitoh, 2014, "Spin-Electricity Conversion Induced by Spin Injection into Topological Insulators," Phys. Rev. Lett. **113**, 196601.

Shuvaev, A. M., A. A. Mukhin, and A. Pimenov, 2011, "Magnetic and magnetoelectric excitations in multiferroic manganites," J. Phys. Condens. Matter **23**, 113201.

Sidoruk, J., J. Leist, H. Gibhardt, O. Sobolev, B. Ouladdiaf, R. Mole, and G. Eckold, 2016, "Kinetics of domain redistribution in $SrTiO_3$ under pulsed electric fields," Ferroelectrics **505**, 200–209.

Singh, M. K., Y. Yang, and C. G. Takoudis, 2009, "Synthesis of multifunctional multiferroic materials from metalorganics," Coord. Chem. Rev. **253**, 2920–2934.

Sinova, J., S. O. Valenzuela, J. Wunderlich, C. H. Back, and T. Jungwirth, 2015, "Spin Hall effects," Rev. Mod. Phys. **87**, 1213–1260.

Skyrme, T. H. R., 1961, "A non-linear field theory," Proc. R. Soc. A **260**, 127.

Slonczewski, J. C., 1996, "Current-driven excitation of magnetic multilayers," J. Magn. Magn. Mater. **159**, L1–L7.

Smolensky, G. A., and I. E. Chupis, 1982, "Ferroelectromagnets," Sov. Phys. Usp. **25**, 475.

Soda, M., T. Ishikura, H. Nakamura, Y. Wakabayashi, and T. Kimura, 2011, "Magnetic Ordering in Relation to the Room-Temperature Magnetoelectric Effect of $Sr_3Co_2Fe_{24}O_{41}$," Phys. Rev. Lett. **106**, 087201.

Song, Q., H. Zhang, T. Su, W. Yuan, Y. Chen, W. Xing, J. Shi, J. Sun, and W. Han, 2017, "Observation of inverse Edelstein effect in Rashba-split 2DEG between $SrTiO_3$ and $LaAlO_3$ at room temperature," Sci. Adv. **3**, e1602312.

Song, Q., *et al.*, 2022, "Evidence for a single-layer van der Waals multiferroic," Nature (London) **602**, 601–605.

Song, T., *et al.*, 2019, "Voltage control of a van der Waals spin-filter magnetic tunnel junction," Nano Lett. **19**, 915–920.

Song, Y., D. Zhang, B. Xu, K. Chang, and C.-W. Nan, 2019, "Electrical control of large Rashba effect in oxide heterostructures," arXiv:1909.03727.

Sosnowska, I., T. P. Neumaier, and E. Steichele, 1982, "Spiral magnetic ordering in bismuth ferrite," J. Phys. C **15**, 4835–4846.

Sosnowska, I., and A. K. Zvezdin, 1995, "Origin of the long period magnetic ordering in $BiFeO_3$," J. Magn. Magn. Mater. **140–144**, 167–168.

Soumyanarayanan, A., N. Reyren, A. Fert, and C. Panagopoulos, 2016, "Emergent phenomena induced by spin-orbit coupling at surfaces and interfaces," Nature (London) **539**, 509–517.

Spaldin, N. A., M. Fiebig, and M. Mostovoy, 2008, "The toroidal moment in condensed-matter physics and its relation to the magnetoelectric effect," J. Phys. Condens. Matter **20**, 434203.

Spaldin, N. A., and R. Ramesh, 2019, "Advances in magnetoelectric multiferroics," Nat. Mater. **18**, 203–212.

Srivastava, T., *et al.*, 2018, "Large-voltage tuning of Dzyaloshinskii-Moriya interactions: A route toward dynamic control of skyrmion chirality," Nano Lett. **18**, 4871–4877.

Stanciu, C. D., F. Hansteen, A. V. Kimel, A. Kirilyuk, A. Tsukamoto, A. Itoh, and Th. Rasing, 2007, "All-Optical Magnetic Recording with Circularly Polarized Light," Phys. Rev. Lett. **99**, 047601.

Steffes, J. J., R. A. Ristau, R. Ramesh, and B. D. Huey, 2019, "Thickness scaling of ferroelectricity in $BiFeO_3$ by tomographic atomic force microscopy," Proc. Natl. Acad. Sci. U.S.A. **116**, 2413–2418.

Stiles, M. D., and A. Zangwill, 2002, "Anatomy of spin-transfer torque," Phys. Rev. B **66**, 014407.

Stolichnov, I., S. W. E. Riester, H. J. Trodahl, N. Setter, A. W. Rushforth, K. W. Edmonds, R. P. Campion, C. T. Foxon, B. L. Gallagher, and T. Jungwirth, 2008, "Non-volatile ferroelectric control of ferromagnetism in (Ga, Mn)As," Nat. Mater. **7**, 464–467.

Stroppa, A., D. Di Sante, P. Barone, M. Bokdam, G. Kresse, C. Franchini, M.-H. Whangbo, and S. Picozzi, 2014, "Tunable ferroelectric polarization and its interplay with spin-orbit coupling in tin iodide perovskites," Nat. Commun. **5**, 5900.

Su, Y., X. Li, M. Zhu, J. Zhang, L. You, and E. Y. Tsymbal, 2021, "van der Waals multiferroic tunnel junctions," Nano Lett. **21**, 175–181.

Sugawara, F., S. Iida, Y. Syono, and S. Akimoto, 1965, "New magnetic perovskites $BiMnO_3$ and $BiCrO_3$," J. Phys. Soc. Jpn. **20**, 1529–1529.

Sugawara, F., S. Iiida, Y. Syono, and S. Akimoto, 1968, "Magnetic properties and crystal distortions of $BiMnO_3$ and $BiCrO_3$," J. Phys. Soc. Jpn. **25**, 1553–1558.

Sun, W., W. Wang, J. Zang, H. Li, G. Zhang, J. Wang, and Z. Cheng, 2021, "Manipulation of magnetic skyrmion in a 2D van der Waals heterostructure via both electric and magnetic fields," Adv. Funct. Mater. **31**, 2104452.

Suzuki, Y., 2001, "Epitaxial spinel ferrite thin films," Annu. Rev. Mater. Res. **31**, 265.

Takahashi, S., and S. Maekawa, 2008, "Spin current in metals and superconductors," J. Phys. Soc. Jpn. **77**, 031009.

Talatchian, P., M. Romera, F. A. Araujo, P. Bortolotti, V. Cros, D. Vodenicarevic, N. Locatelli, D. Querlioz, and J. Grollier, 2020, "Designing Large Arrays of Interacting Spin-Torque Nano-Oscillators for Microwave Information Processing," Phys. Rev. Appl. **13**, 024073.

Talbayev, D., S. A. Trugman, S. Lee, H. T. Yi, S.-W. Cheong, and A. J. Taylor, 2011, "Long-wavelength magnetic and magnetoelectric excitations in the ferroelectric antiferromagnet $BiFeO_3$," Phys. Rev. B **83**, 094403.

Tan, C., J. Lee, S.-G. Jung, T. Park, S. Albarakati, J. Partridge, M. R. Field, D. G. McCulloch, L. Wang, and C. Lee, 2018, "Hard magnetic properties in nanoflake van der Waals $Fe_3GeTe_2$," Nat. Commun. **9**, 1554.

Tan, C., *et al.*, 2021, "Gate-controlled magnetic phase transition in a van der Waals magnet $Fe_5GeTe_2$," Nano Lett. **21**, 5599–5605.

Tanaka, T., H. Kontani, M. Naito, T. Naito, D. S. Hirashima, K. Yamada, and J. Inoue, 2008, "Intrinsic spin Hall effect and orbital Hall effect in 4*d* and 5*d* transition metals," Phys. Rev. B **77**, 165117.

Tang, D. D., P. K. Wang, V. S. Speriosu, S. Le, R. E. Fontana, and S. Rishton, 1995, "An IC process compatible nonvolatile magnetic RAM," in *Proceedings of the International Electron Devices Meeting, Washington, DC, 1995* (IEEE, New York), pp. 997–1000.

Taniguchi, T., J. Grollier, and M. D. Stiles, 2015, "Spin-Transfer Torques Generated by the Anomalous Hall Effect and Anisotropic Magnetoresistance," Phys. Rev. Appl. **3**, 044001.

Tao, L. L., T. R. Paudel, A. A. Kovalev, and E. Y. Tsymbal, 2017, "Reversible spin texture in ferroelectric $HfO_2$," Phys. Rev. B **95**, 245141.

Tao, L. L., and E. Y. Tsymbal, 2018, "Persistent spin texture enforced by symmetry," Nat. Commun. **9**, 2763.

Tao, L. L., and J. Wang, 2016, "Strain-tunable ferroelectricity and its control of Rashba effect in $KTaO_3$," J. Appl. Phys. **120**, 234101.

Tarequzzaman, M., A. S. Jenkins, T. Böhnert, J. Borme, L. Martins, E. Paz, R. Ferreira, and P. P. Freitas, 2018, "Broadband voltage rectifier induced by linear bias dependence in CoFeB/MgO magnetic tunnel junctions," Appl. Phys. Lett. **112**, 252401.

Teague, J. R., R. Gerson, and W. J. James, 1970, "Dielectric hysteresis in single crystal $BiFeO_3$," Solid State Commun. **8**, 1073–1074.

Theis, T. N., and P. M. Solomon, 2010, "It's time to reinvent the transistor!," Science **327**, 1600–1601.

Thiaville, A., S. Rohart, É. Jué, V. Cros, and A. Fert, 2012, "Dynamics of Dzyaloshinskii domain walls in ultrathin magnetic films," Europhys. Lett. **100**, 57002.

Thiele, C., K. Dörr, O. Bilani, J. Rödel, and L. Schultz, 2007, "Influence of strain on the magnetization and magnetoelectric effect in $La_{0.7}A_{0.3}MnO_3/PMN-PT\,(001)$ ($A$=Sr, Ca)," Phys. Rev. B **75**, 054408.

Thompson, D. P., P. Korgul, and A. Hendry, 1983, "The structural characterisation of sialon polytypoids," in *Progress in Nitrogen Ceramics*, edited by F. L. Riley, NATO ASI, Ser. E, Vol. 65 (Springer Netherlands, Dordrecht), pp. 61–74.

Tian, J., C. Şahin, I. Miotkowski, M. E. Flatté, and Y. P. Chen, 2021, "Opposite current-induced spin polarizations in bulk-metallic $Bi_2Se_3$ and bulk-insulating $Bi_2Te_2Se$ topological insulator thin flakes," Phys. Rev. B **103**, 035412.

Tokunaga, Y., N. Furukawa, H. Sakai, Y. Taguchi, T. Arima, and Y. Tokura, 2009, "Composite domain walls in a multiferroic perovskite ferrite," Nat. Mater. **8**, 558–562.

Tokunaga, Y., S. Iguchi, T. Arima, and Y. Tokura, 2008, "Magnetic-Field-Induced Ferroelectric State in $DyFeO_3$," Phys. Rev. Lett. **101**, 097205.

Tokura, Y., S. Seki, and N. Nagaosa, 2014, "Multiferroics of spin origin," Rep. Prog. Phys. **77**, 076501.

Tokura, Y., and Y. Tomioka, 1999, "Colossal magnetoresistive manganites," J. Magn. Magn. Mater. **200**, 1–23.

Tolédano, P., M. Ackermann, L. Bohatý, P. Becker, T. Lorenz, N. Leo, and M. Fiebig, 2015, "Primary ferrotoroidicity in antiferromagnets," Phys. Rev. B **92**, 094431.

Tombros, N., C. Jozsa, M. Popinciuc, H. T. Jonkman, and B. J. van Wees, 2007, "Electronic spin transport and spin precession in single graphene layers at room temperature," Nature (London) **448**, 571–574.

Tornos, J., *et al.*, 2019, "Ferroelectric Control of Interface Spin Filtering in Multiferroic Tunnel Junctions," Phys. Rev. Lett. **122**, 037601.

Trier, F., P. Noël, J.-V. Kim, J.-P. Attané, L. Vila, and M. Bibes, 2022, "Oxide spin-orbitronics: Spin-charge interconversion and topological spin textures," Nat. Rev. Mater. **7**, 258–274.

Trier, F., *et al.*, 2020, "Electric-field control of spin current generation and detection in ferromagnet-free $SrTiO_3$-based nanodevices," Nano Lett. **20**, 395–401.

Tsoi, M., A. G. M. Jansen, J. Bass, W.-C. Chiang, M. Seck, V. Tsoi, and P. Wyder, 1998, "Excitation of a Magnetic Multilayer by an Electric Current," Phys. Rev. Lett. **80**, 4281–4284.

Tsymbal, E. Y., and H. Kohlstedt, 2006, "Tunneling across a ferroelectric," Science **313**, 181–183.

Tulapurkar, A. A., Y. Suzuki, A. Fukushima, H. Kubota, H. Maehara, K. Tsunekawa, D. D. Djayaprawira, N. Watanabe, and S. Yuasa, 2005, "Spin-torque diode effect in magnetic tunnel junctions," Nature (London) **438**, 339–342.

Uchida, K., *et al.*, 2010, "Spin Seebeck insulator," Nat. Mater. **9**, 894–897.

Ullakko, K., 1996, "Magnetically controlled shape memory alloys: A new class of actuator materials," J. Mater. Eng. Perform. **5**, 405–409.

Valencia, S., *et al.*, 2011, "Interface-induced room-temperature multiferroicity in $BaTiO_3$," Nat. Mater. **10**, 753–758.

Valenzuela, S. O., and M. Tinkham, 2006, "Direct electronic measurement of the spin Hall effect," Nature (London) **442**, 176–179.

Valenzuela, S. O., and M. Tinkham, 2007, "Electrical detection of spin currents: The spin-current induced Hall effect (invited)," J. Appl. Phys. **101**, 09B103.

Valet, T., and A. Fert, 1993, "Theory of the perpendicular magnetoresistance in magnetic multilayers," Phys. Rev. B **48**, 7099–7113.

Van Aken, B. B., J.-P. Rivera, H. Schmid, and M. Fiebig, 2007, "Observation of ferrotoroidic domains," Nature (London) **449**, 702–705.

van den Brink, A., G. Vermijs, A. Solignac, J. Koo, J. T. Kohlhepp, H. J. M. Swagten, and B. Koopmans, 2016, "Field-free magnetization reversal by spin-Hall effect and exchange bias," Nat. Commun. **7**, 10854.

Varignon, J., J. Santamaria, and M. Bibes, 2019, "Electrically Switchable and Tunable Rashba-Type Spin Splitting in Covalent Perovskite Oxides," Phys. Rev. Lett. **122**, 116401.

Varignon, J., L. Vila, A. Barthélémy, and M. Bibes, 2018, "A new spin for oxide interfaces," Nat. Phys. **14**, 322–325.

Varotto, S., *et al.*, 2021, "Room-temperature ferroelectric switching of spin-to-charge conversion in germanium telluride," Nat. Electron. **4**, 740–747.

Vaz, C. A. F., J. Hoffman, Y. Segal, M. S. J. Marshall, J. W. Reiner, Z. Zhang, R. D. Grober, F. J. Walker, and C. H. Ahn, 2011, "Control of magnetism in $Pb(Zr_{0.2}Ti_{0.8})O_3/La_{0.8}Sr_{0.2}MnO_3$ multiferroic heterostructures (invited)," J. Appl. Phys. **109**, 07D905.

Vaz, C. A. F., J. Hoffman, Y. Segal, J. W. Reiner, R. D. Grober, Z. Zhang, C. H. Ahn, and F. J. Walker, 2010, "Origin of the Magnetoelectric Coupling Effect in $Pb(Zr_{0.2}Ti_{0.8})O_3/La_{0.8}Sr_{0.2}MnO_3$ Multiferroic Heterostructures," Phys. Rev. Lett. **104**, 127202.

Vaz, D. C., F. Trier, A. Dyrdał, A. Johansson, K. Garcia, A. Barthélémy, I. Mertig, J. Barnaś, A. Fert, and M. Bibes, 2020, "Determining the Rashba parameter from the bilinear magnetoresistance response in a two-dimensional electron gas," Phys. Rev. Mater. **4**, 071001.

Vaz, D. C., *et al.*, 2019, "Mapping spin-charge conversion to the band structure in a topological oxide two-dimensional electron gas," Nat. Mater. **18**, 1187–1193.

Vaz, D. C., *et al.*, 2022, "Functional demonstration of a fully integrated magneto-electric spin-orbit device," in *Proceedings of the 2021 IEEE International Electron Devices, San Francisco, 2021* (IEEE, New York).

Vaz, D. C., *et al.*, 2024, "Voltage-based magnetization switching and reading in magnetoelectric spin-orbit nanodevices," Nat. Commun. **15**, 1902.

Verzhbitskiy, I. A., H. Kurebayashi, H. Cheng, J. Zhou, S. Khan, Y. P. Feng, and G. Eda, 2020, "Controlling the magnetic anisotropy in $Cr_2Ge_2Te_6$ by electrostatic gating," Nat. Electron. **3**, 460–465.

Vicente-Arche, L. M., *et al.*, 2021, "Metal/$SrTiO_3$ two-dimensional electron gases for spin-to-charge conversion," Phys. Rev. Mater. **5**, 064005.

Vistoli, L., *et al.*, 2019, "Giant topological Hall effect in correlated oxide thin films," Nat. Phys. **15**, 67–72.

Voerman, J. A., C. Li, Y. Huang, and A. Brinkman, 2019, "Spin-momentum locking in the gate tunable topological insulator $BiSbTeSe_2$ in non-local transport measurements," Adv. Electron. Mater. **5**, 1900334.

Wadley, P., *et al.*, 2018, "Current polarity-dependent manipulation of antiferromagnetic domains," Nat. Nanotechnol. **13**, 362–365.

Wang, D., J. Weerasinghe, A. Albarakati, and L. Bellaiche, 2013, "Terahertz dielectric response and coupled dynamics of ferroelectrics and multiferroics from effective Hamiltonian simulations," Int. J. Mod. Phys. B **27**, 1330016.

Wang, H., P. Gopal, S. Picozzi, S. Curtarolo, M. Buongiorno Nardelli, and J. Sławińska, 2020, "Spin Hall effect in prototype Rashba ferroelectrics GeTe and SnTe," npj Comput. Mater. **6**, 1–7.

Wang, H., J. Kally, C. Şahin, T. Liu, W. Yanez, E. J. Kamp, A. Richardella, M. Wu, M. E. Flatté, and N. Samarth, 2019, "Fermi level dependent spin pumping from a magnetic insulator into a topological insulator," Phys. Rev. Res. **1**, 012014.

Wang, H., K.-Y. Meng, P. Zhang, J. T. Hou, J. Finley, J. Han, F. Yang, and L. Liu, 2019, "Large spin-orbit torque observed in epitaxial $SrIrO_3$ thin films," Appl. Phys. Lett. **114**, 232406.

Wang, H., *et al.*, 2020, "Above room-temperature ferromagnetism in wafer-scale two-dimensional van der Waals $Fe_3GeTe_2$ tailored by a topological insulator," ACS Nano **14**, 10045–10053.

Wang, J., *et al.*, 2003, "Epitaxial $BiFeO_3$ multiferroic thin film heterostructures," Science **299**, 1719–1722.

Wang, L., *et al.*, 2018, "Ferroelectrically tunable magnetic skyrmions in ultrathin oxide heterostructures," Nat. Mater. **17**, 1087–1094.

Wang, M., *et al.*, 2018, "Field-free switching of a perpendicular magnetic tunnel junction through the interplay of spin-orbit and spin-transfer torques," Nat. Electron. **1**, 582–588.

Wang, W., *et al.*, 2013, "Room-Temperature Multiferroic Hexagonal $LuFeO_3$ Films," Phys. Rev. Lett. **110**, 237601.

Wang, W., *et al.*, 2019, "Anomalous spin-orbit torques in magnetic single-layer films," Nat. Nanotechnol. **14**, 819–824.

Wang, W. G., and C. L. Chien, 2013, "Voltage-induced switching in magnetic tunnel junctions with perpendicular magnetic anisotropy," J. Phys. D **46**, 074004.

Wang, W.-G., M. Li, S. Hageman, and C. L. Chien, 2012, "Electric-field-assisted switching in magnetic tunnel junctions," Nat. Mater. **11**, 64–68.

Wang, X., *et al.*, 2019, "Current-driven magnetization switching in a van der Waals ferromagnet $Fe_3GeTe_2$," Sci. Adv. **5**, eaaw8904.

Wang, Y., J. Hu, Y. Lin, and C.-W. Nan, 2010, "Multiferroic magnetoelectric composite nanostructures," NPG Asia Mater. **2**, 61–68.

Wang, Y. J., Y. L. Tang, Y. L. Zhu, and X. L. Ma, 2023, "Entangled polarizations in ferroelectrics: A focused review of polar topologies," Acta Mater. **243**, 118485.

Wang, Y.-P., X.-Y. Chen, and M.-Q. Long, 2020, "Modifications of magnetic anisotropy of $Fe_3GeTe_2$ by the electric field effect," Appl. Phys. Lett. **116**, 092404.

Wang, Z., H. Zhou, M. Wang, W. Cai, D. Zhu, J.-O. Klein, and W. Zhao, 2019, "Proposal of toggle spin torques magnetic RAM for ultrafast computing," IEEE Electron Device Lett. **40**, 726–729.

Wang, Z., *et al.*, 2018, "Electric-field control of magnetism in a few-layered van der Waals ferromagnetic semiconductor," Nat. Nanotechnol. **13**, 554–559.

Weiler, M., A. Brandlmaier, S. Geprägs, M. Althammer, M. Opel, C. Bihler, H. Huebl, M. S. Brandt, R. Gross, and S. T. B. Goennenwein, 2009, "Voltage controlled inversion of magnetic anisotropy in a ferromagnetic thin film at room temperature," New J. Phys. **11**, 013021.

Weisheit, M., S. Fahler, A. Marty, Y. Souche, C. Poinsignon, and D. Givord, 2007, "Electric field-induced modification of magnetism in thin-film ferromagnets," Science **315**, 349–351.

Wen, Chang H., S. Akita, F. Matsukura, and H. Ohno, 2013, "Hole concentration dependence of the Curie temperature of (Ga, Mn)Sb in a field-effect structure," Appl. Phys. Lett. **103**, 142402.

Wen, Z., and D. Wu, 2020, "Ferroelectric tunnel junctions: Modulations on the potential barrier," Adv. Mater. **32**, 1904123.

White, J. S., I. Živković, A. J. Kruchkov, M. Bartkowiak, A. Magrez, and H. M. Rønnow, 2018, "Electric-Field-Driven Topological Phase Switching and Skyrmion-Lattice Metastability in Magnetoelectric $Cu_2OSeO_3$," Phys. Rev. Appl. **10**, 014021.

White, J. S., *et al.*, 2014, "Electric-Field-Induced Skyrmion Distortion and Giant Lattice Rotation in the Magnetoelectric Insulator $Cu_2OSeO_3$," Phys. Rev. Lett. **113**, 107203.

Wojdeł, J. C., P. Hermet, M. P. Ljungberg, P. Ghosez, and J. Íñiguez, 2013, "First-principles model potentials for lattice-dynamical studies: General methodology and example of application to ferroic perovskite oxides," J. Phys. Condens. Matter **25**, 305401.

Wollan, E. O., and W. C. Koehler, 1955, "Neutron diffraction study of the magnetic properties of the series of perovskite-type compounds $[(1-x)\mathrm{La}, x\mathrm{Ca}]\mathrm{MnO}_3$," Phys. Rev. **100**, 545–563.

Woo, S., *et al.*, 2016, "Observation of room-temperature magnetic skyrmions and their current-driven dynamics in ultrathin metallic ferromagnets," Nat. Mater. **15**, 501–506.

Wood, V. E., and A. E. Austin, 1974, "Possible applications for magnetoelectric materials," Int. J. Magn. **5**, 303.

Wu, H., *et al.*, 2019, "Room-Temperature Spin-Orbit Torque from Topological Surface States," Phys. Rev. Lett. **123**, 207205.

Wu, M., 2021, "Two-Dimensional van der Waals ferroelectrics: Scientific and technological opportunities," ACS Nano **15**, 9229–9237.

Wu, S. M., S. A. Cybart, D. Yi, J. M. Parker, R. Ramesh, and R. C. Dynes, 2013, "Full Electric Control of Exchange Bias," Phys. Rev. Lett. **110**, 067202.

Wu, S. M., S. A. Cybart, P. Yu, M. D. Rossell, J. X. Zhang, R. Ramesh, and R. C. Dynes, 2010, "Reversible electric control of exchange bias in a multiferroic field-effect device," Nat. Mater. **9**, 756–761.

Wu, T., A. Bur, P. Zhao, K. P. Mohanchandra, K. Wong, K. L. Wang, C. S. Lynch, and G. P. Carman, 2011, "Giant electric-field-induced reversible and permanent magnetization reorientation on magnetoelectric $\mathrm{Ni}/[011][\mathrm{Pb}(\mathrm{Mg}_{1/3}\mathrm{Nb}_{2/3})\mathrm{O}_3]_{(1-x)}-[\mathrm{PbTiO}_3]_x$ heterostructure," Appl. Phys. Lett. **98**, 012504.

Wu, Y., *et al.*, 2020, "Néel-type skyrmion in $\mathrm{WTe}_2/\mathrm{Fe}_3\mathrm{GeTe}_2$ van der Waals heterostructure," Nat. Commun. **11**, 3860.

Wulf, Wm. A., and S. A. McKee, 1995, "Hitting the memory wall: Implications of the obvious," SIGARCH Comput. Archit. News **23**, 20–24.

Xie, Y., Q. Zhan, T. Shang, H. Yang, Y. Liu, B. Wang, and R.-W. Li, 2018, "Electric field control of magnetic properties in FeRh/PMN-PT heterostructures," AIP Adv. **8**, 055816.

Xu, J., and C. L. Chien, 2021, "Voltage-controlled spin-orbit torque switching in W/CoFeB/MgO," Appl. Phys. Lett. **118**, 052409.

Xu, Y., F. Zhang, Y. Liu, R. Xu, Y. Jiang, H. Cheng, A. Fert, and W. Zhao, 2023, "Inverse orbital Hall effect discovered from light-induced terahertz emission," arXiv:2208.01866.

Yadav, A. K., *et al.*, 2016, "Observation of polar vortices in oxide superlattices," Nature (London) **530**, 198–201.

Yamada, H., *et al.*, 2013, "Giant electroresistance of super-tetragonal $\mathrm{BiFeO}_3$-based ferroelectric tunnel junctions," ACS Nano **7**, 5385–5390.

Yamanouchi, M., D. Chiba, F. Matsukura, and H. Ohno, 2006, "Current-assisted domain wall motion in ferromagnetic semiconductors," Jpn. J. Appl. Phys. **45**, 3854–3859.

Yan, Y., *et al.*, 2016, "Strong electrical manipulation of spin-orbit torque in ferromagnetic heterostructures," Adv. Electron. Mater. **2**, 1600219.

Yang, F., A. A. Taskin, S. Sasaki, K. Segawa, Y. Ohno, K. Matsumoto, and Y. Ando, 2014, "Top gating of epitaxial $(\mathrm{Bi}_{1-x}\mathrm{Sb}_x)_2\mathrm{Te}_3$ topological insulator thin films," Appl. Phys. Lett. **104**, 161614.

Yang, H., A. Thiaville, S. Rohart, A. Fert, and M. Chshiev, 2015, "Anatomy of Dzyaloshinskii-Moriya Interaction at Co/Pt Interfaces," Phys. Rev. Lett. **115**, 267210.

Yang, H., B. Zhang, X. Zhang, X. Yan, W. Cai, Y. Zhao, J. Sun, K. L. Wang, D. Zhu, and W. Zhao, 2019, "Giant Charge-to-Spin Conversion Efficiency in $\mathrm{SrTiO}_3$-Based Electron Gas Interface," Phys. Rev. Appl. **12**, 034004.

Yang, N., *et al.*, 2019, "Structure dependence of ferroelectricity in high quality $\mathrm{BiMnO}_3$ epitaxial films," Phys. Rev. Mater. **3**, 054402.

Yang, S., K.-W. Moon, T.-S. Ju, C. Kim, H.-J. Kim, J. Kim, B. X. Tran, J.-I. Hong, and C. Hwang, 2021, "Electrical generation and deletion of magnetic skyrmion-bubbles via vertical current injection," Adv. Mater. **33**, 2104406.

Yi, D., J. Liu, S. Okamoto, S. Jagannatha, Y.-C. Chen, P. Yu, Y.-H. Chu, E. Arenholz, and R. Ramesh, 2013, "Tuning the Competition between Ferromagnetism and Antiferromagnetism in a Half-Doped Manganite through Magnetoelectric Coupling," Phys. Rev. Lett. **111**, 127601.

Yin, Y. W., M. Raju, W. J. Hu, X. J. Weng, X. G. Li, and Q. Li, 2011, Coexistence of tunneling magnetoresistance and electroresistance at room temperature in $\mathrm{La}_{0.7}\mathrm{Sr}_{0.3}\mathrm{MnO}_3/(\mathrm{Ba,Sr})\mathrm{TiO}_3/\mathrm{La}_{0.7}\mathrm{Sr}_{0.3}\mathrm{MnO}_3$ multiferroic tunnel junctions," J. Appl. Phys. **109**, 07D915.

Yin, Y. W., *et al.*, 2013, "Enhanced tunnelling electroresistance effect due to a ferroelectrically induced phase transition at a magnetic complex oxide interface," Nat. Mater. **12**, 397–402.

Yoda, H., *et al.*, 2016, "Voltage-control spintronics memory (VoCSM) having potentials of ultra-low energy-consumption and high-density," in *Proceedings of the 2016 IEEE International Electron Devices Meeting (IEDM), San Francisco, 2016* (IEEE, New York), pp. 27.6.1–27.6.4.

Yoda, T., T. Yokoyama, and S. Murakami, 2015, "Current-induced orbital and spin magnetizations in crystals with helical structure," Sci. Rep. **5**, 12024.

Yu, J., *et al.*, 2019, "Long spin coherence length and bulk-like spin-orbit torque in ferrimagnetic multilayers," Nat. Mater. **18**, 29–34.

Yu, P., *et al.*, 2010, "Interface Ferromagnetism and Orbital Reconstruction in $\mathrm{BiFeO}_3$–$\mathrm{La}_{0.7}\mathrm{Sr}_{0.3}\mathrm{MnO}_3$ Heterostructures," Phys. Rev. Lett. **105**, 027201.

Yu, P., *et al.*, 2012, "Interface control of bulk ferroelectric polarization," Proc. Natl. Acad. Sci. U.S.A. **109**, 9710–9715.

Yu, X. Z., N. Kanazawa, Y. Onose, K. Kimoto, W. Z. Zhang, S. Ishiwata, Y. Matsui, and Y. Tokura, 2011, "Near room-temperature formation of a skyrmion crystal in thin-films of the helimagnet FeGe," Nat. Mater. **10**, 106–109.

Yu, X. Z., N. Kanazawa, W. Z. Zhang, T. Nagai, T. Hara, K. Kimoto, Y. Matsui, Y. Onose, and Y. Tokura, 2012, "Skyrmion flow near room temperature in an ultralow current density," Nat. Commun. **3**, 988.

Yu, X. Z., Y. Onose, N. Kanazawa, J. H. Park, J. H. Han, Y. Matsui, N. Nagaosa, and Y. Tokura, 2010, "Real-space observation of a two-dimensional skyrmion crystal," Nature (London) **465**, 901–904.

Yuasa, S., T. Nagahama, A. Fukushima, Y. Suzuki, and K. Ando, 2004, "Giant room-temperature magnetoresistance in single-crystal Fe/MgO/Fe magnetic tunnel junctions," Nat. Mater. **3**, 868.

Zhai, K., P. Lu, Y. Chang, A. Nie, Z. Yu, and Y. Sun, 2020, "Electric field control of nonvolatile two-state magnetoelectric coefficient at room temperature in a hexaferrite," J. Am. Ceram. Soc. **103**, 4384–4389.

Zhang, H. J., S. Yamamoto, Y. Fukaya, M. Maekawa, H. Li, A. Kawasuso, T. Seki, E. Saitoh, and K. Takanashi, 2014, "Current-induced spin polarization on metal surfaces probed by spin-polarized positron beam," Sci. Rep. **4**, 4844.

Zhang, S., and A. Fert, 2016, "Conversion between spin and charge currents with topological insulators," Phys. Rev. B **94**, 184423.

Zhang, S., P. M. Levy, and A. Fert, 2002, "Mechanisms of Spin-Polarized Current-Driven Magnetization Switching," Phys. Rev. Lett. **88**, 236601.

Zhang, S., *et al.*, 2012, "Electric-Field Control of Nonvolatile Magnetization in $Co_{40}Fe_{40}B_{20}/Pb(Mg_{1/3}Nb_{2/3})_{0.7}Ti_{0.3}O_3$ Structure at Room Temperature," Phys. Rev. Lett. **108**, 137203.

Zhang, W., Z. Teng, H. Zeng, H. Zhang, J. Železný, and W. Zhang, 2020, "Tuning spin Hall conductivity in GeTe by ferroelectric polarization," Phys. Status Solidi (b) **257**, 2000143.

Zhang, W., and R.-G. Xiong, 2012, "Ferroelectric metal-organic frameworks," Chem. Rev. **112**, 1163–1195.

Zhang, X., M. Ezawa, and Y. Zhou, 2015, "Magnetic skyrmion logic gates: Conversion, duplication and merging of skyrmions," Sci. Rep. **5**, 9400.

Zhang, X., C. Wang, Y. Liu, Z. Zhang, Q. Y. Jin, and C.-G. Duan, 2016, "Magnetization switching by combining electric field and spin-transfer torque effects in a perpendicular magnetic tunnel junction," Sci. Rep. **6**, 18719.

Zhang, X., Z. Zhang, Y. Liu, and Q. Y. Jin, 2015, "Simulation of electric-field and spin-transfer-torque induced magnetization switching in perpendicular magnetic tunnel junctions," J. Appl. Phys. **117**, 17A701.

Zhang, X., Y. Zhou, M. Ezawa, G. P. Zhao, and W. Zhao, 2015, "Magnetic skyrmion transistor: Skyrmion motion in a voltage-gated nanotrack," Sci. Rep. **5**, 11369.

Zhang, X.-G., and W. H. Butler, 2004, "Large magnetoresistance in bcc Co/MgO/Co and FeCo/MgO/FeCo tunnel junctions," Phys. Rev. B **70**, 172407.

Zhang, Z., P.-F. Li, Y.-Y. Tang, A. J. Wilson, K. Willets, M. Wuttig, R.-G. Xiong, and S. Ren, 2017, "Tunable electroresistance and electro-optic effects of transparent molecular ferroelectrics," Sci. Adv. **3**, e1701008.

Zhao, H. J., P. Chen, C. Paillard, R. Arras, Y.-W. Fang, X. Li, J. Gosteau, Y. Yang, and L. Bellaiche, 2020, "Large spin splittings due to the orbital degree of freedom and spin textures in a ferroelectric nitride perovskite," Phys. Rev. B **102**, 041203.

Zhao, H. J., P. Chen, S. Prosandeev, S. Artyukhin, and L. Bellaiche, 2021, "Dzyaloshinskii-Moriya-like interaction in ferroelectrics and antiferroelectrics," Nat. Mater. **20**, 341–345.

Zhao, T., *et al.*, 2006, "Electrical control of antiferromagnetic domains in multiferroic $BiFeO_3$ films at room temperature," Nat. Mater. **5**, 823–829.

Zhao, Z., M. Jamali, N. D'Souza, D. Zhang, S. Bandyopadhyay, J. Atulasimha, and J.-P. Wang, 2016, "Giant voltage manipulation of MgO-based magnetic tunnel junctions via localized anisotropic strain: A potential pathway to ultra-energy-efficient memory technology," Appl. Phys. Lett. **109**, 092403.

Zhao, Z., A. K. Smith, M. Jamali, and J.-P. Wang, 2020, "External-field-free spin Hall switching of perpendicular magnetic nanopillar with a dipole-coupled composite structure," Adv. Electron. Mater. **6**, 1901368.

Zheng, L. M., *et al.*, 2018, "Ambipolar ferromagnetism by electrostatic doping of a manganite," Nat. Commun. **9**, 1897.

Zheng, Z., *et al.*, 2021, "Field-free spin-orbit torque-induced switching of perpendicular magnetization in a ferrimagnetic layer with a vertical composition gradient," Nat. Commun. **12**, 4555.

Zhong, W., D. Vanderbilt, and K. M. Rabe, 1994, "Phase Transitions in $BaTiO_3$ from First Principles," Phys. Rev. Lett. **73**, 1861–1864.

Zhong, Z., L. Si, Q. Zhang, W.-G. Yin, S. Yunoki, and K. Held, 2015, "Giant switchable Rashba effect in oxide heterostructures," Adv. Mater. Interfaces **2**, 1400445.

Zhou, L., Y. Huang, S. Das, Y. Tang, C. Li, H. Tian, L.-Q. Chen, Y. Wu, R. Ramesh, and Z. Hong, 2022, "Local manipulation and topological phase transitions of polar skyrmions," Matter Radiat. Extremes **5**, 1031–1041.

Zhou, Z., B. M. Howe, M. Liu, T. Nan, X. Chen, K. Mahalingam, N. X. Sun, and G. J. Brown, 2015, "Interfacial charge-mediated nonvolatile magnetoelectric coupling in $Co_{0.3}Fe_{0.7}/Ba_{0.6}Sr_{0.4}TiO_3/Nb:SrTiO_3$ multiferroic heterostructures," Sci. Rep. **5**, 7740.

Zhu, L., and R. A. Buhrman, 2019, "Maximizing Spin-Orbit-Torque Efficiency of Pt/Ti Multilayers: Trade-Off between Intrinsic Spin Hall Conductivity and Carrier Lifetime," Phys. Rev. Appl. **12**, 051002.

Zhu, R., *et al.*, 2022, "Dynamics of Polar Skyrmion Bubbles under Electric Fields," Phys. Rev. Lett. **129**, 107601.

Zhuravlev, M. Ye., R. F. Sabirianov, S. S. Jaswal, and E. Y. Tsymbal, 2005, "Giant Electroresistance in Ferroelectric Tunnel Junctions," Phys. Rev. Lett. **94**, 246802.

Zvezdin, A. K., A. M. Kadomtseva, S. S. Krotov, A. P. Pyatakov, Yu. F. Popov, and G. P. Vorob'ev, 2006, "Magnetoelectric Interaction and magnetic field control of electric polarization in multiferroics," J. Magn. Magn. Mater. **300**, 224–228.